Epidemic Spreading Dynamics on Temporal Networks

Guest Editors: Wei Wang, Luxing Yang, and Chenquan Gan

Epidemic Spreading Dynamics on Temporal Networks

Epidemic Spreading Dynamics on Temporal Networks

Guest Editors: Wei Wang, Luxing Yang, and Chenquan Gan

Contents

WILEY | Hindawi

Retraction

Retracted: Information Spreading on Memory Activity-Driven Temporal Networks

Complexity

This article has been retracted by Hindawi following an investigation undertaken by the publisher [1]. This investigation has uncovered evidence of one or more of the following indicators of systematic manipulation of the publication process:

(1) Discrepancies in scope

(2) Discrepancies in the description of the research reported

(3) Discrepancies between the availability of data and the research described

(4) Inappropriate citations

(5) Incoherent, meaningless and/or irrelevant content included in the article

(6) Manipulated or compromised peer review

The presence of these indicators undermines our confidence in the integrity of the article's content and we cannot, therefore, vouch for its reliability. Please note that this notice is intended solely to alert readers that the content of this article is unreliable. We have not investigated whether authors were aware of or involved in the systematic manipulation of the publication process.

Wiley and Hindawi regrets that the usual quality checks did not identify these issues before publication and have since put additional measures in place to safeguard research integrity.

We wish to credit our own Research Integrity and Research Publishing teams and anonymous and named external researchers and research integrity experts for contributing to this investigation.

The corresponding author, as the representative of all authors, has been given the opportunity to register their agreement or disagreement to this retraction. We have kept a record of any response received.

References

[1] L. Zhong, Y. Bai, C. Liu, J. Du, and W. Pan, "Information Spreading on Memory Activity-Driven Temporal Networks," *Complexity*, vol. 2021, Article ID 8015191, 8 pages, 2021.

WILEY | Hindawi

Retraction

Retracted: Analysis of Factors Influencing Stock Market Volatility Based on GARCH-MIDAS Model

Complexity

This article has been retracted by Hindawi following an investigation undertaken by the publisher [1]. This investigation has uncovered evidence of one or more of the following indicators of systematic manipulation of the publication process:

(1) Discrepancies in scope

(2) Discrepancies in the description of the research reported

(3) Discrepancies between the availability of data and the research described

(4) Inappropriate citations

(5) Incoherent, meaningless and/or irrelevant content included in the article

(6) Manipulated or compromised peer review

The presence of these indicators undermines our confidence in the integrity of the article's content and we cannot, therefore, vouch for its reliability. Please note that this notice is intended solely to alert readers that the content of this article is unreliable. We have not investigated whether authors were aware of or involved in the systematic manipulation of the publication process.

Wiley and Hindawi regrets that the usual quality checks did not identify these issues before publication and have since put additional measures in place to safeguard research integrity.

We wish to credit our own Research Integrity and Research Publishing teams and anonymous and named external researchers and research integrity experts for contributing to this investigation.

The corresponding author, as the representative of all authors, has been given the opportunity to register their agreement or disagreement to this retraction. We have kept a record of any response received.

References

[1] D. Ma, T. Yang, L. Liu, and Y. He, "Analysis of Factors Influencing Stock Market Volatility Based on GARCH-MIDAS Model," *Complexity*, vol. 2022, Article ID 6176451, 10 pages, 2022.

WILEY | Hindawi

Retraction

Retracted: A Study on the Topic-Sentiment Evolution and Diffusion in Time Series of Public Opinion Derived from Emergencies

Complexity

This article has been retracted by Hindawi following an investigation undertaken by the publisher [1]. This investigation has uncovered evidence of one or more of the following indicators of systematic manipulation of the publication process:

(1) Discrepancies in scope

(2) Discrepancies in the description of the research reported

(3) Discrepancies between the availability of data and the research described

(4) Inappropriate citations

(5) Incoherent, meaningless and/or irrelevant content included in the article

(6) Manipulated or compromised peer review

The presence of these indicators undermines our confidence in the integrity of the article's content and we cannot, therefore, vouch for its reliability. Please note that this notice is intended solely to alert readers that the content of this article is unreliable. We have not investigated whether authors were aware of or involved in the systematic manipulation of the publication process.

Wiley and Hindawi regrets that the usual quality checks did not identify these issues before publication and have since put additional measures in place to safeguard research integrity.

We wish to credit our own Research Integrity and Research Publishing teams and anonymous and named external researchers and research integrity experts for contributing to this investigation.

The corresponding author, as the representative of all authors, has been given the opportunity to register their agreement or disagreement to this retraction. We have kept a record of any response received.

References

[1] M. Cai, H. Luo, and Y. Cui, "A Study on the Topic-Sentiment Evolution and Diffusion in Time Series of Public Opinion Derived from Emergencies," *Complexity*, vol. 2021, Article ID 2069010, 23 pages, 2021.

WILEY | Hindawi

Retraction

Retracted: Cascading Failure Dynamics against Intentional Attack for Interdependent Industrial Internet of Things

Complexity

This article has been retracted by Hindawi following an investigation undertaken by the publisher [1]. This investigation has uncovered evidence of one or more of the following indicators of systematic manipulation of the publication process:

(1) Discrepancies in scope

(2) Discrepancies in the description of the research reported

(3) Discrepancies between the availability of data and the research described

(4) Inappropriate citations

(5) Incoherent, meaningless and/or irrelevant content included in the article

(6) Manipulated or compromised peer review

The presence of these indicators undermines our confidence in the integrity of the article's content and we cannot, therefore, vouch for its reliability. Please note that this notice is intended solely to alert readers that the content of this article is unreliable. We have not investigated whether authors were aware of or involved in the systematic manipulation of the publication process.

Wiley and Hindawi regrets that the usual quality checks did not identify these issues before publication and have since put additional measures in place to safeguard research integrity.

We wish to credit our own Research Integrity and Research Publishing teams and anonymous and named external researchers and research integrity experts for contributing to this investigation.

The corresponding author, as the representative of all authors, has been given the opportunity to register their agreement or disagreement to this retraction. We have kept a record of any response received.

References

[1] H. Peng, Z. Qian, Z. Kan, D. Zhao, J. Yu, and J. Han, "Cascading Failure Dynamics against Intentional Attack for Interdependent Industrial Internet of Things," *Complexity*, vol. 2021, Article ID 7181431, 15 pages, 2021.

WILEY | Hindawi

Retraction

Retracted: The Evolution Model of Public Risk Perception Based on Pandemic Spreading Theory under Perspective of COVID-19

Complexity

This article has been retracted by Hindawi following an investigation undertaken by the publisher [1]. This investigation has uncovered evidence of one or more of the following indicators of systematic manipulation of the publication process:

(1) Discrepancies in scope

(2) Discrepancies in the description of the research reported

(3) Discrepancies between the availability of data and the research described

(4) Inappropriate citations

(5) Incoherent, meaningless and/or irrelevant content included in the article

(6) Peer-review manipulation

The presence of these indicators undermines our confidence in the integrity of the article's content and we cannot, therefore, vouch for its reliability. Please note that this notice is intended solely to alert readers that the content of this article is unreliable. We have not investigated whether authors were aware of or involved in the systematic manipulation of the publication process.

Wiley and Hindawi regrets that the usual quality checks did not identify these issues before publication and have since put additional measures in place to safeguard research integrity.

We wish to credit our own Research Integrity and Research Publishing teams and anonymous and named external researchers and research integrity experts for contributing to this investigation.

The corresponding author, as the representative of all authors, has been given the opportunity to register their agreement or disagreement to this retraction. We have kept a record of any response received.

References

[1] Y. Zhang, Z. Li, G. Zhou, N. Xu, and J. Liu, "The Evolution Model of Public Risk Perception Based on Pandemic Spreading Theory under Perspective of COVID-19," *Complexity*, vol. 2021, Article ID 1015049, 10 pages, 2021.

WILEY | Hindawi

Research Article

Quantitative Analysis of COVID-19 Pandemic Responses Based on an Improved SEIR-SD Model

Yang Liu,[1] Bingrui Liu,[2] Yi Deng,[2] and Jia Liu [2]

[1]*School of Management, Wuhan University of Technology, Wuhan, China*
[2]*School of Information and Safety Engineering, Zhongnan University of Economics and Law, Wuhan, China*

Correspondence should be addressed to Jia Liu; whutrobin@163.com

In late 2019, the COVID-19 pandemic began to spread over the world, causing millions of deaths. In the first few months of the pandemic, several countries (such as China) prevented the spread of the pandemic successfully. By contrast, the pandemic in many other countries was not controlled well. For example, India encountered a second serious outbreak of COVID-19 from April 2021 due to the poor resistance measures implemented by the government. To figure out the effective countermeasures to the pandemic, this research proposes a COVID-19 pandemic and its response system, which consists of the infection subsystem, the quarantine subsystem, and the medical subsystem. On this basis, an improved SEIR-SD model is established which is utilized to analyze the response measures to the pandemic quantitatively. This model successfully simulates the actual epidemic scenarios in Wuhan, which verifies its effectiveness. Afterward, the impact of hospital administration rate, quarantine rate, average contact number, and contact infection rate on the cumulative number of infections and deaths are analyzed by simulation. The results show that both the medical and administrative efforts, especially in the early stage of the epidemic, are significant in reducing the number of infections and shortening the epidemic period. In the medical aspect, the more stringent quarantine brings the earlier inflection point of the epidemic; more importantly, improving the treatment rate significantly reduces the scale of the epidemic. In the administrative aspect, enforcing individual protection and strict community closure can effectively cut off the transmission of the virus and curb the spread of the epidemic. Finally, this research proposes several practical suggestions in response to the COVID-19 pandemic. The main contribution of this research is that the effects of different response measures on the number of new infections daily and the cumulative number of deaths of a country or region in the COVID-19 pandemic are estimated quantitatively based on modeling and simulation.

1. Introduction

The COVID-19 epidemic was discovered in Wuhan in late 2019 and spread over the world. After the outbreak, the Chinese national government and Wuhan local government immediately adopted a series of measures to control the spread of the virus. These measures include but are not limited to closing communities, enforcing individual protection, isolating suspected cases, and establishing temporary treatment centers for mildly infected cases. Simultaneously, medical staff and supplies from all over China supported Wuhan rapidly, which greatly reduced the death rate of confirmed cases in Wuhan. However, the pandemic in many other countries was not controlled well.

For example, India encountered a second serious outbreak of COVID-19 from April 2021 due to the poor resistance measures implemented by the government.

From the perspective of system science, the epidemic of infectious diseases in the population is a complex diffusion process. The analysis and prediction of infectious disease spread based on models can help understand the epidemic mechanism and the inherent laws and provide a theoretical basis for the choice of intervention measures. The models are established based on either the micro- or macroperspectives. The micromodels focus on the individuals in the crowd. There is a contact network with individuals. The contact between the infected cases and the suspected ones leads to the state change of the suspected ones, forming the

transmission dynamics process on the network [1]. There are two main research fields of network-based micromodel: the first one is to study the spread of infectious diseases in ideal networks, such as small-world networks and scale-free networks, which partially depict the characteristics of real social networks [2]. The second one is to study the spread of infectious diseases on the real network. The basic method is to carry out actual investigations and construct a contact network close to the real one [3]. Macroscopic modeling regards the population as a whole and focuses on the changes of its state. The composite population method considers the spatial heterogeneity of the population and divides the population into different groups, which are coupled by the flow of people, forming a complex dynamic system [4]. Correspondingly, the single group method shows the epidemic process of infectious diseases in the number of susceptible, infectious, and other types of people. The most popular single population model is the compartment model. One of the classic compartment models is the SIR model, which was proposed by Kermack et al. in 1927 [5]. Based on the SIR model, the SIS model [6], SIRS model [7], and SEIR model [8] are developed. The SEIR model is one of the most representative mathematical models of infectious disease dynamics in a fixed population. The model considers the incubation period of infectious diseases and is suitable for large-scale modeling of the COVID-19 epidemic on the country and city level. Therefore, this paper intends to analyze the COVID-19 epidemic by the improvement of this model.

The system dynamics model [9] was first proposed in 1956 by Forrester of the Massachusetts Institute of Technology. It has been widely used in industry, agriculture, economy, management, medicine, transportation, ecology, environment, energy, military, and many other fields. For example, Assuncao et al. used system dynamics to establish an urban sustainable development system considering the natural factors, physiological feelings, and psychological feelings [10]. Ekinci et al. utilized the model to assess the future impact of various air quality factors on environmental sustainability [11]. As one of the most powerful tools to study complex systems, system dynamics has a broad prospect on public health, in which the combination of system dynamics and the classical models of infectious diseases is a new field of infectious disease research [12, 13]. Li et al. combined the system dynamics with a multicompartment model to predict the development trend of the COVID-19 epidemic [14]. In this study, the system dynamics model is combined with the SEIR model so that the solution process of the SEIR model can be simulated and visualized. More importantly, the effect of different variables on simulation results can be analyzed.

After the outbreak of COVID-19, many scholars engaged in the study of the epidemic by establishing mathematical models. Tang and Zhao used the classical SEIR model to fit the epidemic development trend [15, 16]. Considering quarantine measures and types of the infected population, Wei et al. proposed the SEIR + CAQ model to predict the number of infected cases [17]. In the early stage of COVID-19, many studies focused on the scale prediction of the epidemic. For example, British scholar Jonathan et al. predicted in January 2020 that infected cases in Wuhan would reach 190,000 on February 4th [18]. Shen et al. estimated the basic and effective reproduction times of COVID-19 [19]. They predicted the peak time and scale of the epidemic based on the existing epidemiological data and the dynamic model. They also estimated that the number of infected people would ultimately be less than 20000. Wu et al. calculated the number of infected people in Wuhan by the number of cases in January 2020 and predicted that the number of infected cases on January 25 would exceed 6000 [20]. In terms of epidemic prevention and control measures, Lin et al. proposed a conceptual model of the outbreak of COVID-19 in Wuhan, which was based on the consideration of such interventions as holiday extension, travel restriction, hospitalization, and quarantine [21]. Adam et al. estimated that within two weeks of the restriction, the transmission volume would decrease by nearly a half. The Lancet published an editorial that China has successfully avoided a large number of cases of infection and death because of the strong public countermeasures [22]. They also called on the other countries to learn from China's experience [23]. To sum up, the current research of COVID-19 primarily focuses on the prediction and estimation of epidemic development. There is a lack of modeling and analysis of specific prevention measures. Therefore, this paper focuses on analyzing the effectiveness of the measures such as closing communities, enforcing individual protection, isolating suspected cases, and establishing temporary treatment centers for mildly infected cases.

The dynamic models are utilized to study the effect of various prevention and control measures in the COVID-19 pandemic (He et al., 2020) [24]. For example, Zhao and Chen developed a SUQC model to explicitly parameterize the intervention effects of control measures of the pandemic [25]. Moran's spatial statistic with various definitions of neighbors was used by Kang et al. (2020) to conduct a test to determine whether a spatial association of the COVID-19 infections existed [26]. Linka et al. (2020) combined a global network mobility model with a local epidemiology model to simulate and predict the outbreak dynamics and control of the pandemic in Europe [27]. On this basis, Jia et al. (2020) developed a spatiotemporal risk source model, which can not only forecast the distribution of confirmed cases but also identify regions that have a high risk of transmission at the early stage of the pandemic [28].

This research combines the infectious disease model (hereinafter referred to as "SEIR") with the system dynamics model (hereinafter referred to as "SD"). We analyze the countermeasures of Wuhan by the combined model, and finally, propose feasible suggestions for the response to the epidemic. The model simulates the situation of a large area and scale of individuals within an acceptable complexity. Moreover, the Chinese official data are utilized to fit the model, while the values of the parameters in this model are set by the authoritative data. On this basis, the effectiveness of the model is verified. The remainder of this paper is organized as follows: The second section proposes the COVID-19 epidemic and its response system. The third

section establishes the improved SEIR-SD model for the system. The fourth section makes simulations on several countermeasures according to the real and some hypothetical scenarios in Wuhan. The fifth section is the conclusions and suggestions.

2. COVID-19 Epidemic and Its Response System

The factors in the COVID-19 epidemic and its response forms a complex dynamic feedback system that includes the medical supplies, the hospital beds, the medical staff, the patients, etc. The system consists of the following subsystems: the infection subsystem, the quarantine subsystem, and the medical subsystem.

2.1. Infection Subsystem. In the infection subsystem, the total number of people in the city, the average number of contacts per person daily, and the infection rate have a positive impact on the number of people who are infected and enter the incubation period. The close contacts of patients in the incubation period are infected due to the lack of protective measures, resulting in an increase in the number of infected people daily. After the incubation period, patients begin to develop symptoms. In addition, the number of infected people, the average number of close contacts, and susceptible people were positively correlated with the number of close contacts of symptomatic people. Among the close contacts, some are infected and go into the incubation period, while others are uninfected but still susceptible. There are two important factors to determine whether close contacts are infected or not. The first one is the infection rate of close contacts. The transmission mode of the virus is diverse. It is easy to be infected without any protective measures. After taking measures such as wearing masks and disinfecting, the infection rate of close contacts is greatly reduced. The second one is the quarantine rate. If the infected cases are found precisely and quarantined in time, the probability of secondary infection should decrease significantly.

The causal relationship of the infection subsystem is shown in Figure 1.

The meaning of parameters in Figure 1 is shown in Table 1.

2.2. Quarantine Subsystem. In the quarantine subsystem, the factors that have a positive impact on the number of quarantined close contacts one day are the number of close contacts and the overall proportion of quarantined close contacts (the quarantined rate). Among these quarantined close contacts, some are diagnosed as infected and receive treatment, while others are not infected and released from quarantine. In addition to the number of quarantined close contacts on that day, the influencing factors of the number of these two parts also include the overall proportion of close contacts who are infected. The number of newly quarantined people on that day and the quarantine days positively impact the cumulative number of quarantined people and the number of released people on that day, while the number of
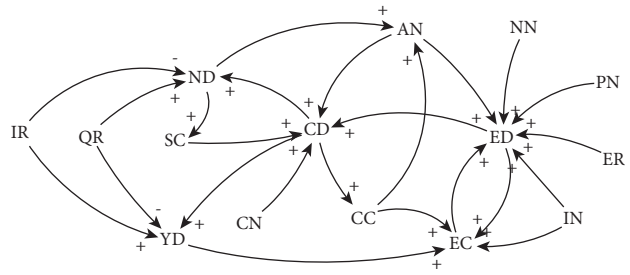
FIGURE 1: Causal relationship of infection subsystem.

released people on that day negatively impacts the cumulative number of quarantined people.

The causal relationship of the quarantine subsystem is shown in Figure 2.

The meaning of parameters in Figure 2 is shown in Table 2.

2.3. Medical Subsystem. In the medical subsystem, the patients who are infected in the incubation period have symptoms after the incubation period, so the number of patients who have symptoms after the incubation period is affected by the average incubation period of the disease and the number of patients who are infected and in the incubation period. Due to the influence of medical supplies and hospital beds, only a part of the people with symptoms can be admitted to the hospital. Therefore, the positive influencing factors of the number of people with symptoms admitted to the hospital one day are the number of people with symptoms and the overall proportion of people with symptoms admitted to the hospital. The number of hospitalized patients directly affects the number of cured patients and the number of deaths. Some of the people who have not been treated can recover by themselves. The number of self-healing people is affected by the average self-healing time, the proportion of patients treated, and the number of patients with symptoms.

The causal relationship of the medical subsystem is shown in Figure 3.

The meaning of parameters in Figure 3 is shown in Table 3.

3. Improved SEIR-SD Model for COVID-19 Epidemic and Its Response

The classical SEIR epidemic model considers four groups of people including the susceptible, exposed, infected, and rehabilitated. It uses a set of differential equations to express the transmission mechanism of infectious diseases. But the model does not consider the strong intervention of management measures. The Chinese government and the local government of Wuhan have implemented a series of effective measures to control the spread of the virus. These measures include but are not limited to closing communities, enforcing individual protection, isolating suspected cases, and establishing temporary treatment centers for mildly infected cases. The spread of the virus has been largely

TABLE 1: Definition of parameters in Figure 1.

Parameter	Definition
IR	The proportion of close contacts infected
QR	The proportion of close contacts found and quarantined (quarantine rate)
ND	The number of uninfected cases in close contact but not quarantined daily
YD	The number of infected cases in close contact but not quarantined daily
CN	The average number of close contacts of infected cases
CD	The number of close contacts of those with symptoms daily
AN	The number of people except for those in quarantine, hospitalization, and death
CC	The cumulative number of close contacts
EC	The cumulative number of infected cases in the incubation period
ED	The number of infected cases going into incubation period daily
NN	The average number of daily contacts per person (average contact number)
PN	Cumulative population
ER	The proportion of infections after contacting infected cases (contact infection rate)
SC	Susceptible population
IN	The number of initial infected cases
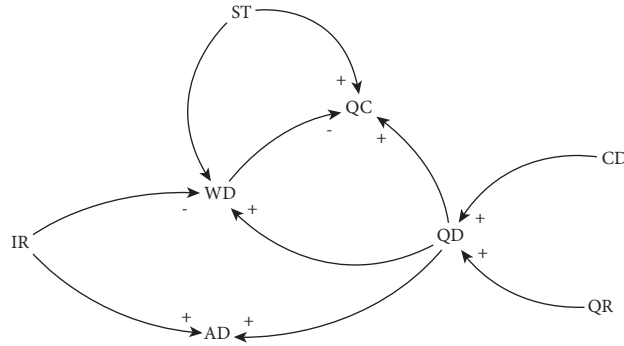
FIGURE 2: Causal relationship of quarantine subsystem.

TABLE 2: Definition of parameters in Figure 2.

Parameter	Definition
WD	The number of close contacts released from quarantine daily
AD	The number of infected cases in quarantine daily
QC	The cumulative number of infected cases in close contacts
QD	The number of quarantined close contacts daily
ST	Quarantine days
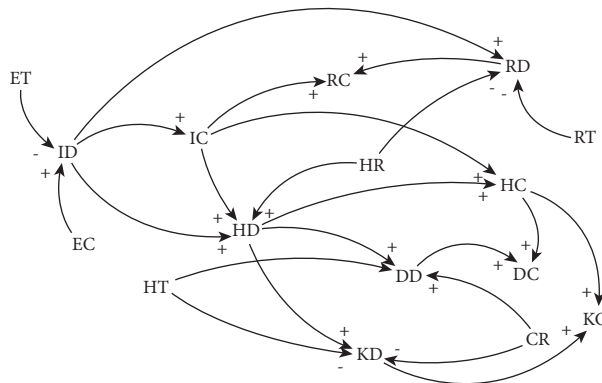
FIGURE 3: Causal relationship of the medical subsystem.

TABLE 3: Definition of parameters in Figure 3.

Parameter	Definition
ET	The average incubation period
ID	The number of new infections daily
IC	The cumulative number of infections
HD	The number of new infections and admitted to the hospital daily
HT	Average hospitalization time
RC	The cumulative number of self-healing
HR	The proportion of patients admitted to hospital (hospital admission rate)
DD	The number of cases cured and discharged daily
KD	The number of new deaths daily
RD	The number of self-healing daily
RT	Average self-healing time
HC	The cumulative number of cases in hospital
DC	The cumulative number of cases cured and discharged
CR	Average cure rate
KC	The cumulative number of deaths

controlled because of the interventions. This study intends to improve the classical SEIR model by adding the variables related to the management measures. Afterward, we combine the improved SEIR model with SD simulation to analyze the influence of management factors, such as the community closure degree, the personal protection degree, the hospital treatment rate, and the quarantine rate of close contacts on the number of confirmed cases and deaths of a country or region.

Based on the COVID-19 epidemic and its response system proposed in Section 2. We propose the flowchart of the infection subsystem (Figure 4), quarantine subsystem (Figure 5), and medical subsystem (Figure 6). There are three types of variables in the flowcharts which are the level variables, rate variables, and auxiliary variables. The level variables in the rectangle represent the cumulative effect of the system over time. The rate variables in the form of a valve control the strength of the system change. Auxiliary variables are used to construct information feedback between the variables.

In the infection subsystem, CC, EC, and SC are selected as the level variables, while the rate variables are CD, ED, and ND. The functional relationships of the infection subsystem are shown in the following equations:

$$\frac{dCC}{dt} = C\,D - Y\,D - N\,D - Q\,D, \tag{1}$$

$$\frac{dEC}{dt} = E\,D + Y\,D - I\,D, \tag{2}$$

$$\frac{dSC}{dt} = N\,D + W\,D - E\,D - C\,D, \tag{3}$$

$$AN = PN - KC - HC - QC, \tag{4}$$

$$E\,D = \begin{cases} SC, & \dfrac{(IC + EC) \cdot NN \cdot ER \cdot SC}{AN} > SC, \\[2ex] \dfrac{(IC + EC) \cdot NN \cdot ER \cdot SC}{AN}, & \dfrac{(IC + EC) \cdot NN \cdot ER \cdot SC}{AN} \le SC, \end{cases} \tag{5}$$

$$N\,D = C\,D \cdot (1 - QR) \cdot (1 - IR), \tag{6}$$

$$C\,D = \begin{cases} SC - E\,D, & I\,D \cdot CN \ge SC - E\,D, \\ I\,D \cdot CN, & I\,D \cdot CN < SC - E\,D, \end{cases} \tag{7}$$

$$Y\,D = C\,D \cdot (1 - QR) \cdot IR, \tag{8}$$
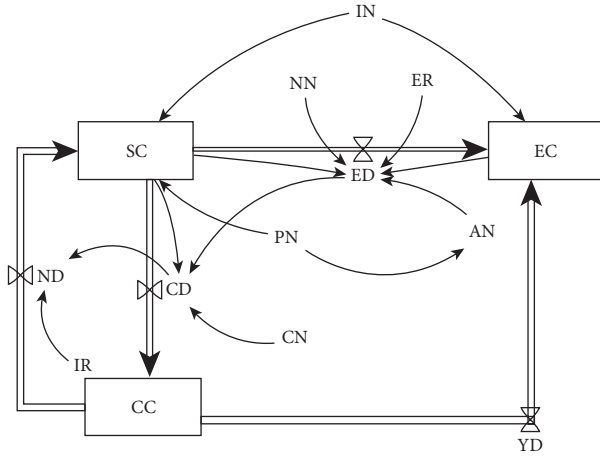
Figure 4: Infection subsystem flowchart.
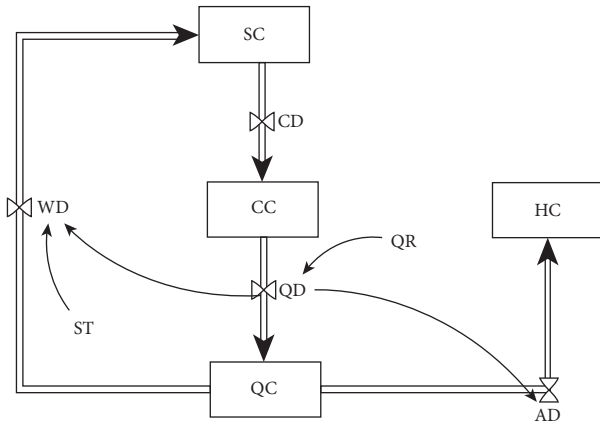
Figure 5: Quarantine subsystem flowchart.
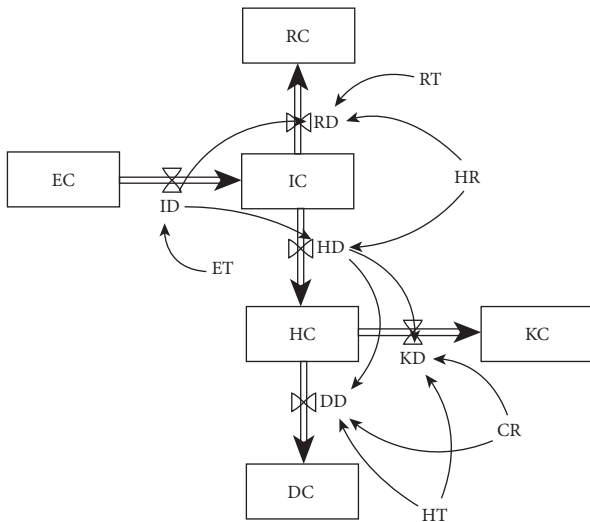
Figure 6: Medical subsystem flowchart.

In the quarantine subsystem, the level variable is QC, while the rate variables are WD, QD, and AD. Equations (9)-(12) show the functional relationships of the quarantine subsystem.

$$\frac{dQC}{dt} = Q\,D - W\,D - A\,D, \tag{9}$$

$$A\,D = \begin{cases} Q\,D \cdot IR, & time \geq 1, \\ 0, & time < 1, \end{cases} \tag{10}$$

$$Q\,D = \begin{cases} C\,D \cdot QR, & time \geq 1, \\ 0, & time < 1, \end{cases} \tag{11}$$

$$W\,D = \begin{cases} Q\,D \cdot (1 - IR), & time \geq ST, \\ 0, & time < ST, \end{cases} \tag{12}$$

In the medical subsystem, the level variables are DC, IC, HC, KC, and RC which are determined by the rate variables DD, ID, HD, KD, and RD. The functional relationships of the medical subsystem are shown in the following equations:

$$\frac{dDC}{dt} = D\,D, \tag{13}$$

$$\frac{dIC}{dt} = I\,D - R\,D - H\,D, \tag{14}$$

$$\frac{dHC}{dt} = H\,D + A\,D - D\,D - K\,D, \tag{15}$$

$$\frac{dKC}{dt} = K\,D, \tag{16}$$

$$\frac{dRC}{dt} = R\,D, \tag{17}$$

$$D\,D = \begin{cases} H\,D \cdot CR, & time \geq HT, \\ 0, & time < HT, \end{cases} \tag{18}$$

$$H\,D = I\,D \cdot HR, \tag{19}$$

$$I\,D = \begin{cases} E\,D, & time \geq ET, \\ 0, & time < ET, \end{cases} \tag{20}$$

$$K\,D = \begin{cases} H\,D \cdot (1 - CR), & time \geq HT, \\ 0, & time < HT, \end{cases} \tag{21}$$

$$R\,D = \begin{cases} I\,D \cdot (1 - HR), & time \geq RT, \\ 0, & time < RT, \end{cases} \tag{22}$$

The improved SEIR-SD model is established, of which the system flowchart is shown in Figure 7 which consists of three parts, i.e., infection part, quarantine part, and medical part. The model considers asymptomatic infection and subclinical cases. The assumptions of the model include: there is only human to human transmission; there is no specific medicine or vaccine for the virus; other diseases do not influence the mortality rate and other parameters; there is no population mobility; deaths occur only in hospital; the isolated cases are immediately tested for nucleic acid

FIGURE 7: System flowchart of the improved SEIR-SD model.

regardless of the existence of symptoms; the close contacts are quarantined within one day if the conditions permit. The isolated cases are tested for nucleic acid within one day. In this model, the initial values of the level variables are zero except SC and EC. The sum of the initial values of SC and EC is equal to the cumulative population, and the initial value of EC is equal to IN.

4. Simulation Results and Analysis

4.1. Simulation of Epidemic Responses in Wuhan

4.1.1. Simulation Parameter Setting. This section tests the simulation effect of the model to ensure the validity and reliability of the model in terms of structure, parameter settings, and functional relationships using the historical data of the COVID-19 epidemic in Wuhan. It was not until February 14th that the number of nucleic acid tests that can be performed in Wuhan every day met the demand. In other words, the number of confirmed cases was reliable after that. Therefore, the initial time of the model is set as February 14th, 2020. The basic parameters of the model are set as follows: initial time = 1, end time = 100, time step = 1.

The parameter values of the model are set based on the official data or authoritative research results that have been published, as shown in Table 4 [22, 29–33].

We set QR = 0.94, HR = 0.9 based on the data published by Hubei Provincial Health Committee and Wuhan Municipal Health Committee.

According to the official announcement ([16, 34–37]), the following variable values are determined. In the initial period of the epidemic, residents can move freely in the city, so we set NN = 2.7 for this period. Since February 5th (time = 35), villages, communities, and units have been closed, so we set NN = 2 for this period. After mid-February (time = 44), all the residential districts had been strictly closed, so we set NN = 0.7 for this period. According to the authoritative news report, in the early stage, there were insufficient personal protective supplies, such as masks, so we set ER = 0.06 for this scenario; in late February (time = 55), the supplies gradually became sufficient, so we set ER = 0.03 for this scenario. We set CR = 0.93 based on the data published on the official website of Wuhan Health and Health Commission for the scenario in the early stage. In the later period (time >38), the public places are requisitioned to build temporary treatment centers and many designated hospitals are renovated to increase available beds, which effectively improves the treatment rate and cure rate, so we set CR = 0.98 for this scenario.

According to the policy and actual situation, the logical functions of NN, ER, and CR can be established as follows:

TABLE 4: Model parameter values.

name	HT	CN	ET	RT	PN	Ir	In	ST
Value	12	2	5.2	9	10000000	0.17	1180	14

$$NN = \text{IF THEN ELSE}\,(\text{Time} < \, = 35, 2.7, \text{IF THEN ELSE}\,(\text{Time} > 35: \text{AND}: \text{Time} < 44, 2, 0.7)),$$

$$ER = \text{IF THEN ELSE}\,(\text{Time} < \, = 55, 0.06, 0.03), \tag{23}$$

$$CR = \text{IF THEN ELSE}\,(\text{Time} < \, = 38, 0.93, 0.98).$$

4.1.2. Simulation Results. The number of confirmed cases in Wuhan officially released by the authority cannot reflect the actual infection number due to the poor nucleic acid testing ability in the early stage of the epidemic. We select a total of 30 days from February 14th to March 14th for simulation. The simulated number of infections daily (ID) and a simulated cumulative number of deaths (KC) are compared with the actual data to verify the effectiveness of the model. The simulation results are shown in Figure 8.

As shown in Figure 8(a), the number of confirmed cases has been steadily decreasing since mid-February until a sharp decline occurred on February 19th. This is because all the cases were admitted and all the close contacts were quarantined compulsorily in Wuhan after February 16th. Figure 8(b) shows that as the cure rate increases, the cumulative number of deaths shows a slower trend.

From the simulation results, the average deviation and its variance between the actual and simulated number of confirmed cases in every single day are −5.24% and 0.0516, respectively. The average deviation and its variance between actual and simulated cumulative deaths are −0.80% and 0.0013, respectively. Therefore, it suggests that the improved SEIR-SD model proposed in this paper is effective.

During the epidemic, Wuhan has adopted the measures such as closing communities, enforcing individual protection, enhancing treatment rate (establishing temporary treatment centers for mildly infected cases, adding hospital beds, and adding medical personnel and supplies), and enhancing quarantine rate (accurate tracking and quick quarantine of close contacts and suspected cases). To study the effect of these measures on the stemming and control of this epidemic, this paper utilizes the improved SEIR-SD model to make simulations according to the measures.

4.2. Simulation Analysis of the COVID-19 Epidemic Response Measures

4.2.1. Impact of Hospital Administration Rate. HR is an important factor affecting the development of the epidemic. Based on the improved SEIR-SD model proposed in the previous section, this section studies the trend of ID and KC with time (T) under different HRs. In this simulation, it is assumed that residents can move freely (NN = 3) while taking extremely limited personal protective measures (ER = 0.06), and other parameter values are the same as those proposed in Section 4.1. HR and T are regarded as the experimental variables, while other variables are regarded as the control variables. The value of HR is set between 0 and 1, while T is between 0 and 30 (days). The simulation results are shown in Figure 9.

Figure 9(a) shows the trend of ID over time under different HRs. It can be seen that ID continues to grow with time, which gives rise to the effect of improving HRs increasingly more obvious. While HR is low, the epidemic spreads increasingly more rapidly, resulting in a substantial increase in the number of infected people; in the middle and late stage of the epidemic, ID has a maximum growth rate and exceeds 200000; after the majority of residents are infected, the growth rate declines. When HR is close to 1, ID increases slowly, and the maximum value is only 16071. Consequently, the growth rate of ID varies greatly under different HRs.

Figure 9(b) shows the trend of KC over time under different HRs. Overall, KC shows an exponential upward trend with time. When HR is lower than 0.5, the number of patients that can be accommodated in the hospital is small, and most of the patients who died from infection are not included in the statistics. Therefore, KC is small in the figure. When HR exceeds 0.5, KC shown in the figure is the actual value. It implies that with the increase of HR, the rising trend of KC gradually decreases.

Therefore, ensuring the adequate supply of medical materials and medical staff, which improves the hospital admission rate, can restrain the development of the epidemic to a great extent. Especially in the early stage of the epidemic, ensuring a high admission rate can effectively prevent large-scale outbreaks.

4.2.2. Impact of Quarantine Rate. Close contacts of infected cases are important carriers of the virus. Therefore, their quarantine rate directly affects the development of the epidemic. This section studies the trend of ID and KC with time (T) under different QRs. The basic assumptions of this simulation are as follows: residents can move freely (NN = 3), the majority of infected cases are admitted to the hospitals (HR = 90%), and few personal protection measures are taken (ER = 0.06). QR and T are regarded as the experimental variables, while other variables are regarded as the control variables. The value of QR is set between 0 and 1, while T is between 0 and 30 (days). The simulation results are shown in Figure 10.

Figure 10(a) shows the trend of ID over time under different QRs. With the passage of time, the number of infected cases increases gradually, and the effect of measures
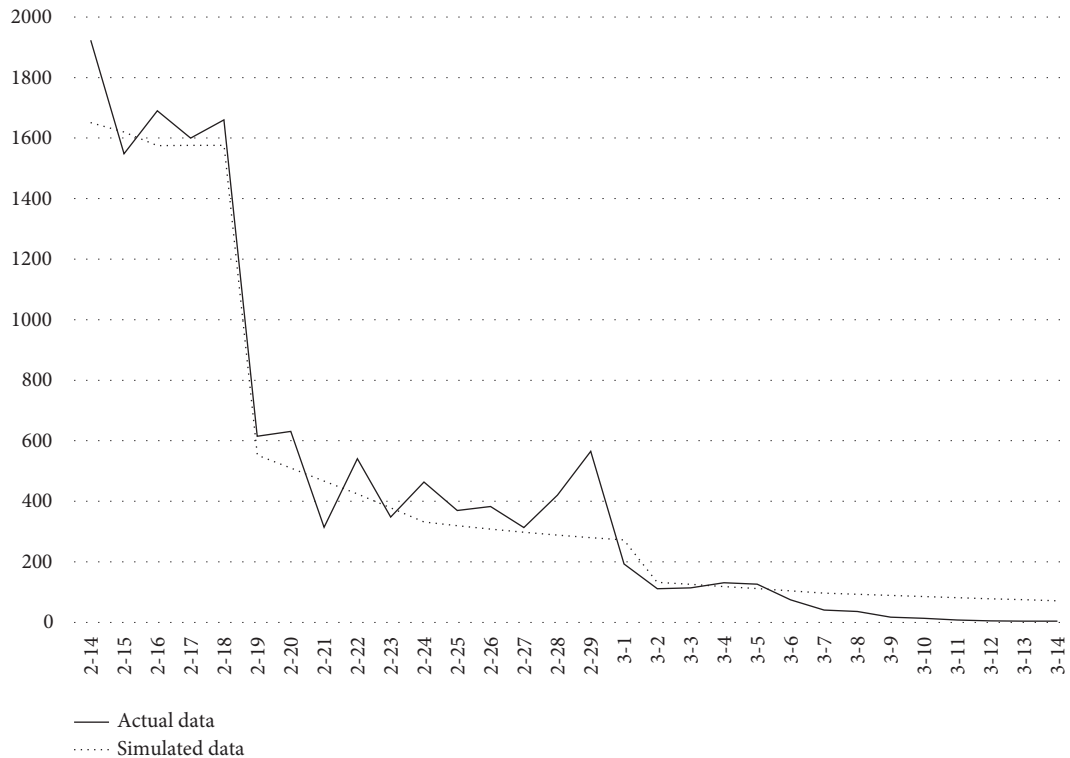
(a)
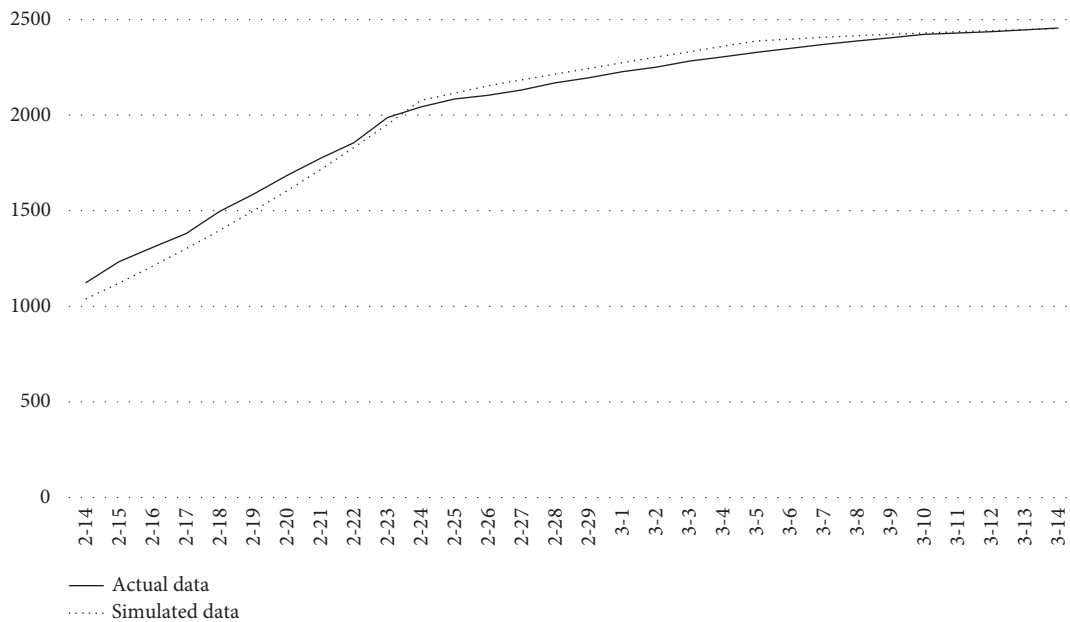
(b)

FIGURE 8: Comparison of simulated and actual data of the COVID-19 in Wuhan. (a) The number of confirmed cases in every single day. (b) The cumulative number of deaths.

to improve QR is more obvious. When QR is relatively low, the speed of disease transmission is the fastest. In this case, ID would reach 202368 on the 30th day. With the gradual increase of QR, the growth of confirmed cases slows down. When QR reaches 0.9, the upper limit of ID is only 19872.

Therefore, there are great differences in the growth of ID under different QRs.

Figure 10(b) shows the trend of KC over time under different QRs. As is shown in the figure, KC increases exponentially with time. When QR is low, the upper limit value

(a)

(b)
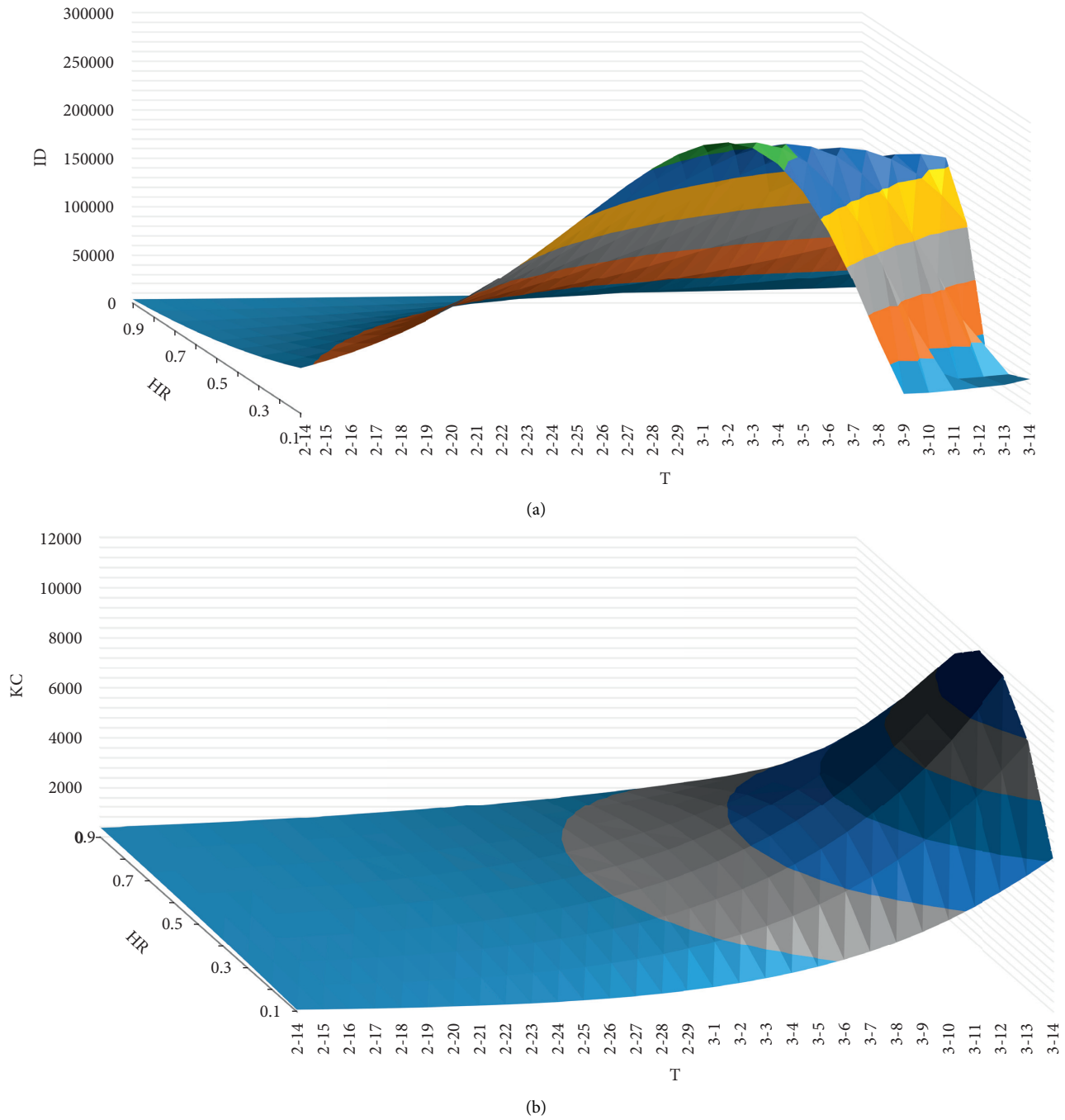
FIGURE 9: Trend of ID and KC under different HRs.

of KC is 13718. By increasing QR, which inhibits the spread of the virus, the growth rate of KC decreases continuously. When QR reaches 0.9, KC should be lower than 3660. Consequently, with the increase of QR, the rising trend of KC gradually decreases.

Therefore, improving the quarantine rate by accurate tracking and rapid quarantine of close contacts of infected cases can effectively reduce the number of infections and deaths. In the early stage of the epidemic, the improvement of the quarantine rate has a more significant impact on the spreading speed of the epidemic.

4.2.3. Impact of Average Contact Number. The degree of community closure directly determines the average contact number of residents. In this section, we study the trend of ID and KC with time (T) under different NNs. The basic assumptions of this simulation are as follows: most infected cases are admitted to the hospitals (HR = 90%), residents can move freely (NN = 3), and few personal protection measures are taken (ER = 0.06). NN and T are regarded as the experimental variables, while other variables are regarded as the control variables. The value of NN is set between 0 and 3, while T is between 0 and 30. The simulation results are shown in Figure 11.

(a)

(b)
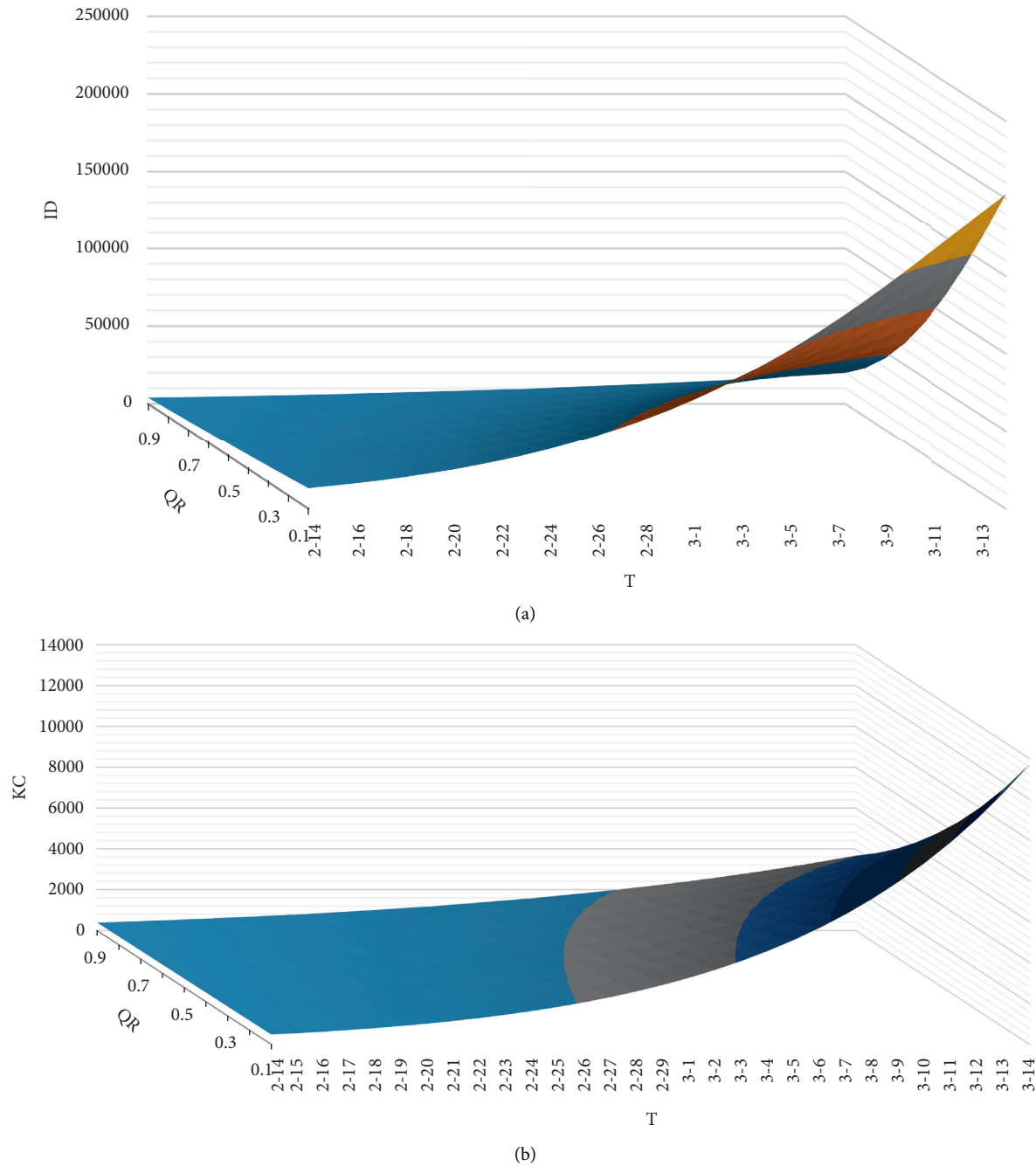
FIGURE 10: Trend of ID and KC under different QRs.

Figure 11(a) shows the trend of ID over time under different NNs. It is not difficult to find that the effect of early adoption of strict community closure measures is extremely obvious. In the case of the free flow of people, NN is the highest, so the epidemic spreads most rapidly. After 30 days, the value of ID reaches 16097. In the case that the government takes compulsory community closure measures, ID decreases significantly, and the maximum number is only 24, which differs significantly from the former case.

Figure 11(b) shows the trend of KC over time with different NNs. Under the condition of the free flow of residents, KC increases exponentially over time, reaching the maximum of 3358 cases. On the contrary, taking the greatest degree of community closure measures leads to a significant decline in the number of deaths (the maximum is only 31 cases). Consequently, strict closure measures can effectively reduce KC.

It implies that the restraint effect of the epidemic should be very significant if strict community closure measures are taken in the early stage of the outbreak. Otherwise, the number of patients would increase exponentially, and the epidemic should be much more difficult to restrain.

(a)

(b)
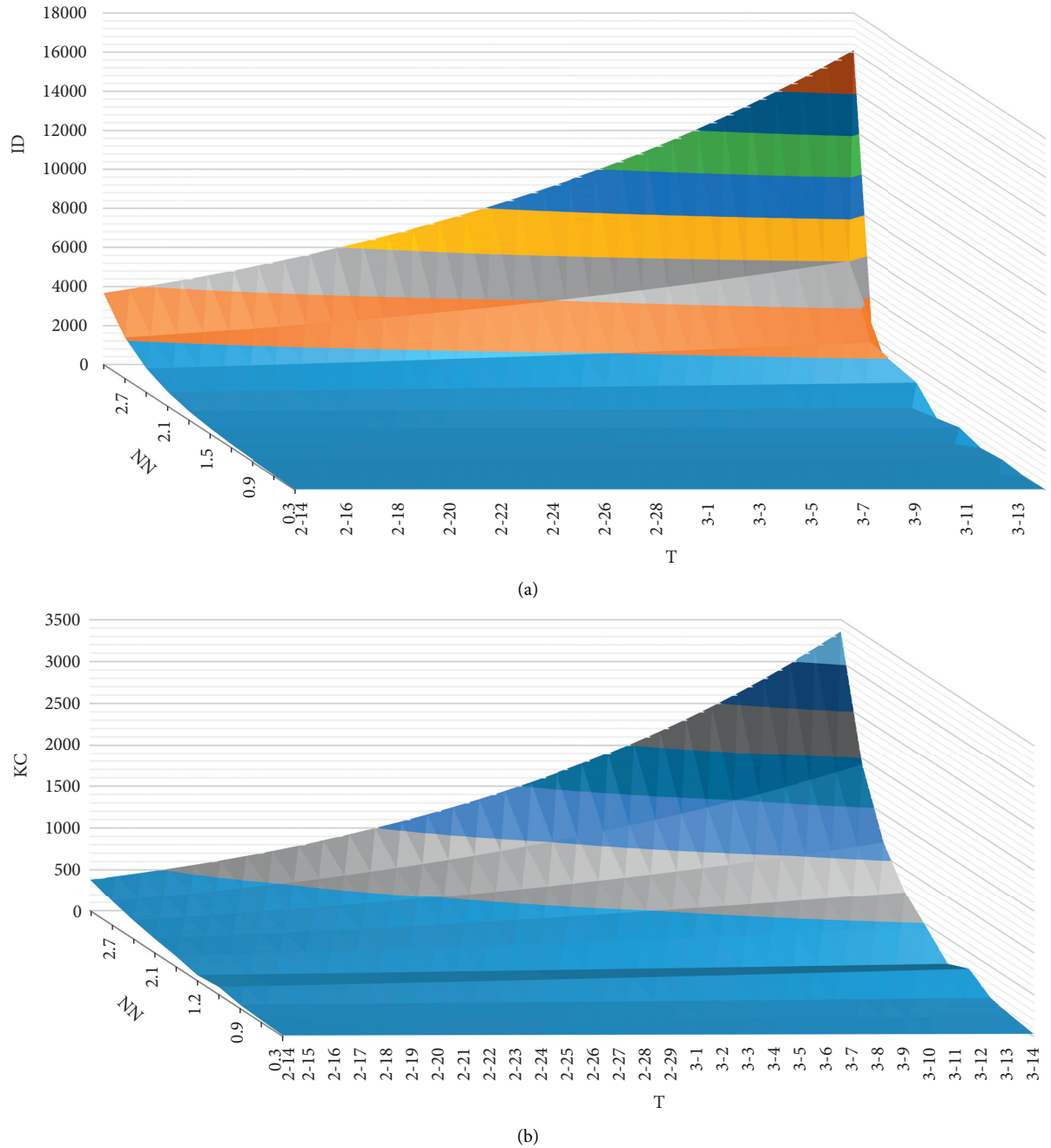
FIGURE 11: Trend of ID and KC under different NNs.

4.2.4. Impact of Contact Infection Rate. In this section, we analyze the impact of ER on ID and KC. In the simulation, QR and HR are set to 0.94 and 0.9, respectively. While people do not take any protective measures, and the contact infection rate is very high. In this case, the maximum value of ER is set to 0.06. By contrast, in the case that people take the most stringent personal protection, ER reaches the minimum (0.03). Therefore, the value of ER is set between 0.030 and 0.060. The simulation results are shown in Figure 12.

Figure 12(a) shows the trend of ID over time under different ERs. At the same level of ER, ID increases with the passage of time. While ER is 0.06, the value of ID on the 30th day of the epidemic can reach four times that at the beginning of the epidemic. At the same time node, the greater the ER, the more the ID. Additionally, with the increase of ER, the increase of ID becomes faster. While ER is 0.042, ID reaches 1000. While ER reaches 0.06, ID could be more than 10000.

Figure 12(b) shows the trend of KC over time under different ERs. At the same level of ER, KC increases with time. While ER is 0.06, KC could increase from 382 to 3359 in 30 days. At the same time node, the greater the ER, the more the KD and KC. By contrast, while the ER is reduced to 0.045, KC would also reduce to less than 1000.
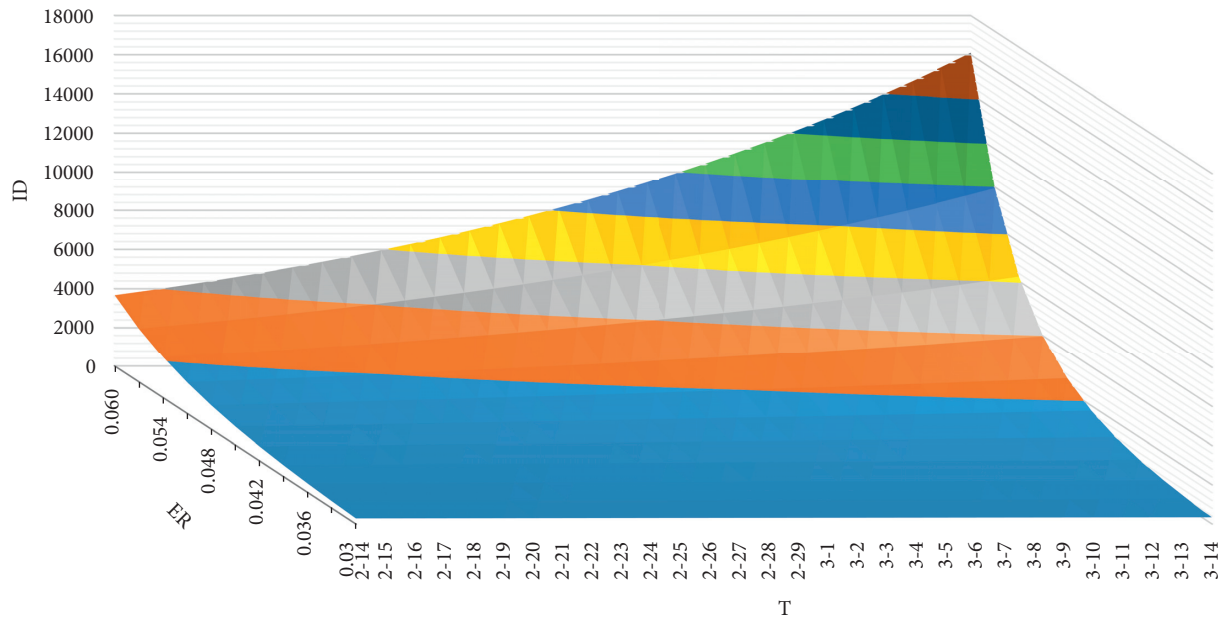
(a)
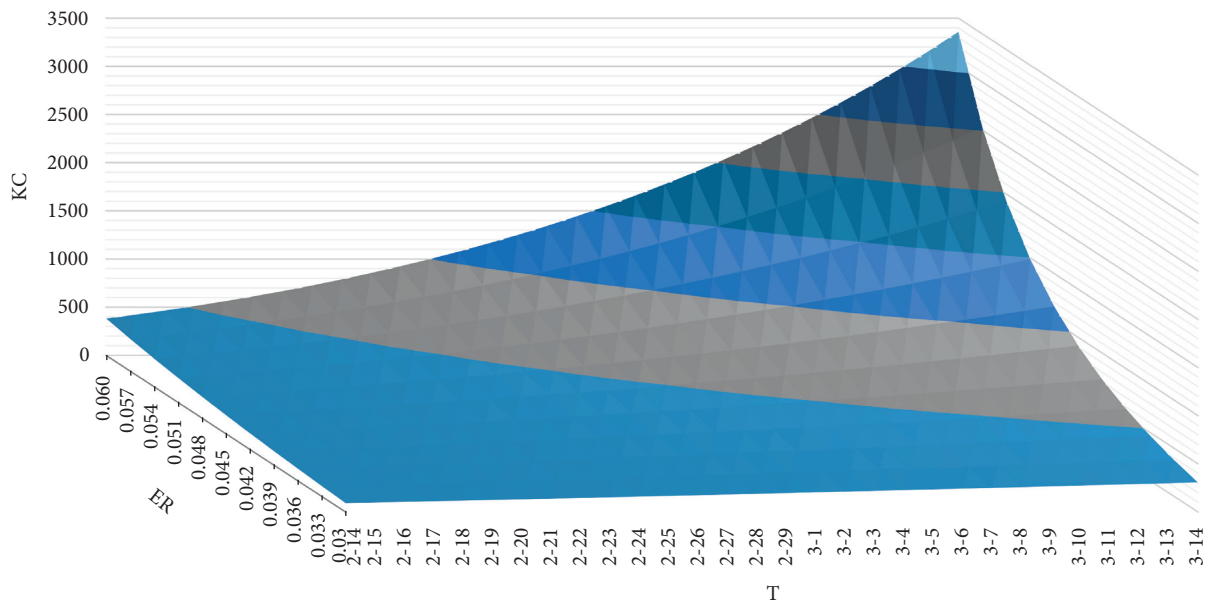
(b)

FIGURE 12: Trend of ID and KC under different ERs.

The simulation results show that when the contact infection rate is high, the number of new infections daily and the total number of deaths increase exponentially. Therefore, the measures such as wearing masks to reduce the contact infection rate are of pivotal importance to restrain the development of the epidemic.

4.2.5. Combined Impact of Hospital Admission Rate and Quarantine Rate. This section studies the values of IC and KC on the 30th day under different HRs and QRs. In this simulation, we assume that residents can move freely

(NN = 3) and take extremely limited personal protection measures (ER = 0.06). HR and QR are regarded as the experimental variables, while other variables are regarded as the control variables. The value of QR is set between 0 and 1, while T is between 0 and 30. The simulation results are shown in Figure 13.

Figure 13(a) shows the values of IC under different HRs and QRs. Given a fixed value of QR, with the increase of HR, IC continues to decline. Specifically, if both QR and HR are 0.1, then IC is 6636770; while HR is increased to 0.9, IC decreases to 1151102. Additionally, Given a fixed value of HR, with the increase of QR, IC decreases. Specifically, while

(a)

(b)
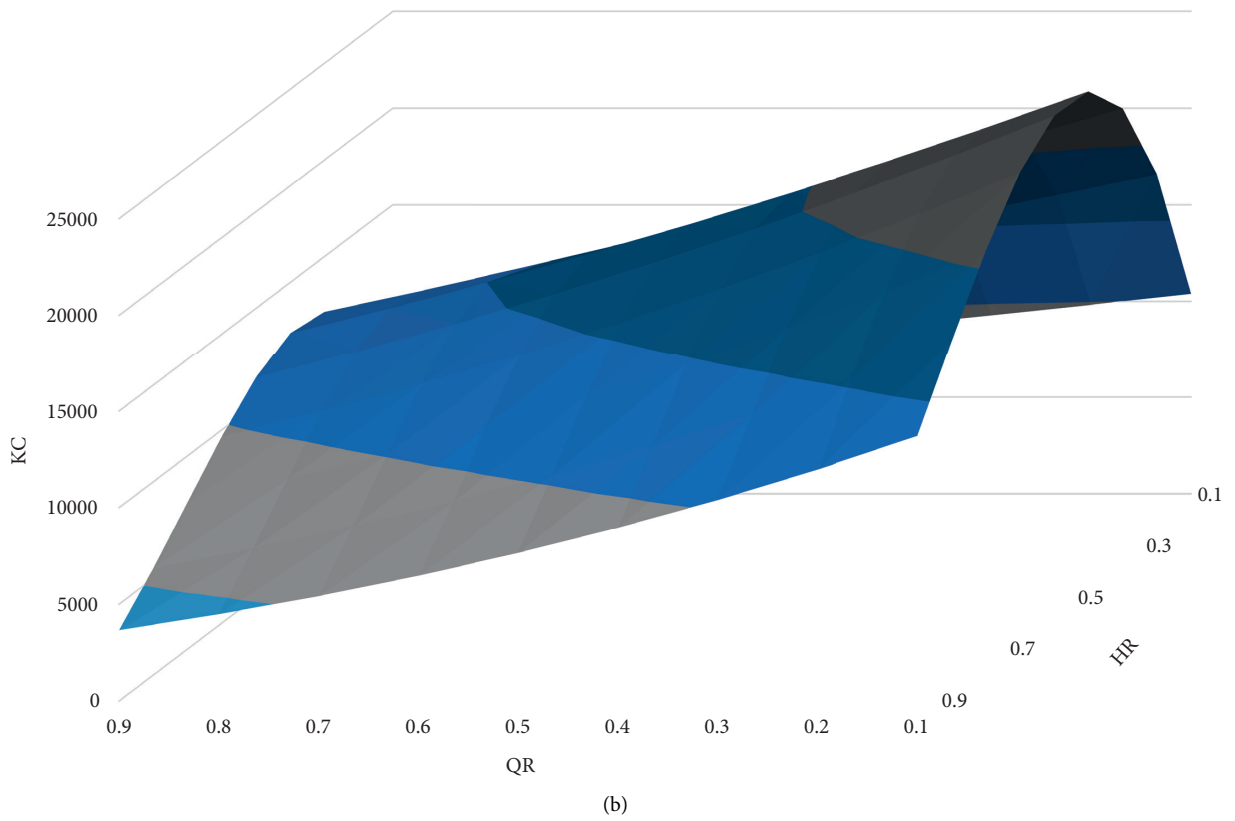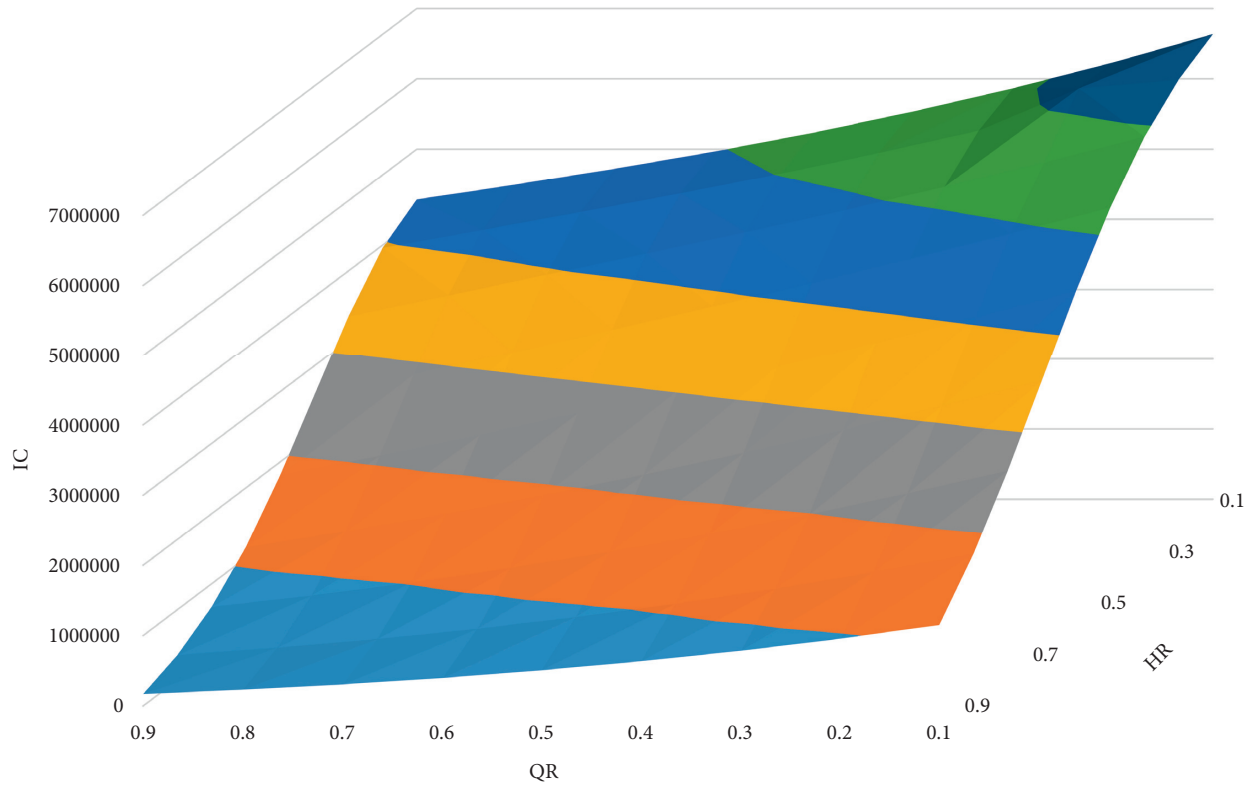
Figure 13: Values of IC and KC under different HRs and QRs.
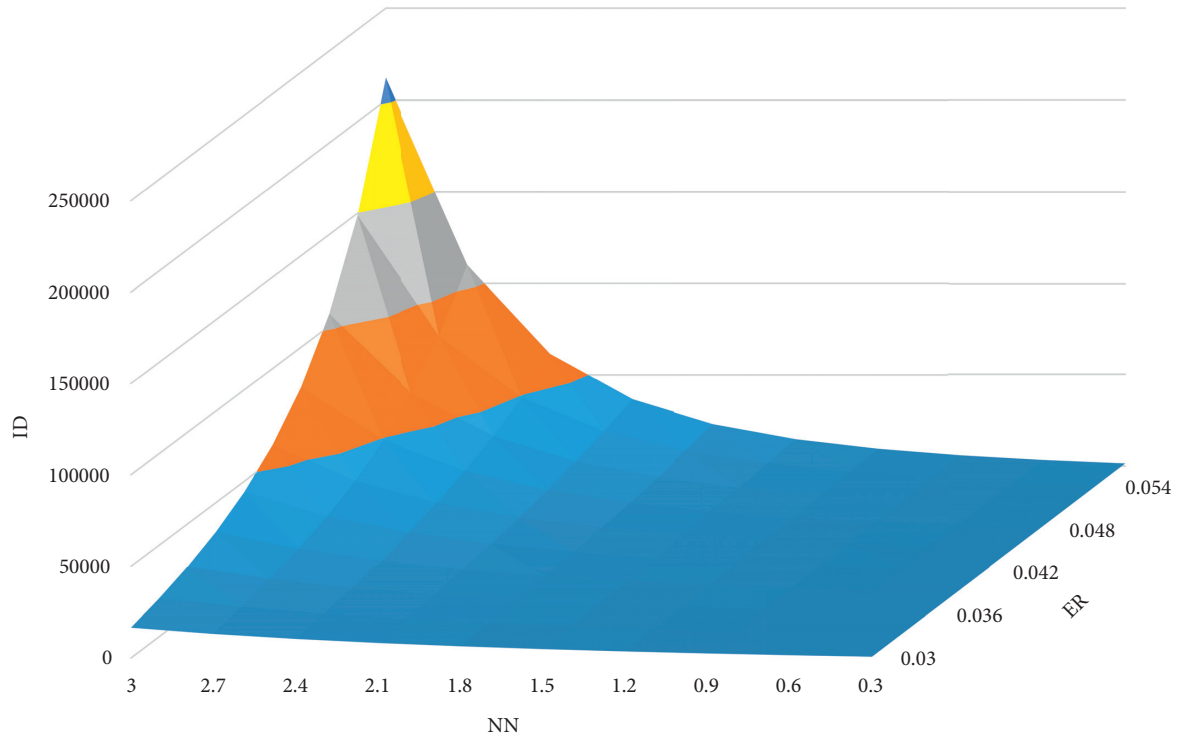
(a)
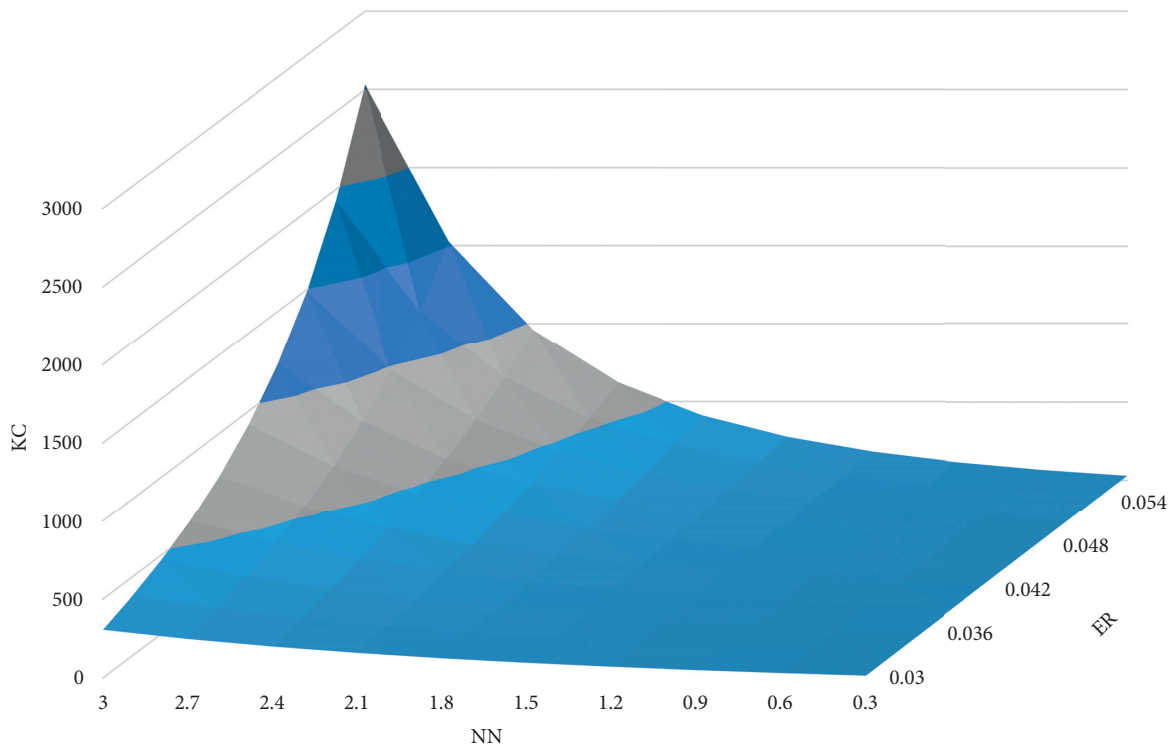
(b)

Figure 14: Values of IC and KC under different NNs and ERs.

HR is 0.1 and QR is 0.9, IC should be 4282985. When the two factors (HR and QR) work together, HR plays a decisive role in the trend of the curve and determines the overall trend of the epidemic situation. By contrast, the growth of QR makes the number of infected people and deaths show a relatively small downward trend.

Figure 13(b) shows the values of KC under different HRs and QRs. Given a fixed value of QR, while HR is within the

interval of [0,0.5], KC increases with HR. At this stage, the number of infected cases that can be accommodated in the hospitals is small, and most of the patients who died from infection are not included in the statistics. While HR is within the interval of [0.5,1], KC gradually decreases with HR. Moreover, given a fixed value of HR, KC decreases with the increase of QR. Specifically, while both HR and QR are 0.1, KC is 10399. By contrast, if QR increases to 0.9, then KC decreases to 6307 correspondingly.

Therefore, the hospital admission rate is more important than the quarantine rate in responding to the epidemic. The increase of the quarantine rate can only delay the peak of the epidemic but cannot determine the scale of the epidemic. On the contrary, enhancing the hospital admission rate (or treatment rate) can radically restrain the epidemic.

4.2.6. Combined Impact of Average Contact Number and Contact Infection Rate. This section studies the values of IC and KC on the 30th day under different NNs and ERs. In this simulation, HR and QR are set as 0.9 and 0.94, respectively. NN and ER were regarded as the experimental variables, while other variables were regarded as the control variables. The value of NN is set between 0 and 3, while ER is between 0.03 and 0.06. The simulation results are shown in Figure 14.

Figure 14(a) shows the values of IC under different NNs and ERs. Given a fixed value of NN, IC increases with ER. Specifically, while NN is 3 and ER drops from 0.057 to 0.03, IC drops from more than 9000 to 300. Additionally, given a fixed value of ER, IC increases with NN. Specifically, while ER is 0.057 and NN increases from 0.3 to 3, IC increase from 23 to more than 9000.

Figure 14(b) shows the values of KC under different NNs and ERs. At the initial stage of the outbreak, the residents do not take the necessary protective measures, resulting in a high ER. With the increase of NN, KC grows rapidly. After the residents make personal protection, ER decreases and the growth rate of KC slows down. Similarly, KC increases with NN, and the growth rate slows down with the decrease of ER.

It implies the increase of average contact number and contact infection rate make the cumulative number of infections and the cumulative number of deaths increase exponentially. Therefore, in the early stage of the epidemic, if the residents can improve their awareness of self-prevention, strictly take scientific protective measures, and reduce outdoor activities, the spread of the epidemic can be restrained to a great extent.

5. Conclusions and Suggestions

This research establishes an improved SEIR-SD model for the COVID-19 epidemic. The real scenarios of the epidemic in Wuhan are simulated successfully by this model, which proves the effectiveness of the model. Afterward, the impact of hospital administration rate, quarantine rate, average contact number, and contact infection rate on the cumulative number of infections and deaths are analyzed by simulation. The results show that both the medical and administrative efforts, especially in the early stage of the epidemic, are significant in reducing the number of infections and shortening the epidemic period. In the medical aspect, the more stringent quarantine brings the earlier inflection point of the epidemic; more importantly, improving the treatment rate significantly reduces the scale of the epidemic. In the administrative aspect, enforcing individual protection and strict community closure can effectively cut off the transmission of the virus and curb the spread of the epidemic. In this regard, this research proposes the following suggestions:

(1) Based on the accurate judgment of the epidemic situation, the government should implement strict and effective community closure measures at the preliminary stage of the epidemic. Specifically, it is necessary to close factories and schools, stop collective activities or large-scale crowd assemblies, and take traffic restrictions in villages, communities, and other areas to reduce close contact among residents.

(2) The residents must improve their protection, such as wearing masks and keeping social distance in public places. The government should ensure an adequate supply of protective supplies and sterilize public places.

(3) The national or regional medical resources, including medical supplies and medical care personnel, should be allocated reasonably. Establishing temporary treatment centers for mild patients and expanding the capacity of the existing hospital for severe patients are important ways to realize the quarantine and treatment of the patients.

(4) Accurate tracking of the close contacts of confirmed cases and the suspected cases is of great importance. It is also necessary to mobilize the social forces and resources to establish quarantine places and conduct quarantine on suspected cases and close contacts to cut off the transmission chain of the virus fundamentally.

(5) In the early stage of the development of the epidemic, we should focus on ensuring the hospital admission rate. On this basis, we should quarantine mild infected cases, which not only reduces the occupation of important medical resources but also helps to restrain the epidemic to a certain extent.

Data Availability

No data were used to support this study.

Conflicts of Interest

The authors declare that they have no conflicts of interest.

Acknowledgments

References

[1] F. Zhang, L. Li, and H. Y. Xuan, "Survey of transmission models of infectious diseases," *System Engineering-Theory & Practice*, vol. 31, no. 9, pp. 1736–1744, 2011.

[2] G.-M. Tang and Z.-X. Wu, "Fragility and robustness of self-sustained oscillations in an epidemiological model on small-world networks," *Chaos: An Interdisciplinary Journal of Nonlinear Science*, vol. 29, no. 2, Article ID 023119, 2019.

[3] S. Eubank, H. Guclu, V. S. Anil Kumar et al., "Modelling disease outbreaks in realistic urban social networks," *Nature*, vol. 429, no. 6988, pp. 180–184, 2004.

[4] L. Hufnagel, D. Brockmann, and T. Geisel, "Forecast and control of epidemics in a globalized world," *Proceedings of the National Academy of Sciences*, vol. 101, no. 42, pp. 15124–15129, 2004.

[5] W. O. Kermack and A. G. Mckendrick, "Contributions to the mathematical theory of epidemics," *Proceedings of the Royal Society of London*, vol. 115, pp. 700–721, 1927.

[6] B. Jhun, M. Jo, and B. Kahng, "Simplicial SIS model in scale-free uniform hypergraph," *Journal of Statistical Mechanics: Theory and Experiment*, vol. 2019, no. 12, Article ID 123207, 2019.

[7] X. Mu, Q. Zhang, and L. Rong, "Optimal vaccination strategy for an SIRS model with imprecise parameters and Lévy noise," *Journal of the Franklin Institute*, vol. 356, no. 18, Article ID 11385, 2019.

[8] H. Inaba, "Age-structured homogeneous epidemic systems with application to the MSEIR epidemic model," *Journal of Mathematical Biology*, vol. 54, no. 1, pp. 101–146, 2007.

[9] J. W. Forrester, "Industrial dynamics: a breakthrough for decision makers," *Harvard Business Review*, vol. 4, pp. 37–66, 1958.

[10] E. R. G. T. R. Assunção, F. A. F. Ferreira, I. Meidutė-Kavaliauskienė, C. Zopounidis, L. F. Pereira, and R. J. C. Correia, "Rethinking urban sustainability using fuzzy cognitive mapping and system dynamics," *The International Journal of Sustainable Development and World Ecology*, vol. 27, no. 3, pp. 261–275, 2020.

[11] E. Ekinci, Y. Kazancoglu, and S. K. Mangla, "Using system dynamics to assess the environmental management of cement industry in streaming data context," *The Science of the Total Environment*, vol. 715, Article ID 136948, 2020.

[12] Y. Shi, "Stochastic dynamic model of SARS spreading," *Chinese Science Bulletin*, vol. 48, no. 13, pp. 1287–1292, 2003.

[13] D. R. Zeng, X. H. Cheng, and J. A. Huang, "Study on the mathematical model of SARS epidemic prediction and control-an improved method based on the infectious disease model," *Chinese Journal of Safety Science*, vol. 14, pp. 41–45, 2004.

[14] Q. Li, X. Guan, P. Wu et al., "Early transmission dynamics in Wuhan, China, of novel coronavirus–infected pneumonia," *New England Journal of Medicine*, vol. 382, pp. 1199–1207, 2020.

[15] B. Tang, X. Wang, Q. Li et al., "Estimation of the transmission risk of the 2019-nCoV and its implication for public health interventions," *Journal of Clinical Medicine*, vol. 9, no. 2, p. 462, 2020.

[16] S. Zhao, Q. Lin, J. Ran et al., "Preliminary estimation of the basic reproduction number of novel coronavirus (2019-nCoV) in China, from 2019 to 2020: a data-driven analysis in the early phase of the outbreak," *International Journal of Infectious Diseases*, vol. 92, pp. 214–217, 2020.

[17] Y. Y. Wei, Z. Z. Lu, and Z. C. Du, "Fitting and forecasting the trend of COVID-19 by SEIR+ CAQ dynamic model," *Chinese Journal of Epidemiology*, vol. 41, no. 04, pp. 470–475, 2020.

[18] J. M. Read, J. R. Bridgen, and D. A. Cummings, "Novel coronavirus 2019-nCoV: early estimation of epidemiological parameters and epidemic predictions," *Philosophical Transactions of the Royal Society B: Biological Sciences*, vol. 376, no. 1829, Article ID 20200265, 2020.

[19] M. W. Shen, Z. H. Peng, and Y. N. Xiao, "Modeling the epidemic trend of the 2019 novel coronavirus outbreak in China," *The Innovation*, vol. 1, no. 3, Article ID 100048, 2020.

[20] J. T. Wu, K. Leung, and G. M. Leung, "Nowcasting and forecasting the potential domestic and international spread of the 2019-nCoV outbreak originating in Wuhan, China: a modelling study," *The Lancet*, vol. 395, no. 10225, pp. 689–697, 2020.

[21] Q. Lin, S. Zhao, D. Gao et al., "A conceptual model for the coronavirus disease 2019 (COVID-19) outbreak in Wuhan, China with individual reaction and governmental action," *International Journal of Infectious Diseases*, vol. 93, pp. 211–216, 2020.

[22] J. K. Adam, W. R. Timothy, and D. Charlie, "Early dynamics of transmission and control of COVID-19: a mathematical modeling study," *The Lancet Infectious Diseases*, vol. 20, no. 5, pp. 553–558, 2020.

[23] The Lancet, "COVID-19: too little, too late?" *The Lancet*, vol. 395, no. 10226, p. 755, 2020, https://www.sciencedirect.com/science/article/pii/S0140673620305225.

[24] S. He, Y. Peng, and K. Sun, "SEIR modeling of the COVID-19 and its dynamics," *Nonlinear Dynamics*, vol. 101, no. 3, pp. 1667–1680, 2020.

[25] S. Zhao and H. Chen, "Modeling the epidemic dynamics and control of COVID-19 outbreak in China," *Quantitative Biology*, vol. 8, no. 1, pp. 11–19, 2020.

[26] D. Kang, H. Choi, J.-H. Kim, and J. Choi, "Spatial epidemic dynamics of the COVID-19 outbreak in China," *International Journal of Infectious Diseases*, vol. 94, pp. 96–102, 2020.

[27] K. Linka, M. Peirlinck, F. Sahli Costabal, and E. Kuhl, "Outbreak dynamics of COVID-19 in Europe and the effect of travel restrictions," *Computer Methods in Biomechanics and Biomedical Engineering*, vol. 23, no. 11, pp. 710–717, 2020.

[28] J. S. Jia, X. Lu, and Y. Yuan, "Population flow drives spatio-temporal distribution of COVID-19 in China," *Nature*, vol. 582, no. 7812, 2020.

[29] G. Wei-jie, N. Zheng-yi, H. Yu, and L. Wenhua, "Clinical characteristics of 2019 novel coronavirus infection in China," *New England Journal of Medicine*, vol. 382, no. 18, pp. 1708–1720, 2020.

[30] M. Peirlinck, K. Linka, F. Sahli Costabal, and E. Kuhl, "Outbreak dynamics of COVID-19 in China and the United States," *Biomechanics and Modeling in Mechanobiology*, pp. 1–15, 2020.

[31] F. Zhou, T. Yu, R. Du et al., "Clinical course and risk factors for mortality of adult inpatients with COVID-19 in Wuhan, China: a retrospective cohort study," *The Lancet*, vol. 395, no. 10229, pp. 1054–1062, 2020.

[32] Wuhan Statistics Bureau, *Wuhan Statistical Yearbook*, Wuhan Publishing House, Wuhan, China, 2018.

[33] B. David, X. L. Qi, K. Nielsen-Saines, M Didier, P Léo, and F Guillaume, "Real estimates of mortality following COVID-

19 infection," *The Lancet Infectious Diseases*, vol. 20, no. 7, p. 773, 2020.

[34] D. M. Studdert and M. A. Hall, "Disease control, civil liberties, and mass testing - calibrating restrictions during the covid-19 pandemic," *New England Journal of Medicine*, vol. 383, no. 2, pp. 102–104, 2020.

[35] M. Peirlinck, K. Linka, C. F. Sahli, and K Ellen, "Outbreak dynamics of COVID-19 in China and the United States," *Biomechanics and Modeling in Mechanobiology*, pp. 1–15, 2020.

[36] P. Neal and T. Theparod, "The basic reproduction number, R0, in structured populations," *Mathematical Biosciences*, vol. 315, p. 108224, 2019.

[37] Y. Chen, A. H. Wang, B. Yi, K. Q. Ding, H Wang, and J Wang, "The epidemiological characteristics of infection in close contacts of COVID-19 in Ningbo city," *Chinese Journal of Epidemiology*, vol. 41, no. 5, pp. 667–671, 2020.

WILEY | Hindawi

Retraction

Retracted: Analysis of Factors Influencing Stock Market Volatility Based on GARCH-MIDAS Model

Complexity

This article has been retracted by Hindawi following an investigation undertaken by the publisher [1]. This investigation has uncovered evidence of one or more of the following indicators of systematic manipulation of the publication process:

(1) Discrepancies in scope

(2) Discrepancies in the description of the research reported

(3) Discrepancies between the availability of data and the research described

(4) Inappropriate citations

(5) Incoherent, meaningless and/or irrelevant content included in the article

(6) Manipulated or compromised peer review

The presence of these indicators undermines our confidence in the integrity of the article's content and we cannot, therefore, vouch for its reliability. Please note that this notice is intended solely to alert readers that the content of this article is unreliable. We have not investigated whether authors were aware of or involved in the systematic manipulation of the publication process.

Wiley and Hindawi regrets that the usual quality checks did not identify these issues before publication and have since put additional measures in place to safeguard research integrity.

We wish to credit our own Research Integrity and Research Publishing teams and anonymous and named external researchers and research integrity experts for contributing to this investigation.

The corresponding author, as the representative of all authors, has been given the opportunity to register their agreement or disagreement to this retraction. We have kept a record of any response received.

References

[1] D. Ma, T. Yang, L. Liu, and Y. He, "Analysis of Factors Influencing Stock Market Volatility Based on GARCH-MIDAS Model," *Complexity*, vol. 2022, Article ID 6176451, 10 pages, 2022.

WILEY | Hindawi

Research Article

Analysis of Factors Influencing Stock Market Volatility Based on GARCH-MIDAS Model

Dan Ma [ID],[1] Tianxing Yang [ID],[2] Liping Liu [ID],[3,4] and Yi He [ID][5]

[1]*School of Statistics, Southwestern University of Finance and Economics, Chengdu 610071, China*
[2]*School of Big Data Statistics, Guizhou University of Finance and Economics, Guiyang 550025, China*
[3]*School of Mathematics and Statistics, Guizhou University of Finance and Economics, Guiyang 550025, China*
[4]*Guizhou Key Laboratory of Big Data Statistical Analysis, Guiyang 550025, China*
[5]*School of Accountancy, Guizhou University of Commerce, 550025 Guiyang, China*

Correspondence should be addressed to Liping Liu; llping@mail.gufe.edu.cn

This paper further extends the existing GARCH-MIDAS model to deal with the effect of microstructure noise in mixed frequency data. This paper has two highlights. First, according to the estimation of the long-term volatility components of the GARCH-MIDAS model, rAVGRV is adopted to substitute for the RV estimator. rAVGRV uses the rich data sources in tick-by-tick data and significantly corrects the impact of the microstructure noise on volatility estimation. Second, besides introducing macroeconomic variables (i.e., macroeconomic consistency index (MCI), deposits in financial institutions (DFI), industrial value-added (IVA), and M2), Chinese Economic Policy Uncertainty (CEPU) index and Infectious Disease Equity Market Volatility Tracker (EMV) are introduced in the long-run volatility component of the GARCH-MIDAS model. As indicated by the results of this paper, the rAVGRV-based GARCH-MIDAS is slightly better than the RV model-based GARCH-MIDAS. In addition to the common macroeconomic variables significantly impacting stock market volatility, CEPU also substantially impacts stock market volatility. Nevertheless, the effect of EMV on the stock market is insignificant.

1. Introduction

Traditional econometric models have been extensively used to analyze macroeconomic and financial consistent sampling frequency data. On the whole, the research methods using such data consist of VAR-type models, GARCH-type models, cointegration tests, and Granger causality tests. Most of the mentioned studies complied with low-frequency data models to examine the correlation between macroeconomics and stock market volatility. Over the past few years, among the studies on modeling problems of variables at different sampling frequencies, the Mixed Data Sampling (MIDAS) proposed by Ghysels et al. [1] has aroused the biggest attention. Such a model can develop a linear correlation between high-frequency explanatory variables and low-frequency explanatory variables, and it has been extensively applied in studies on macroeconomics, stock market, and crude oil futures for its ability to fully draw upon available information. Based on the MIDAS regression model, Engel et al. [2] developed a GARCH-MIDAS model, decomposing volatility into long-term and short-term components. Their model is adopted to study the correlation between stock market volatility and macroeconomic variables. Subsequently, Asgharian et al. [3] examined the effect of U.S. macroeconomic variables on stock market volatility by adopting the GARCH-MIDAS model.

The reason why this model outperforms the conventional GARCH-class models is that it can decompose the total conditional variance of the conventional GARCH model into two parts, that is, short-term volatility at a high frequency captured by a GARCH process and long-term volatility at a low frequency. To calculate the sum of squares of intraday yield data, Andersen et al. [4] proposed the GARCH-MIDAS model with a long-run component based

on realized volatility (RV). For the RV estimator, most scholars exploited return data with a 5-minute sampling frequency to determine high-frequency realized volatility (Wang and Ghysels [5]; Conrad and Kleen [6]). Though intraday high-frequency data involves sufficient data information and can increase the estimation efficiency of stock volatility, it is difficult to estimate due to considerable data. Moreover, when high-frequency data are used to estimate the stock market volatility, prices are sampled at finer intervals, and microstructure issues turn out to be more pronounced.

RV proposed by Andersen et al. [4] is justified based on the assumption of a continuous stochastic process to meet the challenge from market microstructure noise in practical applications (Aït-Sahalia et al. [7]). Zhang et al. [8] proposed realized volatility through subsample averaging (rAVGRV) that exploited the abundant sources in tick-by-tick data; to a great extent, it could correct the effect of the microstructure noise on volatility estimation. As indicated by Liu et al. [9], rAVGRV is a more theoretically and empirically reliable estimator than RV.

When predicting financial market volatility, macroeconomic indicators are important (Andersen et al. [4]; Conrad and Loch [10]; Dorion [11]). The GARCH-MIDAS model has been the most popular model adopted to investigate the correlations between aggregate financial volatility and macroeconomic or financial variables (Conrad et al. [12]; Conrad et al. [13]; Pan et al. [14]; Su et al. [15]; Conrad and Kleen [6]; Opschoor et al. [16]; Dominicy and Vander Elst [17]; Lindblad [18]; Amendola et al. [19]; Conrad et al. [12]; and Borup and Jakobsen [20]).

The study is different from existing studies, and the long-run volatility component of the GARCH-MIDAS model is impacted by realized volatility and other explanatory variables. The explanatory variables here included the macroeconomic variables, that is, macroeconomic consistency index (MCI), deposits in financial institutions (DFI), industrial value-added (IVA), and M2, as well as Chinese Economic Policy Uncertainty (CEPU) index and Infectious Disease Equity Market Volatility Tracker (EMV). The reason for selecting CEPU and EMV variables is twofold. On the one hand, although China's stock market has been leaping forward over the past two decades, it is still emerging. It is not sufficiently mature to require the government to stabilize it by releasing and implementing necessary policies. The government's policies are overly frequent, and the constant modifications in policies increase internal and external uncertainties, thereby increasing stock market volatility. On the other hand, the coronavirus (COVID-19) outbreak in December 2019 has significantly affected global macroeconomy and financial markets. Intuitively, stock market reacts to such a pandemic more promptly and directly than other sectors in economic and financial system. Accordingly, the two mentioned variables should be included in this paper.

The paper further extends the existing studies, and the highlights focus on two aspects. (1) In the estimation of the long-term volatility components of the GARCH-MIDAS model, rAVGRV is used to replace the RV estimator.

rAVGRV uses the rich sources in tick-by-tick data and to a great extent corrects the effect of the microstructure noise on volatility estimation. Accordingly, the rAVGRV-based GARCH-MIDAS model should be able to characterize the volatility of the stock market more effectively. As a matter of fact, the study by Liu et al. [9] confirmed that rAVGRV exhibited a better performance than RV. (2) Besides introducing macroeconomic variables MCI, IVA, DFI, and M2, CPEU and EMV were also introduced in the long-run volatility component of the GARCH-MIDAS model. The Chinese government's policies are too frequent, and the constant modifications in policies increase internal and external uncertainties. Moreover, COVID-19 has imposed great burden on global macroeconomy and financial markets. For this reason, CEPU and EMV should be introduced.

The rest of the study is organized as follows. The second section elucidates the GARCH-MIDAS model. The third section refers to an empirical study that explores the estimation, forecasting the GARCH-MIDAS model built in the study at several levels. The fourth section presents the application of the model to the portfolio. The fifth section is the robustness analysis of this paper. The last section concludes the present study.

2. GARCH-MIDAS Model

In accordance with Campbell [21], the correlation between the variations of unanticipated and expected returns in the stock market can be set below:

$$
\begin{aligned}
& r_{i,t} - E_{i-1,t}\left(r_{i,t}\right) \\
& = \left(E_{i,t} - E_{i-1,t}\right) \sum_{j=0}^{\infty} \rho^j \Delta d_{i+j,t} - \left(E_{i,t} - E_{i-1,t}\right) \sum_{j=1}^{\infty} \rho^j \Delta d_{i+j,t},
\end{aligned}
\tag{1}
$$

where $r_{i,t}$ denotes the logarithmic stock return on day i of month t; $d_{i,t}$ expresses the logarithmic dividend on day i of month t; $d_{i,t}$ represents the discount factor; $E_{i-1,t}(.)$ denotes the conditional expectation for a given set of information $I_{i-1,t}$ up to moment $i-1$.

Engle and Rangel [22] argued that unanticipated returns can be determined based on future cash flows or expected returns:

$$
r_{i,t} - E_{i-1,t}\left(r_{i,t}\right) = \sqrt{\tau_t g_{i,t}} \varepsilon_{i,t},
\tag{2}
$$

where the volatility consists of at least two components, and the volatility of stock returns falls into short-term $g_{i,t}$ and long-term τ_t components, where $g_{i,t}$ represents the volatility on day i of month t, and τ_t denotes the volatility at month t. Moreover, it is assumed that the random perturbation term $\varepsilon_{i,t}$ follows with the conditional standard normal distribution, that is, $\varepsilon_{i,t}|I_{i-1,t} \sim N(0,1)$.

Thus, the conditional variance of stock returns is written as

$$
\sigma_{i,t}^2 = E\left[\left(r_{i,t} - E_{i-1,t}\left(r_{i,t}\right)\right)^2\right] = \tau_t g_{i,t}.
\tag{3}
$$

Assume that $E_{i-1,t}(r_{i,t}) = u$, so equation (2) can be written as

$$r_{i,t} = \mu + \sqrt{\tau_t g_{i,t}} \varepsilon_{i,t}. \qquad (4)$$

For the short-term volatility component, it follows a mean-reverting unit-variance GJR-GARCH (1, 1) process:

$$g_{i,t} = (1 - \alpha - \beta - 0.5\gamma) + \left(\alpha + \gamma I_{\{r_{i-1,t}<0\}}\right)\frac{\left(r_{i-1,t} - \mu\right)^2}{\tau_t} + \beta g_{i-1,t}, \qquad (5)$$

where $I_{\{\}}$ is an indicator function, which means that the function takes a value of one if the condition is satisfied and zero otherwise. The short-run parameters are subject to $\alpha > 0; \beta \geq 0; \gamma \geq 0; \alpha + \beta + \gamma/2 < 1$. Parameter γ contains the information of asymmetry.

The long-term volatility component with a single explanatory variable takes the following form:

$$\log(\tau_t) = m + \theta \sum_{j=1}^{K} \varnothing_j(\omega_1, \omega_2) RV_{t-j},$$
$$RV_t = \sum_{i=1}^{N_i} r_{i,t}^2, \qquad (6)$$

where K denotes the number of periods over which the volatility is smoothed. If t represents a day, RV_t denotes daily realized volatility; if the sampling frequency of intraday high-frequency data is 5 min, the value of N_i is 48; if t represents a month, the monthly realized volatility is written as

$$RV_t = \frac{1}{22} \sum_{i=1}^{22} RV_{i,t}. \qquad (7)$$

Compared with daily return data, intraday high-frequency data containing rich data information and realized volatility estimation based on high-frequency data can significantly increase the estimation efficiency of volatility, whereas the effect of market microstructural noise on realized volatility cannot be ignored. When noise is present, the estimator RV is biased, and applying it to the GARCH-MIDAS model will adversely affect the estimation of this model. To address the mentioned problem, this paper also considered applying the RV via subsample averaging (rAVGRV) proposed by Zhang et al. [8] to the GARCH-MIDAS model to substitute for the RV estimator. Thus, the single-factor GARCH-MIDAS model is expressed as

$$\log(\tau_t) = m + \theta \sum_{j=1}^{K} \varnothing_j(\omega_1, \omega_2) \text{rAVGRV}_{t-j}. \qquad (8)$$

The rAVGRV estimator can effectively eliminate the effect of noise. rAVGRV is defined as follows.

Assume that, in period t, there are N equispaced returns $r_{i,t}$ and Δ is set to equal alignPeriod. For $i \geq \Delta$, the sub-sampled Δ-period return is defined as

$$\tilde{r}_{i,t} = \sum_{k=0}^{\Delta-1} r_{i-k,t}. \qquad (9)$$

It is defined that $N^*(j) = N/\Delta$ if $j = 0$; otherwise, $N^*(j) = N/\Delta - 1$. The j-th component of the rAVGRV estimator is expressed by

$$RV_t^j = \sum_{i=1}^{N^*(j)} \tilde{r}_{j+i-\Delta}^2. \qquad (10)$$

Take the average across the different $RV_t^j, j = 0, \ldots, \Delta - 1$, and the rAVGRV estimator is defined.

When Y_t is the MIDAS term, the long-run component of the GARCH-MIDAS model is

$$\log(\tau_t) = m + \theta \sum_{j=1}^{K} \varnothing_j(\omega_1, \omega_2) Y_{t-j}, \qquad (11)$$

where Y denotes the macroeconomic variable.

In the GARCH-MIDAS model expressed in equations (8) and (11), $\varnothing_j(\omega_1, \omega_2)$ is obtained from the weight function proposed by Ghysels et al. [1], and the equation is expressed as

$$\varnothing_j(\omega_1, \omega_2) = \frac{(j/K)^{\omega_1-1}(1-j/K)^{\omega_2-1}}{\sum_{i=1}^{K}(i/K)^{\omega_1-1}(1-i/K)^{\omega_2-1}}. \qquad (12)$$

To ensure that the weights of the lagged variables are in a decaying form, $w_1 = 1$ is generally fixed. Thus, equation (12) can be defined as

$$\varnothing_j(\omega_2) = \frac{(1-j/K)^{\omega_2-1}}{\sum_{i=1}^{K}(1-i/K)^{\omega_2-1}}. \qquad (13)$$

The single-factor GARCH-MIDAS model presented in the previous section considers only the rAVGRV volatility estimator or macroeconomic variable in the MIDAS term. However, numerous studies have shown that both realized volatility and macroeconomic variables have a significant impact on stock market volatility. With Y denoting the macroeconomic variable, as inspired by Engle et al. [2], equation (4) can be modified as

$$r_{i,t} = \mu + \sqrt{\tau(Y_t)g_{i,t}} \varepsilon_{i,t}. \qquad (14)$$

As a result, the long-run volatility component expressed in equations (8) and (11) can be rewritten as

$$\log(\tau_t) = m + \theta_1 \sum_{j=1}^{K} \varnothing_j(\omega_{1,R}, \omega_{2,R}) \text{rAVGRV}_{t-j}$$
$$+ \theta_2 \sum_{j=1}^{K} \varnothing_j'(\omega_1, \omega_2) Y_{t-j}. \qquad (15)$$

Equations (14) and (15) represent multifactor GARCH-MIDAS model.

3. Empirical Analysis

3.1. Data

3.1.1. Stock Market Data. This paper considers daily log-returns on the SSE Composite Index, calculated as $r_{i,t} = 100 * (\ln(p_{i,t}) - \ln(p_{i,t-1}))$, for the 2006 : M1 to 2021 : M6 period. To assess the volatility forecasts, this paper employed daily realized variances $RV_{i,t}$ and $\text{rAVGRV}_{i,t}$, where $RV_{i,t}$ is calculated from 5 min intraday log-returns. The data can be obtained from Wind database.

3.1.2. Explanatory Variables. Explanatory variables consist of macroeconomic consistency index (MCI), deposits in financial institutions (DFI), industrial value-added (IVA), and M2, as well as economic policy uncertainty index (EPUI) and Infectious Disease Equity Market Volatility Tracker (EMV). They are monthly data.

The monthly data of the Chinese Economic Policy Uncertainty (CEPU) index built by Huang et al. [23] are used. The index using 10 mainland Chinese newspapers can capture a wide range of uncertainty timely [24]. The Infectious Disease Equity Market Volatility Tracker (EMV) was built by Baker et al. [25]. Note that this paper aims to investigate whether and how infectious disease pandemic can affect the stock market volatility from a long-term perspective, instead of focusing on a single public health emergency, so the data from January 2006 to June 2021 are selected.

Table 1 reports the descriptive statistics of these time series. EMV is found with much larger standard deviation than those of stock indices. All the series have significant autocorrelation up to 10th lag, and they are not normally distributed.

The entire sample falls into two parts (i.e., estimation and forecast), in which the length of the estimation interval is from January 2006 to December 2020 (total 3647 days). The size of the forecast interval is from January 2021 to June 2021 (total 118 days). Both the daily closing rate data and the intraday high-frequency data are obtained from the RESSET database. Notably, when forecasting the volatility of SSE Composite Index, this paper uses a one-step forward rolling time window method. In other words, the first estimation interval $t = 1, 2, \ldots, 3647$ is adopted to estimate the parameters of the GARCH-MIDAS model to determine the volatility value of SSE Composite Index, which is used as the volatility prediction value on day 3648. By keeping the length of the estimation interval constant, the estimated sample interval is shifted back one day, and the second estimation interval is $t = 2, 3, \ldots, 3648$, in which the parameters of the GARCH-MIDAS model are estimated again, and the volatility of the 3649th day is predicted. Next, the volatility prediction of the 118th day is conducted.

3.2. In-Sample Performance

3.2.1. Analysis Based on Single-Factor GARCH-MIDAS Model. In the estimation of the GARCH-MIDAS model, the choice of weights w and lags K is of high significance. For the choice of weights, this paper follows the study by Engle et al. [2], in which the first weight is taken, and the second weight is chosen during the estimation of the model to ensure that the weights decrease with the increase in the number of lags.

K is the number of lags in MIDAS; since we use monthly data in the MIDAS equation, the lag order K can be taken as 12 according to Engle et al. [2].

The single-factor GARCH-MIDAS model considers only the rAVGRV (RV) estimator or macroeconomic variable in the MIDAS term. The estimation results of single-factor GARCH-MIDAS model are listed in Table 2.

From Table 2, the following conclusions are drawn: (1) besides macroeconomic variable MCI, macroeconomic variables IVA, M2, and DFI are significant, thereby demonstrating that they significantly impact the volatility of the stock market. (2) Chinese Economic Policy Uncertainty (CEPU) index significantly impacts stock market volatility. The government's policies are overly frequent, and the constant changes in policies increase internal and external uncertainties, thereby increasing stock market volatility. (3) Infectious Disease Equity Market Volatility Tracker (EMV) does not significantly impact the stock market, probably because timely actions by the Chinese authorities can reduce the volatility of their stock market, as also verified by Ali et al. [26] in the recent COVID-19 pandemic. (4) The coefficients θ corresponding to RV and rAVGRV are significant and are taken as positive values, which demonstrates that RV and rAVGRV can significantly improve the volatility of the Chinese stock market. Moreover, the loss functions MSE and QLIKE values of the GARCH-MIDAS (rAVGRV) model are smaller, which demonstrates that the model can be made better by using the rAVGRV estimator instead of the RV estimator in the GARCH-MIDAS model.

3.2.2. Analysis Based on Multifactor GARCH-MIDAS Model. The multifactor GARCH-MIDAS model built with equations (14) and (15) is estimated using data within the sample interval, and the estimation results are listed in Table 3.

According to Table 3, (1) for all multifactor GARCH-MIDAS models, the rAVGRV estimator still significantly improves the Chinese stock market. (2) Consistent with the results of the single-factor GARCH-MIDAS model shown in Table 2, macroeconomic variables IVA, M2, and DFI significantly impact the volatility of the stock market. Chinese Economic Policy Uncertainty (CEPU) index significantly impacts stock market volatility. Infectious Disease Equity Market Volatility Tracker (EMV) insignificantly impacts the stock market.

Figure 1 illustrates the long-term components of stock market volatility of the GARCH-MIDAS model incorporating significant macroeconomic variables and CEPU, basically complying with the overall trend of the total conditional variance. Thus, the GARCH-MIDAS model incorporating macroeconomic variables and CEPU is suggested to have high goodness of fit.

Table 1: Descriptive statistics.

	RV_t	$rAVGRV_t$	MCI	IVA	M2	DFI	CEPU	EMV
Frequency	Monthly	Monthly	Monthly	Monthly	Monthly	Monthly	Monthly	Monthly
Mean	2.294	1.999	1.992	0.101	5.974	5.975	2.284	−0.294
Std	0.217	0.074	0.018	0.046	0.257	0.255	0.369	0.491
Skewness	2.582***	2.043***	−0.935***	0.532***	−0.384***	−0.355***	0.194***	2.259***
Kurtosis	11.113***	6.930***	4.310***	2.185***	1.894**	1.887**	2.210	8.708***
JB stat	693.668***	241.078***	39.153***	13.477***	13.593***	13.085***	5.810*	397.347***
Q (5)	232.73***	226.1***	517.89***	627.17***	814.5***	814.36***	556.5***	398.03***
Q (10)	322.64***	324.34***	623.98***	1045.6***	1493***	1494.6***	917.41***	486.07***

Notes: the Jarque-Bera statistic test for the null hypothesis of normality in sample returns distribution. $Q(n)$ is the Ljung-Box statistics of the return series for up to nth order serial correlation. ***, **, and * indicate rejection at the 1%, 5%, and 10% significance level, respectively.

Table 2: Estimation results of single-factor GARCH-MIDAS ($K = 12$).

	α	β	γ	m	θ	w_2	MSE	QLIKE
GARCH-MIDAS (RV)	0.0457***	0.951***	0.006	2.031***	0.434**	1.328***	42.217	1.632
	(≤0.001)	(≤0.001)	(0.606)	(≤0.001)	(0.049)	(0.002)		
GARCH-MIDAS (rAVGRV)	0.045***	0.951***	0.005	2.013***	0.456*	1.558***	41.659	1.601
	(≤0.001)	(≤0.001)	0.642	(≤0.001)	(0.084)	(0.005)		
GARCH-MIDAS (MCI)	0.065	0.933***	0.003	2.061	−16.070	7.553	42.197	1.628
	(0.128)	(0.966)	(0.966)	(0.341)	(0.944)	(0.973)		
GARCH-MIDAS (IVA)	0.062***	0.933***	0.008	2.147***	9.062***	4.965***	42.087	1.628
	(≤0.001)	(≤0.001)	(0.655)	(≤0.001)	(≤0.001)	(≤0.001)		
GARCH-MIDAS (M2)	0.064**	0.933***	0.005	2.152***	1.296*	2.312	42.189	1.629
	(0.024)	(≤0.001)	(0.782)	(0.001)	(0.095)	(0.997)		
GARCH-MIDAS (DFI)	0.063***	0.933***	0.005	2.095***	−1.598***	1.928***	42.190	1.629
	(≤0.001)	(≤0.001)	(0.766)	(≤0.001)	(≤0.001)	(≤0.001)		
GARCH-MIDAS (CEPU)	0.060***	0.935***	0.007	2.096***	−3.480**	2.359***	42.206	1.626
	(≤0.001)	(≤0.001)	(0.667)	(≤0.001)	(0.019)	(≤0.001)		
GARCH-MIDAS (EMV)	0.064***	0.933***	0.005	2.081***	0.438	2.801***	42.235	1.629
	(≤0.001)	(≤0.001)	(0.766)	(≤0.001)	(0.448)	(≤0.001)		

Notes: the bracketed numbers are the p value of the estimations. ***, **, and * indicate rejection at the 1%, 5%, and 10% significance level, respectively.

3.3. Forecast Comparisons. To assess the predictive performance exhibited by different models, the following loss functions are employed in the study:

$$\text{MSE} = \frac{1}{N} \sum_{t=1}^{N} \left(h_t - \widehat{h}_t \right)^2,$$

$$\text{MAE} = \frac{1}{N} \sum_{t=1}^{N} \left| h_t - \widehat{h}_t \right|,$$

$$\text{MSD} = \frac{1}{N} \sum_{t=1}^{N} \left(\sqrt{h_t} - \sqrt{\widehat{h}_t} \right)^2, \quad (16)$$

$$\text{MAD} = \frac{1}{N} \sum_{t=1}^{N} \left| \sqrt{h_t} - \sqrt{\widehat{h}_t} \right|,$$

$$\text{QLIKE} = \frac{1}{N} \sum_{t=1}^{N} \left| \frac{h_t}{\widehat{h}_t} - \log\left(\frac{h_t}{\widehat{h}_t} \right) \right|.$$

N in the loss function represents the length of the prediction interval, with $N = 118$ days. h_t and $\widehat{h}_t$ denote the actual and predicted values of stock market volatility, respectively. Since the actual value of stock market volatility is unobservable, as suggested by Pan et al. [27], an estimate of RV based on the 5 min frequency was used instead of h_t. A minor loss function indicates higher accuracy and better out-of-sample predictive power of the model. To verify whether the differences between the different prediction models are significant, the MCS proposed by Hansen et al. [28] is introduced for testing. The first step of the MCS test takes $M = M_0$, M_0 denotes the candidate model, and the significant level is set to a. If the null hypothesis is rejected, the worse-performing prediction model will be eliminated. The process continues till there is no more rejection of the null hypothesis to obtain the set of surviving models, which will be recorded as $\widehat{M}_a^*$. The model contained in $\widehat{M}_a^*$ refers to the optimal prediction model at the $1 - a$ confidence level. A condition for a model belonging to M is that its p value of the MCS test exceeds the significant level. In other words, the larger the p value of the prediction model is, the stronger the model's predictive power will be. Table 4 lists the results of the MCS tests based on different models.

The benchmark p value of the MCS test is set to 0.1. Given the principle of the MCS test, if the corresponding p value of the model is less than 0.10, the out-of-sample predictive ability of the model will be poor and will be rejected in the MCS test process. A larger p value reveals that the out-of-sample predictive ability of the model is better. As

Table 3: Estimation results of multifactor GARCH-MIDAS model ($K = 12$).

	α	β	m	θ_1	θ_2	ω_1	ω_2	LLF
GARCH-MIDAS	0.070***	0.909***	−0.017	0.342***	0.142	1.858***	4.433	−5902.481
(rAVGRV + MCI)	(≤0.001)	(≤0.001)	(0.998)	(≤0.001)	(0.971)	(≤0.001)	(0.917)	
GARCH-MIDAS	0.069***	0.898***	−0.585*	0.325***	7.403***	2.017***	1.001	−5894.395
(rAVGRV + IVA)	(0.002)	(≤0.001)	(0.083)	(0.001)	(0.006)	(0.001)	(0.920)	
GARCH-MIDAS	0.068***	0.897***	6.035*	0.306***	−0.972*	2.292***	2.037	−5896.277
(rAVGRV + M2)	(≤0.001)	(≤0.001)	(0.086)	(≤0.001)	(0.093)	(≤0.001)	(0.386)	
GARCH-MIDAS	0.067***	0.898***	7.458**	0.289***	−1.207**	2.182***	1.608	−5895.538
(rAVGRV + DFI)	(≤0.001)	(≤0.001)	(0.032)	(≤0.001)	(0.035)	(≤0.001)	(0.354)	
GARCH-MIDAS	0.067***	0.906***	1.872***	0.332***	−0.724***	1.941***	38.808	−5894.433
(rAVGRV + CEPU)	(≤0.001)	(≤0.001)	(0.001)	(≤0.001)	(0.003)	(≤0.001)	(0.248)	
GARCH-MIDAS	0.069***	0.909***	0.282	0.341***	0.084	1.891***	4.151	−5902.443
(rAVGRV + EMV)	(≤0.001)	(≤0.001)	(0.528)	(≤0.001)	(0.748)	(≤0.001)	(0.763)	

Notes: LLF indicates maximum likelihood function value. The bracketed numbers are the p value of the estimations. ***, **, and *indicate rejection at the 1%, 5%, and 10% significance level, respectively.

indicated by the above Table, the p value of the GARCH-MIDAS model based on the rAVGRV statistic is also slightly larger than the p value of the GARCH-MIDAS model based on the RV statistic, and the ranking of the model is higher after a two-by-two comparison. Thus, the results above demonstrate that the GARCH-MIDAS (rAVGRV) model can be better than the GARCH-MIDAS (RV) model to some extent, since the rAVGRV statistic removes the effect of noise in the estimation, and the estimated realized volatility can be more accurate.

4. Application in the Portfolio

To verify the effectiveness of various types of volatility forecasting models in practice, they can be applied to a portfolio. It is assumed that the investor invests his money in equities and risk-free assets, respectively. In a standard mean-variance portfolio, the optimal weighting of an investor's investment in a stock is determined a priori based on the predicted variance. A volatility timing strategy popular in forecasting literature (Campbell and Thompson [29]; Ferreira and Santa-Clara [30]; Neely et al. [31]) is adopted in this paper. To be specific, at the end of day t, the investor calculates the optimal weight of the stock index according to the following equation for the next day $t + 1$:

$$w_t = \frac{1}{\delta} \frac{\widehat{R}_{t+1} - R_{f,t}}{\widehat{h}_{t+1}}. \tag{17}$$

In the above equation, δ denotes the risk aversion coefficient, $\widehat{R}_{t+1}$ represents the predicted value of stock returns that exceed the risk-free rate $R_{f,t}$, and here this paper selected the benchmark bank 1-year time deposit rate in place of the risk-free rate. $\widehat{h}_{t+1}$ expresses the predicted value of stock market volatility. The weight of an investor's investment in equities is expressed as w_t, and the remainder weight $1 - w_t$ is assigned to the risk-free asset. Certainly, the optimal weight of stock is affected by the value of risk coefficient δ. For robustness check, four different δ's of 5, 10, 15, and 20 are adopted.

Then the return of the portfolio is expressed as

$$R_{p,t+1} = w_t R_{t+1} + R_{f,t}. \tag{18}$$

To assess the portfolio performance, the measure of certainty equivalent return (CER) is adopted as follows:

$$\text{CER}_p = \mu_p - \frac{1}{2} \delta \sigma_p^2, \tag{19}$$

where μ_p and σ_p^2 denote the mean and variance of the portfolio returns, respectively. The CER values of the portfolios by using different volatility models are listed in the tables below.

Tables 5 and 6 list the annualized percentage values. (1) The economic value corresponding to the GARCH-MIDAS model significantly exceeds that of the GARCH model, so the GARCH-MIDAS model can have high performance in the portfolio, regardless of the risk aversion coefficient. (2) GARCH-MIDAS (rAVGRV) model is slightly better than GARCH-MIDAS (RV) model, and the application of the GARCH-MIDAS (rAVGRV) model to a portfolio can create a higher economic value.

5. Robustness Checks

To verify whether it is better to use rAVGRV instead of the RV estimator in the GARCH-MIDAS model, the GARCH-MIDAS-X model (Amendola et al. [24]; Engle and Patton [32]) is applied for further analysis. GARCH-MIDAS-X models are built for MCI, IVA, DFI, CEPU, EWV, and M2, respectively. RV or rAVGRV is included as a daily lagged variable in the short-run component (the so-called "–X" term). In this paper, the SSE Composite Index data from January 2006 to December 2020 are still used. The estimation results of the GARCH-MIDAS-X model are listed in Table 7.

As indicated by the results in Table 7, (1) for all GARCH-MIDAS-X models, the corresponding loss functions MSE and QLIKE are significantly smaller when the X term is the rAVGRV estimator, which demonstrates that the GARCH-MIDAS-X model built based on rAVGRV is better. (2) According to the parameter term z, when the X term is the rAVGRV estimator, it significantly impacts the Chinese stock market in most cases.
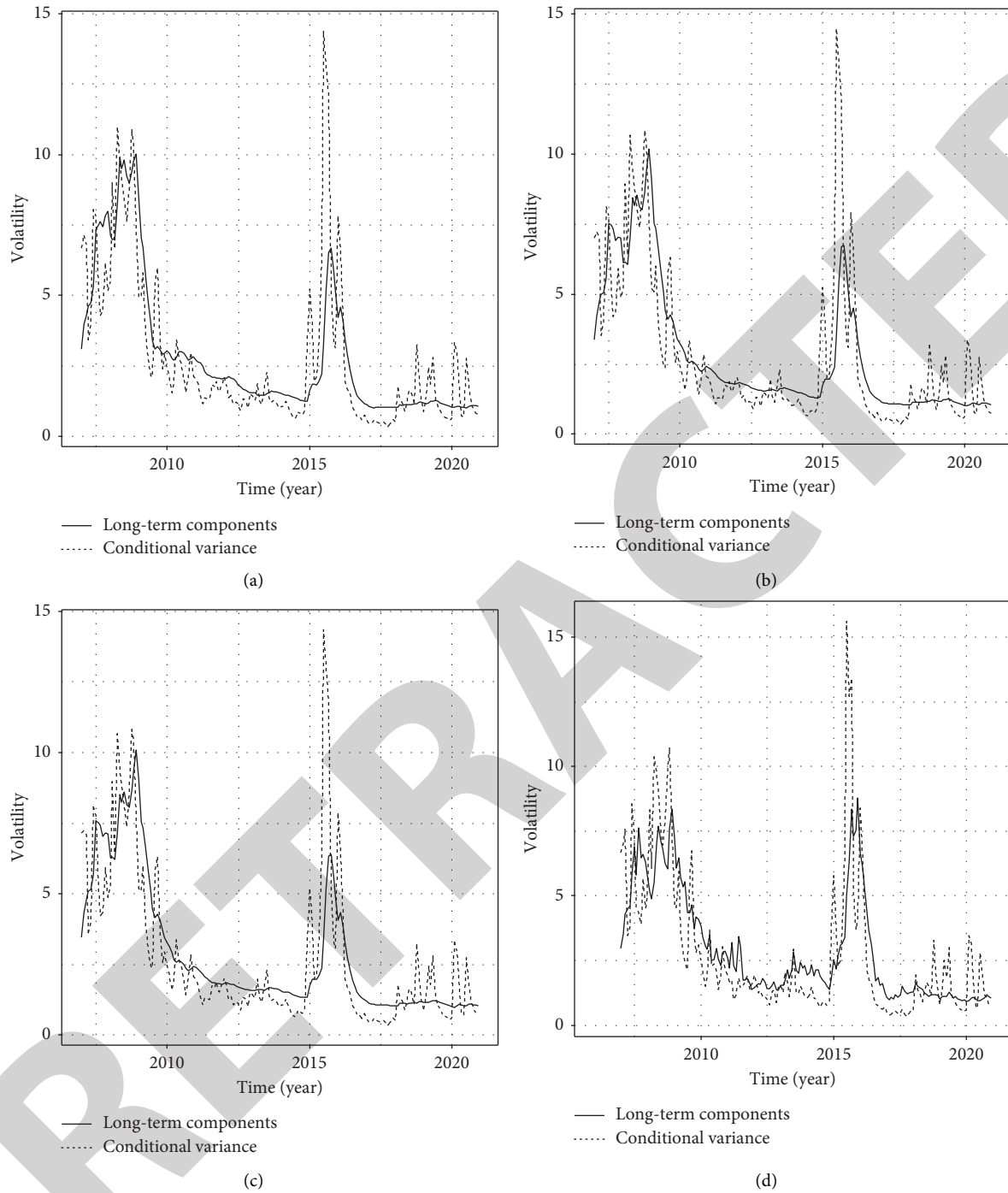
Figure 1: Fitting of conditional variance and long-run components of volatility for the multifactor GARCH-MIDAS model incorporating macroeconomic variables and CEPU. (a) rAVGRV + IVA. (b) rAVGRV + M2. (c) rAVGRV + DFI. (d) rAVGRV + CEPU.

To test the robustness of the research results in the previous section, CSI 300 index is also used as a proxy variable for the Chinese stock market. The selected data estimation interval remains from January 2006 to December 2020. Moreover, the estimation results are listed in Table 8.

According to Table 8, (1) the coefficients θ_1 corresponding to rAVGRV are significant and are taken as a positive value, so rAVGRV estimator can exert a significantly positive effect on the volatility of the Chinese stock market. (2) Variables IVA, M2, DFI, and CEPU still

Table 4: The MCS tests of GARCH-MIDAS model.

Loss function	MSE	MAE	MSD	MAD	QLIKE	Rank_M
GARCH-MIDAS (rAVGRV)	1.000	1.000	1.000	1.000	1.000	1
GARCH-MIDAS (RV)	0.845	0.793	0.845	0.762	0.813	2
GARCH-MIDAS (rAVGRV + MCI)	1.000	1.000	1.000	1.000	1.000	1
GARCH-MIDAS (RV + MCI)	0.743	0.803	0.790	0.746	0.802	2
GARCH-MIDAS (rAVGRV + IVA)	1.000	1.000	1.000	1.000	1.000	1
GARCH-MIDAS (RV + IVA)	0.751	0.698	0.821	0.792	0.880	2
GARCH-MIDAS (rAVGRV + M2)	1.000	1.000	1.000	1.000	1.000	1
GARCH-MIDAS (RV + M2)	0.797	0.813	0.796	0.808	0.779	2
GARCH-MIDAS (rAVGRV + DFI)	1.000	1.000	1.000	1.000	1.000	1
GARCH-MIDAS (RV + DFI)	0.862	0.787	0.794	0.838	0.745	2
GARCH-MIDAS (rAVGRV + CEPU)	1.000	1.000	1.000	1.000	1.000	1
GARCH-MIDAS (RV + CEPU)	0.812	0.799	0.852	0.884	0.802	2

Notes: numbers in the table indicate the p values of the MCS test based on different loss functions. Rank_M indicates the ranking of the model.

Table 5: Investment performance of different models based on RV.

δ	GARCH	GARCH-MIDAS (RV)	GARCH-MIDAS (RV + MCI)	GARCH-MIDAS (RV + IVA)	GARCH-MIDAS (RV + M2)	GARCH-MIDAS (RV + DFI)	GARCH-MIDAS (RV + CEPU)
5	1.545	1.670	1.801	1.790	1.840	1.805	1.796
10	1.329	1.503	1.664	1.595	1.699	1.686	1.599
15	1.260	1.332	1.493	1.320	1.582	1.480	1.436
20	1.065	1.252	1.325	1.295	1.399	1.373	1.311

Table 6: Investment performance of different models based on rAVGRV.

δ	GARCH-MIDAS (rAVGRV)	GARCH-MIDAS (rAVGRV + MCI)	GARCH-MIDAS (rAVGRV + IVA)	GARCH-MIDAS (rAVGRV + M2)	GARCH-MIDAS (rAVGRV + DFI)	GARCH-MIDAS (rAVGRV + CEPU)
5	1.789	1.880	1.822	1.900	1.873	1.815
10	1.585	1.662	1.718	1.826	1.800	1.770
15	1.330	1.465	1.604	1.684	1.612	1.592
20	1.112	1.340	1.482	1.526	1.493	1.391

Table 7: Estimation results of GARCH-MIDAS-X ($K = 12$).

	X	β	z	m	θ	w_2	MSE	QLIKE
GARCH-MIDAS-X (MCI)	RV	0.800**	0.081	1.072***	−4.976***	2.263	52.488	2.02
	rAVGRV	0.928***	0.024**	1.033***	−20.493***	1.618	46.380	1.913
GARCH-MIDAS-X (IVA)	RV	0.808***	0.078	1.076***	7.569	9.130***	52.435	2.021
	rAVGRV	0.926***	0.027**	1.040***	8.172***	9.013***	46.800	1.931
GARCH-MIDAS-X (DFI)	RV	0.798***	0.081*	1.071***	0.264**	1.967	52.363	2.02
	rAVGRV	0.925***	0.025*	1.037***	0.825***	2.088	46.322	1.913
GARCH-MIDAS-X (CEPU)	RV	0.801***	0.08	1.0740***	−0.13	8.928***	52.361	2.021
	rAVGRV	0.930***	0.021	1.055***	−0.893**	5.674	45.488	1.878
GARCH-MIDAS-X (EMV)	RV	0.801***	0.08	1.068***	0.574	2.025**	52.189	2.021
	rAVGRV	0.930***	0.004*	1.462***	−0.632*	1.001**	42.907	1.689
GARCH-MIDAS-X (M2)	RV	0.797***	0.082	1.071***	1.710***	2.287***	52.759	2.024
	rAVGRV	0.927***	0.024**	0.950***	16.540*	18.302**	46.004	1.896

Notes: ***, **, and *indicate rejection at the 1%, 5%, and 10% significance level, respectively. X represents RV or rAVGRV. z represents the coefficients corresponding to X term. Other parameters are consistent with Table 2.

TABLE 8: Estimation results of multifactor GARCH-MIDAS model based on CSI 300 ($K = 12$).

	α	β	γ	m	θ_1	θ_2	ω_1	ω_2	LLF
GARCH-MIDAS	0.065***	0.914***	0.016	−0.700	0.302***	0.562	1.827***	1.003	−6201.200
(rAVGRV + MCI)	(≤0.001)	(≤0.001)	(0.321)	(0.650)	(0.001)	(0.393)	(≤0.001)	(0.782)	
GARCH-MIDAS	0.064***	0.911***	0.015	−0.321	0.276***	7.175***	1.838***	6.663**	−6193.656
(rAVGRV + IVA)	(0.001)	(≤0.001)	(0.360)	(0.251)	(≤0.001)	(0.004)	(0.001)	(0.037)	
GARCH-MIDAS	0.061***	0.909***	0.018	9.231**	0.217**	−1.461**	2.059***	2.576	−6194.839
(rAVGRV + M2)	(≤0.001)	(≤0.001)	(0.265)	(0.026)	(0.014)	(0.030)	(0.002)	(0.665)	
GARCH-MIDAS	0.061***	0.908***	0.018	8.742**	0.228***	−1.382**	2.096***	4.214	−6194.75
(rAVGRV + DFI)	(≤0.001)	(≤0.001)	(0.261)	(0.031)	(0.008)	(0.036)	(0.001)	(0.481)	
GARCH-MIDAS	0.061***	0.915***	0.017***	2.200***	0.277***	−0.780***	1.868***	56.843***	−6191.956
(rAVGRV + CEPU)	(≤0.001)	(≤0.001)	(0.006)	(≤0.001)	(≤0.001)	(0.001)	(≤0.001)	(0.002)	
GARCH-MIDAS	0.064***	0.917***	0.015	0.534	0.282***	0.073	1.710**	3.458	−6201.44
(rAVGRV + EMV)	(0.001)	(≤0.001)	(0.389)	(0.484)	(0.003)	(0.803)	(0.048)	(0.684)	

Notes: LLF indicates maximum likelihood function value. The bracketed numbers are the p value of the estimations. ***, **, and *indicate rejection at the 1%, 5%, and 10% significance level, respectively.

significantly impact the volatility of the stock market, and the impact of EMV on the stock market remains insignificant. In brief, the conclusions drawn from Table 8 comply with Table 3. Thus, the findings of this paper are verified to be robust.

6. Conclusion

We further extend the existing GARCH-MIDAS model. This paper has two highlights. First, the rAVGRV estimator considering noise effects is adopted to estimate the long-term volatility components of the GARCH-MIDAS model. Second, in the GARCH-MIDAS model, the Infectious Disease Equity Market Volatility Tracker (EMV) and Chinese Economic Policy Uncertainty (CEPU) index are introduced besides macroeconomic variables to more comprehensively analyze the factors of Chinese stock market volatility based on the research in the study. Moreover, the following conclusions are drawn:

The GARCH-MIDAS (rAVGRV) model is slightly better than the GARCH-MIDAS (RV) model, since the effect of noise on the stock market in high-frequency data cannot be ignored. rAVGRV statistic removes the effect of noise in the estimation. As a result, the estimated realized volatility can be more accurate.

In single-factor GARCH-MIDAS model, the coefficients θ corresponding to RV and rAVGRV are significant and are taken as positive values, which demonstrates that RV and rAVGRV significantly improve the volatility of the Chinese stock market.

For all GARCH-MIDAS models, macroeconomic variables IVA, M2, and DFI significantly impact stock market volatility. Likewise, Chinese Economic Policy Uncertainty (CEPU) index impacts stock market volatility significantly, the government's policies are overly frequent, and the constant changes in policies cause more internal and external uncertainties, which increases stock market volatility. Besides, Infectious Disease Equity Market Volatility Tracker (EMV) insignificantly impacts the stock market, since timely actions by the Chinese authorities can reduce the volatility of their stock market, which is also verified by Amendola et al. [24] in the recent COVID-19 pandemic.

Data Availability

The stock data used in this article can be obtained from the Wind database. The macroeconomic consistency index (MCI), industrial value-added (IVA), M2, and deposits of financial institutions (DFI) can be obtained from the official website of the People's Bank of China (https://www.pbc.gov.cn/diaochatongjisi/116219/index.html) or the Oriental Fortune website (https://data.eastmoney.com/cjsj/xfzxx.html). The Chinese Economic Policy Uncertainty (CEPU) index (https://economicpolicyuncertaintyinchina.weebly.com/) was constructed by Huang et al. [23]. The Infectious Disease Equity Market Volatility Tracker (EMV) (http://www.policyuncertainty.com/infectious_EMV.html) was constructed by Baker et al. [25]. To save space, we will not show all the data in this article, but they can be provided upon request.

Conflicts of Interest

The authors solemnly declare that that there are no conflicts of interest regarding the publication of this paper.

Acknowledgments

References

[1] E. Ghysels, A. Sinko, and R. Valkanov, "MIDAS regressions: further results and new directions," *Econometric Reviews*, vol. 26, no. 1, pp. 53–90, 2007.

[2] R. F. Engle, E. Ghysels, and B. Sohn, "Stock market volatility and macroeconomic fundamentals," *The Review of Economics and Statistics*, vol. 95, no. 3, pp. 776–797, 2013.

[3] H. Asgharian, A. J. Hou, and F. Javed, "The importance of the macroeconomic variables in forecasting stock return variance: a GARCH-MIDAS approach," *Journal of Forecasting*, vol. 32, pp. 600–612, 2013.

Retraction

Retracted: A Study on the Topic-Sentiment Evolution and Diffusion in Time Series of Public Opinion Derived from Emergencies

Complexity

This article has been retracted by Hindawi following an investigation undertaken by the publisher [1]. This investigation has uncovered evidence of one or more of the following indicators of systematic manipulation of the publication process:

(1) Discrepancies in scope

(2) Discrepancies in the description of the research reported

(3) Discrepancies between the availability of data and the research described

(4) Inappropriate citations

(5) Incoherent, meaningless and/or irrelevant content included in the article

(6) Manipulated or compromised peer review

The presence of these indicators undermines our confidence in the integrity of the article's content and we cannot, therefore, vouch for its reliability. Please note that this notice is intended solely to alert readers that the content of this article is unreliable. We have not investigated whether authors were aware of or involved in the systematic manipulation of the publication process.

Wiley and Hindawi regrets that the usual quality checks did not identify these issues before publication and have since put additional measures in place to safeguard research integrity.

We wish to credit our own Research Integrity and Research Publishing teams and anonymous and named external researchers and research integrity experts for contributing to this investigation.

The corresponding author, as the representative of all authors, has been given the opportunity to register their agreement or disagreement to this retraction. We have kept a record of any response received.

References

[1] M. Cai, H. Luo, and Y. Cui, "A Study on the Topic-Sentiment Evolution and Diffusion in Time Series of Public Opinion Derived from Emergencies," *Complexity*, vol. 2021, Article ID 2069010, 23 pages, 2021.

WILEY | Hindawi

Research Article

A Study on the Topic-Sentiment Evolution and Diffusion in Time Series of Public Opinion Derived from Emergencies

Meng Cai ,[1] Han Luo ,[1] and Ying Cui [2]

[1]*School of Humanities and Social Sciences, Xi'an Jiaotong University, Xi'an 710049, China*
[2]*School of Mechano-Electronic Engineering, Xidian University, Xi'an 710071, China*

Correspondence should be addressed to Meng Cai; mengcai@xjtu.edu.cn

With the development of the Internet, social media has become an important platform for people to deal with emergencies and share information. When a public health emergency occurs, the public can understand the topics of the event and perceive the sentiments of others through social media, thus building a cooperative communication network. In this study, we took the public health emergency as the main research object and the natural disaster, accident, and social security event as the secondary research object and further revealed the law of the formation and evolution of public opinion through the analysis on temporal networks of topics and sentiments in social media platforms. Firstly, we identified the derived topics by constructing the topic model and used the sentiment classification model to divide the text sentiments of the derived topics into two types: positive sentiment and negative sentiment. Then, the ARIMA time series model was used to fit and predict the evolution and diffusion rules of topics and sentiments derived from public opinions on temporal networks. It was found that the evolution law of derived public opinions had similarities and differences in various types of emergencies and was closely related to government measures and media reports. The related research provides a foundation for the management of network public opinion and the realization of better emergency effects.

1. Introduction

With the development of the economy and the deepening of the social transformation period, social contradictions are further aggravated, and the frequent occurrence of emergencies has become a severe test faced by social governance [1]. Based on relevant research, the emergency is defined as the event that poses a serious threat to human life, health, property, and safety and is further divided into four types: natural disaster, accident, public health, and social security event [2, 3]. For example, the COVID-19 outbreak in 2020 is a typical public health event, which has brought serious economic losses and human casualties to all countries in the world and posed serious challenges to the governance of social order and the maintenance of social stability. When public health events or other types of emergencies occur, people will carry out heated discussions on social media around the relevant events and try to obtain information

related to the event and understand the situation related to the event with the convenience of social media, to reduce the impact brought by the uncertainty [4]. However, the immediacy of emergency makes the response of the government and media lag, which cannot meet the explosive demand of the public for the information related to the event, often leaving the public in the situation of lack of information and psychological anxiety. At this time, the public is vulnerable to the influence of false information and tends to form negative emotions, which makes emergency management more complex, weakens social cohesion, impacts social order and social stability, and finally causes social crisis [5].

In recent years, as an integral part of modern society, social media has penetrated everyone's daily life. According to the statistics of relevant agencies, the global users of social media have exceeded 4.7 billion in 2021, which means that, on average, 6 out of 10 people in the world are using social

media [6]. Through the social network established in the social media platform, on one hand, the public can express their views conveniently, share their experiences and thoughts, and make comments on the event. On the other hand, they can also interact with other social media users through functions such as thumb up, retweet, and comment [7]. The advantages of social media in instant communication and interaction also make it play an increasingly important role in the emergency management of emergencies [8]. Therefore, when an emergency occurs, the public tends to use social media to collect and disseminate information and form a cooperative communication network on the social media platform through the exchange of pictures, texts, and other information, to realize information sharing and the exchange of views [9], which also provides favorable conditions for rescue and management after the occurrence of emergencies.

In addition, the occurrence of emergencies is often not isolated, but there will be further evolution and development in the context of time and space and under the action of the environment derive to other related events. When an emergency occurs, the public's discussion and concern about the emergency itself is usually defined as the original public opinion of the emergency, and the public's discussion and concern about the related events evolved in the context of time and space of the emergency is defined as the derived public opinion [10]. In short, the communication process of emergencies on social media is influenced by various external factors and thus forms other interrelated event contents. Derived public opinions are derived from the public's discussion and attention on related events after the differentiation of emergencies in social networks. The typical characteristic of derived public opinion is the transfer of evaluation object, which is different from the research object of original public opinion. Compared with the original public opinion, the derived public opinion of an emergency is more concealable. In the early stage of an emergency, it hides in the evolution of the original public opinion and is difficult to attract public attention. However, when the original public opinion of the emergency has evolved to a certain stage, or when the control and treatment measures for the emergency are ineffective, the derived public opinion will often break out quickly. On the one hand, it attracts the attention of the public and becomes a hot topic in society, further expanding the scope of impact and the degree of function of the emergency [11]. On the other hand, it will have an impact on the original public opinion, aggravate and upgrade the public opinion, increase the difficulty of public opinion management in the social network, and further impact the social order and social stability [12]. Therefore, the relevant analysis of public opinion derived from emergencies based on public health events is not only conducive to the prediction and emergency management of emergencies but also to reducing the negative impact of online public opinion, which is an important guarantee for the realization of network security governance and the maintenance of social order and social stability.

In this study, we take the public opinion derived from public health emergencies as the main research object and introduce other types of emergencies such as natural disasters, accidents and disasters, and social security as the secondary research object. Combined with the time series analysis method, this study attempts to explore the topic-sentiment evolution law of public opinions derived from the public health event on temporal networks and further compares the commonality and difference of topic-sentiment evolution law in different types of emergencies. Through the above analysis, this study attempts to answer the following questions:

(1) What are the characteristics of the topic evolution of public opinions derived from public health emergencies on temporal networks? Are there any differences from other types of emergencies?

(2) What are the characteristics of the emotional evolution of public opinions derived from public health emergencies on temporal networks? Are there any differences from other types of emergencies?

The rest of this paper is structured as follows. In the next section, the study will review the public opinion derived from emergencies and the related studies on topic-sentiment evolution. The third part introduces the method of this paper, mainly including the principle and advantages of the model used in this paper. The fourth part introduces the research design of this paper, including data collection and preprocessing, topic model, sentiment model, and time series model. The fifth part shows the research findings of this paper and reveals the topic and sentiment evolution rules of derived public opinions on temporal networks. The sixth part is the research conclusion of this paper, which summarizes the foregoing and puts forward the further direction for the follow-up research.

2. Related Studies

2.1. Research on Public Opinion Derived from Emergencies. Derivative public opinion is formed in the discussion and interaction of social media users on related events under the evolution of emergencies. These related events are often referred to as secondary or derivative events, which evolve from the original events. Among them, original events usually refer to the emergent events that first appear and then evolve and spread, while secondary events and derivative events are a series of related events that evolved from original events under the action of the spatiotemporal situation [10]. The difference between the two is that the secondary event and the original event are consistent in terms of type and cause of the occurrence, with continuity and linkage, while the derivative event is quite different from the original event in terms of type and cause of occurrence [11]. In short, the secondary event is triggered by the original event, acts on the same object as the original event, and is of the same type as the original event. In addition, the derived event is also the event caused by the original event, but the research object has changed and the type is different from the original event. For example, the governance and prevention events caused by public health events are called secondary events, but the changes in stock prices caused by

public health events belong to the derived event. In addition, from the perspective of the content of related events, some scholars believe that related events are reflections of original events from different aspects, and they name related events as subevents [12, 13]. However, there are few studies on the definition and feature description of associated events, and there is a lack of authoritative definition standards and discriminant framework. Therefore, to facilitate the follow-up research work, a series of related events evolving in the context of time and space of emergencies are uniformly referred to as derivative events.

Online public opinion on emergencies refers to the synthesis of attitudes, opinions, and sentiments expressed on social networks around the occurrence and dissemination of emergencies in a certain time and space with social media platforms as communication channels [14]. Derived public opinion refers to the social media users expressing their views, opinions, and evaluations on the derivative events of emergencies through the network platform [15]. Existing related studies that take derived public opinion as the research object mainly focus on the dissemination and prediction of derived public opinion, the evolution mechanism of derived public opinion, the formation and response of derived public opinion, and so on. Among them, the dissemination and prediction of derived public opinion are mainly studied. On the one hand, information mining methods are used to understand the dissemination mechanism of derived public opinion; on the other hand, methods such as machine learning are used to realize the prediction of derived public opinion. For example, some scholars established a digital model to simulate the propagation dynamics of network rumors in social networks, to identify the propagation characteristics of network rumors, a special derivative public opinion, in social networks [16]. In addition, some scholars established a control model and explained the propagation mode of derived public opinion based on the propagation mechanism, to realize the control of derived public opinion [17]. As for the prediction of the derived public opinion, on the one hand, recent studies use machine learning algorithms such as HDP to analyze the text semantics to realize the classification of the derived public opinion [18]. On the other hand, deep learning algorithms such as neural networks are used to realize the prediction of the derived public opinion through the analysis of social media data [19].

At present, the research on the evolution mechanism of derived public opinions mainly adopts the method of case study and analyzes the evolution of derived public opinions in social networks by selecting specific emergencies as research objects. Some studies choose a single emergency event as the research object. For example, based on the investigation of an emergency accident and disaster event, the evolution path and internal logic of derived public opinions are explored from the interaction and game among the government, media, and the public [20]. There are also studies taking large-scale emergent event data sets as research objects. For example, based on the analysis of 101 emergent event data sets, the changes of online public opinion in time and space are explored, providing a rich research basis for the evolution mechanism of derived public opinion [21]. The third aspect of related research on derivative public opinion focuses on the formation reasons and coping strategies of derivative public opinion and provides theoretical summarization of derivative public opinion from a multidisciplinary perspective. For example, some scholars described the propagation mode of derived public opinions in social networks through the epidemiological model and explained the reason why expert intervention and government action cannot play a role from the perspective of time delay [22]. From the perspective of competitive diffusion, some scholars also proposed network interruption strategy and balance strategy to deal with the spread of derivative public opinions in social networks, to control the derivative public opinions, and reduce the damage caused by negative public opinions such as rumors [23].

To sum up, the emergence of derivative public opinion has attracted the attention of all sectors of society and become a key topic of research by scholars. However, the current research on derivative public opinion mainly focuses on the formation reasons and countermeasures of the derivative public opinion, and there is a lack of sufficient exploration of the evolution of the derivative public opinion in the time scale. Therefore, we introduce the time series model to analyze the evolution law of public opinion derived from emergencies in social networks from the perspective of time series, to make contributions to the governance of public opinion derived from emergencies and the maintenance of network order.

2.2. Topic Research on Network Public Opinion. With the development of the Internet and information technology, people have become accustomed to getting information from social media. However, the complexity and diversity of information in social media make it more difficult for us to find the information we want. Using the topic discovery method to analyze topics from event news can not only help people better understand the occurrence and evolution of the event but also analyze the issues of public concern and understand the public opinion and focus. Therefore, the analysis method of topic discovery has attracted the attention of many scholars and has been widely applied in the related research of online public opinion [24].

At present, the topic research of online public opinion on emergencies mainly focuses on the topic discovery and transmission evolution of online public opinion. Among them, the topic discovery of network public opinion is mainly aimed at the identification of the unexpected event topic in social networks, or the improvement and optimization of the accuracy of the prediction model based on the original model. Cluster analysis and topic models are usually adopted in the research. The former is mainly based on the clustering assumption that the similarity of documents of the same class is large and the similarity of documents of different classes is small, and then the text information is transformed into digital information and processed by the machine learning method. For example, some studies use the large-scale text data in social media to detect the tweet event

monitoring system based on subdivision and, based on considering the frequency distribution and the similarity of information content, detect the tweet segments of emergency events as event fragments and then cluster the event fragments into the events to realize the identification of relevant events [25]. There are also studies on the use of machine learning clustering algorithms to identify topic trends in social media and provide meaningful analysis to synthesize accurate descriptions of each topic [26]. The latter is based on the topic discovery tool widely used in text mining to automatically find the potential hidden topics and model them from the large-scale text data. The most widely used model is LDA (Latent Dirichlet Allocation) model and its improved model [27]. For example, the LDA model is used to detect and classify the evolution of topics in social networks when public health emergencies occur [28]. Based on the LDA model, TS-LDA (Trend Sensitive-Latent Dirichlet Allocation) model is proposed to extract potential topics from text information more effectively [29].

The transmission evolution of network public opinion mainly focuses on the communication mechanism and evolution law of emergency topics in social networks. Through the analysis of large-scale social media data, it tries to depict the communication path of event topics in social networks based on the evolution model. Relevant researches focus on establishing the evolution model of the emergency topic in the social network or realizing it by dividing the evolution life cycle of the emergency topic in the social network. For example, based on the OLDA (Online LDA) topic evolution model, combined with the correlation between topics in different time segments, the topic evolution of online public opinion has been effectively tested [30]. Some studies combine the LDA model with the improved Birch hierarchical clustering method to propose a new text enhancement strategy, to expand the content of social media with short text characteristics, and then extract the topic evolution characteristics of network public opinions [31]. In addition to the research based on topic models such as LDA, some scholars had also introduced social network analysis method to construct topic evolution model based on the network matrix formed by forwarding relationship and further explored the interaction and evolution mechanism of event topics under the influence of environment in the communication of public opinion [32]. In addition, the evolution of the topic of emergencies in the life cycle has also attracted the attention of many scholars. For example, based on the amount of information about the event topic in different periods, the evolution of online public opinion is divided into four stages: initial stage, outbreak stage, decline stage, and end stage [33]. Or based on the nature of the events, such as choosing a public health emergency as the research object, the network public opinion is divided into different stages according to the local evolution of the virus and hot trends [34]. Some studies also analyze the propagation characteristics of emergencies in different life cycle stages, such as propagation period, control period, and stable period, by simulating the time evolution process of multiple emergencies in social networks [21].

To sum up, the topic research of network public opinion is relatively mature and has achieved good results, but few studies take the topic of derived public opinion as to the research object. Given this, we take the derived public opinion as to the research object, explore the propagation evolution law of the derived public opinion topic, and compare and further explore the derived public opinion law of different types of emergencies.

2.3. Sentiment Research on Network Public Opinion. With the development of Internet technology, the public has become accustomed to using social media in their daily life. Through the extraction of users' posts, comments, tweets, blogs, discussions, and other content in social media, we can analyze the opinions and attitudes of social media users and then infer the individual sentimental trends and behavioral preferences [35]. This method of analysis is often referred to as sentiment analysis, sometimes also referred to as viewpoint analysis, opinion mining [36]. As a branch of natural language processing, it is widely used in information retrieval, text mining, and other fields [37]. For example, based on the test set, relevant researchers conduct retrieval evaluation by making use of the correlation judgment of information objects and topics, to verify the validity and reliability of the information collected by the test set in the retrieval evaluation [38]. In addition, there are also studies based on social network analysis methods to conduct sentiment analysis on the large-scale text data of emergencies in social networks, to understand the communication structure and characteristics of event content [39].

Similar to topic research, transmission evolution is also the focus of online public opinion sentiment research. The sentiment research of network public opinion mainly focuses on two aspects, namely the influencing factors of sentiment and the evolution mechanism of sentiment. Based on the analysis of text information, we can not only understand what factors will affect sentiments but also understand the changes of sentiments in different times and spaces, to realize the analysis and prediction of sentiments. Among them, in the field of commercial products, the influence factor analysis of sentiment is most commonly used. For example, some studies divide the review text of mobile phone products on Amazon into emotions such as joy, sadness, trust, and anger, and understand the influencing factors of consumers' emotions through the analysis of the review text, to provide feedback for mobile phone manufacturers [40]. According to the content characteristics of product reviews, some studies are conducted to understand the influencing factors of user preferences in the reviews, to improve the effectiveness of user perception information in the shopping platform, and provide better suggestions for users in the choice of products [41]. In addition to the research on the influencing factors of emotion, we can also use the sentiment of users in social media to analyze the evolutionary transmission mechanism of network public opinion, to realize the prediction of emergencies. For example, based on the transference and infectivity of sentiment, scholars have used social media data to predict

national political elections based on sentiment analysis methods and achieved good results [42, 43]. Some scholars also used opinion mining and sentiment analysis to predict stock price indexes and trends based on public comments and opinions published on social media platforms [44, 45].

Before we can do sentiment analysis, we need to first categorize the sentiments. The commonly used research methods are mainly divided into two categories: sentiment classification based on sentiment dictionary and sentiment classification based on machine learning [46]. The former is mainly based on the meaning of words and phrases in the document to mark the sentimental direction of the document, through manual screening, based on the existing dictionary, or based on the method of corpus construction. For example, NRC Sentiment Dictionary is used to calculate the sentimental performance of news headlines in eight dimensions when an emergency occurs [47], or taking emergencies as an example, the method of point mutual information based on existing sentiment dictionaries is used to construct emoji dictionaries to calculate text sentiments [48]. The latter needs to use supervised, semisupervised, and unsupervised machine learning methods, such as support vector machine, Naive Bayes, and neural network, to classify sentiments based on labeled data as the training set. For example, SVM is used as a classifier to classify text data sets by mapping emojis and word vectors into sentiment space [49], or N-gram is used as the text feature and Naive Bayes as the classifier to identify the sentimental types of netizens [50]. With the development of deep learning technology, more and more studies use deep learning models as a classifier to replace the traditional machine learning model for sentiment analysis of short texts. For example, through the sentimental data analysis framework, the convolutional neural network is used to realize the recognition of different sentimental types on text, video, and other data [51], or based on the cyclic neural network, the long and short memory model (CLSTM) is introduced to make the cyclic neural network better store the sentimental information [52]. These studies have achieved good results, making deep learning one of the most popular methods in sentiment classification. The success of these studies has made deep learning one of the most popular methods of sentiment classification.

To sum up, the study of online public opinion by using sentiment analysis has always been a hot topic of research. However, the difference of sentimental evolution in the social network by comparing derivative public opinion of different emergencies with derivative public opinion as the research object has received less attention from scholars. Given this, we combine the deep learning method to classify sentiments and attempt to make further study on the sentimental evolution of derived public opinions in social networks based on time series analysis. In addition, we also compare and explore the law of public opinion derived from public health events and other types of emergencies.

3. The Proposed Methodology

In this part, we introduce the research methods used in the study and mainly build three models, namely, the topic identification of online public opinion, the sentiment classification of online public opinion, and the time series model of online public opinion. In the topic identification model, the research mainly used the Word2Vec word vector model to convert text data into word vectors and then used the clustering method to realize topic identification. In the sentiment classification model, the biLSTM model was mainly used to realize the identification of text sentiment based on the training set, and it was divided into positive and negative sentiment types. In the time series model, the research mainly used the ARIMA model to make topic-sentiment analysis of public opinion derived from emergencies and further compared different types of emergencies, to explore the evolutionary commonalities and differences between the public health event and other types of emergencies on temporal networks. In this section, we will briefly introduce the principle and advantages of the Word2Vec word vector model, biLSTM sentiment classification model, and ARIMA time series model.

3.1. The Construction of Topic Identification Model.
Social media provides a convenient channel for people to understand the information related to emergencies. However, the large scale of network data, the large amount of useless information, and the existence of noise make it more difficult to extract effective information. To timely and accurately discover important information, the topic identification method has been widely used in event detection and information extraction of social media [53]. However, in social media platforms such as Twitter and Facebook, which are dominated by short text information, the traditional topic identification model represented by LDA is not applicable, and the effectiveness of topic identification cannot be well guaranteed [54]. As a typical topic model, LDA mainly uses the soft clustering method to cluster documents and, through the study of document matrix, realizes topic clustering by using the cooccurrence relationship of words in documents. However, when the topic model is applied to short text documents, the problem of sparse data often occurs. Specifically, on the one hand, the number of words in short documents is smaller than that in long documents, so it is difficult for the model to distinguish the document semantics by a small number of words. On the other hand, the number of contexts in short texts limits the application of the model, making it difficult for the thematic model to accurately identify the meanings of ambiguous words. To further improve the accuracy of topic recognition, researchers proposed a series of topic identification and text mining methods based on deep learning, among which the most representative model is Word2vec, which can generate word vectors and is represented by a shallow and two-layer neural network structure [55]. Compared with the topic model represented by LDA, Word2vec is mainly expressed as the word embedding model with neural network structure. By learning context-word matrix, words are converted into word vectors, which shows better results in topic recognition of short text information.

Word2vec word vector model can be regarded as a simplified neural network model. Firstly, the text is

processed by using a shallow neural network, and based on using a large data set as a training set, the relationship between words and context is obtained. Secondly, the semantic of the word is mapped to the vector space, and the word is transformed into a distributed word vector by representing it as a similar semantic word [56]. Among them, word vector training of the Word2vec model is mainly completed by the Skip-Gram model and Continuous Bag-of-Words (CBOW) model. The difference is that the former mainly realizes the prediction of the context words through the semantics of the current word, while the latter mainly realizes the prediction of the current word through the semantics of the context. Although the Skip-Gram model is more accurate in obtaining word vectors of all texts after traversing all texts, the CBOW model has been adopted by researchers for its higher efficiency and faster speed in the analysis of large-scale social media data sets [57]. Considering that this paper adopts a relatively large data set, we use the CBOW model to carry out topic analysis on the public opinions derived from emergencies.

As a shallow neural network model, the CBOW model is composed of the input layer, projection layer, and output layer. It is a word bag model formed based on continuously distributed word representation methods [58]. The objective function of the CBOW model is usually expressed as a logarithmic likelihood function, as shown in (1), where C represents the objective function of the model, w is the central word to be studied, and n is a given sequence of training words, which means that n words are taken before and after the central word w.

$$C = \sum_{w \in n} p(w|\text{Context}(w)). \tag{1}$$

The CBOW model is a prediction of the central word based on the context words with a probability of $p(w_i|\text{Context}(w_i))$. Assume that T is the number of training words in the corpus, and $\omega_{w(t)}$ is the t the component value of vector ω. Based on the context information of the central word w_i, the model combined with softmax function for normalization calculation and finally generated the vector value of w_i. The specific calculation is shown in

$$p(w_i|\text{Context}(w_i)) = \frac{\exp(\omega_{w(i)})}{\sum_{t=1}^{T} \exp(\omega_{w(t)})}. \tag{2}$$

The structure of the CBOW model is shown in Figure 1. Firstly, the model enters the context word of the target word and passes it to the embedding layer initialized with random weights. Secondly, the model transfers the word embeddings of the context words to the lambda layer to obtain the averaged word embeddings. Thirdly, we pass the averaged word vectors to the dense layer and match the predicted words with the target words based on the prediction of the target words by the softmax function. Finally, loss calculation and embedding layer updating are implemented by categorical cross-entropy and back-propagation, respectively.

3.2. The Construction of Sentiment Classification Model.
In recent years, sentiment classification models based on deep learning have achieved good results in tests and have been widely applied [59]. Among them, in natural language processing studies that have requirements on the length of input variables, recurrent neural networks (RNN) have become an important tool in the field of sentiment analysis by the high efficiency of information processing [60]. In this study, a bidirectional long short-term memory model was used to realize sentiment classification based a recurrent neural network.

The long short-term memory model, as a variant of the recurrent neural network, is widely used in sentiment analysis. On the one hand, it is because the design structure of the model can capture remote dependencies and solve the short-term memory problem of traditional recurrent neural networks. On the other hand, it can not only consider the order of text data but also save or delete information in the training process, so it has a great advantage in the processing of sequential text data. The realization of the model is mainly divided into three stages: selective memory, forgetting, and output stage. Selecting memory is the input stage, selectively recording input information. The forgetting stage is the second extraction of information, forgetting unimportant information and recording important information, to achieve the selection of information recording. The output phase determines what information is ultimately output into the current state.

Corresponding to the implementation stage of the model, the long short-term memory model selects information through the "gate" to realize the selective passage of information. The structure of the model is composed of an input gate, forgetting gate, output gate, and memory unit. The model mainly realizes the selection of information to be forgotten through the forgetting gate, and the specific formula is shown in (3). The symbol of forgetting gate is represented by f_t, σ is the activation function, W_f and b_f, respectively, represent the weight and standard deviation of forgetting gate, h_{t-1} represents the hidden state at the previous moment, and μ_t represents the input of text information at the current moment.

$$f_t = \sigma(W_f h_{t-1} + W_f \mu_t + b_f). \tag{3}$$

The input gate is corresponding to the selected memory stage of the model, which mainly determines the input of text information and realizes the preservation of memory information. The specific calculation equation is shown below, where i_t represents the input gate, $\tilde{C}_t$ represents the temporary memory unit, W_i and b_i respectively represent the weight and standard deviation of the input gate, W_C and b_C respectively represent the weight and standard deviation of the memory unit, and C_{t-1} represents the memory unit of the previous moment.

$$\begin{aligned} i_t &= \sigma(W_i h_{t-1} + W_i \mu_t + b_i), \\ \tilde{C}_t &= \tanh(W_C h_{t-1} + W_C \mu_t + b_C), \\ C_t &= C_{t-1} f_t + \tilde{C}_t i_t. \end{aligned} \tag{4}$$
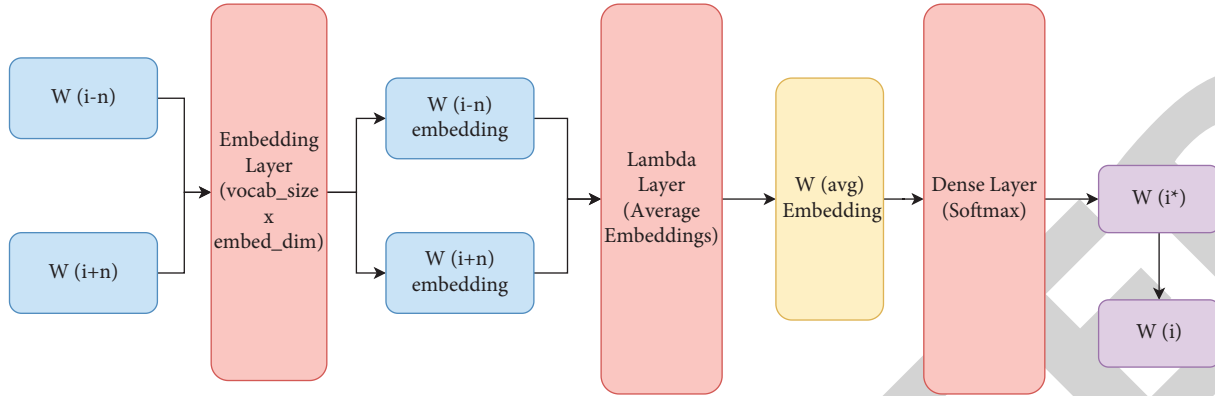
FIGURE 1: The structure of the CBOW model.

Similar to the input gate, the output gate corresponds to the output stage of the model and mainly determines the output of the text information in the memory unit at the next moment. The specific calculation equation is as follows, where the output gate is represented by the symbol o_t, the memory unit is represented by the symbol C_t, W_o and b_o represent the weight and standard deviation of the output gate, respectively, and h_{t-1} and h_t represent the hidden state of the memory unit at the previous moment and the current moment, respectively.

$$
\begin{aligned}
o_t &= \sigma\left(W_o h_{t-1} + W_o \mu_t + b_o\right), \\
h_t &= o_t \tanh\left(C_t\right).
\end{aligned}
\tag{5}
$$

Long short-term memory model can effectively process sequential text and solve the short-term memory problem of recurrent neural networks, which has been recognized by many scholars. However, the LSTM also has some defects. It can only process data from the front to the back, ignoring the backward feature of text information and being unable to encode information from the back to the front. Therefore, to further improve the accuracy of the classification effect, we adopted the bidirectional long short-term memory model to achieve the sentiment classification work in this paper. The bidirectional long- and short-term memory model is composed of two forward and backward long- and short-term memory models, including all forward and backward information. It can complete the learning of sequence data from both front and back directions and, finally, get the output results with more accuracy. The model structure is shown in Figure 2 below. Firstly, the model inputs text data in the pretraining embedding layer and transform it into word vectors. Secondly, the forward and backward LSTM models are used to obtain the information before and after the word vectors, and then they are spliced. Finally, the complete information is input into the softmax function layer to output the probability distribution of positive and negative sentiments based on the function prediction.

3.3. The Construction of Time Series Model.

Time series is a sequence formed by ordering the observation values of the same object in the order of time. The purpose is to use the

existing historical data to predict future data [61]. To realize the prediction of observations, stochastic and dynamic models based on time series data have been established. Common models include Autoregressive (AR), Moving Averages (MA), and Vector Auto-Regression (VAR), as well as Auto-Regressive Moving Average (ARMA) and Auto-Regressive Integrated Moving Average (ARIMA) models based on AR and MA models. Compared with other models that directly use the past value to predict the future value, the ARIMA model first weights the past data and corrects the error value, showing a better prediction effect, so it is widely used in time series analysis [62]. Based on existing studies, this study mainly uses the ARIMA model to realize topic-sentiment evolution analysis of public opinion derived from emergencies and then explores the internal formation and propagation rules of public health emergencies and other three kinds of emergencies.

ARIMA model is a composite model based on time series, where AR refers to the autoregressive model, and it mainly makes regression predictions based on the correlation between lag data and observed data. p is used to represent the number of autoregressive items. We refer to Integration and it is expressed as a single integer order. At the same time, it is also the number of times of making the time series stationary and making a difference. The stationarity of the time series is maintained by measuring the observed values in different periods, where the number of differences for the stationary time series is usually represented by d. MA refers to the Moving Averages model which measures the correlation between the observed value and the residual term, where the number of moving average items is often expressed by q. Therefore, ARIMA (p, d, q) is also commonly used in research to represent the autoregressive differential moving average model [63].

The basic principle of the ARIMA model is to approximate the data change of the observed object in time through mathematical methods and realize the prediction of the future based on the fitting of historical data. The general p order Autoregressive (AR) model equation is shown in (6). Among them, the stationary data series is represented by z_t, the autoregressive coefficient is represented by φ_n, ω_t represents the random error term of the time series, also known as the white noise series, and c represents the constant.
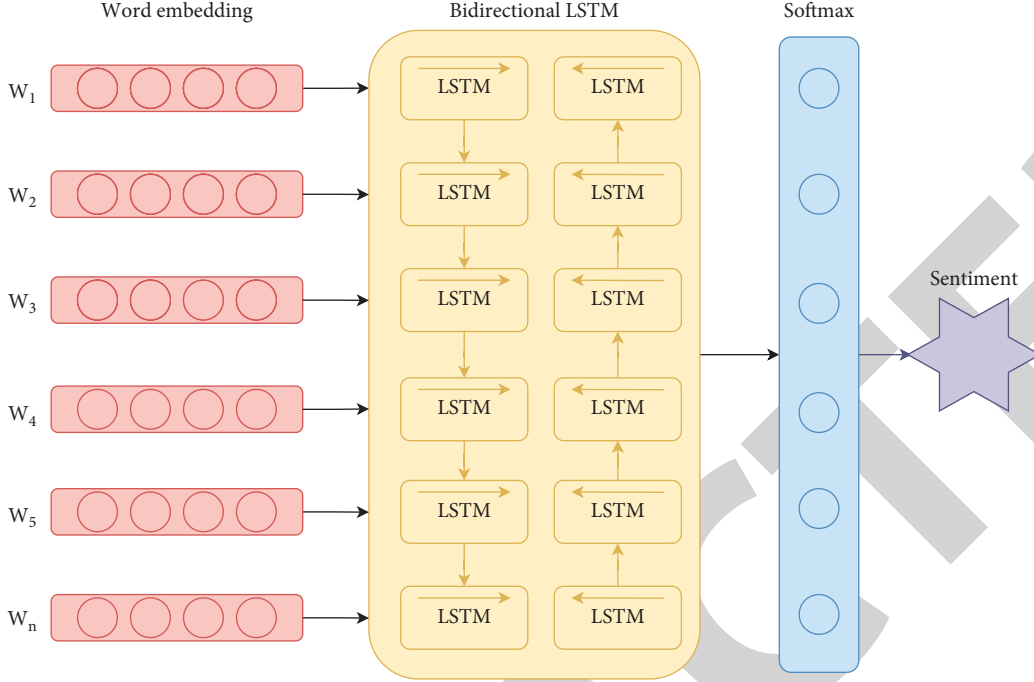
FIGURE 2: The architecture of the biLSTM model.

$$z_t = c + \sum_{n=1}^{p} \varphi_n z_{t-n} + \omega_t. \tag{6}$$

The Moving Averages (MA) model equation of order q is shown in (7), where β_n represents the moving average coefficient, ω_t represents the white noise process of the time series, and ε represents the expectation of the stationary time series, which is usually assumed to be equal to 0.

$$z_t = \varepsilon + \sum_{n=0}^{q} \beta_n \omega_{t-n}. \tag{7}$$

ARIMA model is obtained by combining AR, MR model, and difference, and the model equation is shown in (8), where z_t' represents the data series after difference, to convert the nonstationary time into a stationary time series. The parameter p represents the order of the AR model, the parameter q represents the order of the MA model, ω_t represents the white noise sequence, and c represents the constant.

$$z_t' = c + \sum_{n=1}^{p} \varphi_n z_{t-n} + \omega_t + \sum_{n=0}^{q} \beta_n \omega_{t-n}. \tag{8}$$

The use of the ARIMA model to analyze the derivative public opinion in the time scale mainly involves the following steps. Firstly, the stability test of the derived public opinion should be carried out. If it is not stable, the nonstationary sequence should be converted into a stationary one using differential transformation or other methods. In this paper, we mainly use the graph method to check the stationarity of time series data. After the production of the time sequence map with the release time of microblog as the abscissa and the number of texts as the ordinate, it can judge whether the time series data are stable by observing the trend of the derived public opinions on temporal networks. Secondly, the form of the model is determined by the autocorrelation coefficient and partial correlation coefficient, and the parameters of the ARIMA (p, d, q) model are determined according to the fitting degree of the model. Finally, the white noise test is carried out on the residual sequence to judge the effect of extracting useful information from the model, to achieve accurate prediction of derived public opinion.

4. Research Design

In the study, we first captured the public health event as our main research object and then captured the microblog data sets of three different types of emergencies, the natural disaster, accident, and social security event, for comparative analysis. In addition, we complete the text preprocessing by removing stop words, word segmentation, and filtering text content. Secondly, we use Word2Vec and K-means clustering methods to extract the topics of various types of emergencies and divide the identified topics into original topics and derived topics and further obtain the derived topic data sets of each emergency through calculation. Thirdly, based on the training data set, we combined the bidirectional long short-term memory model to realize the sentiment classification of text information and divided it into two types: positive sentiment and negative sentiment. Finally, we use the time series analysis method to model the derived public opinion, explore the topic-sentiment evolution mechanism of the derived public opinion in public health events, draw the evolution map, and make a

comparison with other three kinds of emergencies to understand the commonality and difference of the evolution law. The research framework is shown in Figure 3.

4.1. Data Collection and Preprocessing.

The research mainly takes the public health emergency as the main research object and, through the comparison with other three kinds of emergencies, reveals the topic-sentiment evolutionary commonality and difference of public opinion derived from emergencies on temporal networks. Therefore, we selected four representative emergencies in recent years as our case materials and obtained data sources through Sina Weibo. Among them, we selected the case of "virus cruise ship" (the large-scale virus infection in Japanese luxury cruise ships) as our main research object in public health events. This is because it not only involves a massive viral transmission in a confined space, which has captured the world's attention, but it is also so typical of its relevance to COVID-19. In addition, the forest fire, gold mine explosion, and hostage-taking incident are selected as natural disasters, accidents, and social security cases, respectively.

Sina Weibo is one of the most representative and influential information interaction and exchange platforms in China. Similar to Twitter, Facebook, and other social media platforms, users share their experiences, express their views on events, and interact with each other on Weibo, thus building an information exchange and sharing network. Through the method of limited time and searching keywords, the researchers obtained the event posts and time information of the four types of emergency cases on the platform, which provided sufficient data support for our subsequent research.

Before data analysis, to further improve the efficiency of model operation and the accuracy of results, some data preprocessing steps need to be taken. First, we did a preliminary browsing of the data we obtained to remove invalid posts and filtered the text content through methods such as regular expressions. Second, we used the Jieba tool for word segmentation of Chinese text to solve the problem of lack of space in Chinese text compared with English text. Finally, to further process the invalid words in the text data, we used the HIT Chinese stop word table to label the part of speech and deleted the stop word.

4.2. The Design of Topic Identification Model.

Before using the Word2vec model to transform text information into a word vector, we first extract feature words through the TF-IDF model to reduce the interference of useless information and noise in text data. Based on weighted processing, we extract the 20 most important keywords from each text data and use them as corpus sets for word vector transformation. Second, we use the CBOW model in Word2vec to transform the word vector of the data set, convert the text into a word vector, and use the common text mining method k-means to cluster the text. Finally, we divide the extracted topics into different clusters according to the similarity between texts to realize the recognition of text topics.

After using Word2Vec word vector model and K-means clustering method to realize topic identification of text data, we divided the identified topics into original topics and derived topics according to the judgment criteria of derived events. In the existing studies, it is very common to detect derived events based on topic identification based on the clustering method [64]. Considering that the evaluation subjects involved in public opinions of emergencies in social networks are easy to identify, combining with existing studies, we regard the change of evaluation subjects as the criterion for the classification of original topics and derived topics. If the subject of evaluation in the topic has changed, the topic will be identified as a derived topic, and a data set containing the derived topic will be further established for analysis [65].

To analyze the derived public opinion, we need to establish the derived public opinion data set according to the identified topics. First of all, we need to give all text data corresponding topics according to the topic identification model to distinguish the text data of each event and divide it into data sets of different topics. Secondly, we use Q_m to represent the topics identified by the topic model and W_{mn} to represent the keywords of each topic. The sequence number of the topic is m, the sequence number of the keyword is n, and the topic (keyword) is Q_m (W_{mn}). For example, the first keyword of the first topic can be expressed as Q_1 (W_{11}), and the first keyword of the third topic can be expressed as Q_3 (W_{31}), etc. Thirdly, we use K_{mn} to represent the frequency of occurrence of a certain keyword n in topic m, and m values of K_{mn} can be obtained from any text data. Finally, we compare the K_{mn} value among different text data. The higher the value is, the more likely the text data is to belong to a certain topic, to obtain the data sets of the original topic and derived topic. After obtaining the data set of the derived topics, we counted the relationship between the time of microblog posting and the number of microblog postings in the derived topic data set, and then obtained the time-series data that can be analyzed.

4.3. The Design of Sentiment Classification Model.

In this paper, we mainly use the bidirectional long- and short-term memory model to realize sentiment classification, but before using the deep learning model for sentiment classification of text data, we need to train and test the sentiment classification model based on the test training set data of Weibo. Combined with the existing research, we use the public data set of microblog sentiment classification evaluation in 2013 and 2014 of the NLPCC International Conference as our model data set. We divide sentiments into two types: "positive sentiment" and "negative sentiment," among which positive sentiment includes emotions such as love and happiness, while negative sentiment includes emotions such as disgust, fear, anger, and sadness.

The reason why we choose the NLP&CC data set for training and testing is that the NLP&CC data set has been widely used in the training and evaluation of fine-grained Chinese sentiment classification models in recent years and has achieved good results [66, 67]. On the other hand, the
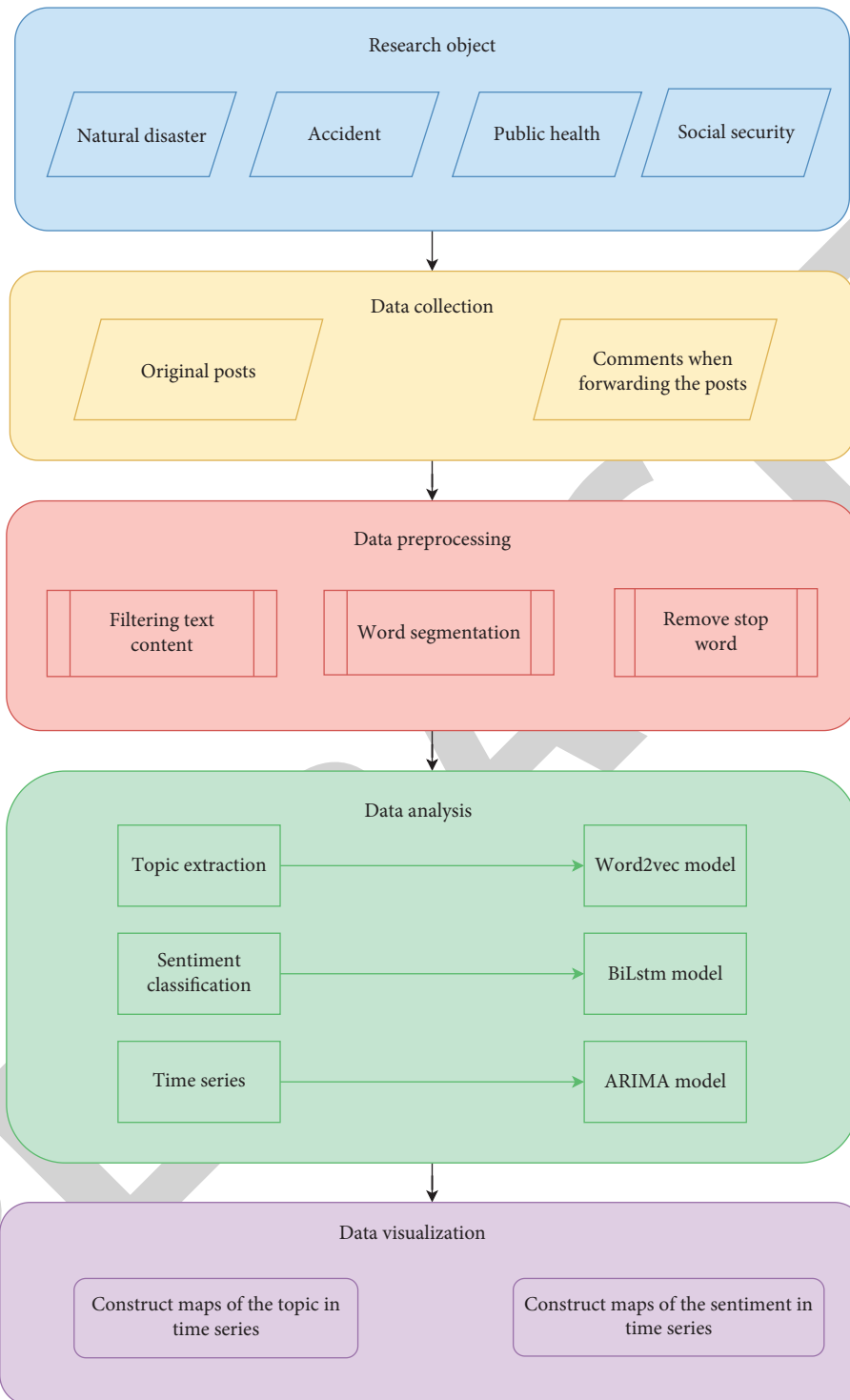
Figure 3: Research framework.

NLP&CC data set comes from the Sina Weibo platform, which is consistent with our data sources and is suitable for our sentiment analysis research. At the same time, considering that some new words that were not originally included in the training data set are now widely used, the corpus may change over time. Before adopting the biLSTM model to achieve sentiment classification, we randomly captured and filtered 200,000 microblogs, carried out pretraining by using the CBOW method, and obtained semantic representation and semantic similarity of words through the pretrained word embedding model. Therefore, when the input statement contains a word that does not appear in the training corpus but appears in the pretraining corpus, the prediction model can also grasp its sentimental meaning and

further improve the prediction accuracy and generalization ability of the model. After the pretraining of the sentiment classification model, we carried out sentiment recognition on the microblog data set, divided the microblog posts into positive and negative sentiment types, and assigned the corresponding sentiment labels to each text data. The accuracy of the model was 0.71, which met the needs of our research.

4.4. The Design of Time Series Model. To realize the topic-sentiment analysis of the derived public opinion on temporal networks, we used the ARIMA model to analyze the derived data set. Based on obtaining the data set of derived public opinion, the research mainly establishes a time graph with the number of texts as the ordinate and the time scale as the abscess, to observe the evolution of the topic and sentiment of derived public opinion in the time scale. Among them, the steps for obtaining topic-based time series data of derived public opinion are as follows.

First of all, topic clustering of text data is carried out through a topic identification model, and corresponding topic tags are assigned to each microblog. Secondly, we divide the topics identified by the topic model into original topics and derived topics and extract the text data containing all the derived topics according to the calculation method of the derived topic data set. Thirdly, we select a derived topic that needs to be analyzed, filtered, and extracted in the data set and establish the derived topic data set. Finally, we set up a two-dimensional coordinate graph according to the release time and text quantity of the derived topic data set to carry out the time series analysis of the derived topic.

The acquisition method of time series data based on sentiment-derived public opinion is similar to that of topic data. Firstly, sentiment classification is carried out on text data and a corresponding sentiment type is given to each post. Secondly, all text data containing derived topics are extracted according to the computation method of the derived topic data set. Thirdly, according to the needs of analyzing a certain sentiment type, the sentiment data set derived from the event is established by screening and extraction in the data set. Finally, according to the release time and the number of texts in the data set, the coordinate map is established to analyze the change of sentiment derived from public opinion on the time scale.

5. Results and Discussion

5.1. Descriptive Analysis of Data. In this paper, we take public health emergencies as the main research object and further explore the evolution mechanism of public opinions derived from public health events on temporal networks by comparing public health events with natural disasters, accidents and disasters, and social security events. We chose the "Japanese Virus Cruise" as a public health case, which occurred during the COVID-19 transmission. During the period of January and February 2020, 712 people of 3,711 crew members and tourists were infected and many died in an outbreak on a Japanese luxury cruise ship. At the same time, forest fire (March 30, 2019, to April 10, 2019), gold mine explosion (January 10, 2021, to February 5, 2021), and hostage taking (January 22, 2021, to February 10, 2021) were selected as natural disaster, accident disaster, and social security event cases. After the occurrence of these events, they all attracted the general attention of the public on the Weibo platform. The public carried out relevant discussions around the topic and formed a large amount of text data, which provided abundant analytical materials for our research.

Under the condition of the specified time, we crawled relevant data from the Weibo platform by searching keywords. For example, we crawled posts related to public health events on Weibo between January 19, 2020, and February 21, 2020, based on search keywords such as "COVID-19 virus cruise ship" and "cruise ship outbreak". The posts included users' comments on the event itself and interactions with other people's comments. Finally, the number of complete and valid posts reached 85,551. The number of posts of each emergency is shown in Table 1.

5.2. Derivative Public Opinion Data Set Based on Topic Identification. In this study, the Word2Vec word vector model was used to transform text data into vectors, and the K-means clustering method was used to realize topic identification. Considering that the main object of the study is the formation and development of derived public opinions, we only show the clustering results of public health emergencies in the following Table 2 and realize the identification of derived topics according to the judgment criteria of derived events.

According to the difference of K value, the results of K value clustering will also change greatly. Combined with data volume and data content, we chose the appropriate K value to achieve text clustering. The clustering results are shown in Table 2. The text data of the public health emergency after clustering by the K-means method can be divided into 9 categories. Considering the limited space in the paper, we only show part of the keywords in the table. For example, topics 1 and keywords can be expressed as $Q_1\{W_{12}, W_{13}, W_{14}, W_{15}, W_{16}, \ldots, W_{1n}\}$, namely, the topic "police arrest sabotage resistance to disease" by {"eliminate," "arrest," "nuisance," "inspection authority," "police," "Jinan Municipal Party Committee," "playing mahjong," "industry"} as keywords.

In the topic clustering of the public health emergency, we can find that the topics together form the development vein of public health emergencies. For example, topic 3 "the latest news about a massive virus outbreak on ships" and topic 6 "cruise ship epidemic prevention and control are ineffective, becoming a disaster area" were the beginning of our selected public health events. COVID-19 spreads rapidly in the cruise ships during this period. Then topic 4 "medical personnel are on board to help infected people" and topic 9 "the government held a press conference to give details of the virus outbreak about the ship" represented the government's concern and response to this public health event. Topic 5 "people prayed for the safe return of those infected" and

TABLE 1: The number of posts of each emergency.

Event types	Microblog entries
Natural disaster	99612
Accident	110505
Public health	85551
Social security	101734

topic 8 "the public accused officials of shirking their responsibility" were not only the public's care and blessing for the infected people on the ship, but also the evaluation of the behavior of government officials in public health emergencies. Topic 1 "the police arrested those who were obstructing the fight against the epidemic," topic 2 "people called for a common fight against the epidemic," and topic 7 "the news media reported the situation of the epidemic" were divided into derived topics according to the judgment criteria of derived events because of the change of evaluation subjects.

Combined with the acquisition method of derived public opinion data sets, we can obtain the data sets of various topics in the public health emergency. For example, there were 2,308, 4,138, and 7,447 data on the topics of "the police arrested those who were obstructing the fight against the epidemic," "people called for a common fight against the epidemic," and "the news media reported the situation of the epidemic," respectively. In addition, we could also calculate the heat of each topic based on the proportion of the topic data set to the total data set. Among them, there were 85,551 data sets of public health emergencies, and the data quantities and heat ratios of each topic are shown in Table 3.

As can be seen from Table 3, among the topics after the clustering of the public health emergency, the topic with the highest popularity was "the latest news about a massive virus outbreak on ships," which had aroused the most heated attention and discussion in cyberspace. The topic with the least popularity was "cruise ship epidemic prevention and control is ineffective, becoming a disaster area," and the data set obtained was the least. This phenomenon showed that online public opinion was susceptible to the influence of the event itself in the transmission process, and the initial major progress of the event was easy to attract public attention, but with the passage of time and the impact of other news it had weakened. Among the three topics derived from public opinion, the topic "the news media reported the situation of the epidemic" had the highest popularity, ranking second among all the topics. The topic of "the police arrested those who were obstructing the fight against the epidemic" and the topic of "people called for a common fight against the epidemic" had weakened in popularity, but they also ranked high among all the topics. On the one hand, this confirmed the importance of derivative public opinion, which had a broad scope of influence and a large degree of influence. On the other hand, from the perspective of content, it was also confirmed that derived topics played an important role in propaganda and guidance during the transmission of COVID-19 and lead to the differentiation of content in the transmission process.

To compare the differences between the spread of the public health emergency and other types of emergencies on temporal networks, we conducted topic clustering for different types of emergencies. In addition, we combined the number of topic data sets in each emergency to calculate the heat of the topic. The topic clustering and heat comparison results of various types of emergencies are shown in Table 4.

According to the transfer of evaluation subjects in the topics, the identified topics could be divided into original topics and derived topics. Considering the differences in the influence of various derived topics on temporal networks, we selected the two derived topic data sets with the highest topic popularity from each emergency for further analysis. The topic data sets derived from the natural disaster event were "guard mountains and rivers and guard homeland" and "salute every hero who carries the burden." Derived topic data sets of the accident included "a foreign trade dispute arose in the mineral trade" and "improve the system to prevent the recurrence of the tragedy." The derived topic data sets of the public health event were "the news media reported the situation of the epidemic" and "the public accused officials of shirking their responsibility." Derived topic data sets of the social security event were "protect fairness and justice and reduce tragedy" and "malignant incident caused the net friend onlookers."

5.3. Topic Analysis of Derived Public Opinions Based on Time Series. After obtaining the derived public opinion data set, we used the time series analysis method to analyze the extracted derived public opinions on the time scale. Considering that the period of all the data sets of public opinion adopted in the study lasted for about one month, it was not suitable for slicing with the unit of "day." In addition, to further refine the time scale and more intuitively show the evolution trend of derived public opinions, we finally chose to slice the time data in the unit of "three hours." The relationship between the release date and the number of posts in the data set was counted, and the analyzable time series data {time, time_number} were finally constructed.

The specific steps of time series analysis were as follows. Firstly, we imported the sliced post publishing time and number data {time, time_number} into the analysis software and observed the stationarity through the observation of the sequence diagram. Secondly, since the acquired data were all nonstationary series, we used the difference method to carry out the first-order difference and the second-order difference respectively to make the data stable. It was found that the second-order difference is more suitable for the data obtained by us, and the data after the difference was transformed into a stationary time series. Thirdly, we carried out autocorrelation and partial correlation tests on the data after difference and determined the values of coefficient p and coefficient q in the ARIMA model by combining ACF autocorrelation diagram and PACF partial correlation diagram. Finally, the results of ARIMA models with different coefficients were compared, and the appropriate coefficients were selected to draw the formation and evolution graphs of each derived topic on temporal networks. The ARIMA model test results of each derived topic are shown in Table 5. The overall fitting effect of the model is represented by

TABLE 2: Topic clustering of the public health emergency.

No.	Topic	Keyword
1	The police arrested those who were obstructing the fight against the epidemic	Eliminate, arrest, nuisance, inspection authorities, police, Jinan municipal party committee, playing mahjong, industry
2	People called for a common fight against the epidemic	Together voice, power, advice, conviction, total amount, complete, colleges and universities, having been square, each way
3	Latest news about a massive virus outbreak on ships	Latest news, docked, new coronet, passenger, infection, confirmed, risk, patient, crew, institute
4	Medical personnel are on board to help infected people	Unknown, number, critical, patient, CDC, team healing, sea, deterioration, body
5	People prayed for the safe return of those infected	Home country, thanks, family members, science, coping, disaster, crisis, family, family
6	Cruise ship epidemic prevention and control is ineffective, becoming a disaster area	Hard-hit areas, rescue teams, living hell, high incidence areas, drugs, find out, blacklist, suicide note, location
7	The news media reported the situation of the epidemic	huanqiu.com, TV, cases, reports, people's daily, infected persons, Japan broadcasting association, health department
8	The public accused officials of shirking their responsibility	Shirk responsibility, malpractice, flaunt, show, shine a magic mirror, empty talk, distinguish, hear, post
9	The government held a press conference to give details of the virus outbreak about the ship	Epidemic, media, journalists, proliferation, control, data, acknowledgment, press release, disclosure, epidemic

TABLE 3: Comparison of the number of posts and heat on various topics in the public health emergency.

Ranking	Topic	Microblog Number	The heat of the topic
1	Latest news about a massive virus outbreak on ships	49213	0.575
2	The news media reported the situation of the epidemic	7447	0.087
3	People prayed for the safe return of those infected	6499	0.076
4	The public accused officials of shirking their responsibility	6490	0.076
5	The government held a press conference to give details of the virus outbreak about the ship	6295	0.074
6	People called for a common fight against the epidemic	4138	0.048
7	The police arrested those who were obstructing the fight against the epidemic	2308	0.027
8	Medical personnel are on board to help infected people	1711	0.020
9	Cruise ship epidemic prevention and control is ineffective, becoming a disaster area	1450	0.017

stationary R^2, and the range of R^2 is 0-1. The closer the value is to 1, the better the fitting effect of the model will be. The information criterion of the model is represented by BIC, and the model is selected according to the fit degree of the model. In addition, the residuals of each model were not correlated, and the residuals of the time series data conformed to the distribution of random series, and there was no outlier, showing a good fitting effect.

According to the test results of the ARIMA model of each derived topic, as shown in Table 5, we established the measured and fitting graphs of the formation and evolution of each derived topic on temporal networks. The curves of actual and predicted values for each derived topic are shown in Figure 4, where the abscissa is the time of posting posts after slicing and the ordinate is the number of posts. Moreover, the red curve represents the actual value, the blue curve represents the predicted value, and the confidence intervals UCL and LCL are represented by the purple curve and the pink curve, respectively. In addition, Figures 4(a) and 4(b) respectively represent the derived topics with the highest and second-highest popularity among the topics of the natural disaster emergency. Figures 4(c) and 4(d) respectively represent the derived topics with the highest and second-highest topic

popularity in the accident event. Figures 4(e) and 4(f) represent the derived topics with the highest and second-highest topic popularity among the public health event, respectively. Figures 4(g) and 4(h) represent the derived topics with the highest and second-highest topic popularity among the social security event, respectively.

As can be seen from Figure 4, the two derived topics of the natural disaster event had an obvious "long tail effect" in the time series, and the heat of the event had an obvious outbreak phenomenon at the beginning of its occurrence, and it gradually flattened out over time. Among them, the mean value of the derived public opinion data in Figure 4(a) was about 514.08, the standard deviation was about 717.463, the maximum value was 3747, the minimum value was 0, the skewness was 2.440, and the kurtosis was 7.033. The data fluctuated violently and had the characteristics of sharp peak and right bias. The mean value of the derived public opinion data in Figure 4(b) was about 42.75, the standard deviation was 64.142, the maximum value was 394, the minimum value was 0, the skewness was 3.057, and the kurtosis was 12.358. The fluctuation of the data was still relatively severe, but it was a little gentle compared with Figure 4(a), and it had more obvious sharp peaks and right-skewed characteristics.

Table 4: Topic clustering and heat comparison of various types of emergencies.

No.	Topic	Data	Heat	Is it derivative?
N-1	The list of martyrs was announced	47759	0.480	No
2	Guard mountains and rivers, and guard the homeland	39412	0.396	Yes
3	The forest fire is under control	3816	0.038	No
4	Salute every hero who carries the burden	3424	0.034	Yes
5	Relatives commemorate the martyrs	1833	0.018	No
6	Remember the spirit of serving the motherland	1600	0.016	Yes
7	Internet users have been detained for insulting martyrs	1323	0.013	Yes
8	The citizens bid a tearful farewell to the martyrs	445	0.004	No
A-1	The survival of the trapped miners	47553	0.430	No
2	The public hoped for the safe return of the miners	32346	0.293	No
3	A foreign trade dispute arose in the mineral trade	14782	0.134	Yes
4	There was an explosion at the gold mine site	7545	0.068	No
5	The results of the accident investigation were announced	6342	0.057	No
6	Improve the system to prevent the recurrence of the tragedy	1057	0.010	Yes
7	Carry out the investigation and rectification of risks and hidden dangers	880	0.008	Yes
P-1	Latest news about a massive virus outbreak on ships	49213	0.575	No
2	The news media reported the situation of the epidemic	7447	0.087	Yes
3	People prayed for the safe return of those infected	6499	0.076	No
4	The public accused officials of shirking their responsibility	6490	0.076	Yes
5	The government held a press conference to give details of the virus outbreak about the ship	6295	0.074	No
6	People called for a common fight against the epidemic	4138	0.048	Yes
7	The police arrested those who were obstructing the fight against the epidemic	2308	0.027	Yes
8	Medical personnel are on board to help infected people	1711	0.020	No
9	Cruise ship epidemic prevention and control is ineffective, becoming a disaster area	1450	0.017	No
S-1	A hostage-taking incident took place in Kunming	47288	0.465	No
2	Protect fairness and justice, and reduce the tragedy	21844	0.215	Yes
3	The public prayed for the safety of the injured	15358	0.151	No
4	Details of the hijacking were relayed to the authorities	4876	0.048	No
5	The public discussed the specific circumstances of the hijacking case	4687	0.046	No
6	Malignant incident caused the net friend onlookers	3943	0.039	Yes
7	Formulate policies and improve relevant systems	2991	0.029	Yes
8	Discuss the offender's motive and condemn the offender	747	0.007	No

Table 5: ARIMA model test results of the topic data set.

Types	Model	Stationary R^2	BIC
N-01	ARIMA (5, 2, 7)	0.712	13.396
N-02	ARIMA (5, 2, 6)	0.686	8.773
A-01	ARIMA (12, 2, 14)	0.778	11.858
A-02	ARIMA (12, 2, 16)	0.819	3.816
P-01	ARIMA (8, 2, 3)	0.684	10.906
P-02	ARIMA (6, 2, 3)	0.682	8.566
S-01	ARIMA (3, 2, 1)	0.651	15.038
S-02	ARIMA (3, 2, 3)	0.475	10.822

According to the observation of Figures 4(c) and 4(d), it can be found that the derived topics of the accident emergency all passed a stable period before the outbreak, which was also consistent with the development of the event itself. Combined with the text data, the accident did not arouse public attention immediately after its occurrence but took a period of fermentation before it finally aroused public opinion. Among them, the mean value of the derived public opinion data in Figure 4(c) was about 73.97, the standard deviation was about 294.524, the maximum value was 3117, the minimum value was 0, the skewness was 7.673, and the kurtosis was 68.851. Moreover, the fluctuation range of the

data was large, and the characteristics of the peak were very obvious and skewed to the right. In Figure 4(d), the mean value of the derived public opinion data was 1.60, the standard deviation was 0.371, the maximum value was 47, the minimum value was 0, the skewness was 6.505, and the kurtosis was 49.248, showing obvious characteristics of sharp peak and right skewness, but the range of data changes was smaller than that in Figure 4(c).

Based on Figures 4(e) and 4(f), the variation of the derived topics of the public health event over time scales was reflected. Compared with other types of emergencies, the time-series images of the public health event showed unique characteristics. According to Figures 4(e) and 4(f), we can intuitively feel the difference in the propagation of derived topics. The former fluctuated more violently and experienced several successive periods of fluctuation, while the latter erupted more gently and discontinuously. Combining the textual data, we found that this was due to the nature of the selected public health event. The frequent occurrence of COVID-19 around the world and its great depredation had attracted more attention and discussion on the derived topic of "the news media reported the situation of the epidemic," and its popularity remained high. The change in the timing trend of the topic "the public accused officials of shirking
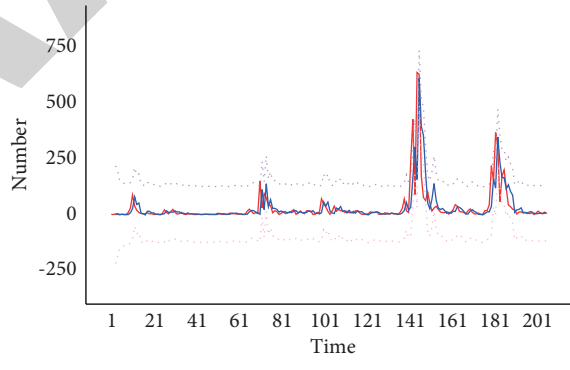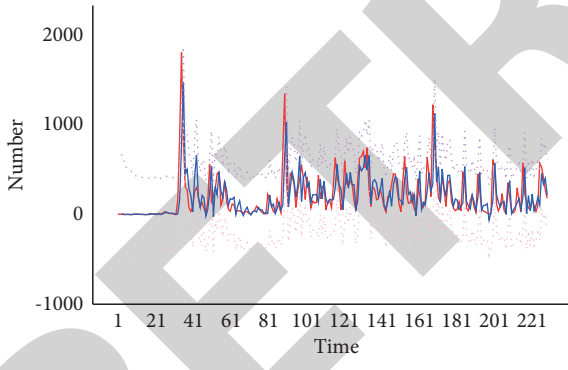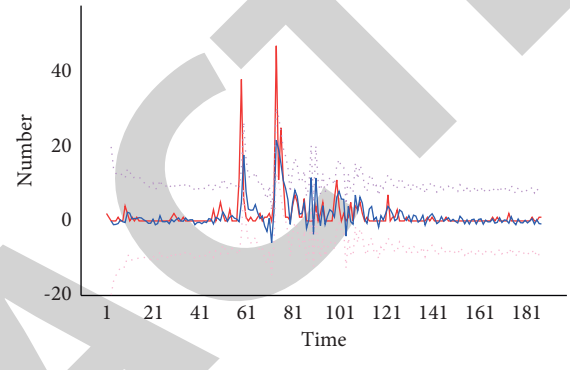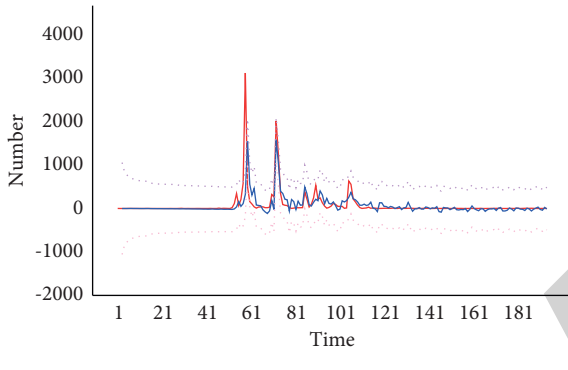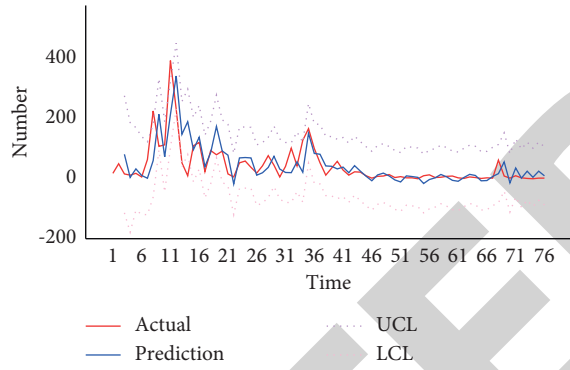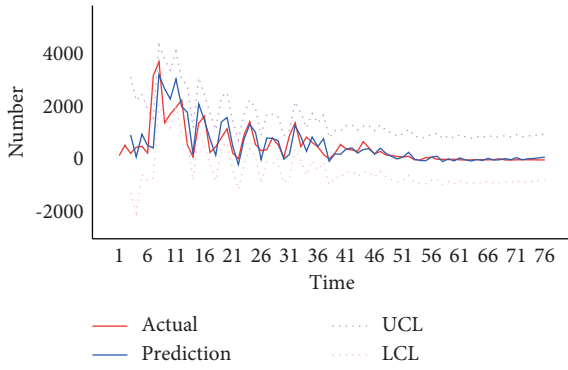
(a)

(b)

(c)

(d)

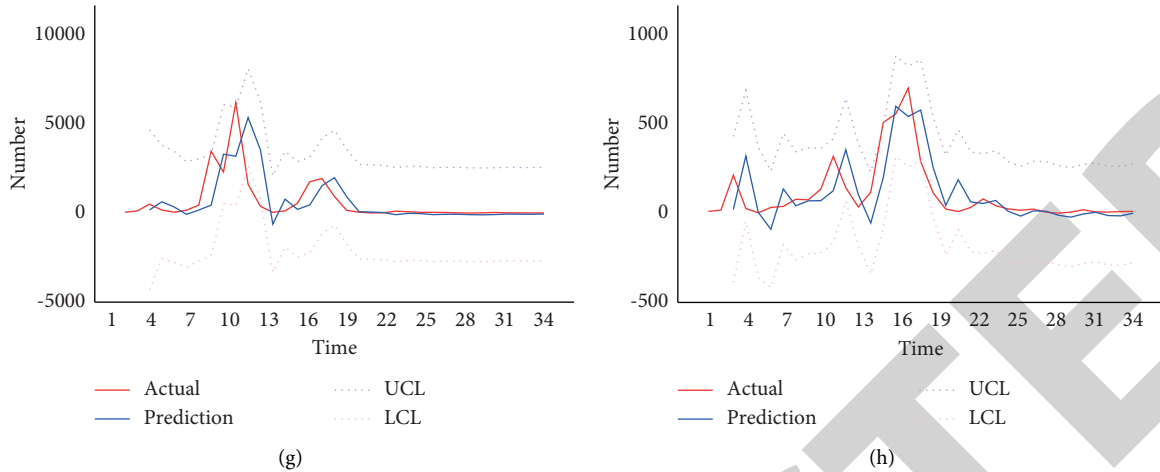(e)

(f)

Figure 4: Continued.

(g)

(h)

Figure 4: Actual and predicted values with ARIMA models in derivative topic. (a) Natural disaster 1. (b) Natural disaster 2. (c) Accident 1. (d) Accident 2. (e) Public health 1. (f) Public health 2. (g) Social security 1. (h) Social security 2.

their responsibility" was due to the influence of the press conference and the improvement of the way to deal with the epidemic, and the popularity did not last and gradually faded. In short, the reason why the opinion dissemination of public health events on temporal networks was different from other emergencies was mainly related to the characteristics of public health events themselves. Different from other emergencies, public health events tended to last for a long time and were prone to drastic changes under the influence of the external environment. In addition, compared with other events, public health events had a wider range of regional impacts, and the extent of impacts varied with the governance measures and environmental differences in different regions. In Figure 4(e), the mean value was 209.21, the standard deviation was 243.799, the maximum value was 1811, the minimum value was 0, the skewness was 2.494, and the kurtosis was 10.211. The data fluctuated sharply, with a large number of peaks, and had obvious right-skewness characteristics. In Figure 4(f), the mean value was 31.16, the standard deviation was 81.708, the maximum value was 634, the minimum value was 0, the skewness was 5.219, and the kurtosis was 31.352. Compared with Figure 4(e), the mean value was smaller and the fluctuation was relatively gentle, but the sharp peak and right skewness were more obvious.

Based on Figures 4(g) and 4(h), we can observe the changes of the derived topics of the social security event on temporal networks. Both of them experienced relatively intense fluctuations at the beginning of the event, and as time goes on, the heat gradually cooled down and the curve gradually became flat. In Figure 4(g), the mean value of the data was 140.55, the standard deviation was 646.252, the maximum value was 6208, the minimum value was 0, the skewness was 6.929, and the kurtosis was 55.914. The fluctuation of the data was relatively violent, and the feature of the peak was especially obvious, and it was right-skewed. In Figure 4(h), the mean value of the data was 7.511, the standard deviation was 92.606, the maximum value was 703, the minimum value was 0, the skewness was 5.319, and the

kurtosis was 30.702. Compared with the mean value of Figure 4(g), the fluctuation of the data was relatively gentle, and the characteristics of sharp peak and right skewness were not obvious.

5.4. Sentiment Analysis of Derived Public Opinions Based on Time Series. After sentiment classification of public opinion data sets by the biLSTM model, we gave each text data the corresponding positive sentiment or negative sentiment label and established a derivative public opinion data set through data screening. Then, we extracted the positive sentiment data set and negative sentiment data set from the derived public opinion data sets respectively and established the ARIMA model to analyze them on temporal networks. Among them, the ARIMA model test results of the sentiment data set derived from public opinion are shown in Table 6. In addition, we selected appropriate model coefficients to draw a map of the evolution of positive and negative sentiments derived from public opinion in the time series. The fitting degree of the selected model was higher than that of other coefficient values, which achieved better results, and also met the conditions that the residual sequence was uncorrelated and the outlier value was 0.

After determining the coefficients of the time series models of positive and negative sentiments, we drew the corresponding time series maps of public opinions derived from emergencies. For example, the evolution trend of positive sentiment derived from public opinion over time is shown in Figure 5. The legend was consistent with the time series of the topic. The red and blue curves represent the actual and predicted values, and the purple and pink curves represent the upper and lower limits of confidence intervals, respectively.

It can be seen from Figures 5(a) and 5(b) that the public opinion derived from the type of the natural disaster event had a relatively obvious positive sentiment fluctuation at the initial stage of the event, and it was relatively gentle as time goes on. Combined with the text material, it mainly came

TABLE 6: ARIMA model test results of the sentiment data set.

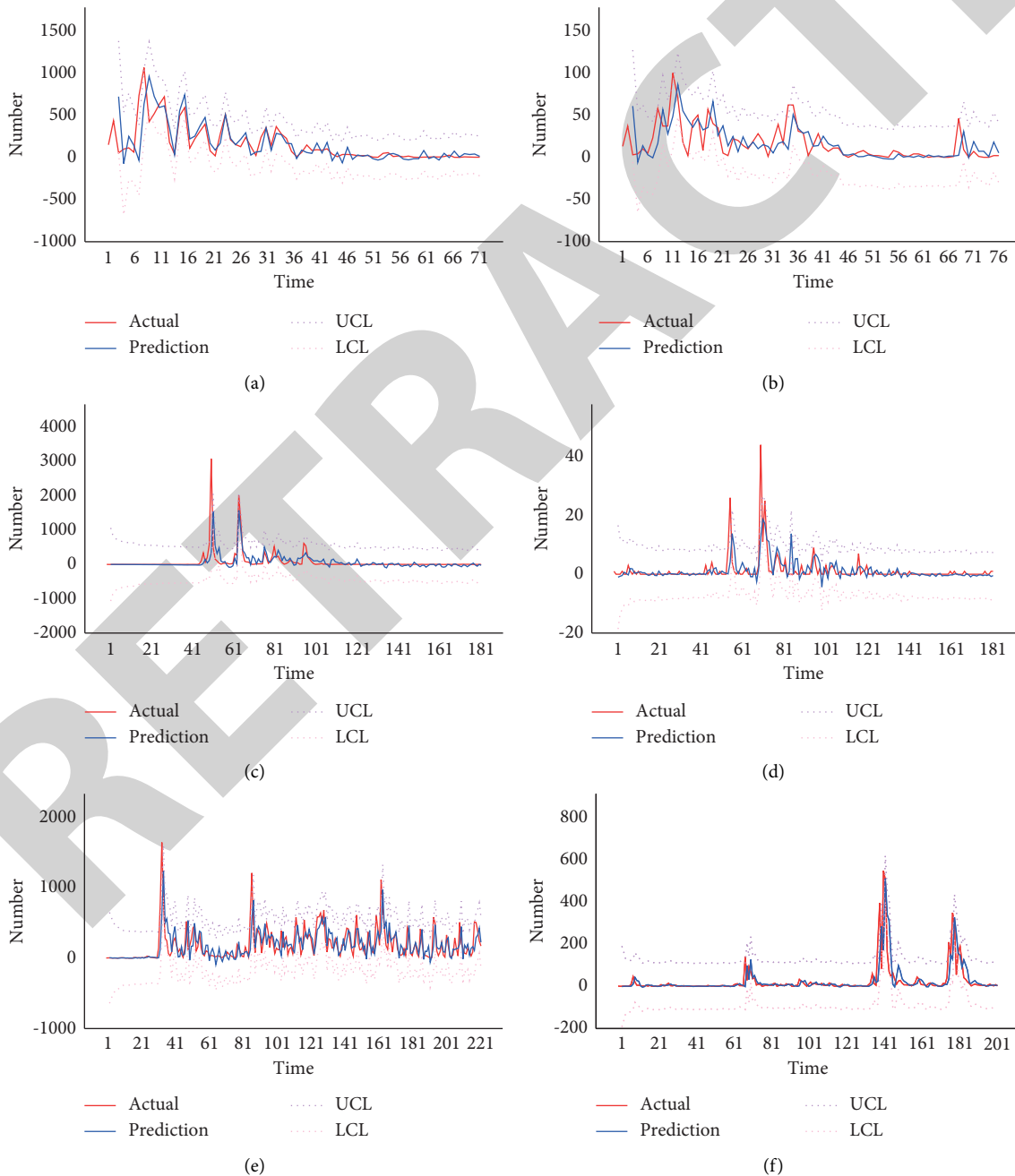| Types	Positive sentiment			Negative sentiment		
	Model	Stationary R^2	BIC	Model	Stationary R^2	BIC
N-01	ARIMA (6, 2, 16)	0.677	12.001	ARIMA (5, 2, 10)	0.707	12.862
N-02	ARIMA (6, 2, 3)	0.660	6.588	ARIMA (5, 2, 6)	0.656	8.026
A-01	ARIMA (12, 2, 14)	0.776	11.891	ARIMA (8, 2, 1)	0.707	2.717
A-02	ARIMA (12, 2, 16)	0.805	3.655	ARIMA (4, 2, 1)	0.717	1.086
P-01	ARIMA (10, 2, 8)	0.691	10.900	ARIMA (8, 2, 10)	0.694	6.378
P-02	ARIMA (8, 2, 1)	0.688	8.302	ARIMA (8, 2, 3)	0.676	4.906
S-01	ARIMA (4, 2, 2)	0.711	13.463	ARIMA (3, 2, 2)	0.650	13.907
S-02	ARIMA (3, 2, 1)	0.549	10.362	ARIMA (3, 2, 3)	0.450	7.313

(a)

(b)
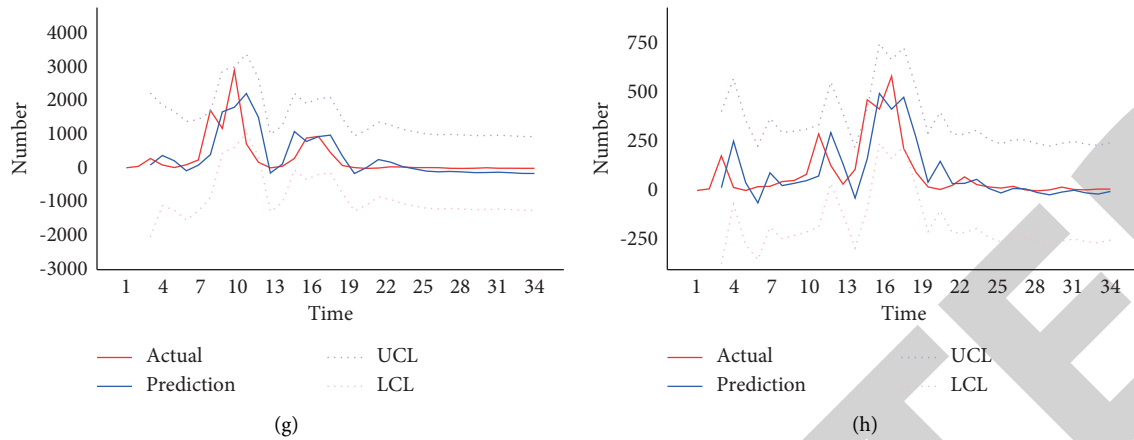
(c)

(d)

(e)

(f)

FIGURE 5: Continued.

(g)

(h)

Figure 5: Actual and predicted values of ARIMA model in positive sentiment. (a) Natural disaster 1. (b) Natural disaster 2. (c) Accident 1. (d) Accident 2. (e) Public health 1. (f) Public health 2. (g) Social security 1. (h) Social security 2.

from the public's respect and love for the heroes that emerged at the beginning of the event. Compared with Figure 5(a), the positive sentiment in Figure 5(b) formed a wave peak again at the end of time and became the focus of people's attention. This was because the announcement of the list of heroes suffering in emergencies at this time caused people to spontaneously form respect and gather positive sentiment.

According to Figures 5(c) and 5(d), it can be found that the sentimental evolution of public opinions derived from the accident was similar to the topic evolution map, both of which realized rapid outbreak after fermentation. Combined with the materials, the positive sentiment gathered at this time was mostly from the recognition of the emergency management department's handling speed and handling methods, as well as the admiration of the disaster victims' tenacious will to survive.

Based on Figures 5(e) and 5(f), we can observe the evolution of positive sentiment of the public health event in time series. The former formed a continuous outbreak of fluctuations in the transmission process, and the sympathy and encouragement of people around the world for the victims of the disaster became the mainstream of communication on social media. The latter had undergone a period of fermentation. It was not until the specific ways and arrangements of the event emerged that positive sentiment emerged from the public, which mainly focused on the prayers and wishes for the victims.

According to Figures 5(g) and 5(h), we can observe the evolution process of the positive sentiment of the social security event in the time series. The fluctuation trend of the two was relatively similar, both of which presented inverted "U" fluctuation at the initial stage of the outbreak of the event. The content of the material focused on the hope that public justice can be protected and the relevant system can be improved. Meanwhile, it was also the joy of the success of rescuing hostages and the recognition of rescuers.

When an emergency occurs, the distribution of negative sentiment derived from various public opinions in the time series is shown in Figure 6. From Figures 6(a) and 6(b), it can

be found that the negative sentiment change of public opinion derived from the natural disaster event in the time series presented an "M" shape and had a long tail effect. The burst curve of negative sentiment was similar to that of positive sentiment, both rising sharply at the onset of the event, but the difference was that the duration of negative sentiment was shorter than that of positive sentiment. Combined with the text, it may be related to the media propaganda content. At the initial stage of the event, relevant media publicity focused on the economic losses and human casualties caused by the natural disaster, but after the outbreak of the event, it focused on paying tribute to the heroes emerging from the emergency and praising the people's spirit of protecting their homes, which gathered more positive sentiment rather than negative sentiment.

Figures 6(c) and 6(d) show the change of negative sentiment in the time series of public opinions derived from the accident, which were similar to positive sentiment. The outbreak of negative sentiment was mainly concentrated in the intermediate stage after the occurrence of the accident, which was related to the lag of public attention caused by the accidents. With positive sentiment being different, negative sentiment also produced intense fluctuation change but far less than on a change in positive sentiment. This may be because, after the event, the rescue workers searched the relevant locations of the victims in time and made supplies, which weakened the formation of negative emotions such as anxiety and fear.

According to Figures 6(e) and 6(f), we can observe the negative sentiment change of public opinion derived from the public health event in the time series, and the trend of curve change was consistent with the positive sentiment. The curve of negative sentiment in Figure 6(e) fluctuated up and down continuously, while the curve of negative sentiment in Figure 6(f) formed a sharp outbreak trend after passing the lag period in the initial stage. Combined with the text, this may be determined by the nature of the study of the public health emergency. Although COVID-19 had brought heavy disasters to the people of the world, people were also inspired by the heroes emerging from the disasters. In addition, the
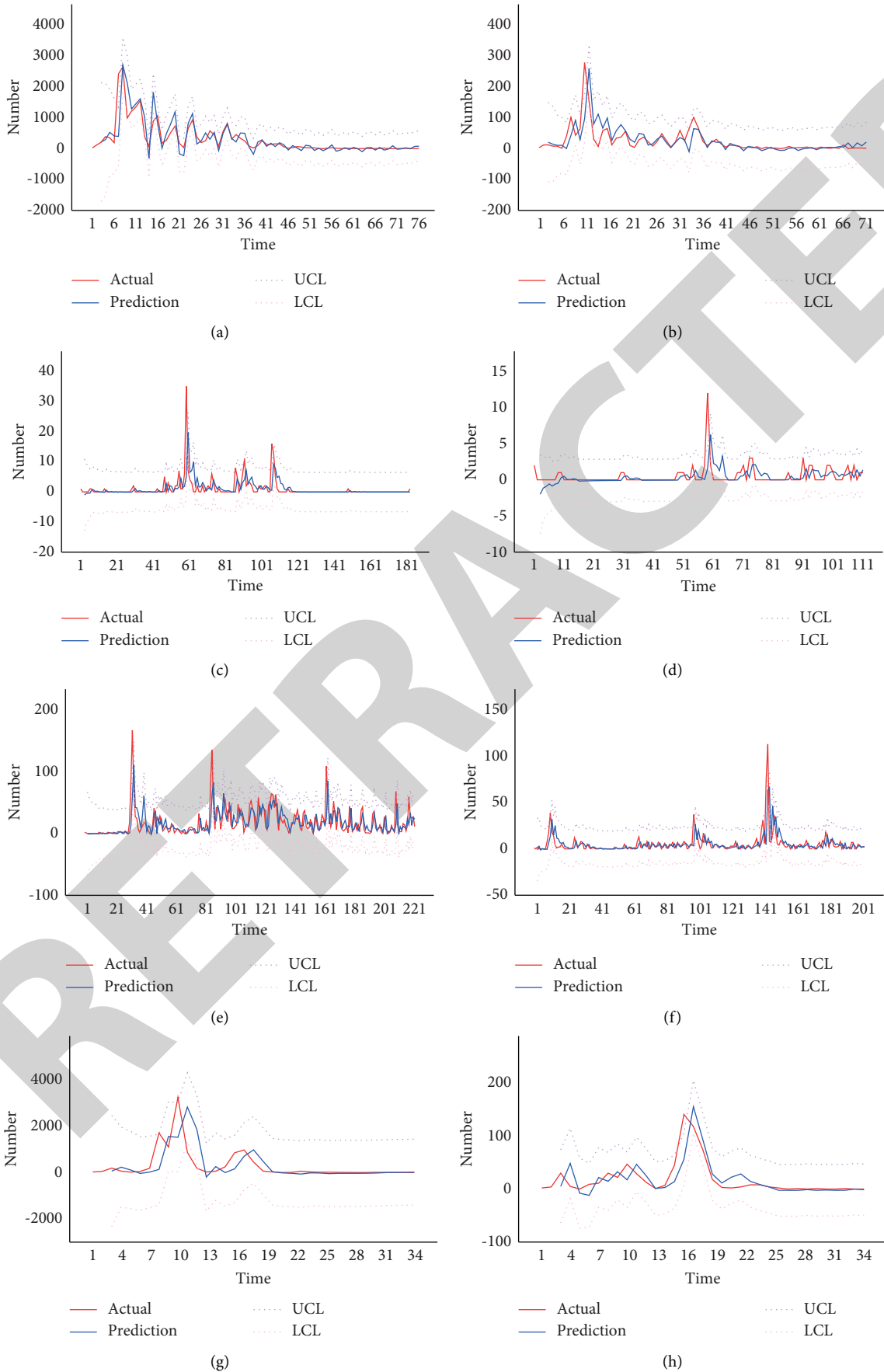
FIGURE 6: Actual and predicted values of ARIMA model in negative sentiment. (a) Natural disaster 1. (b) Natural disaster 2. (c) Accident 1. (d) Accident 2. (e) Public health 1. (f) Public health 2. (g) Social security 1. (h) Social security 2.
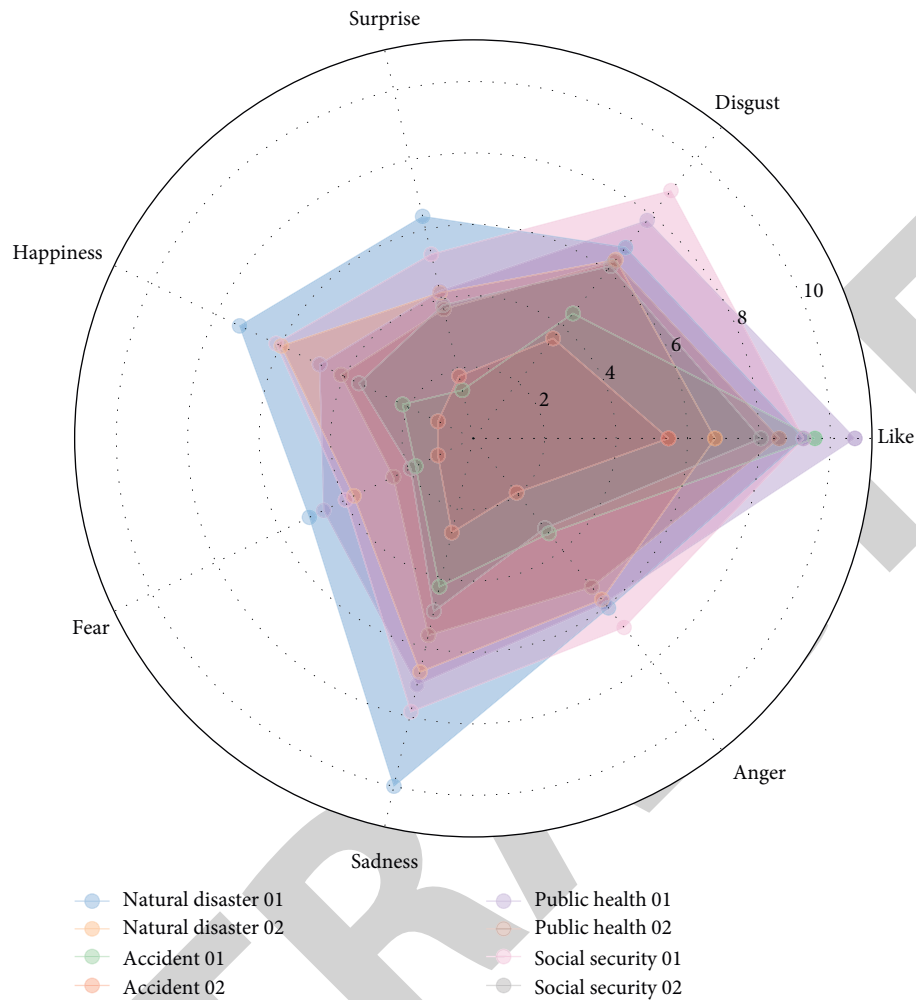
FIGURE 7: Multidimensional emotion radar diagram of public opinion derived from emergencies.

continuous overcoming of the epidemic management difficulties had brought confidence to the people, and positive sentiment and negative sentiment were accompanied by each other.

Based on Figures 6(g) and 6(h), it can be found that the emotional distribution of public opinions derived from the social security event in the time series was similar to positive sentiment, both of which showed an inverted "U" shaped trend. But the evolution curve of negative sentiment was steeper and more dramatic, and it was also associated with the rapid changes of social security events, which were less predictable. When the hostage taker made the corresponding action of threatening the hostage, the negative sentiment of the public was produced sharply and fluctuated accordingly.

Combined with the above analysis, we found that the evolution and distribution of public opinions derived from different types of events were significantly different in time series. Based on the topic analysis, it was found that influenced by the nature of events, the evolution of the derived topics of the public health event in time series was more volatile than that of other emergencies and fluctuated continuously with time. In addition, it also had a certain

continuity. This was also because the public health event was dynamic in time and a long-term process of continuous development. In space, it involved the vast majority of people and had a broader scope of time and space. From the sentiment analysis, it was found that the positive and negative sentiments of the public health event were similar to those of other emergencies, and both had a certain range of ups and downs. But more than any other emergencies, the emotional evolution of the public health event had spiked and revived rather than leveling off over time. At the same time, the occurrence curve of positive sentiment and negative sentiment in the public health event was closer, and the disasters brought by the epidemic caused people to continuously form negative sentiment. However, the formation of negative sentiment was not independent, and the emergence of heroes in the public health event and the good news of overcoming difficulties would also promote the generation of positive sentiment.

5.5. Emotional Distribution of Derived Public Opinion in Emergencies. To have a deeper understanding of the emotional dynamics of public opinions derived from

emergencies in social media, we further subdivided sentiments into seven emotion types: "like," "fear," "sadness," "surprise," "anger," "happiness," and "disgust," and used the radar chart to describe the distribution of each derived public opinion on different emotions. The details are shown in Figure 7. To facilitate the understanding of the graph, we took the logarithm of the number of microblogs containing different emotions.

As can be seen from Figure 7, in the derived public opinion of various emergencies, the emotion of like occupies a dominant position. Combined with the text materials, the emotion of like mainly came from paying tribute to the heroes who emerged in the emergency. Despite the huge material losses and casualties caused by all kinds of emergencies, the heroic deeds and the spirit of cooperation that emerged in the emergencies also brought hope to the public. Among them, compared with other emergencies, the distribution of public opinion derived from public health events was also in the first place. This may have something to do with the fact that the public health event was larger in scope and involved the largest number of people, resulting in the largest number of heroic acts and acts of resistance. Secondly, disgust and sadness played an important role in the derivative public opinion of all kinds of emergencies. Combined with the text materials, the aversion mainly came from the resistance of the public to the disaster and the resistance to some behaviors of seeking personal interests during the disaster. Much of the sadness came from mourning the loss of life. This finding also corresponds to our previous conclusion that the spread of derived public opinions in social media was accompanied by the spread of different emotions, and the distribution of emotions also helped us to further understand the influence of derived public opinions.

6. Conclusion

In this paper, the main research object of our study was the public health emergency, and through the comparison with the natural disaster, accident, and social security emergency, we revealed the evolution law of public opinion on temporal networks. Firstly, we used the topic clustering method to construct the topic model of emergencies and divided the identified topics into original topics and derived topics. Secondly, we extracted the derived topic data set according to the keywords of the derived topics and used the sentiment classification model to assign the corresponding sentiment labels to the text data. Finally, we used the time series model to analyze the formation and evolution rules of public opinions derived from emergencies and compared the topic-sentiment evolution rules of the public health event with other emergencies in common and different.

It is found that compared with other types of emergencies, the public opinions derived from the public health event had unique characteristics in the evolution of topics and sentiments. In the topic analysis, the public opinion derived from public health events had more obvious dynamic characteristics and fluctuated with time. Through sentiment analysis, it was found that the public opinion

curve derived from public health events had more spikes and did not gradually stabilize over time, but formed a new growth curve. But at the same time, combined with the text materials, it was found that the government's measures and media reports would deeply affect the fluctuations of public opinion derived from emergencies on temporal networks. The public not only paid attention to the development of original events but also paid great attention to the development of derivative public opinions. Through correlation analysis, we can have a clearer understanding of the propagation characteristics of derived public opinions on temporal networks. At the same time, it can also make a certain contribution to the emergency management of public opinion, reduce the public's negative emotions, and maintain the network order and society.

By using deep learning methods, we can more easily understand the propagation and evolution of public health events on temporal networks. However, there is still room for further development of the relevant research carried out by the deep learning method in this paper, such as selecting a more appropriate clustering model and classification model and selecting larger data sets for training. We will also take this study as a starting point and carry out further research in the future.

Data Availability

The data of this article are available from the corresponding author upon request.

Conflicts of Interest

The authors declare no conflicts of interest.

Acknowledgments

References

[1] L. Yijun, C. Sijia, H. Yuan, M. Ning, W. Guanghui, and N. Wenyuan, "The analysis and policy recommendations on the spread of network public opinion in major production safety accidents—a case study of the 8·12 Tianjin port explosion," *Management Review*, vol. 28, no. 3, p. 221, 2016.

[2] "UK government advice on definition of an emergency," 2007, http://www.ukresilience.info/upload/assets/www.ukresilience.info/15mayshortguide.pdf.

[3] "National overall emergency plan for public emergencies," 2006, http://www.gov.cn/jrzg/2006-01/08/content_150878.htm.

[4] K. H. Kwon, C. C. Bang, M. Egnoto, and H. Raghav Rao, "Social media rumors as improvised public opinion: semantic network analyses of twitter discourses during Korean saber rattling 2013," *Asian Journal of Communication*, vol. 26, no. 3, pp. 201–222, 2016.

[5] W. Zhang, M. Wang, and Y.-c. Zhu, "Does government information release really matter in regulating contagion-evolution of negative emotion during public emergencies? From the perspective of cognitive big data analytics," *International Journal of Information Management*, vol. 50, pp. 498–514, 2020.

[6] "Digital 2021: April global statshot," 2021, https://datareportal.com/reports/digital-2021-april-global-statshot.

[7] A. M. Aladwani, "Facilitators, characteristics, and impacts of twitter use: theoretical analysis and empirical illustration," *International Journal of Information Management*, vol. 35, no. 1, pp. 15–25, 2015.

[8] A. Sarcevic, L. Palen, J. White, K. Starbird, M. Bagdouri, and K. Anderson, "Beacons of hope" in decentralized coordination: learning from on-the-ground medical twitterers during the 2010 Haiti earthquake," in *Proceedings of the ACM 2012 Conference on Computer Supported Cooperative Work*, Seattle, WA, USA, 2012.

[9] Y. Kryvasheyeu, H. Chen, N. Obradovich et al., "Rapid assessment of disaster damage using social media activity," *Science Advances*, vol. 2, no. 3, Article ID e1500779, 2016.

[10] M. Li, J. Chen, T. Chen, and H. Yuan, "Probability for disaster chains in emergencies," *Journal of Tsinghua University Science and Technology*, vol. 50, no. 8, pp. 1173–1177, 2010.

[11] A. Lu and L. Qian, "A probe into secondary derived events of emergencies based on hot topic recognition," *Information and Documentation Services*, vol. 41, no. 6, pp. 26–35, 2020.

[12] R. Srivastava and M. P. S. Bhatia, "Real-time unspecified major sub-events detection in the twitter data stream that cause the change in the sentiment score of the targeted event," *International Journal of Information Technology and Web Engineering*, vol. 12, no. 4, pp. 1–21, 2017.

[13] D. Pohl, A. Bouchachia, and H. Hellwagner, "Automatic sub-event detection in emergency management using social media," in *Proceedings of the 21st International Conference on World Wide Web*, Lyon, France, 2012.

[14] E. Zhang and T. Li, "Research on public opinion countermeasures of incidents based on Weibo," *Intelligence Science*, vol. 12, pp. 94–98, 2016.

[15] O. Soffer and G. Gordoni, "Opinion expression via user comments on news websites: analysis through the perspective of the spiral of silence," *Information, Communication & Society*, vol. 21, no. 3, pp. 388–403, 2018.

[16] W. Liu, X. Wu, W. Yang, X. Zhu, and S. Zhong, "Modeling cyber rumor spreading over mobile social networks: a compartment approach," *Applied Mathematics and Computation*, vol. 343, pp. 214–229, 2019.

[17] L. Zhu and B. Wang, "Stability analysis of a SAIR rumor spreading model with control strategies in online social networks," *Information Sciences*, vol. 526, pp. 1–19, 2020.

[18] P. K. Srijith, M. Hepple, K. Bontcheva, and D. Preotiuc-Pietro, "Sub-story detection in twitter with hierarchical Dirichlet processes," *Information Processing & Management*, vol. 53, no. 4, pp. 989–1003, 2017.

[19] G. Bekoulis, J. Deleu, T. Demeester, and C. Develder, "Sub-event detection from twitter streams as a sequence labeling problem," 2019, https://arxiv.org/abs/1903.05396.

[20] Y. Liu and Y. Wang, "The generating and evolution of "secondary public sentiment" in public crisis: based on the focus on "8·12 Tianjin port explosion"," *Chinese Journal of Journalism & Communication*, vol. 9, pp. 116–133, 2017.

[21] S. Li, Z. Liu, and Y. Li, "Temporal and spatial evolution of online public sentiment on emergencies," *Information Processing & Management*, vol. 57, no. 2, Article ID 102177, 2020.

[22] A. Jain, J. Dhar, and V. Gupta, "Rumor model on homogeneous social network incorporating delay in expert intervention and government action," *Communications in Nonlinear Science and Numerical Simulation*, vol. 84, Article ID 105189, 2020.

[23] L. Yang, Z. Li, and A. Giua, "Containment of rumor spread in complex social networks," *Information Sciences*, vol. 506, pp. 113–130, 2020.

[24] X. Yan, J. Guo, Y. Lan, J. Xu, and X. Cheng, "A probabilistic model for bursty topic discovery in microblogs," in *Proceedings of the AAAI Conference on Artificial Intelligence*, Austin, TX, USA, 2015.

[25] C. Li, A. Sun, and A. Datta, "Twevent: segment-based event detection from tweets," in *Proceedings of the 21st ACM International Conference on Information and Knowledge Management, Association for Computing Machinery*, pp. 155–164, Maui, HI, USA, 2012.

[26] M. Mathioudakis and N. Koudas, "Twittermonitor: trend detection over the twitter stream," in *Proceedings of the 2010 ACM SIGMOD International Conference on Management of Data*, Indianapolis, IN, USA, 2010.

[27] S. Stieglitz, M. Mirbabaie, B. Ross, and C. Neuberger, "Social media analytics—challenges in topic discovery, data collection, and data preparation," *International Journal of Information Management*, vol. 39, pp. 156–168, 2018.

[28] L. An, C. Yu, X. Lin, T. Du, L. Zhou, and G. Li, "Topical evolution patterns and temporal trends of microblogs on public health emergencies," *Online Information Review*, vol. 42, no. 6, pp. 821–846, 2018.

[29] M.-C. Yang and H.-C. Rim, "Identifying interesting twitter contents using topical analysis," *Expert Systems with Applications*, vol. 41, no. 9, pp. 4330–4336, 2014.

[30] Y. Hu, L. Bai, and W. Zhang, "OLDA-based method for online topic evolution in network public opinion analysis," *Journal of National University of Defense Technology*, vol. 34, no. 1, pp. 150–154, 2012.

[31] A. Wang and J. Zhang, "Topic discovery method based on topic model combined with hierarchical clustering," in *Proceedings of the 2020 IEEE 5th Information Technology and Mechatronics Engineering Conference (ITOEC)*, Chongqing, China, 2020.

[32] H. Wei-dong, W. Qian, and C. Jie, "Tracing public opinion propagation and emotional evolution based on public emergencies in social networks," *International Journal of Computers, Communications & Control*, vol. 13, no. 1, pp. 129–142, 2018.

[33] J. Yamin, A. Lu, and L. Gang, "On the online information dissemination pattern of city emergencies," *Journal of Intelligence*, vol. 34, no. 4, pp. 91–96, 2015.

[34] J. Zhang, Y. Chen, Y. Zhao, D. Wolfram, and F. Ma, "Public health and social media: a study of Zika virus-related posts on Yahoo! Answers," *Journal of the Association for Information Science and Technology*, vol. 71, no. 3, pp. 282–299, 2020.

[35] A. Yadav and D. K. Vishwakarma, "Sentiment analysis using deep learning architectures: a review," *Artificial Intelligence Review*, vol. 53, no. 6, pp. 4335–4385, 2020.

[36] F. Hemmatian and M. K. Sohrabi, "A survey on classification techniques for opinion mining and sentiment analysis," *Artificial Intelligence Review*, vol. 52, no. 3, pp. 1495–1545, 2019.

WILEY | Hindawi

Retraction

Retracted: The Evolution Model of Public Risk Perception Based on Pandemic Spreading Theory under Perspective of COVID-19

Complexity

This article has been retracted by Hindawi following an investigation undertaken by the publisher [1]. This investigation has uncovered evidence of one or more of the following indicators of systematic manipulation of the publication process:

(1) Discrepancies in scope

(2) Discrepancies in the description of the research reported

(3) Discrepancies between the availability of data and the research described

(4) Inappropriate citations

(5) Incoherent, meaningless and/or irrelevant content included in the article

(6) Peer-review manipulation

The presence of these indicators undermines our confidence in the integrity of the article's content and we cannot, therefore, vouch for its reliability. Please note that this notice is intended solely to alert readers that the content of this article is unreliable. We have not investigated whether authors were aware of or involved in the systematic manipulation of the publication process.

Wiley and Hindawi regrets that the usual quality checks did not identify these issues before publication and have since put additional measures in place to safeguard research integrity.

We wish to credit our own Research Integrity and Research Publishing teams and anonymous and named external researchers and research integrity experts for contributing to this investigation.

The corresponding author, as the representative of all authors, has been given the opportunity to register their agreement or disagreement to this retraction. We have kept a record of any response received.

References

[1] Y. Zhang, Z. Li, G. Zhou, N. Xu, and J. Liu, "The Evolution Model of Public Risk Perception Based on Pandemic Spreading Theory under Perspective of COVID-19," *Complexity*, vol. 2021, Article ID 1015049, 10 pages, 2021.

WILEY | Hindawi

Research Article

The Evolution Model of Public Risk Perception Based on Pandemic Spreading Theory under Perspective of COVID-19

Yi-Cheng Zhang,[1,2] Zhi Li,[2] Guo-Bing Zhou,[3] Nai-Ru Xu [1] and Jia-Bao Liu [4]

[1]*School of Business, Anhui Xinhua University, Hefei 230088, China*
[2]*School of Management, University of Science and Technology of China, 96 JinZhai Road, Hefei, Anhui 230026, China*
[3]*Center for Financial Engineering of Soochow University, Suzhou, Jiangsu 215031, China*
[4]*School of Mathematics and Physics, Anhui Jianzhu University, Hefei, China*

Correspondence should be addressed to Jia-Bao Liu; liujiabaoad@163.com

After the occurrence of public health emergencies, due to the uncertainty of the evolution of events and the asymmetry of pandemic information, the public's risk perception will fluctuate dramatically. Excessive risk perception often causes the public to overreact to emergencies, resulting in irrational behaviors, which have a negative impact on economic development and social order. However, low-risk perception will reduce individual awareness of prevention and control, which is not conducive to the implementation of government pandemic prevention and control measures. Therefore, it is of great significance to accurately evaluate public risk perception for improving government risk management. This paper took the evolution of public risk perception based on the COVID-19 region as the research object. First, we analyze the characteristics of infectious diseases in the evolution of public risk perception of public health emergencies. Second, we analyze the characteristics of risk perception transmission in social networks. Third, we establish the dynamic model of public risk perception evolution based on SEIR, and the evolution mechanism of the public risk perception network is revealed through simulation experiments. Finally, we provide policy suggestions for government departments to deal with public health emergencies based on the conclusions of this study.

1. Introduction

After the occurrence of public health emergencies, due to the uncertainty of the evolution of events and the asymmetry of pandemic information, the public's risk perception will fluctuate dramatically. The public takes various protective measures, such as collecting relevant information about the pandemic, forwarding and spreading information about the pandemic, producing violent emotional reactions, buying protective goods, and even leaving the pandemic area [1, 2]. In early March 2020, more than 50,000 people across the country were surveyed about their psychological stress and emotional state according to the Shanghai Mental Health Center; the survey showed: about 35% of the interviewees suffered from psychological distress and had obvious emotional stress reaction; about 5.14% of the interviewees suffered from serious psychological distress. During

COVID-19, there has been frantic buying of face masks and disinfectants across the country and around the world. Moreover, public risk perceptions are highly contagious, and excessive risk perceptions by some members of the public can lead to irrational behavior by more members of the public, jeopardizing social harmony and stability. Therefore, we should pay attention to the public's risk perception and emotional guidance, face up to the psychological needs of the public to vent their emotions, and reasonably guide the public's emotional fluctuations and behavioral reactions. These become an important task of COVID-19 pandemic prevention and control [3].

Public risk perception refers to the concern or anxiety expressed by the public about something [4], which reflects the process of the public's subjective evaluation of a specific risk state [5, 6]. When the public is aware of risks, it stimulates the psychological state of coping with risks and

further generates the demand for risk-related information and emergency behavior based on subjective judgment. Too high risk perception often leads the public to overreact to risk events, resulting in a variety of irrational and unnecessary behaviors, which have an unnecessary impact on economic development and social stability. However, when risk perception is too low, the public may give up taking effective self-protection behaviors. Public risk perception is a collection, selection, and understanding of the process of crisis information and response [7, 8]. In the all-media information age dominated by the network, the public's information demand, information channel, and information content are characterized by diversification and complexity. It leads to dynamic change and unpredictability of public risk perception, which further increases the difficulty of health emergency prevention and control.

Therefore, after the occurrence of major public health emergencies, the dynamic evolution law of public risk perception along with the development of the events should be grasped. It is helpful for the government to adopt active and effective risk management policies and measures.

2. Literature Review

2.1. Risk Perception.
Scholars generally believe that the public's risk perception is mainly affected by individual characteristics, time, event progress, risk information, and other factors [9]. A questionnaire survey through a psychological scale is the most effective method to study the influencing factors and differences of risk perception. Peacock et al. take hurricane as the research scenario and explore the influencing factors of the formation process of public risk perception from two dimensions of socioeconomic and demographic characteristics [10]. In order to study the characteristics and influencing factors of public risk perception, Slovic carried out a series of empirical studies and summarized 15 different characteristics of risk perception [11].

In the field of behavioral science and psychology, many scholars focus on the important role of memory in individual behavioral decision-making [12], Most of their research results support that individual memory system has a decisive influence on behavioral decision-making [13]. Welch et al. believed that the information obtained through news media and informal communication channels of social networks all belonged to the information used for behavioral decision-making in the individual memory system [14]. The same conclusion can also be reached when scholars introduce individual memory to build mathematical models. For example, Mullainathan took consumers' memories of previous products and wages as the basis for purchasing decisions and constructed a consumer memory decision model [15]. Mehta et al. studied the relationship between consumers' forgetting rate of brands and purchasing decisions and believed that when consumers are faced with many brands, their memory and perception of these brands play an important role in consumers' choice [16]. Wei et al. constructed an evolution model of individual memory perception and corporate reputation to study the optimal

strategy of CSR activities of enterprises [17]. Wei et al. introduced the recency effect, Lenovo effect, and read-back effect and built the public risk perception evolution model based on crisis information flow. This model uses the crisis information growth model, stakeholder influence model, and stakeholder memory model to measure the process of crisis information release, information diffusion, and information perception. The diffusion coefficient and forgetting coefficient of crisis information are introduced to explain the transmission mechanism of crisis information in the population. It is found that there are lag effect, cumulative effect, and jump phenomenon in the evolution of public risk perception [18].

2.2. Communicable Disease Model Network Public Opinion Spread.
The infectious disease model is a mathematical model that uses an ordinary differential equation to describe the spread and prevalence of the infectious disease. Consider the similarity between the spread of information and the spread of infectious diseases. Daley et al. applied the infectious disease dynamics model to information transmission, dividing individuals into three categories: susceptible, sprayer, and immune and then constructing the classic DK model [19]. Subsequently, some scholars further refined the communication process and improved the model [20, 21]. However, with the rapid development of information technology and the explosion of social networks, the mode of information transmission has undergone profound changes. The classical infectious disease model can no longer accurately describe the geometric progression fission propagation process of network information [22]. One of the important reasons is that the spread of infectious diseases is unconscious, and the transmission of diseases by infected people is not based on people's subjective will. However, the essence of information communication is social communication, and further research needs to consider the attributes of network information content, public society, and other factors [23–25].

Shang et al. integrated the social network and communication dynamics model and proposed a simulation planning method taking public emergencies as scenarios [26]. Zhu et al. [27] established an infectious disease model based on the transmission rules of the Ebola virus. Wang et al. considered the interdependence of online and offline activities and constructed an information transmission model of a two-layer social network based on complex network theory and communication dynamics [28]. Liu et al. considered the influence of network dynamic evolution and constructed a dynamic network diffusion information transmission model of public emergencies [29]. Wang et al. defined the types of the public and the role of government intervention, and combined with the characteristics of emergency information communication, they constructed a public opinion communication control model under government intervention [30]. Zhong et al. considered the relationship between public status transition and the influence of government intervention, constructed the SEIRS model of public opinion communication control under government intervention, and used control factors to realize effective intervention of online public opinion in emergencies

[31]. Yin et al. [32] considered that users may enter into another related topic after discussing one topic and proposed a multi-information susceptibility discussion immunity (M-SDI) model, effectively predicted the trend of online public opinion communication of public health emergencies through the fitting analysis of COVID-19 public opinion data obtained from China's Sina Weibo. Wang et al. analyzed the mutual influence of multiple public opinion communication and the rule of state transfer among different groups after an emergency occurred and proposed the 3SI3R model [33].

So that's all, at present, the research on infectious disease models is relatively mature, and most of them are applied in the field of information dissemination and network public opinion dissemination. However, there are few literature on the evolution of applying the infectious disease model to public risk perception. Therefore, in the context of COVID-19, this paper analyzes the spread characteristics and rules of public risk perception by using the infectious disease model. Considering the propagation properties of the social network, such as social reinforcement effect, containment mechanism, and forgetting mechanism, we constructed the evolution dynamics model of public risk perception based on SEIR, which better delineated the evolution of public risk perception and provided decision-making suggestions for the government in formulating the risk management of public health emergencies.

3. Model Construction

3.1. Characteristics of the Evolution of Public Risk Perception in the COVID-19.
The essence of an infectious disease is that the carrier of the pathogen transmits its own germs to the person who comes into contact with it through contact with other individuals. In the context of COVID-19, the spread of public risk perception has the characteristics of infectious disease, and individuals who perceive risk will transmit their perceived risk to other individuals who communicate with them through various communication channels. The transmission of infectious diseases between hosts needs to break a certain threshold, and the spread of the public's perceived risk in the context of COVID-19 also needs certain conditions, as the perceived risk exceeds their own tolerance. Therefore, in the context of COVID-19, the spread of public risk perception has the characteristics of risk sources, transmission media, infectivity, and immunity.

3.1.1. Risk Source.
The source of risk is the precondition of risk transmission. If there is no source of risk, there is no risk transmission. Risk sources are equivalent to pathogens in infectious diseases. The public health emergency caused by the COVID-19 outbreak in late December 2019 is a risk source for the spread of public risk perception. As the core of the process of risk communication, the source of risk causes public panic and panic buying of medical equipment depending on the communication media.

3.1.2. Propagation Medium.
The transmission medium is the carrier of risk source transmission. After the outbreak of COVID-19, the media of public risk perception are the Internet, TV, newspapers, Weibo, and other mass media. The pandemic information permeates the entire social cyberspace, and the public receives the pandemic information and transmits the perceived risk incorrectly, thus causing panic among the general public.

3.1.3. Contagious.
Infectivity is the most fundamental characteristic of infectious diseases. If there are only pathogens and infectious media, but pathogens do not have infectivity, they do not belong to infectious disease. Risk source of contagion will spread the risk to the environment, when individuals perceive more risk than they can bear, they will spread the risk perception to the outside world through their closely related kinship, work and neighborhood relationships.

3.1.4. Immunity.
Some people are immune to certain infections because they have antibodies or have been vaccinated against them. In the process of risk transmission caused by the outbreak of COVID-19, some individuals show different immunity based on their psychological quality and knowledge. For example, individuals with poor mental health and inadequate knowledge of novel coronavirus and the spread of the virus have much lower immunity than individuals with high mental health and abundant protective behaviors against COVID-19. At the same time, the individual's gender, personality, and living environment will affect their immune ability.

Therefore, in the context of COVID-19, the transmission process of public risk perception has the characteristics of the transmission process of infectious diseases. The infectious disease model is used to analyze and simulate the transmission process of risk perception so as to understand the principle of risk perception transmission and provide a reference for the formulation of risk perception control measures.

3.2. Factors Influencing the Evolution of Public Risk Perception.
Public risk perception is widely spread through the Internet, TV, newspapers, Weibo, and other mass media in the social network space such as the circle of relatives, neighbors, and friends who are closely related to individuals. The dissemination of public risk perception is a complex process, which is not only affected by individual factors such as interindividual intimacy, knowledge background, and life experience [34–36] but also affected by social factors such as information memory effect, social reinforcement effect, interest attenuation effect, containment mechanism, authority effect, broken window effect, and responsibility dispersion effect [37–40]. This paper focuses on the influence of the forgetting mechanism, social reinforcement effect, and containment mechanism on public risk perception transmission.

3.2.1. Forgetting Mechanism.
German psychologist Ebbinghaus revealed the nonlinear attenuation of information value with the passage of time through the method of relearning. It reflects the significant impact of

attenuation characteristics on information dissemination. Relevant literature call this phenomenon a forgetting mechanism [41], and it is proved by simulation that this mechanism can inhibit information diffusion and reduce the scale of information dissemination [42]. Scholars have shown that the rate of forgetting has a significant impact on the density of spreaders and immunizers in rumor-spreading experiments. The higher the forgetting probability or the faster the forgetting speed, the weaker the spreading power of rumors [43]. Then, in major public health emergencies, the public risk perception transmission characteristics will be the same.

3.2.2. Social Reinforcement Effect.
In the process of information transmission, individuals tend to be skeptical of information, and the probability of transmitting information after receiving it only once is very limited. However, if the neighbor repeatedly prompts the same information so that the individual receives the same information many times, the probability of the individual believing the information and spreading it will greatly increase. In social networks, information is dense, and a lot of information is mixed with truth and false. It is difficult for ordinary people to make a reasonable judgment. At this time, most people will use others' judgment to form their own opinions. Therefore, the social reinforcement effect is very obvious in the information dissemination of social networks.

Literature [44] constructed a rumor propagation model with social reinforcement effect and interest attenuation effect based on the social network and believed that the social reinforcement effect and interest attenuation effect would simultaneously act on the propagation state node, which would be converted into the connected state by interest attenuation effect, and the connected state would be converted into the propagation state by the social reinforcement effect. Therefore, this paper defines the propagation probability function of public risk perception in the social network caused by the social reinforcement effect as follows:

$$\lambda(m) = 1 - (1 - \beta)e^{-b(m-1)}, \tag{1}$$

where β is the initial transmission rate, which represents the probability that an individual will transmit the pandemic information after receiving it only once; b is the strengthening factor; and m is the number of messages received when $m = 1$ and $\lambda(1) = \beta$.

Figure 1 shows that under the action of different reinforcement coefficient b, the propagation probability of individual risk perception changes with the change of m. Initial value $\lambda(1) = \beta = 0.5$ represents the transmission probability of risk perception of susceptible individuals receiving information of an pandemic.

Based on the above considerations, this paper focuses on the local environment of individuals to describe the forgetting mechanism, social reinforcement effect, and containment mechanism of the spread of public risk perception and analyzes how these factors affect the spread of risk perception through simulation.
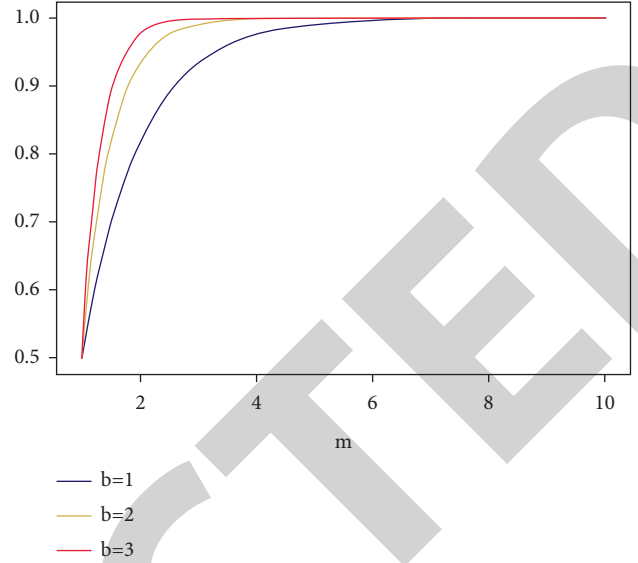

FIGURE 1: Influence of different reinforcement coefficients on propagation probability.

3.3. Dynamic Evolution Model of Public Risk Perception in COVID-19.
The individual in the social network is represented as the node in the network, and the relationship between individuals is represented by the connection between nodes, so the social network is represented as a concrete network structure. The individuals in the social network are represented as nodes in the network, and the relationships between individuals are represented by the links between nodes, thus representing the social network as a specific network structure. In the process of risk perception propagation, it can only be propagated between neighboring nodes. When a node propagates risk perception to its neighboring nodes, if the neighboring nodes choose to believe and accept the information, then the neighboring nodes continue to propagate risk perception to its neighbors. If the neighboring node does not accept the risk perception, the neighboring node does not propagate it again.

When the risk perception spreads from the risk source to the whole network, there will be different psychological states for the same information due to the different interests and knowledge of nodes in the network. Therefore, nodes have different attitudes on whether to accept the spread of risk perception and ultimately lead to different trends in the spread of risk perception. So that, the nodes in the social network can be divided into four states: the susceptible state (S), the latent state (E), the onset state (I), and the recovering state (R). Among them, the susceptible state refers to the public who has not received the pandemic information. The latent status refers to receiving information but not disseminating risk perception. In other words, it refers to receiving pandemic information for the first time and perceiving risk but not breaking one's maximum risk tolerance. The onset state refers to the state of panic and anxiety when receiving information, which is spreading risk perception. The recovery status refers to the public who rationally see the pandemic and do not spread it.

The proportions of these four groups in the total population at time t are, respectively, $S(t)$, $E(t)$, $I(t)$, $R(t)$, and $S(t) + E(t) + I(t) + R(t) = 1$.

Considering the social reinforcement effect, forgetting mechanism, and containment mechanism of public risk perception, the following risk perception communication rules are proposed:

(1) When the susceptible individual S_i receives the information transmitted from an infected individual I_j, the susceptible individual S_i may change to the latent state E_i with probability α or may change to the onset state I_i with the initial rate of transmission β and transmit the pandemic information to other individuals. The state transition can be expressed as follows:

$$S_i + I_j \xrightarrow{\alpha} E_i + I_j, S_i + I_j \xrightarrow{\beta} I_i + I_j. \quad (2)$$
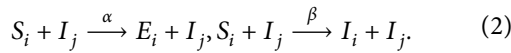
(2) The nodes in the latent state are suspicious of the pandemic information and will receive the information transmitted from the nodes in the neighboring pandemic state many times. Under the influence of the social reinforcement effect, the nodes in the latent state E_i will be transformed into the onset state I_i with the probability of transmission λ. The latent node E_i that has not been transformed into the disease state may be transformed into the recovering state R_i with probability θ. The E_i transition process of the latent state can be expressed as follows:

$$E_i \xrightarrow{\lambda} I_i, E_i \xrightarrow{\theta} R_i. \quad (3)$$
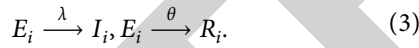
(3) Since the onset node has already believed the pandemic information and spread it, the transmission state will not be affected by the social strengthening effect. However, the onset state I_i is affected by the social containment mechanism, the nodes in the onset state I_i will be transformed into the recovery state R_i with the probability of transmission ε. The I_i transition process of the onset state can be expressed as follows:

$$I_i \xrightarrow{\varepsilon} R_i. \quad (4)$$
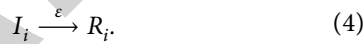
(4) With the passage of time, the recovering state R_i was affected by the amnesia mechanism and changed to the susceptible state S_i with a probability of δ. The R_i transfer process of the healing state can be expressed as follows:

$$R_i \xrightarrow{\delta} S_i. \quad (5)$$

According to the above analysis, the evolution model of the public risk perception network in COVID-19 is shown in Figure 2.

In summary, the public risk perception communication dynamics model is as follows:
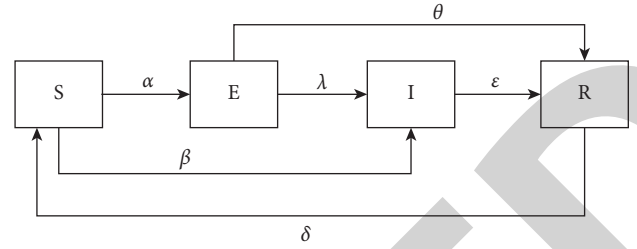

Figure 2: State transition diagram of social network nodes.

$$\frac{dS(t)}{dt} = -\alpha S(t)I(t) - \beta S(t)I(t) + \delta R(t),$$

$$\frac{dE(t)}{dt} = \alpha S(t)I(t) - \lambda E(t) - \theta E(t),$$

$$\frac{dI(t)}{dt} = \beta S(t)I(t) + \lambda E(t) - \varepsilon I(t),$$

$$\frac{dR(t)}{dt} = \theta E(t) + \varepsilon I(t) - \delta R(t).$$

$$(6)$$

3.4. Analysis of the Basic Reproduction Number of the Model.
In this paper, the next-generation matrix method is used to calculate the basic reproduction number R_0.

States 1, 2, 3, and 4 represent the states of E, I, S, and R, respectively. The density of class 4 node states is denoted by x_i, that is $x = (x_1, x_2, x_3, x_4)^T$. Constructor $F(x)$: $F_i(x)$ represents the probability of new diseased nodes in state i; according to the above information, when $i = 1$, the probability of new diseased node in latent state E is αSI; when $i = 2$, the probability of new diseased node in onset state is βSI; and when $i = 3, 4$, there were no new disease nodes in susceptible nodes and recovered nodes. Therefore,

$$F(x) = \begin{bmatrix} F_1(x) \\ F_2(x) \\ F_3(x) \\ F_4(x) \end{bmatrix} = \begin{bmatrix} \alpha SI \\ \beta SI \\ 0 \\ 0 \end{bmatrix}. \quad (7)$$

Constructor $V(x)$: $V_1(x)$, $V_2(x)$, $V_3(x)$, and $V_4(x)$, respectively, represents the probability of change of state nodes of E, I, S, and R; hypothesis $V_i(x) = V_i^-(x) - V_i^+(x)$, where $V_i^+(x)$ represents the probability of changing from another state node to the i state and $V_i^-(x)$ represents the probability of transition from the i state node to another state; therefore,

$$V(x) = \begin{bmatrix} V_1(x) \\ V_2(x) \\ V_3(x) \\ V_4(x) \end{bmatrix} = \begin{bmatrix} \lambda E + \theta E \\ \varepsilon I - \lambda E \\ \alpha SI + \beta SI - \delta R \\ \delta R - \theta E - \varepsilon I \end{bmatrix}. \quad (8)$$

Obviously, when there is no diseased node in the network system, all nodes are susceptible to infection, that is, $E_0 = (0, 0, S^*, 0)$ is the equilibrium point of the system, The derivative of $F(x)$ and $V(x)$ at E_0 is as follows:

$$\begin{cases} DF(E_0) = \begin{pmatrix} F & 0 \\ 0 & 0 \end{pmatrix}, \\ DV(E_0) = \begin{pmatrix} V & 0 \\ J_3 & J_4 \end{pmatrix}, \end{cases} \tag{9}$$

where

$$\begin{cases} F = \begin{pmatrix} 0 & \alpha \\ 0 & \beta \end{pmatrix}, \\ V = \begin{pmatrix} \lambda + \theta & 0 \\ -\lambda & \varepsilon \end{pmatrix}. \end{cases} \tag{10}$$

Therefore, we calculated that

$$FV^{-1} = \begin{bmatrix} \dfrac{\alpha\lambda}{(\lambda + \theta)\varepsilon} & \dfrac{\alpha}{\varepsilon} \\[3ex] \dfrac{\beta\lambda}{(\lambda + \theta)\varepsilon} & \dfrac{\beta}{\varepsilon} \end{bmatrix}. \tag{11}$$

The spectral radius of FV^{-1} is expressed as $\rho(FV^{-1})$, that is, the basic regeneration number R_0 is

$$R_0 = \rho(FV^{-1}) = \frac{\alpha\lambda + \beta(\lambda + \theta)}{\varepsilon(\lambda + \theta)}. \tag{12}$$

In the analysis of the network information transmission process, the basic regeneration number R_0 is an important parameter to measure whether network information can be spread on a large scale. It represents the average number of people affected by introducing a disease state node when all the network space is susceptible to infection without intervention. When $R_0 < 1$, the network information will not be widely diffused. When $R_0 > 1$, the network information will present a large-scale diffusion trend.

It can be seen from equation (12) that the basic regeneration number is closely related to the social effects of public risk perception, and these social effects have an important influence on whether the public risk perception spreads on a large scale. Among them, when other factors remain unchanged, the initial transmission rate of public risk perception keeps increasing, so that the basic regeneration number R_0 gradually changes from a value less than 1 to a value greater than 1, and the public panic gradually spreads. With the increase of the basic regeneration number R_0, the diffusion scale becomes larger and larger.

4. Numerical Simulation and Analysis

This part will verify the rationality and stability of the evolutionary model of public risk perception through simulation experiments and analyze the propagation mechanism of risk perception. In the simulation experiments, the initial conditions given are: $S(0) = 1$, $E(0) = 0.00$, $I(0) = 0.00$, and $R(0) = 0.00$.

4.1. Analysis of the Density of State Nodes in the Network. Set the initial parameter to $\alpha = 0.2, \beta = 0.5, \lambda = 0.5, \theta = 0.3, \varepsilon = 0.2, \delta = 0.1$ and substitute into equation (12); the calculation gives the basic regeneration number R_0 as 3.125, The theory suggests that public risk perceptions undergo mass diffusion, which is consistent with the results in the figure.

From Figure 3, it can be seen that the node density of the susceptible state decreases rapidly at the initial stage and eventually tends to stabilize; the node density of the latent state increases rapidly to a peak of 0.31, then gradually decreases, and eventually tends to 0; the node density of the pathogenic state increases rapidly at the early stage of propagation and reaches a peak of 0.63, after which the node density gradually decreases and eventually stabilizes at 0.32; the node density of the healed state rapidly increases during the propagation process and eventually reaches a stable at 0.61. The density of nodes in the healed state increased rapidly during propagation and eventually reached a stable level of 0.61.

4.2. Impact of Initial Propagation Rate on the Evolution of Public Risk Perception. The node density of the morbidity state represents the active degree of risk perception transmission; the node density of the healing state represents the degree of risk perception transmission final state. Therefore, the impact of public health pandemics on public risk perception is investigated by analyzing the change in node density of morbidity and healing states with the initial transmission rate β. Figures 4 and 5 depict how public risk perceptions vary over time in terms of the density of morbidity status and healing status under the influence of different initial transmission probabilities. Set the initial parameter $\alpha = 0.2, \lambda = 0.5, \theta = 0.3, \varepsilon = 0.2, \delta = 0.1$; take three cases $\beta = 0.2, \beta = 0.5$, and $\beta = 0.8$; and substitute into equation (12); the calculation can get the basic regeneration number R_0 as 1.625, 3.125, and 4.625, respectively; theoretically, the public risk perception will carry out large-scale diffusion, which is consistent with the results in the figure. As can be seen in Figures 4 and 5, both the onset state and the healing state R density maxima increase with increasing initial transmission probability β. That is, the greater the initial probability of transmission, the more the public is inclined to spread risk perceptions, and the shorter the time it takes to reach the peak. After the node density of the disease state reaches its peak, as the government's emergency work advances, such as the effective implementation of pandemic prevention and control measures, some members of the public believe that the pandemic is temporarily controllable, and the number of publics spreading information about the pandemic begins to decrease, and eventually, all change to the disease state. Therefore, the greater the initial rate of transmission of public risk perception, the faster the network transmission that is not only fast but also on a large scale.

4.3. The Impact of Social Reinforcement Effects on the Evolution of Public Risk Perceptions. Set the initial parameter to $\alpha = 0.2, \beta = 0.5, \theta = 0.3, \varepsilon = 0.2, \delta = 0.1$ and take the three cases $b = 1, m = 1, b = 1, m = 2$, and $b = 2, m = 2$. Figure 6 depicts the change in the density of morbidity status nodes
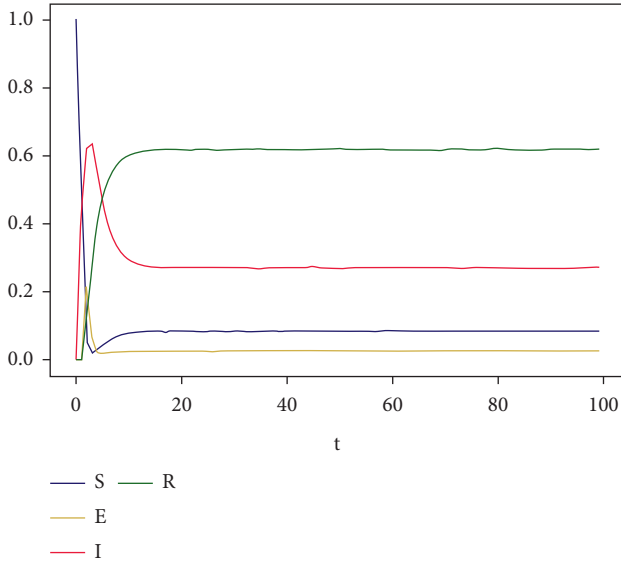
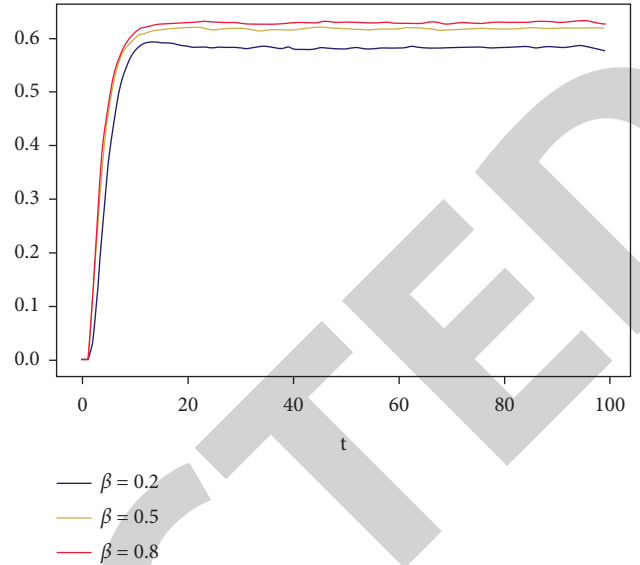FIGURE 3: Trend of state changes of various nodes in the SEIR model.

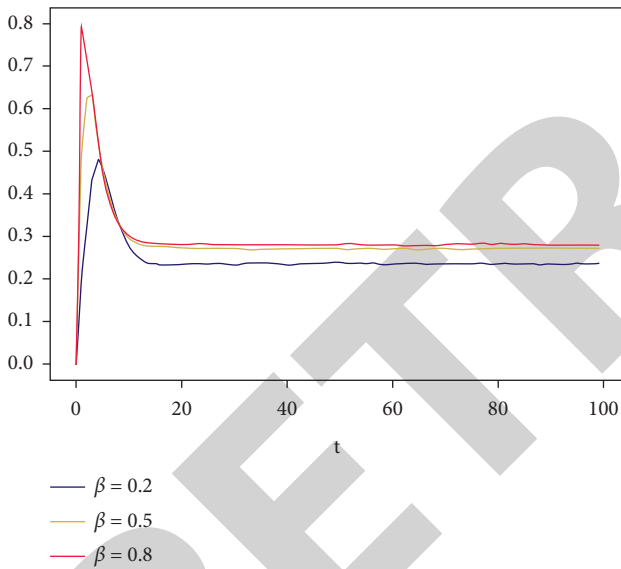FIGURE 4: Effect of initial transmission rate on the density of nodes in the onset state.

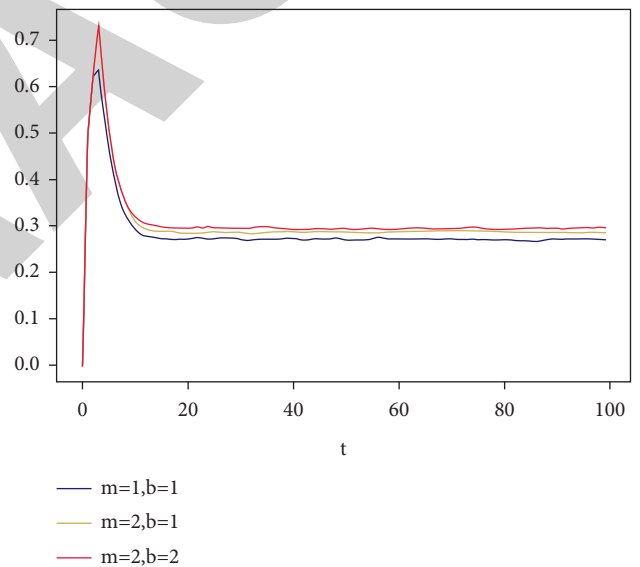FIGURE 5: Effect of initial propagation rate on node density in the healed state.

FIGURE 6: Effect of reinforcement effects on the density of nodes in the onset state.

over time for different social reinforcement effects on public risk perception. As can be seen in Figure 6, the greater the number of times an individual receives information about an pandemic, the greater the density of morbidity status nodes, for the same reinforcement factor. Similarly, the higher the reinforcement factor, the higher the density of onset nodes, given the same number of times an individual received information about the pandemic. This suggests that the public is more inclined to disseminate risk perceptions in the presence of social reinforcement effects.

4.4. Impact of Containment Mechanisms on the Evolution of Public Risk Perceptions. Set the initial parameter to $\alpha = 0.2, \beta = 0.5, \lambda = 0.5, \theta = 0.3, \delta = 0.1$ and take the three cases

$\varepsilon = 0.2$, $\varepsilon = 0.4$, and $\varepsilon = 0.6$. Substituting into equation (12), the corresponding basic regeneration numbers R_0 are 3.125, 1.56, and 1.04, respectively, and the nodal densities of onset states when public risk perception transmission reaches stability are 0.27, 0.16, and 0.1, respectively. From Figure 7, it can be seen that the maximum value of the onset state node density decreases with the increase of the containment mechanism ε. Since ε represents the strength of the containment mechanism, this means that the stronger the containment mechanism, the easier it is for the onset state nodes to be influenced by other nodes and stop spreading, the faster the network reaches a stable state, and the smaller the density of onset state nodes after the network is stable. Therefore, the containment
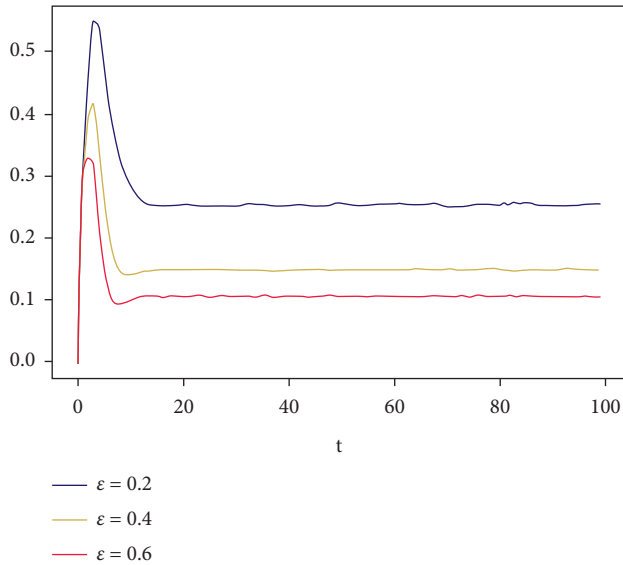
FIGURE 7: Effect of containment mechanisms on node density in the onset state.

FIGURE 8: Effect of forgetting mechanisms on the density of nodes in the onset state.

mechanism curbs the spread of public risk perception to a certain extent, reducing the speed and scope of transmission.

4.5. The Impact of Forgetting Mechanisms on the Evolution of Public Risk Perception. Set the initial parameter to $\alpha = 0.2, \beta = 0.5, \lambda = 0.5, \theta = 0.3, \varepsilon = 0.2$; take the three cases of $\delta = 0.1$, $\delta = 0.4$, and $\delta = 0.7$, and substitute into (12); the corresponding basic regeneration numbers are all 3.125. The node densities of onset states when network propagation is stable are 0.28, 0.52, and 0.61, respectively.

As can be seen from Figure 8, the maximum value of the onset state node density increases with the increase of the forgetting rate δ. Since δ represents the intensity of forgetting, this means that the greater the degree of forgetting, the easier it is for sick state nodes to forget the received pandemic information and the easier it is for them to become susceptible nodes again to receive pandemic information and propagate risk perceptions, making the density of sick state nodes greater when the network is stable.

5. Research Conclusions and Policy Recommendations

5.1. Research Conclusions. In this paper, based on COVID-19, first, we analyzed the infectious characteristics of public risk perception in public health emergencies. Second, according to the characteristics of public risk perception transmission in social networks, we established the evolution dynamics model of public risk perception and solved the basic regeneration number. Finally, we revealed the evolution mechanism of the public risk perception network through parameter selection and simulation experiments. Therefore, the significance of this study is reflected in the following three aspects:
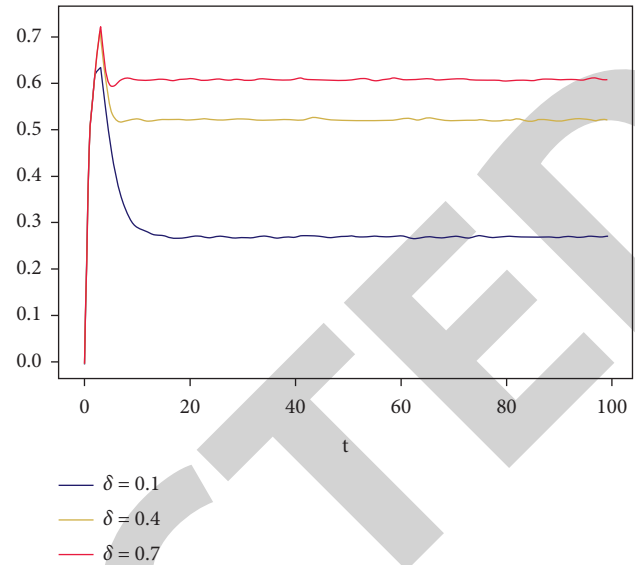
(1) Systematically summarize the characteristics of public risk perception of infectious diseases in public health emergencies, including risk sources, transmission media, infectivity, and immunity. It provides a theoretical basis for the establishment of a public risk perception model.

(2) Systematically analyze the influencing factors of public risk perception of public health emergencies. From two dimensions of individual and social factors, we focused on analyzing the influence of the forgetting mechanism, social reinforcement effect, and containment mechanism on the spread of risk perception and established the evolution dynamics model of the public risk perception based on SEIR. The stability of the model is proved theoretically by solving the basic regeneration number.

(3) The infectious disease model is applied to the evolution model of risk perception of public health emergencies; through simulation experiments, we revealed the evolution mechanism of public risk perception network. The greater the initial rate of diffusion, the greater the speed and scope of network diffusion; the stronger the social reinforcement effect, the greater the speed and scope of network diffusion; the stronger the rate of forgetting, the greater the speed and scope of network diffusion; and the stronger the rate of containment, the weaker the speed of network diffusion and the smaller the scale of network diffusion.

5.2. Policy Recommendations. The conclusions of this study can provide the following suggestions for relevant government departments to deal with major public health emergencies:

(1) The government should immediately launch the emergency plan to rescue the affected public, shrink the scope of the emergency, reduce the level of the emergency, cut down the influence of the emergency, and weaken the public risk perception so as to reduce the negative impact of the online public opinion of the emergency and maintain social harmony and stability.

(2) The government should undertake the responsibility of supervision, regulation, and management. First, on the premise of satisfying the public's right to know, gradually relax the control on news media, and standardize the system of information disclosure and dissemination. In the process of information disclosure, the government should establish two-way communication channels: on the one hand, timely inform the public of the truth of the incident and, on the other hand, invite experts to objectively analyze and release authoritative information. Second, the government has a responsibility to know the source of the public's fear and respect the public's perception of risk. The risk that may be overestimated by the public through various ways has to be reduced, so as to reduce the public's risk perception level and relieve the public's panic.

(3) News media should abide by professional ethics and report objectively and fairly, which will help reduce the risk perception of the public. The media is the reporter of the risk information of public health emergencies, the interpreter of dynamic information, and the guide of the public's risk perception. After the occurrence of public health emergencies, the public relies more on media reports because of asymmetric information. Therefore, the media should report information objectively, accurately and timely so that the potential risks can be recognized by the public so as to cut down the public's risk perception and panic and ultimately reduce the change from vulnerable groups to latent groups or disease groups.

(4) The public should maintain a positive and optimistic attitude, collect emergency information rationally and objectively, and reduce the overestimated risk perception because of information insufficient. Instead of passively receiving information, the public should actively acquire and screen information. The analysis must be rational and objective so as to avoid herd behavior.

In a word, in the face of public health emergencies, the government should establish an early warning and response mechanism for public risk perception. The media should report the emergency objectively and fairly in order to guide public opinion correctly. The public should remain positive and optimistic, enhance the awareness of discrimination, reduce unnecessary panic, and improve the confidence to overcome difficulties.

Data Availability

No data were used to support this study.

Conflicts of Interest

The authors declare that there are no conflicts of interest regarding the publication of this paper.

Acknowledgments

References

[1] M. K. Lindell and R. W. Perry, "The protective action decision model: theoretical modifications and additional evidence," *Risk Analysis*, vol. 32, no. 4, pp. 616–632, 2012.

[2] S. Shapira, L. Aharonson-Daniel, and Y. Bar-Dayan, "Anticipated behavioral response patterns to an earthquake: the role of personal and household characteristics, risk perception, previous experience and preparedness," *International Journal of Disaster Risk Reduction*, vol. 31, pp. 1–8, 2018.

[3] J. Wei, "The present and future research on public risk perception evolution and protective action decision amid public health emergencies," *China Science Foundation*, vol. 6, pp. 776–785, 2020.

[4] Y. Sun and Z. Han, "Climate change risk perception in taiwan: correlation with individual and societal factors," *International Journal of Environmental Research and Public Health*, vol. 15, no. 1, p. 91, 2018.

[5] P. Bubeck, W. J. W. Botzen, and J. C. J. H. Aerts, "A review of risk perceptions and other factors that influence flood mitigation behavior," *Risk Analysis*, vol. 32, no. 9, pp. 1481–1495, 2012.

[6] C. Peng, J. Wei, and G. Yue, "Who should be blamed? the attribution of responsibility for a city smog event in China," *Natural Hazards: Journal of the International Society for the Prevention and Mitigation of Natural Hazards*, vol. 85, no. 2, pp. 669–689, 2017.

[7] G. Wachinger, O. Renn, C. Begg, and C. Kuhlicke, "The risk perception paradox-implications for governance and communication of natural hazards," *Risk Analysis*, vol. 33, no. 6, pp. 1049–1065, 2013.

[8] B. Liu-Lastres, A. Schroeder, and L. Pennington-Gray, "Cruise line customers' responses to risk and crisis communication messages: an application of the risk perception attitude framework," *Journal of Travel Research*, vol. 58, no. 5, pp. 849–865, 2019.

[9] J. Zeng, *Public's Risk Response-Behavior and Information Communication Research in the Situation of Nuclear Power Plants Construction*, Doctoral dissertation, University of Science and Technology of China, Hebei, China, 2017.

[10] W. G. Peacock, S. D. Brody, and W. Highfield, "Hurricane risk perceptions among Florida's single family homeowners," *Landscape and Urban Planning*, vol. 73, no. 2, pp. 120–135, 2005.

[11] P. Slovic, "Perception of risk," *Science*, vol. 236, no. 4799, pp. 280–285, 1987.

[12] A. O. Hirschman, *A Propensity to Self-Subversion*, Harvard University Press, Cambridge, MA, USA, 1995.

[13] A. B. Hollingshead, "Cognitive interdependence and convergent expectations in transactive memory," *Journal of Personality and Social Psychology*, vol. 81, no. 6, pp. 1080–1089, 2001.

WILEY | Hindawi

Research Article

Analysis of a Tuberculosis Infection Model considering the Influence of Saturated Recovery (Treatment)

Fatima Sulayman [ID][1,2] **and Farah Aini Abdullah** [ID][1]

[1]*School of Mathematical Sciences, Universiti Sains Malaysia USM, 11800 Penang, Malaysia*
[2]*Department of Mathematical Sciences, Ibrahim Badamasi Babangida University, Lapai, P. M. B. 11, Niger State, Nigeria*

Correspondence should be addressed to Farah Aini Abdullah; farahaini@usm.my

Tuberculosis (TB) is a serious global health threat that is caused by the bacterium *Mycobacterium tuberculosis*, is extremely infectious, and has a high mortality rate. In this paper, we developed a model of TB infection to predict the impact of saturated recovery. The existence of equilibrium and its stability has been investigated based on the effective reproduction number R_C. The model displays interesting dynamics, including backward bifurcation and Hopf bifurcation, which further results in the stable disease-free and stable endemic equilibria to be coexisting. Bifurcation analysis demonstrates that the saturation parameter is accountable for the phenomenon of backward bifurcation. We derive a condition that guarantees that the model is globally asymptotically stable using the Lyapunov function approach to global stability. The numerical simulation also reveals that the extent of saturation of TB infection is the mechanism that is fuelling TB disease in the population.

1. Introduction

Modeling and simulation are significant decision tools for controlling human diseases [1, 2]. Although every disease demonstrates its own series of biological characteristics, the models should be adjusted to every case in order to tackle real-world scenarios [3, 4].

Tuberculosis (TB) kills more people every year than any other infectious disease, including HIV and malaria, making it one of the most serious global health challenges [5]. Despite the fact that TB is a curable and preventable disease, it is still one of the top ten causes of mortality worldwide [5, 6]. TB is usually caused by the bacterium *Mycobacterium tuberculosis*. In 2018, there were 10 million new cases of TB reported, with 8.6% of those living with HIV [5]. To be infected with TB, a person just has to inhale a few TB bacteria [5, 6]. The infection may also affect other areas of the body, like the kidneys, brain, skin, and spine, in some cases. The TB infection is not new to the community, yet it has a long history of presence since antiquity in China, Egypt, and India [7]. Tuberculosis is transferred from one infected individual to another by germ-infested air droplets. When a person with active tuberculosis germs spits, talks, coughs, or sneezes, the TB germs are propelled into the air [5]. TB can be contracted effectively from relatives and companions. An individual becomes contaminated effectively when they inhale a couple of TB germs. Approximately ten percent of TB-infected people develop active TB infection, while the other ninety percent remain latent [5]. TB infection is not transmitted by people who are latently sick. Individuals with TB may be identified by skin or blood testing. People with immunocompromised diseases are more susceptible to TB (HIV and diabetic patients). A cough that lasts longer than three weeks, fever, coughing up blood, chest pain, fatigue, weight loss, exhaustion, and night sweats are all symptoms of active tuberculosis [5, 8]. TB is a transferable disease, which can be treated with medication therapy [5, 8].

Treatment is a significant and viable technique that can be used within a population to control the spread of infectious diseases. In modeling techniques, the role of treatment function addresses the likelihood of treatment against the disease at a given time for each infected person.

In standard epidemic models, the treatment rate is proportional to the infective's population size; however, in general, the rate of recovery is determined by medical resources such as medications, vaccinations, hospital beds, isolation areas, and the effectiveness of the treatments. It is understood in practice that societies have limited medical services for the treatment of infections, so offering these services places considerable pressure on facilities for public health. It is therefore more realistic to consider treatment functions of the saturated form, which appear to be large as the number of infectives increases [9–11]. Wang and Ruan [12] proposed an SIR model with a constant treatment as follows:

$$h(I) \begin{cases} \tau, & I > 0, \\ 0, & I = 0, \end{cases} \tag{1}$$

that modeled a treatment capacity limit. The following piecewise linear treatment function was considered by Wang and Ruan [12]:

$$h(I) \begin{cases} \tau I, & 0 \le I \le I_0, \\ \tau I_0, & I > I_0, \end{cases} \tag{2}$$

where I_0 is the infectious threshold at which the healthcare system gains capacity; that is, treatment rises linearly with I until capacity is achieved, and then it takes its maximal value, τI. This appears to be more realistic than the standard linear function. Eckalbar and Eckalbar [13] built the following SIR model using a quadratic treatment function:

$$T(I) = \max\{\tau I - gI^2, 0, \quad r, g > 0. \tag{3}$$

Apart from that, we are aware that delaying treatment for infective persons has a negative impact on treatment efficiency. Zhang and Liu [9] employed a saturated treatment function that was both continuous and differentiable, $h(I) = \tau I/(1 + kI)$, where $\tau > 0, \tau$ corresponds to the cure rate, and the quantity k represents the delay in treatment.

It has been noted that saturation in recovery or treatment function allows multiple endemic equilibria to occur when R_0 changes [9, 10, 14–17]. For $R_0 < 1$, the presence of backward bifurcation (the existence of endemic equilibrium along with disease-free equilibrium) implies that only $R_0 < 1$ is insufficient to eradicate the disease from the community [9, 14, 16, 17].In this situation, an endemic equilibrium is established along with the stable disease-free equilibrium (bistability of equilibria when $R_0 < 1$). Moreover, some researchers have observed the presence of limit cycles alongside the stable disease-free equilibrium when $R_0 < 1$ [16, 17]. Subsequently, if $R_0 < 1$, the occurrence of a stable endemic equilibrium and oscillations in the infective population indicate that maximum efforts are needed to eliminate or monitor the disease [14, 16, 17].

Moreover, when $R_0 > 1$, some different scenarios, for example, Hopf bifurcation and the occurrence of several endemic equilibria, also have been observed as a result of saturated recovery or treatment [12, 14, 15, 17]. For example, Cui et al. [14] proposed and investigated an SIS model with saturated recovery rate and discovered the occurrence of

oscillatory behavior in the population via Hopf bifurcation because of the treatment capacity limitations. Wang and Ruan [12] presented and analyzed an SIR model with a constant treatment rate of infective. They noticed that when $R_0 > 1$, the system experiences different bifurcations including saddle-node bifurcation and Hopf bifurcation. Global stability is observed without removal rate, while oscillatory behavior for constant removal rate was discovered. The behaviour of SEIR epidemic model with saturated treatment function is investigated by [18], a backward bifurcation that results in bistability emergence, and numerical result work suggested that they should improve the medical conditions to control the epidemic [19]. To fully understand the influence of delayed treatment on transmission of the dynamics of disease, Zhang et al. [20] considered an SEIR model approach with saturated incidence and saturated treatment method. Their finding recommends that to eliminate the disease, they should raise the effectiveness and extend the capacity of treatment. In other words, our medical technology and contribution of more drugs and beds provide timely treatment to patients.

In this paper, we incorporated saturated recovery which was excluded in previous four-dimensional SEIR-like models with exogenous infection used to study the phenomenon of backward bifurcation (see [21, 22]).

2. Construction of the Model

We examined the transmission dynamics of TB by employing a nonlinear ODE system of $S_t E_t I_t R_t$ type system, which was developed in [21, 22]. Our aim is to better understand the interplay between exogenous reinfection and saturated treatment (recovery) rate in determining the outbreaks of TB. The whole population $N_t(t)$ is classified into four (9) compartments, S_t, E_t, I_t, and R_t, which, respectively, denote susceptible, exposed, infected, and treated individuals. A normal mass action known as density-dependent incidence form interaction for the TB epidemic is examined and the population is considered to also be homogeneously mixed. The S_t, E_t, I_t, R_t process of TB spreading is shown in Figure 1.

2.1. The Model with Saturated Recovery Rate.
The nonlinear model that is considered in this study consists of a system of ordinary differential equations (ODEs):

$$\frac{dS_t}{dt} = \Lambda - \mu S_t - \beta S_t I_t,$$

$$\frac{dE_t}{dt} = \beta S_t I_t - p\beta E_t I_t - (\kappa + \mu)E_t,$$

$$\frac{dI_t}{dt} = p\beta E_t I_t + \kappa E_t - (\mu + \tau + \delta)I_t - \frac{cI}{1 + \varpi I_t}, \tag{4}$$

$$\frac{dR_t}{dt} = \frac{cI_t}{1 + \varpi I_t} + \tau I_- \mu R_t,$$
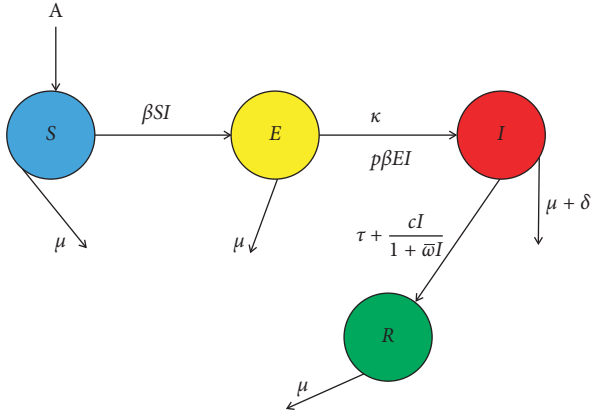
with the initial conditions given by the following equation:

FIGURE 1: Schematic diagram showing the dynamics of TB infection with saturated recovery.

$$S_t(0) = S_{t0} > 0,$$
$$E_t(0) = E_{t0} > 0,$$
$$I_t(0) = I_t > 0,$$ (5)
$$R_t(0) = R_{t0} > 0.$$

In this epidemiological system, the susceptible compartment is increased by recruiting individuals, either by immigration or birth, into the population at the constant rate Λ. The term μ is the natural death rate. The exposed compartment becomes infectious at the rate of κE and progresses to actively infected state. Exogenous reinfection can enable individuals that are already infected to develop active TB. This happens when they contract new infection from infectious individuals at a constant rate $p\beta EI$. Infected individuals are decreased in number because of treatment, which is given at the rate τI, $cI/(1 + \varpi I)$. δ respectively. The term $cI/(1 + \varpi I)$ is the saturation form of treatment (recovery) to the infected populations with the recovery rate c, and the parameter ϖ determines the magnitude of the impact of delaying the treatment of infected individuals.

3. Basic Properties of the TB Model with Saturated Recovery

Following the technique in [23, 24] (and furthermore the proof in [24]), it is not hard to demonstrate that when all model parameters remain nonnegative, the state variables $S_t, E_t, I_t,$ and R_t are all positive for all time t given they are initially positive.

Theorem 1. *The region*

$$\Phi = \left\{(S_t, E_t, I_t, R_t) \in R_+^4, \quad N_t \leq \frac{\Lambda}{\mu}\right\},$$ (6)

is positively invariant and attracts all nonnegative solutions of model system (4).

Proof. As mentioned in the study of [23], considering the nonlinear system of model (4), we take the first equation and let $\lambda = \beta I_t$.

$$\frac{dS_t}{dt} = \Lambda - (\lambda + \mu),$$ (7)

that is,

$$\frac{dS_t}{dt} \geq -(\lambda + \mu)S,$$ (8)

$$\Longrightarrow \frac{dS_t}{S_t} \geq (\lambda + \mu)dt.$$ (9)

Integrating (9) by separation of variables gives

$$\int \frac{dS_t}{S_t} \geq \int (\lambda + \mu)dt,$$ (10)

and therefore

$$S_t(t) \geq S_{(0)}e^{-(\lambda+\mu)t} \geq 0.$$ (11)

Similarly, it can also been shown that $E_t(t) > 0$, $I_t(t) > 0$, $R_t(t) > 0$, for all $t > 0$.

3.1. Invariant Region

Theorem 2. *The solution of TB model system (4) is enclosed in the region Φ subset $\in \in R_+^6$, given by*

$$\Phi = \left\{(S_t, E_t, I_t, R_t) \in R_+^4, \quad N_t \leq \frac{\Lambda}{\mu}\right\},$$ (12)

for the initial conditions (5) in Φ.

4. Analysis of Disease-Free Equilibrium (DFE), P_0, and Effective Basic Reproduction Number R_C

The disease-free equilibrium (DFE) state, P_0, of system model (4) is obtained by setting the right-hand side of (4) to zero which is given by

$$P_0 = (S_t, E_t, I_t, R_t)\left(\frac{\Lambda}{\mu}, 0, 0, 0\right).$$ (13)

The basic reproduction number of system model (4) was calculated using the next generation operator approach (see [25, 26]), where it is obtained to be

$$R_C = \frac{\beta\kappa\Lambda}{\mu(\mu + \kappa)(\mu + \delta + \tau + c)},$$ (14)

where R_C is the effective reproduction number of system model (4). The following outcomes would guaranty the stability of P_0, when the threshold quantity $R_C < 1$ ascertains that the system will be free from TB infection under a threshold condition. A significant result is the following theorem.

Theorem 3. *The disease-free equilibrium state, P_0, of model system (4) is locally asymptotically stable (LAS) when $R_C < 1$ and unstable if $R_C > 1$.*

Proof. Consider model system (4), and the Jacobian of system (4) at P_0 is given by

$$\Sigma(P_0) = \begin{pmatrix} -\mu & 0 & \dfrac{-\beta\Lambda}{\mu} & 0 \\ 0 & -(\kappa+\mu) & \dfrac{\beta\Lambda}{\mu} & 0 \\ 0 & \kappa & -(\mu+\delta+\tau+c)(R_C-1) & 0 \\ 0 & 0 & \tau+c & -\mu \end{pmatrix}. \tag{15}$$

Then, the root characteristic equation of $\Sigma(P_0)$ is $-\mu$, $-(\kappa+\mu)$, $-\mu$, and $-(\mu+\delta+\tau+c)(R_C-1)$. If $R_C < 1$, all the characteristic roots are negative and thus P_0 is locally asymptotically stable and unstable when $R_C > 1$.

4.1. Global Stability of P_0 State. In order to ensure that TB is independent of the initial size of the subpopulations of model system (4), it is necessary to show that P_0 is globally asymptotically stable (GAS) [27–30]. Several approaches, such as the Lyapunov theorem, [27, 29, 31, 32] and global stability theorem have been used to prove the global stability of the disease free equilibrium, P_0. Here, we shall apply the method that was introduced in [32].

Theorem 4. *The disease-free equilibrium P_0 of model system (4) is global asymptotically stable in Ω if $R_C < 1$ and conditions (H_1) and (H_2) are satisfied as given in [32].*

Proof. The two conditions (H_1) and (H_2) in Castillo-Chavez global stability theorem must be satisfied for $R_C < 1$ to ascertain the global stability of the P_0. Write system model (4) in the following form:

$$\frac{dX}{dt} = F(X, Z),$$

$$\frac{dZ}{dt} = G(X, Z); \quad G(X, Z) = 0. \tag{16}$$

Here, the components $X = (S_\iota^*, R_\iota^*)$ and $Z = (E_\iota^*, I_\iota^*)$ where $X \in R^2$ denotes uninfected population and $Z \in R^2$ denotes the infected population. The disease-free equilibrium is defined by

$$P_0 = (X^*, 0), \tag{17}$$

where

$$X^* = \left(\frac{\Lambda}{\mu}, 0\right). \tag{18}$$

For condition H_1 (the global asymptotical stability of X^*) to be fulfilled, we have

$$\frac{dX}{dt} = F(X, 0) \begin{pmatrix} \Lambda - \mu S_\iota^* \\ \mu R_\iota^* \end{pmatrix}, \tag{19}$$

written in the form of linear differential equations as follows:

$$\frac{dS_\iota^*}{dt} = \Lambda - \mu S_\iota^*,$$

$$\frac{dR_\iota^*}{dt} = \mu R_\iota. \tag{20}$$

Solving linear differential equation (20) yields

$$S_\iota^*(t) = \frac{\Lambda}{\mu} + S_\iota^*(0)e^{-\mu t},$$

$$R_\iota^*(t) = R_\iota^*(0)e^{-(\mu)t}. \tag{21}$$

Now, clearly $R_\iota^*(t) \longrightarrow 0$ and $S_\iota^*(t) \longrightarrow (\Lambda/\mu)$ as $t \longrightarrow \infty$, regardless of the value of $S_\iota^*(0)$ and $R_\iota^*(0)$.

Hence, $X^* = ((\Lambda/\mu), 0)$ is globally asymptotically stable.

Next, applying second condition of the theorem proposed in [32], that is, $\widehat{G}(X, Z) = AZ - G(X, Z)$, $\widehat{G}(X, Z) \geq 0$, we have

$$G(X, Z) = \begin{bmatrix} G_1(X, Z) \\ G_2(X, Z) \end{bmatrix} = \begin{bmatrix} \beta S_\iota I_\iota - (\mu+\kappa+p\beta I_\iota)E_\iota \\ \kappa E_\iota - \left(\mu+\delta+\tau+\dfrac{cI_\iota}{1+\varpi}\right)I_\iota \end{bmatrix},$$

$$A) = \frac{\partial G}{\partial Z}(X^*, 0) \begin{bmatrix} -(\mu+\kappa) & 0 \\ \kappa & -\left(\mu+\delta+\tau+\dfrac{c}{\varpi}\right) \end{bmatrix}. \tag{22}$$

This is certainly an M- matrix (the off-diagonal elements of A are nonnegative) [32].

Since

$$G(X, Z) = \begin{bmatrix} -(\mu+\kappa)E_\iota^* & 0 \\ \kappa E^* & -\left(\mu+\delta+\tau+\dfrac{c}{\varpi}I_\iota^*\right) \end{bmatrix}, \tag{23}$$

then,

$$\widehat{G}(X, Z) = AZ - G(X, Z)$$

$$
= \begin{bmatrix} -(\mu + \kappa) & 0 \\ \\ \kappa & -\left(\mu + \delta + \tau + \dfrac{c}{\omega}\right) \end{bmatrix} \begin{bmatrix} E_\iota^* \\ \\ I_\iota^* \end{bmatrix} - \begin{bmatrix} -(\mu + \kappa)E_\iota^* & 0 \\ \\ \kappa E_\iota^* & -\left(\mu + \delta + \tau + \dfrac{c}{\omega}I_\iota^*\right) \end{bmatrix}
$$ (24)

$$
= \begin{bmatrix} -(\mu + \kappa)E_\iota^* & 0 \\ \\ \kappa E_\iota^* & -\left(\mu + \delta + \tau + \dfrac{c}{\omega}I_\iota^*\right) \end{bmatrix} - \begin{bmatrix} -(\mu + \kappa)E_\iota^* & 0 \\ \\ \kappa E_\iota^* & -\left(\mu + \delta + \tau + \dfrac{c}{\omega}I_\iota^*\right) \end{bmatrix} = \begin{bmatrix} 0 \\ 0 \end{bmatrix},
$$

so that

$$\widehat{G}(X, Z) = AZ - G(X, Z) = \begin{bmatrix} 0 \\ 0 \end{bmatrix}. \quad (25)$$

Since $\widehat{G}(X_1, X_2) \geq 0$, we have showed that condition $H2$ of the theorem proposed in [32, 33] is satisfied by our model. This shows that regardless of the initial population of infected, TB still can be controlled.

4.2. Endemic Equilibria and Bifurcation Analysis. To find endemic equilibrium $(S_\iota^*, E_\iota^*, I_\iota^*, R_\iota^*)$ as before, we set the right-hand side of system model (4) to zero. Solving for S_ι^*, E_ι^*, and R_ι^* from first, third, and last equation of (4), respectively, we have

$$S_\iota^* = \frac{\Lambda}{\mu + \beta I_\iota^*}, \quad (26)$$

$$E_\iota^* = \frac{(M + (c/(1 + \omega I_\iota^*)))I_\iota^*}{p * \beta I_\iota^*}, \quad (27)$$

where $M = (\mu + \tau + \delta)$ and

$$R_\iota^* = \frac{(\tau + (c/(1 + \omega I_\iota^*)))I_\iota^*}{\mu}. \quad (28)$$

By substituting and simplifying equations (26)–(28), we get the following equation in I_ι^*:

$$F(I_\iota^*) = \widetilde{A}I_\iota^3 + \widetilde{B}I_\iota^2 + \widetilde{C}I_\iota + \widetilde{D} = 0, \quad (29)$$

where

$$
\begin{aligned}
\widetilde{A} &= \omega p \beta^2 M, \\
\widetilde{B} &= (p(-\omega\Lambda + M + c)\beta + \omega M((p+1)\mu + \kappa))\beta, \\
\widetilde{C} &= \left(-p\omega\Lambda\beta^2 + ((p+1)(M + c)\mu + \kappa(-\omega\Lambda + M + c))\beta + \mu\omega M(\kappa + \mu)\right), \\
\widetilde{D} &= (\kappa + \mu)(\mu + \tau + \delta + c)(1 - R_C).
\end{aligned}
$$ (30)

Clearly, $\widetilde{A} > 0$. When $R_C > 1$, then $\widetilde{D} < 0$ and thus $F(0) < 0$. Furthermore, as as $I_\iota \longrightarrow \infty$, $F(\infty) > 0$. Accordingly, from the continuity of $F(0)$, at least one positive I_ι exists, such that $F(I_\iota) = 0$, and thus there will be at least one endemic equilibrium of the model system (4). Notice that if $R_C > 1$ and $\widetilde{B}, \widetilde{C}$ are positive, then model system (4) has a unique endemic equilibrium defined as $P^* = (S_\iota^*, E_\iota^*, I_\iota^*, R_\iota^*)$ from Descartes' rule of sign. The number of possible positive real roots of the cubic polynomial (29) depends on the signs of $\widetilde{B}, \widetilde{C}$, and $\widetilde{D}$. We, therefore, propose the following results.

Theorem 5. *The TB model system (4) has*

(1) *A unique endemic equilibrium when $R_C > 1$.*

(2) *One or more than one endemic equilibrium when $\widetilde{B} < 0, \widetilde{C} > 0$, and $R_C < 1$.*

(3) *No endemic equilibrium when $R_C < 1$.*

Now we will look at the polynomial in (29) to see how it influences the existence of endemic equilibrium.

If $\omega = 0$, the polynomial (29) reduces to a linear equation in I_ι^*, with a unique solution

$$I_\iota^* = -\frac{\widetilde{D}}{\widetilde{C}}, \quad (31)$$

which is positive if and only if $R_C > 1$. As a result, we can now say that if $\omega = 0$, then a unique endemic equilibrium exist if $R_C > 1$ and there cannot be an endemic equilibrium when $R_C < 1$. To put it in another way, if the treatment of certain infected outpatients is not delayed, when the effective reproduction number is smaller than unity, an endemic steady state solution is not possible, ignoring the possibility of a backward bifurcation in this scenario.

4.3. Local Stability of Endemic Equilibrium (P^*). The Jacobian matrix of (4) at P^* is given as

$$\Sigma(P^*) = \begin{pmatrix} \Upsilon & 0 & \chi & 0 \\ \beta I_\iota & -(\kappa + \mu + p\beta I_\iota) & -p\beta E_\iota + \beta S_\iota & 0 \\ 0 & p\beta I_\iota + \kappa & \Psi & 0 \\ 0 & 0 & \Xi & -\mu \end{pmatrix}. \quad (32)$$

Here

$$\Upsilon = -\mu + \beta I_\iota,$$

$$\chi = -\beta S_\iota,$$

$$\Psi = p\beta E_\iota - M - \frac{c}{1 + \varpi I_\iota} + \frac{c\varpi I_\iota}{(1 + \varpi I_\iota)^2}, \quad (33)$$

$$\Xi = \tau + \frac{c}{1 + \varpi I_\iota} - \frac{c\varpi I_\iota}{(1 + \varpi I_\iota)^2}.$$

We obtain the characteristic equation after some row and column operations of $\Sigma(P^*)$ given by

$$\lambda^4 + A_1\lambda^3 + A_2\lambda^2 + A_3\lambda + A_4 = 0, \quad (34)$$

where

$$A_1 = p\beta I_\iota - \Psi + \kappa + 2\mu - \Upsilon,$$

$$A_2 = p(pE_\iota - S_\iota)I_\iota\beta^2 + ((\kappa E_\iota + (\mu - \Psi - \Upsilon))pI_\iota - S_\iota\kappa)\beta$$
$$+ (\mu - \Psi - \Upsilon)\kappa + \mu^2 + (-2\Psi - 2\Upsilon)\mu + \Psi\Upsilon,$$

$$A_3 = p(pE_\iota - S_\iota)\mu I_\iota + (pE_\iota - S_\iota)\Upsilon + \chi I_\iota)\beta^2 + ((pI_\iota\Upsilon + (\kappa E_\iota - \Psi I_\iota)p - \kappa S_\iota$$
$$+ ((-\kappa E_\iota + \Psi_\iota)p + \kappa S_\iota)\Upsilon - \kappa\chi I_\iota)\beta + (-\Upsilon + \Psi)\mu^2 + ((2\Psi - \kappa)\Upsilon - \kappa\Psi)\mu + \kappa\Psi\Upsilon,$$

$$A_4 = \mu((pI_\iota(pE_\iota + S_\iota)\beta^2 + (P\Psi I_\iota - \kappa(pE_\iota - S_\iota))\beta + \Psi(\kappa + \mu))\Upsilon - \beta\chi I_\iota((p\beta I_\iota + \kappa)).$$

$$(35)$$

Thus, all the roots of the characteristic equation $\Sigma(P^*)$ are with negative real parts if $A_1 > 0$, $A_3 > 0$, $A_4 > 0$, and $A_1A_2A_3 > A_3^2 + A_1^2A_4$. Therefore, from Routh–Hurwitz criterion [34], the endemic equilibrium state P^* is locally asymptotically stable if these conditions are true. The following result can be obtained.

Theorem 6. *If $R_C > 1$ and $\bar{B}$ and $\tilde{D}$ are positive, then the unique endemic equilibrium P^* of system model (4) is locally asymptotically stable provided $A_3 > 0, A_4 > 0$, and $A_1A_2A_3 > A_3^2 + A_1^2A_4$.*

4.4. Analysis of Backward Bifurcation. The existence and stability of endemic equilibrium are determined by investigating the possibility of backward or forward bifurcation due to the existence of endemic equilibrium. To investigate the possibility of backward or forward bifurcation of model system (4), we use the center manifold theory [35, 36]. Let the bifurcation parameter be $\beta = \beta^*$.

Firstly, we obtained the bifurcation parameter at $R_0 = 1$, and thus

$$\frac{\beta\kappa\Lambda}{\mu(\kappa + \mu)(\mu + \delta + \tau + c)} = 1, \quad (36)$$

and therefore

$$\beta = \beta^* = \frac{\mu(\kappa + \mu)(\mu + \delta + \gamma + c)}{\Lambda\kappa}. \quad (37)$$

To investigate the use of center manifold theory in [35], it is convenient to make simplification and transform the variables on model system (4). This is done by rewriting our system model (4).

Let

$$x_1 = S_\iota,$$
$$x_2 = E_\iota,$$
$$x_3 = I_\iota,$$
$$x_4 = R_\iota.$$
$$(38)$$

Moreover, by using the vector notation $V = (x_1, x_2, x_3, x_4)^T$, model system (4) can be restated in the form of $(dV/dt) = (f_1, f_2, f_3, x_4)^T$ as follows:

$$\frac{dx_1}{dt} = \Lambda - \beta x_1 x_3 - \mu x_1 = f_1,$$

$$\frac{dx_2}{dt} = \beta x_1 x_3 - p\beta x_2 x_3 - (\kappa + \mu)x_2 = f_2,$$

$$\frac{dx_3}{dt} = \kappa x_2 + p\beta x_2 x_3 - (\mu + \delta + \tau)x_3 - \frac{cx_3}{1 + \varpi x_3} = f_3,$$

$$\frac{dx_4}{dt} = \tau x_3 + \frac{cx_3}{1 + \varpi x_3} - \mu x_4 = f_4.$$

$$(39)$$

We next show that the Jacobian matrix of (4) at the point (P_0, β^*) has a simple zero eigenvalue, that is,

$$\Sigma(P_0, \beta^*) = \begin{pmatrix} -\mu & 0 & \dfrac{-\beta^*\Lambda}{\mu} & 0 \\ 0 & -(\kappa + \mu) & \dfrac{\beta^*\Lambda}{\mu} & 0 \\ 0 & \kappa & -(\mu + \delta + \tau + c) & 0 \\ 0 & 0 & \tau + c & -\mu \end{pmatrix}. \quad (40)$$

With $\beta = \beta^*$, system model (39) has a simple zero real part eigenvalue, and all other eigenvalues are negative (i.e., has a hyperbolic equilibrium point). The center manifold theory [35] can therefore be used to examine the dynamics of the system (39) close to $\beta = \beta^*$. It is practicable to derive the right eigenvectors of $\Sigma(P_0, \beta^*)$ represented by $\omega = (\omega_1, \omega_2, \omega_3, \omega_4)^T$, where

$$\omega_1 = \frac{\beta\Lambda}{\mu}(\mu + \kappa),$$

$$\omega_2 = \frac{\mu + \tau + \delta + c}{\kappa},$$

$$\omega_3 = 1,$$

$$\omega_4 = \frac{\tau + c}{\mu}.$$

$$(41)$$

Conversely, the left eigenvectors represented as $v = (v_1, v_2, v_3, v_4)^T$ are easy to obtain, where

$$v_1 = 0,$$

$$v_2 = \frac{\kappa}{2\mu\kappa + \tau\delta + c},$$

$$\frac{\kappa + \mu}{2\mu\kappa + \tau\delta + c},$$

$$v_4 = 0.$$

$$(42)$$

4.5. *Computation of a and b.* Hence, associated bifurcation coefficients are denoted by a and b, respectively; as explained in [35], when bifurcation coefficients a and b are both negative, then the system undergoes a backward bifurcation; otherwise, forward bifurcation will occur.

It is convenient to find both a and b defined by [35]

$$a = \sum_{k,i,j=1}^{4} v_k w_i w_j \frac{\partial^2 f_k}{\partial x_i \partial x_j}(P_0, \beta^*), \quad (43)$$

$$b = \sum_{k,i=1}^{4} v_k w_i \frac{\partial^2 f_k}{\partial x_i \partial \beta}(P_0, \beta^*). \quad (44)$$

Taking into account model system (39) and examining a and b only, which are not equal to zero derivatives, for the terms

$$\left(\frac{\partial^2 f_k}{\partial x_i \partial x_j}\right)(P_0, \beta^*),$$

$$\left(\frac{\partial^2 f_k}{\partial x_i \partial \beta}\right)(P_0, \beta^*), \quad (45)$$

we get

$$a = 2v_1\omega_1 w_\varpi \frac{\partial^2 f_1}{\partial x_1 \partial x_4}(P_0, \beta^*) + 2v_2\omega_2\omega_4 \frac{\partial^2 f_2}{\partial x_2 \partial x_4}(P_0, \beta^*)$$

$$+ 2v_3\omega_1\omega_4 \frac{\partial^2 f_3}{\partial x_1 \partial x_4}(P_0, \beta^*) + 2v_3\omega_2\omega_4 \frac{\partial^2 f_3}{\partial x_3 \partial x_4}(P_0, \beta^*)$$

$$+ 2v_3\omega_3\omega_4 \frac{\partial^2 f_3}{\partial x_3 \partial x_4}(P_0, \beta^*) + 2v_4\omega_3\omega_4 \frac{\partial^2 f_4}{\partial x_3 \partial x_4}(P_0, \beta^*),$$

$$b = 2v_1v_4 \frac{\partial^2 f_1}{\partial x_4 \partial \beta}(P_0, \beta^*) + v_3\omega_2\omega_4 \frac{\partial^2 f_3}{\partial x_4 \partial \beta}(P_0, \beta^*).$$

$$(46)$$

Now considering (43) and (44), we obtain

$$a = 2\frac{2(\mu + \kappa)}{2\mu + \tau + \delta + c}\left[-\frac{(\mu + \kappa)(\mu + \tau + \delta + c)}{\kappa\Lambda\mu}\right.$$

$$\left. - (\mu + \tau + \delta + c) + c\varpi\right], \quad (47)$$

$$b = \frac{\kappa}{2\mu + \kappa + \tau + \delta + c}\frac{\Lambda}{\mu}.$$

As indicated by the result shown in [35], our system experiences backward bifurcation at $\beta = \beta^*$, only when both a and b are positive at (P_0, β^*). Obviously, b is consistently positive. Hence, the positivity of a offers the threshold circumstance for the phenomenon of backward bifurcation.

4.6. *Analysis of Hopf Bifurcation.* Hopf bifurcation of system (4) around endemic equilibrium point will be considered in this section. We employ the criterion that was derived in [37]

to show that Hopf bifurcation exists. Let $P^{**} = (S_t^*, E_t^*, I_t^*, R_t^*)$ be an endemic equilibrium of system (4) when $R_C > 1$ and β be a bifurcation parameter for which P^{**} is locally stable when $\beta < \beta_o$ and unstable when $\beta > \beta_o$. At $\beta = \beta_o$, P^{**} loses its stability and periodic solutions emerge. The characteristic equation at endemic equilibrium equivalent to model system (4) at P^{**} is given by

$$X^4 + A_1 X^3 + A_2 X^2 + A_3 X + A_4 = 0. \tag{48}$$

It was also observed that the component of the endemic equilibrium P^{**} smoothly relies on β, and the corresponding characteristic equation is given as

$$X^4 + A_1(\beta)X^3 + A_2(\beta)X^2 + A_3(\beta)X + A_4(\beta) = 0. \tag{49}$$

To this place, the coefficient is a smooth function of β. Following the approach in [38], a Hopf bifurcation occurs when the following two conditions are satisfied:

The Jacobian matrix $J(P^{**}, \beta_o)$ has a pair of purely imaginary eigenvalues and the remaining eigenvalues have negative real parts.

$(d(\mathrm{Re}(A))/d\beta)|_{\beta=\beta_o} \neq 0$.

According to [37], the coefficients of the characteristic equation have to meet the prerequisite for a pair of purely imaginary eigenvalues, which are

$$A_4 > 0, \ A_4 > 0 \text{ and } A_3 A_2 - A_4 A_1 > 0.$$
$$\Delta_2 = A_3 A_2 A_1 - A_3^2 - A_4 A_1^2 = 0.$$

To complete the discussion, we need to drive the transversality condition (ii). For this reason, we let $\pm i\alpha$ be a pair of purely imaginary eigenvalues corresponding to β_o. Here, differentiating characteristic equation (48) with respect to β, we get

$$\left(4X^3 + 3A_1 X^2 + 2A_2 X + A_3\right)\frac{dX}{d\beta} + X^3 \frac{dA_1}{d\beta} + X^2 \frac{dA_2}{d\beta}$$

$$+ X\frac{dA_3}{d\beta} + \frac{dA_4}{d\beta} = 0. \tag{50}$$

Further, we get

$$\left(\frac{dX}{d\beta}\right)^{-1} = -\frac{4X^3 + 3A_1 X^2 + 2A_2 X + A_3}{X^3(dA_1/d\beta) + X^2(dA_2/d\beta) + X(dA_3/d\beta) + (dA_4/d\beta)}. \tag{51}$$

The following relation will be used.

$$\mathrm{sign}\left[\frac{d(R_e(X))}{d\beta}\right]_{X=i\alpha, \Delta_2=0} = \mathrm{sign}\left[\mathrm{Re}\left(\frac{dX}{d\beta}\right)^{-1}\right]_{X=i\alpha, \Delta_2=0}$$

$$= \mathrm{sign}\left[\mathrm{Re}\left[-\frac{\left(A_3 - 3A_1\alpha^2\right) + \left(2A_2\alpha - 4\alpha^3\right)i}{\left((dA_4/d\beta) - (dA_2/d\beta)\alpha^2\right) + \left((dA_3/d\beta)\alpha - (dA_1/d\beta)\alpha^3\right)i}\right]\right] \tag{52}$$

$$= \mathrm{sign}[\Upsilon].$$

Here

$$\Upsilon = -\frac{\left(A_3 - 3A_1\alpha^2\right)\left((dA_4/d\beta) - (dA_2/d\beta)\alpha^2\right) + \left(2A_2\alpha - 4\alpha^3\right)\left((dA_3/d\beta)\alpha - (dA_1/d\beta)\alpha^3\right)}{\left((dA_4/d\beta) - (dA_2/d\beta)\alpha^2\right)^2 + \left((dA_3/d\beta)\alpha - (dA_1/d\beta)\alpha^3\right)^2}. \tag{53}$$

If $(A_3 - 3A_1\alpha^2)((dA_4/d\beta) - (dA_2/d\beta)\alpha^2) + (2A_2\alpha - 4\alpha^3)((dA_3/d\beta)\alpha - (dA_1/d\beta)\alpha^3) < 0$, then $\text{sign}[d(R_e(X))/d\beta]_{\beta_o,\alpha} > 0$. We then summarize this result in the following equation:

$$\left(A_3 - 3A_1\alpha^2\right)\left(\frac{dA_4}{d\beta} - \frac{dA_2}{d\beta}\alpha^2\right) + \left(2A_2\alpha - 4\alpha^3\right)$$
$$\left(\frac{dA_3}{d\beta}\alpha - \frac{dA_1}{d\beta}\alpha^3\right) < 0. \tag{54}$$

Therefore, the transversality condition holds, and the system undergoes the phenomena of Hopf bifurcation at $\beta_o = \alpha$. Thus, transmission rate β_o crosses its critical value, $\beta_o = \alpha$, and individuals start oscillating around endemic equilibrium point P^{**}. This ends the proof of the theorem.

4.7. Global Stability of Endemic Equilibrium When $R_C > 1$.

To prove the global stability of endemic equilibrium state P^{**} of system model (4), we consider the case when exogenous reinfection parameter $p = 0$. We employed the Lyapunov function method and LaSalle's invariance principles [39, 40]. System model (4) with $p = 0$ therefore reduces to

$$\frac{dS_t}{dt} = \Lambda - \mu S_t - \beta S_t I_t,$$

$$\frac{dE_t}{dt} = \beta S_t I_t - (l_1)E_t,$$

$$\frac{dI_t}{dt} = \kappa E_t - (l_2)I_t - f(I_t), \tag{55}$$

$$\frac{dR_t}{dt} = f(I_t) + \tau I_- \mu R_t,$$

with

$$l_1 = \mu + \kappa,$$

$$l_2 = \mu + \tau + \delta, \tag{56}$$

$$f(I_t) = \frac{cI_t}{1 + \varpi I_t}.$$

Furthermore, define

$$\Gamma_o = \{(S_t, E_t, I_t, R_t) \geq \Gamma: E_t = I_t = R_t = 0\}. \tag{57}$$

The following result is obtained.

Theorem 7. *If $R_C > 1$, then the endemic equilibrium state P^{**} given by (55) is GAS in $\Gamma \backslash \Gamma_o$.*

Proof. Consider the model without exogenous reinfection given by (55), and $R_C > 1$, so that the endemic equilibrium P^{**} of the model (55) exists. In addition, consider the following Lyapunov function method of this type which has been utilized in the study of epidemiology and ecology, such as in [29, 41–43], for model system (55) comprising the first three equations of (55), defined by the following. Define the Lyapunov function

$$U(S_t, E_t, I_t) = S_t - S_t^{**} - S_t^{**} \ln\left(\frac{S}{S_t^{**}}\right)$$

$$+ E_t - E_t^{**} - E_t^{**} \ln\left(\frac{E}{E_t^{**}}\right) \tag{58}$$

$$+ \frac{l_1}{\kappa}\left[I_t - I_t^{**} - I_t^{**} \ln\left(\frac{I}{I_t^{**}}\right)\right],$$

and the derivatives of U are given by

$$\acute{U} = \acute{S}_t - \frac{S_t^{**}}{S_t}\acute{S} + \acute{E} - \frac{E_t^{**}}{E_t}\acute{E}_t + \frac{l_1}{\kappa}\left(\acute{I}_t - \frac{I_t^{**}}{I_t}\acute{I}_t\right). \tag{59}$$

Filling in the derivatives and using (55) in U', we have

$$= \Lambda - \beta S_t I_t - \mu S_t - \frac{S_t^{**}}{S_t}(\Lambda - \beta S_t I_t - \mu S_t) + \beta S_t I_t - l_1 E_t$$

$$- \frac{E_t^{**}}{E_t}(\beta S_t I_t - l_1 E_t) + \frac{l_1}{\kappa}\left[\kappa E_t - l_2 I_t - \frac{I_t^{**}}{I_t}(\kappa E_t - l_2 I_t)\right], \tag{60}$$

$$\acute{U} = \Lambda\left(1 - \frac{S_t^{**}}{S_t}\right) - \mu S_t\left(1 - \frac{S_t^{**}}{S_t}\right) + \left(\beta S_t^{**} - \frac{l_1 l_2}{\kappa}\right)$$
$$- \frac{E_t^{**}\beta S_t I_t}{E_t} + l_1 E_t^{**} - \frac{l_1 I_t^{**} E_t}{I_t} + \frac{l_1 l_2}{\kappa}. \tag{61}$$

At the endemic steady state, it can be observed that

$$\beta S_t^{**} = \frac{(\mu + \kappa)(\mu + \tau + \delta + f)}{\kappa} = \frac{l_1 l_2}{\kappa}. \tag{62}$$

Using expression (62) in equation (61) yields

$$\dot{U} = \Lambda\left(1 - \frac{S_t^{**}}{S_t}\right) - \mu S_t\left(1 - \frac{S_t^{**}}{S_t}\right) - \frac{E_t^{**}\beta S_t I_t}{E_t} + E_t^{**}l_1 - \frac{l_1 I_t^{**} E_t}{I_t} + \beta S_t^{**}I_t^{**},$$

$$\dot{U} = (\beta S_t^{**}I_t^{**} + \mu S_t^{**})\left(1 - \frac{S_t^{**}}{S_t}\right) - \mu S_t\left(1 - \frac{S_t^{**}}{S_t}\right) - \frac{E_t^{**}\beta S_t I_t}{E_t} + E_t^{**}l_1 - \frac{l_1 I_t^{**} E_t}{I_t} + \beta S_t^{**}I_t^{**}, \tag{63}$$

$$\dot{U} = \mu S_t^{**}\left(2 - \frac{S_t^{**}}{S_t} - \frac{S_t}{S_t^{**}}\right) + \beta S_t^{**}I_t^{**} - \frac{\beta S_t^{**\,2}}{S_t} - \frac{\beta S_t I_t E_t^{**}}{E_t} + l_1 E_t^{**} - \frac{l_1 I_t^{**} E_t}{I_t} + \beta S_t^{**}I_t^{**}.$$

We also observed from (55) at steady state that

$$l_1 E_t^* = \beta S_t^{**} I_t^{**}. \tag{64}$$

Using expression (64) in equation (63) gives

$$\dot{U} = \mu S_t^{**}\left(2 - \frac{S_t^{**}}{S_t} - \frac{S_t}{S_t^{**}}\right) + \beta S_t^{**}$$

$$I_t^{**}\left(3 - \frac{S_t^{**}}{S_t} - \frac{S_t I_t E_t^{**}}{S_t^{**}I_t^{**}E_t} - \frac{EI_t^{**}}{I_t E_t^{**}}\right). \tag{65}$$

We can simplify the first term in the last equation of (65) as follows.

$$\left(2 - \frac{S_t^{**}}{S_t} - \frac{S_t}{S_t^{**}}\right) = \frac{2S_t S_t^{**} - S_t^{**\,2} - S_t^2}{S_t S_t^{**}} = -\frac{(S_t - S_t^{**})^2}{S_t - S_t^{**}} \le 0. \tag{66}$$

Finally, it follows that since the arithmetic mean exceeds the geometric mean,

$$\left(3 - \frac{S_t^{**}}{S_t} - \frac{S_t I_t E_t^{**}}{S_t^{**}I_t^{**}E_t} - \frac{EI_t^{**}}{I_t E_t^{**}}\right) \le 0. \tag{67}$$

Accordingly, it follows from this that $U \le 0$ when $R_C >$ with $U = 0$ if and only if $S_t = S_t^{**}$, $E_t = E_t^{**}$, and $I_t = I_t^{**}$. Thus, U is a Lyapunov function for system model (55) in $\Gamma\setminus\Gamma_0$. Thus, the largest compact invariant set where $U = 0$ is a singleton $\{(S_t, E_t, I_t) = (S_t^{**}, E_t^{**}, I_t^{**})\}$, and therefore it follows that by [39], $S_t(t) \longrightarrow S_t^{**}$, $E_t(t) \longrightarrow E_t^{**}$, and $I_t(t) \longrightarrow I_t^{**}$ as $t \longrightarrow \infty$.

5. Numerical Simulation and Discussion

To confirm the feasibility of theoretical findings regarding stability and bifurcation of model system (4), we employed numerical continuation package XPPAUT [44] to perform one parameter bifurcation analysis and Matlab to perform numerical experiment. Motivated by some epidemiological literature of TB model [21, 45], model system (4) was validated by choosing a set of parameter values as illustrated in TB relevant literature, and the estimated parameters used are captured in each respective figure.

Figure 2 demonstrates the population of exposed individuals as the transmission rate β is varied from 0 to 2. The y-axis defines the exposed individuals and x-axis defines the transmission rate beta (β). The red and black lines represent stable and unstable steady states, respectively. The green (blue, respectively) cycles illustrated the

occurrence of stable and unstable limit cycles in this epidemiological system. In general, this epidemiological system demonstrates rich bifurcation dynamics which are epidemiologically important. Several dynamical behaviors of the system are observed as β changes. As demonstrated in Figure 2, the system is identified by Sub $\cdot$ H, BP, LP, and LPC, which corresponded to Hopf bifurcation, transcritical bifurcation, saddle-node bifurcation, and saddle-node bifurcation of cycles. van Voorn [46] stated that "when an unstable limit cycle is born, while the equilibrium becomes stable, we have a subcritical Hopf bifurcation." Hence, the bifurcation is subcritical. Indeed, Figure 2 reveals that for the bifurcation point, the stable equilibrium (red line) becomes unstable (black line). In addition, stable and unstable limit cycles also emerge. As the bifurcation parameter β increases, the unstable limit cycles collide with stable limit cycles via a saddle-node bifurcation of cycles LPC.

Figure 3 depicts a codimension-two bifurcation graph as β and τ are changed. To examine the interaction of subcritical Hopf, saddle-node, and transcritical bifurcations, we conducted a codimension-two bifurcation analysis of TB model (4) as we varied the transmission rate β and recovery parameter τ, and the result can be seen in Figure 3. There is indeed a codimension-2 point, black curve with red point, referring to cycle saddle-node bifurcation. This kind of bifurcation frequently occurs as a result of a collision between stable limit cycles (green curve) and unstable limit cycles (blue curve). In general, the codimension-2 bifurcation point serves as an organizing center, separating the parameter space into various curves with distinct qualitative findings: red curve corresponds to saddle-node bifurcation, blue curve corresponds to Hopf bifurcation, and cyan curve corresponds to transcritical bifurcation as demonstrated in previous result (that is, Figure 2, which illustrates the same qualitative mechanisms as Figure 3).

In Figures 4 and 5, we set the parameter values as $\Lambda = 4$, $\mu = 0.18$, $\delta = 0.08$, $\kappa = 0.03$, $p = 0.5$, $c = 0.02$, and $\varpi = 0.1$, and β is varied around the critical value $\beta_o = 1.7$. The threshold quantity $R_C = 2.3670 > 1$, and the eigenvalues are $(-0.2163698605 + 1.349717265I, -3.652541848, -0.2163698605 - 1.349717265I)$ and the model system endemic equilibrium is given as $(2.53865, 3.9028, 0.820965)$. Here, P^* is found to be unstable. The endemic equilibrium P^* is stable for $\beta < \beta_o$ and unstable for $\beta > \beta_o$. We discover that the condition for Hopf bifurcation is fulfilled resulting in the presence of periodic oscillations around P^*. The graphs for the results obtained are given in Figures 4 and 5.
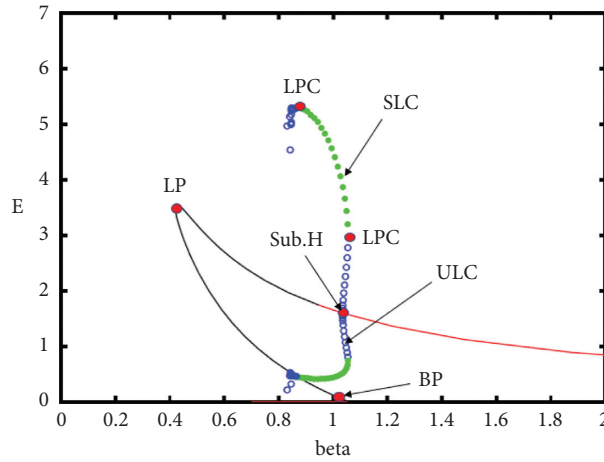
FIGURE 2: One-parameter bifurcation diagram of exposed individuals (E) with transmission rate (β) as a bifurcation parameter. The fixed parameters are $\mu = 0.18$, $\Lambda = 4$, $p = 0.5$, $\kappa = 0.03$, $c = 0.02$, $b = 0.2$, $\delta = 0.08$, and $\tau = 2$. The Hopf bifurcation points occurred at $\beta = 1.035$. Sub · H corresponds to subcritical Hopf bifurcation, LPC corresponds to saddle-node bifurcation of cycles, LP corresponds to saddle-node bifurcation, BP corresponds to transcritical bifurcation, SLC corresponds to stable limit cycle, and ULC corresponds to unstable limit cycle.
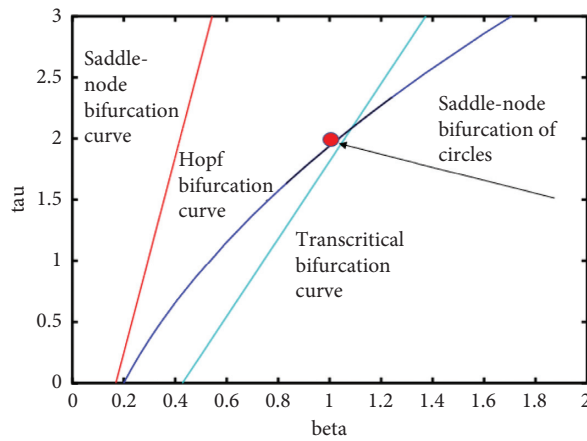

FIGURE 3: Two-parameter bifurcation diagram of model system (9) in the (τ, β)-plane. The fixed parameters are $\mu = 0.18$, $\Lambda = 4$, $p = 0.5$, $\kappa = 0.03$, $c = 0.02$, $b = 0.2$, $\delta = 0.08$, and $\tau = 2$. Red curve denotes saddle-node bifurcation, blue curve denotes Hopf bifurcation, cyan curve denotes transcritical bifurcation, and black curve at (red point) denotes saddle-node bifurcation of cycles.
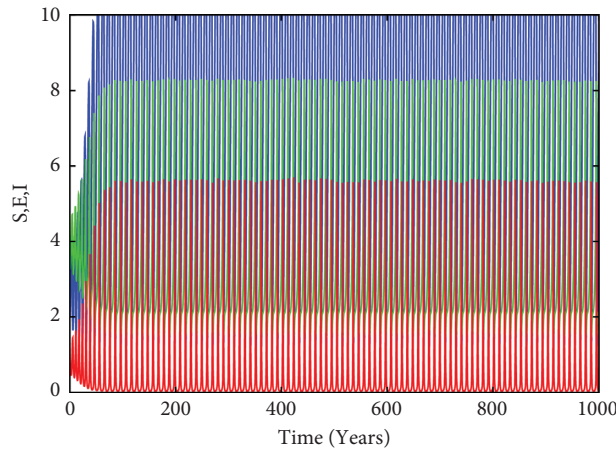

FIGURE 4: The oscillatory simulation of susceptible individuals (blue colour), exposed individuals (green colour), and infected individuals (red colour). Parameters are $\beta = 1.7$, $\Lambda = 4$, $\mu = 0.18$, $\delta = 0.08$, $\kappa = 0.03$, $p = 0.5$, $c = 0.02$, and $\varpi = 0.1$ which give $R_C = 2.3670 > 1$. The oscillatory solution is unstable for some initial conditions. Those used to produce the figure are $S(0) = 2$, $E(0) = 3$, and $I(0) = 1.5$.
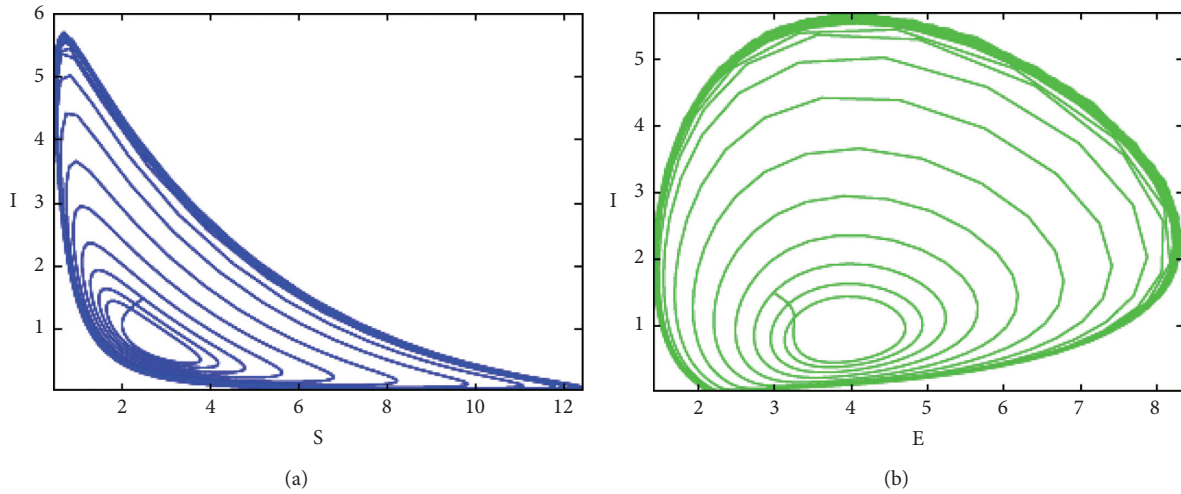
(a)

(b)

FIGURE 5: Phase trajectory for model system (4). The solution approaches periodic orbit around endemic equilibrium when $R_C > 1$. (a) Phase diagram of S, I- plane. (b) Phase diagram of E, I-plane.
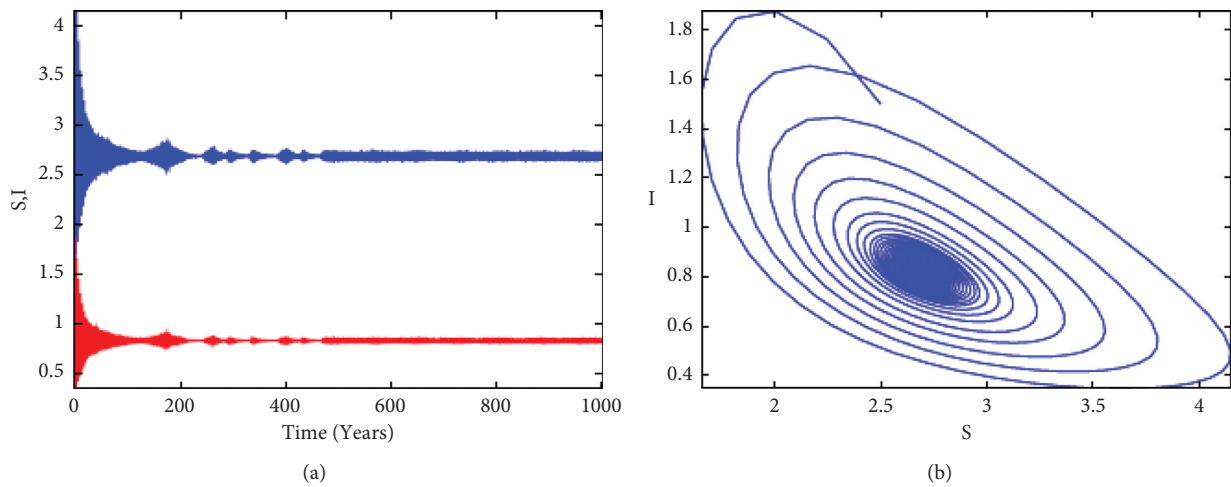

(a)

(b)

FIGURE 6: The trajectories and phase diagram of S, I-plane of model system (4). (a) Profile of S, I with respect to time when $p = 0$. (b) Phase trajectory for S, I-plane when $p = 2$.
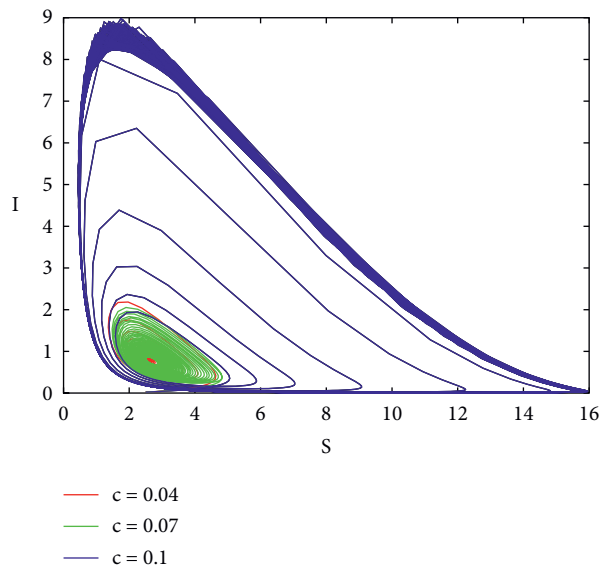

—— c = 0.04
—— c = 0.07
—— c = 0.1

FIGURE 7: The phase diagram of S and I planes with different values of saturated recovery c. Here, there are two limit cycles. The inner one is unstable and the outer one is stable.
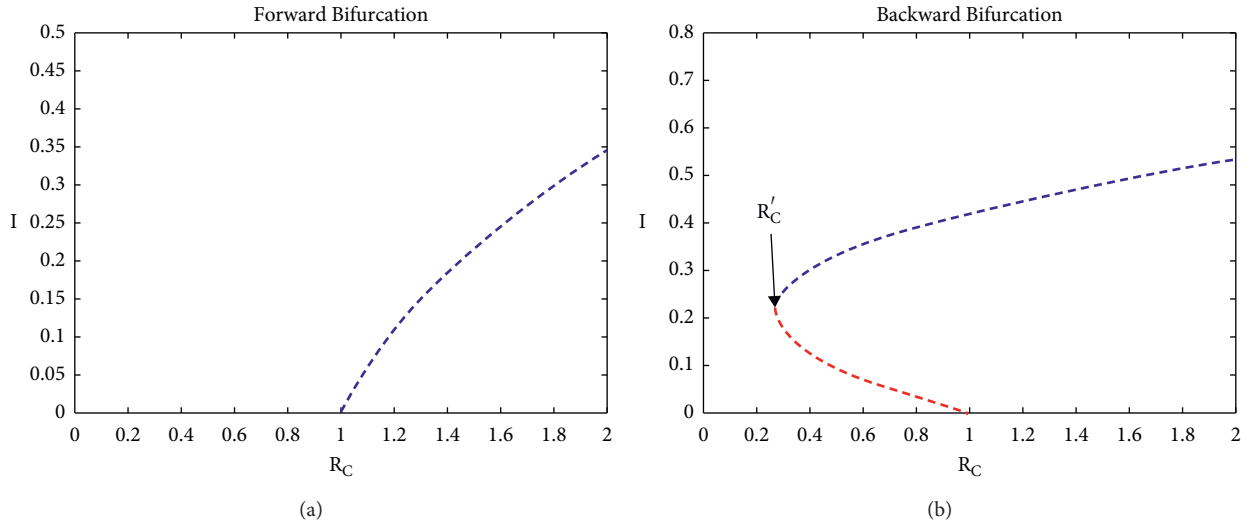
FIGURE 8: (a) Forward bifurcation and (b) backward bifurcation of endemic equilibria where the infected individuals are plotted as a function of R_C. The blue dash line represents the stable equilibrium while the red dash line represents the unstable equilibrium. (a) shows forward bifurcation at the critical value $R_C = 1$, and the parameter values used include $\mu = 0.18$, $\delta = 0.12$, $\kappa = 0.03$, $\beta = 1.6$, $p = 0.12$, $c = 0.9$, $\varpi = 0.1$, and $3.5 \leq \Lambda \leq 5$, while (b) represents backward bifurcation and parameters used are the same as in (a) except $\varpi = 0.25$.
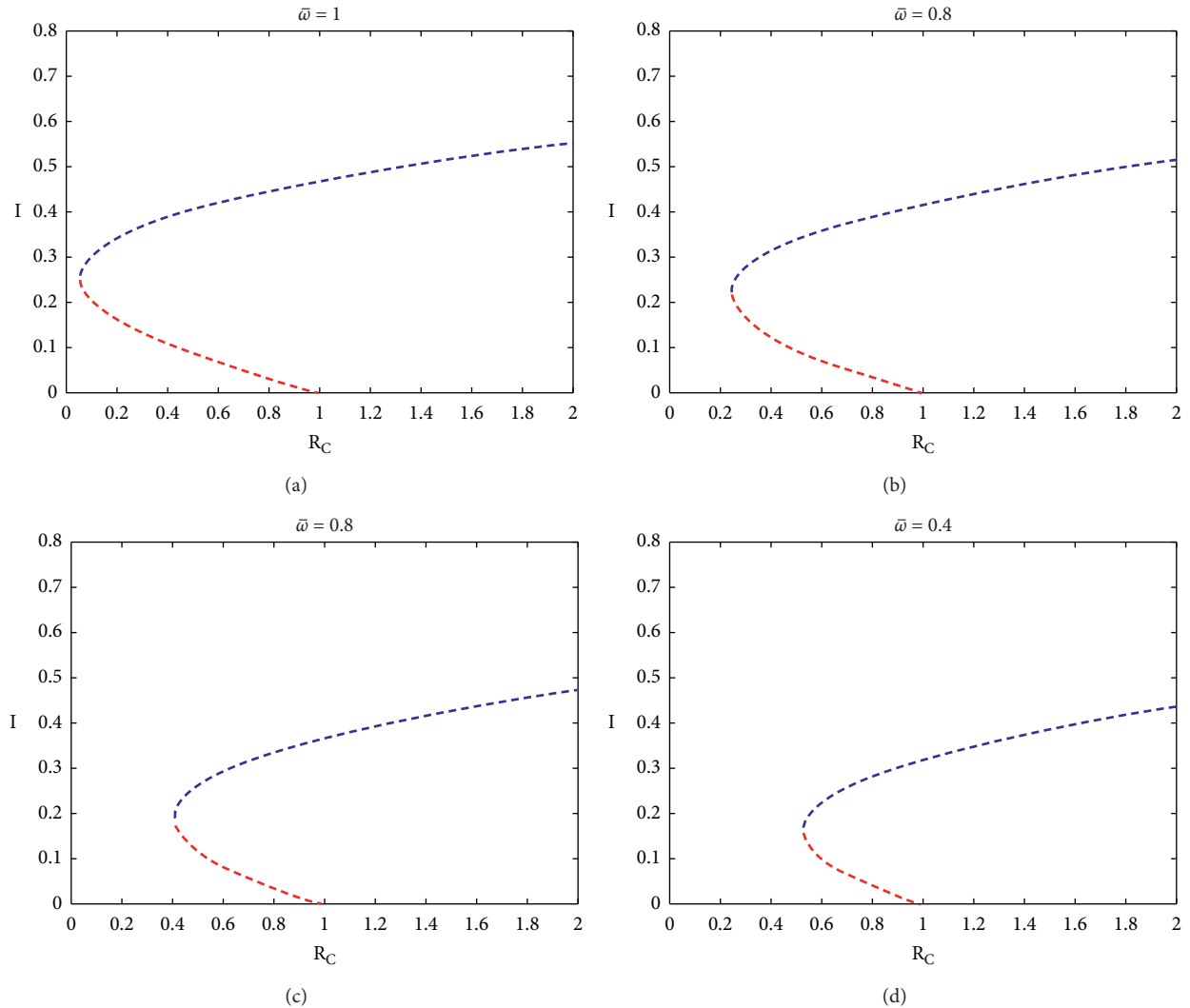

FIGURE 9: Demonstrations of the impact of varying the parameter that accounts for delaying the treatment of infected individuals. Here the parameters are the same as in Figure 8 except $c = 1.2$ while ϖ is shown on top of the figure. (a) Forward bifurcation. (b) Backward bifurcation. (c) Forward bifurcation. (d) Backward bifurcation.

Furthermore, we consider another set of representative parameters as $\Lambda = 4$, $\mu = 0.18$, $\delta = 0.04$, $\kappa = 0.03$, $p = 2$, $c = 0.02$, $\varpi = 0.1$, and $\beta = 1.7$. The threshold quantity $R_C = 2.4093 > 1$, and the equilibrium is (2.11674, 0.997134, 1.0057) while the eigenvalues are given as (-0.231843, $-0.231843 \pm 5.08514I$). We can conclude that P^* is stable since all of the eigenvalues are negative or negative real parts (see Figure 6).

Figure 7 depicts the phase diagram of S_t and I_t planes with different values of saturated recovery c and with $\mu = 0.18$, $\Lambda = 4$, $p = 0.5$, $\kappa = 0.03$, $b = 0.1$, and $\tau = 2$. When $c = 0.04$, the endemic equilibrium is unstable, and as we increase the value of c to 0.1, the endemic equilibrium becomes stable; furthermore, we observed the appearance of two (5) stable limit cycles. We observed that the stability endemic equilibrium state changes from stable to unstable, and this kind of bifurcation is called subcritical Hopf bifurcation (see [46, 47]).

Figure 8 illustrates a typical bifurcation graphs of system model (4). In this diagram, the recruitment rate is changed, whereas other parameters are kept constant. The set of representative parameter values which result in Figure 8 are $\mu = 0.18$, $\delta = 0.12$, $\kappa = 0.03$, $\beta = 1.6$, $p = 0.12$, $c = 0.9$, $\varpi = 0.11$, and $3.5 \leq \Lambda \leq 5$. Figure 8(a) demonstrates the scenario of forward bifurcation that when $R_C < 1$, the TB-free equilibrium is globally asymptotically stable, while if $R_C > 1$, the TB infection can persist. Conversely, as we observed from Figure 8(b), increasing the value of the parameter ϖ from 0.1 to 0.25, the TB infection can persist once defined for the range of R_C values below unity which suggests the occurrence of the phenomenon of backward bifurcation. This suggests that diminishing R_C below one will not be fundamentally enough for the eradication of TB epidemic from the population. When R_C is adequately reduced such that $R_C < R_C^*$, the positive equilibrium does not exist anymore and TB epidemic will cease to develop and will gradually fall from its generally high endemic to the TB-free equilibrium. From Figure 8(b), we observed that when $R_C^* < R_C < 1$, there are stable endemic equilibrium, an unstable endemic equilibrium, and a stable TB-free equilibrium, whereas when $R_C < 1$, there is just one steady endemic equilibrium.

Figure 9 illustrates the backward bifurcation diagram of system model (4) as the effective basic reproduction number (R_C) varies against the infected population (I). Figures 9(a)–9(d) demonstrate that increasing the value of ϖ contributes to the extension of the region of bistability, while reducing the value of ϖ brings about contraction of the bistability region. The TB eradication quantity also known as critical reproduction number shifts from left to the right when ϖ decreases and vice versa. Here, high value of ϖ means insufficient treatment for a huge population of TB infections; therefore, we prefer a scenario where there will be consistent TB epidemics within the population despite the fact that $R_C < 1$.

6. Conclusions

Dynamical models of TB infection have been analyzed by numerous authors [21, 22, 48–50]. However, they all proposed linear recovery function to investigate transmission dynamic behavior of their model. However, we discovered that recovery from TB infection depends upon numerous factors such as antibiotic treatment and the number of hospital beds. This leads to nonlinearity in the number of recoveries. The nonlinear recovery function rate principle was then introduced to reveal some insight into the eradication of TB disease by examining the effect of antibiotic treatment and the number of hospital beds.

The main goal of this study is to investigate the qualitative dynamics of the TB infection incorporating saturated recovery (treatment) of the form $cI_t/(1 + \varpi I_t)$ into the model proposed in [21, 22] which gives a more realistic model. On the other hand, complicated dynamic behaviors, including oscillations, can be caused by saturated recovery [9, 10, 14–17].

Typically in epidemiology, the criterion for the persistence and extinction of an infection is vital. The effective reproduction number is computed and the conditions for the local stability of equilibria and the existence of backward bifurcation and Hopf bifurcation are determined. Under the condition of $R_C < 1$, the infection disappears completely from Theorem 3. But if $R_C > 1$, then according to Theorem 3, there will be endemic disease. In reality, the epidemic cannot be eliminated except that the basic reproduction number is reduced under a lower level to such an extent that $R_C^* < R_C < 1$ (see Figure 8(b)). The mathematical analysis of the TB model system (1) has shown two important mathematical phenomena: bistability and periodicity (oscillatory), which have been observed in some other infectious diseases. In the bistability phenomenon, which usually comes with a conversation of backward bifurcation (see [21] and the references therein), the system exhibits multiple endemic equilibria despite $R_C < 1$. In such situation, a stable endemic equilibrium has been shown to compete with a stable disease-free equilibrium. From these results, it has been confirmed that decreasing $R_C < 1$ cannot control the spread of TB infection in the population. The second phenomenon undergoes oscillatory behavior under some certain conditions. The occurrence of limit cycles supports the behavior stated in several studies on the dynamics of some contagious diseases such as whooping cough, measles, rubella, and so on [51–54]. Numerical findings indicate that ϖ which is the saturation parameter is accountable for backward bifurcation. Inability to intervene before TB infection has accumulated in the population will prompt a circumstance where a TB epidemic exists despite the fact that the $R_C < 1$. Improving existing medical technologies and channeling adequate resources in medicines can essentially encourage early intervention by ensuring that individuals infected with TB get treatment immediately.

Data Availability

Conflicts of Interest

The authors declare that they have no conflicts of interest.

Acknowledgments

References

[1] R. M. Anderson and R. M. May, "Population biology of infectious diseases: Part I," *Nature*, vol. 280, no. 5721, pp. 361–367, 1979.

[2] H. R. Thieme, *Mathematics in Population Biology*, Princeton University Press, Princeton, NJ, USA, 2018.

[3] F. Brauer, C. Castillo-Chavez, and C. Castillo-Chavez, *Mathematical Models in Population Biology and Epidemiology*, Springer, vol. 2, p. 508, New York, NY, USA, 2012.

[4] D. Yan and H. Cao, "The global dynamics for an age-structured tuberculosis transmission model with the exponential progression rate," *Applied Mathematical Modelling*, vol. 75, pp. 769–786, 2019.

[5] World Health Organization, *Global Tuberculosis Report 2013*, World Health Organization, Geneva, Switzerland, 2019.

[6] M. A. Khan, S. Ullah, and M. Farooq, "A new fractional model for tuberculosis with relapse via Atangana–Baleanu derivative," *Chaos, Solitons & Fractals*, vol. 116, pp. 227–238, 2018.

[7] D. Morse, D. R. Brothwell, and P. J. Ucko, "Tuberculosis in ancient Egypt," *American Review of Respiratory Disease*, vol. 90, no. 4, pp. 524–541.

[8] I. Ullah, S. Ahmad, M. U. Rahman, and M. Arfan, "Investigation of fractional order Tuberculosis (TB) model via caputo derivative," *Chaos, Solitons & Fractals*, vol. 142, Article ID 110479, 2021.

[9] X. Zhang and X. Liu, "Backward bifurcation of an epidemic model with saturated treatment function," *Journal of Mathematical Analysis and Applications*, vol. 348, no. 1, pp. 433–443, 2008.

[10] X. Zhang and X. Liu, "Backward bifurcation and global dynamics of an SIS epidemic model with general incidence rate and treatment," *Nonlinear Analysis: Real World Applications*, vol. 10, no. 2, pp. 565–575, 2009.

[11] Á.G. Pérez, E. Avila-Vales, and G. E. García-Almeida, "Bifurcation analysis of an SIR model with logistic growth, nonlinear incidence, and saturated treatment," *Complexity*, vol. 2019, Article ID 9876013, 21 pages, 2019.

[12] W. Wang and S. Ruan, "Bifurcations in an epidemic model with constant removal rate of the infectives," *Journal of Mathematical Analysis and Applications*, vol. 291, no. 2, pp. 775–793, 2004.

[13] J. C. Eckalbar and W. L. Eckalbar, "Dynamics of an epidemic model with quadratic treatment," *Nonlinear Analysis: Real World Applications*, vol. 12, no. 1, pp. 320–332, 2011.

[14] J. Cui, X. Mu, and H. Wan, "Saturation recovery leads to multiple endemic equilibria and backward bifurcation," *Journal of Theoretical Biology*, vol. 254, no. 2, pp. 275–283, 2008.

[15] Z. Hu, W. Ma, and S. Ruan, "Analysis of SIR epidemic models with nonlinear incidence rate and treatment," *Mathematical Biosciences*, vol. 238, no. 1, pp. 12–20, 2012.

[16] B. Song, W. Du, and J. Lou, "Different types of backward bifurcations due to density-dependent treatments," *Mathematical Biosciences and Engineering : MBE*, vol. 10, no. 5-6, pp. 1651–68, 2013.

[17] J. Wang, S. Liu, B. Zheng, and Y. Takeuchi, "Qualitative and bifurcation analysis using an SIR model with a saturated treatment function," *Mathematical and Computer Modelling*, vol. 55, no. 3-4, pp. 710–722, 2012.

[18] X. Zhou and J. Cui, "Analysis of stability and bifurcation for an SEIR epidemic model with saturated recovery rate," *Communications in Nonlinear Science and Numerical Simulation*, vol. 16, no. 11, pp. 4438–4450, 2011.

[19] W. Wang, "Backward bifurcation of an epidemic model with treatment," *Mathematical Biosciences*, vol. 201, no. 1-2, pp. 58–71, 2006.

[20] J. Zhang, J. Jia, and X. Song, "Analysis of an SEIR epidemic model with saturated incidence and saturated treatment function," *The Scientific World Journal*, vol. 2014, Article ID 910421, 11 pages, 2014.

[21] T. K. Kar and P. K. Mondal, "Global dynamics of a tuberculosis epidemic model and the influence of backward bifurcation," *Journal of Mathematical Modelling and Algorithms*, vol. 11, no. 4, pp. 433–459, 2012.

[22] I. M. Wangari, S. Davis, and L. Stone, "Backward bifurcation in epidemic models: problems arising with aggregated bifurcation parameters," *Applied Mathematical Modelling*, vol. 40, no. 2, pp. 1669–1675, 2016.

[23] C. Obasi and G. C. E. Mbah, "On the stability analysis of a mathematical model of Lassa fever disease dynamics," *Journal of the Nigerian Society for Mathematical Biology*, vol. 2, pp. 135–144, 2019.

[24] H. Tang, M. Li, X. Yan, Z. Lu, and Z. Jia, "Modeling the dynamics of drug spreading in China," *International Journal of Environmental Research and Public Health*, vol. 18, no. 1, p. 288, 2021.

[25] P. Van den Driessche and J. Watmough, "Further notes on the basic reproduction number," in *Mathematical Epidemiology*, pp. 159–178, Springer, Berlin, Germany, 2008.

[26] F. Sulayman, F. A. Abdullah, and M. H. Mohd, "An SVEIRE model of tuberculosis to assess the effect of an imperfect vaccine and other exogenous factors," *Mathematics*, vol. 9, no. 4, p. 327, 2021.

[27] H. F. Huo and M. X. Zou, "Modelling effects of treatment at home on tuberculosis transmission dynamics," *Applied Mathematical Modelling*, vol. 40, no. 21-22, pp. 9474–9484, 2016.

[28] G. P. Sahu and J. Dhar, "Analysis of an SVEIS epidemic model with partial temporary immunity and saturation incidence rate," *Applied Mathematical Modelling*, vol. 36, no. 3, pp. 908–923, 2012.

[29] S. Ullah, M. A. Khan, M. Farooq, and T. Gul, "Modeling and analysis of tuberculosis (tb) in Khyber Pakhtunkhwa, Pakistan," *Mathematics and Computers in Simulation*, vol. 165, pp. 181–199, 2019.

[30] H.-F. Huo and L.-X. Feng, "Global stability for an HIV/AIDS epidemic model with different latent stages and treatment," *Applied Mathematical Modelling*, vol. 37, no. 3, pp. 1480–1489, 2013.

[31] C. C. McCluskey, "Lyapunov functions for tuberculosis models with fast and slow progression," *Mathematical Biosciences and Engineering*, vol. 3, no. 4, pp. 603–614, 2006.

[32] C. Castillo-Chavez, Z. Feng, and W. Huang, "On the computation of R0 and its role on global stability," *Mathematical Approaches for Emerging and Reemerging Infectious Diseases: An Introduction*, vol. 125, pp. 229–250, 2002.

[33] S. Liao, *Mathematical Models and Stability Analysis of Cholera Dynamics*, Old Dominion University, Norfolk, VA, USA, 2010.

[34] P. Lawrence, *Differential Equations and Dynamical Systems*, Springer, Berlin, Germany, 1991.

[35] C. Castillo-Chavez and B. Song, "Dynamical models of tuberculosis and their applications," *Mathematical Biosciences and Engineering*, vol. 1, no. 2, pp. 361–404, 2004.

[36] S. M. Garba, A. B. Gumel, and M. R. Abu Bakar, "Backward bifurcations in dengue transmission dynamics," *Mathematical Biosciences*, vol. 215, no. 1, pp. 11–25, 2008.

[37] W. M. Liu, "Criterion of Hopf bifurcations without using eigenvalues," *Journal of Mathematical Analysis and Applications*, vol. 182, no. 1, pp. 250–256, 1994.

[38] J. Guckenheimer and P. Holmes, *Nonlinear Oscillations, Dynamical Systems, and Bifurcations of Vector Fields*, vol. 42Springer Science & Business Media, Berlin, Germany.

[39] J. P. La Salle, *The Stability of Dynamical Systems*, Society for Industrial and Applied Mathematics, Philadelphia, PA, USA, 1976.

[40] J. P. La Salle and S. Lefschetz, *"Stability by Liapunov's Direct Method with Applications by Joseph L Salle and Solomon Lefschetz"*, Elsevier, Amsterdam, Netherlands, 2012.

[41] H. I. Freedman and J. W.-H. So, "Global stability and persistence of simple food chains," *Mathematical Biosciences*, vol. 76, no. 1, pp. 69–86, 1985.

[42] I. Ullah, S. Ahmad, Q. Al-Mdallal, Z. A. Khan, H. Khan, and A. Khan, "Stability analysis of a dynamical model of tuberculosis with incomplete treatment," *Advances in Difference Equations*, vol. 2020, no. 1, pp. 1–14, 2020.

[43] C. C. McCluskey and P. V. d. Driessche, "Global analysis of two tuberculosis models," *Journal of Dynamics and Differential Equations*, vol. 16, no. 1, pp. 139–166, 2004.

[44] O. J. Omaiye and M. H. Mohd, "Computational dynamical systems using XPPAUT," in *SEAMS School on Dynamical Systems and Bifurcation Analysis*, pp. 175–203, Springer, Singapore, 2018.

[45] S. Khajanchi, D. K. Das, and T. K. Kar, "Dynamics of tuberculosis transmission with exogenous reinfections and endogenous reactivation," *Physica A: Statistical Mechanics and Its Applications*, vol. 497, pp. 52–71, 2018.

[46] G. A. K. van Voorn, *PhD Mini Course: Introduction to Bifurcation Analysis*, Vrije Universiteit de Boelelaan, Amsterdam, Netherlands, 2006.

[47] Y. A. Kuznetsov, *Elements of Applied Bifurcation Theory*, Vol. 112, Springer Science & Business Media, Berlin, Germany, 2013.

[48] S. Fatimaa and A. A. Mishra, "SEIRS model of tuberculosis infection model with vital dynamics, early treatment for latent patients and treatment of infective," *IJ Mathematical Sciences and Computing*, vol. 3, pp. 42–52, 2020.

[49] D. J. Gerberry, "Practical aspects of backward bifurcation in a mathematical model for tuberculosis," *Journal of Theoretical Biology*, vol. 388, pp. 15–36, 2016.

[50] Z. Feng, C. Castillo-Chavez, and A. F. Capurro, "A model for tuberculosis with exogenous reinfection," *Theoretical Population Biology*, vol. 57, no. 3, pp. 235–247, 2000.

[51] D. J. Earn, P. Rohani, B. M. Bolker, and B. T. Grenfell, "A simple model for complex dynamical transitions in epidemics," *Science*, vol. 287, no. 5453, pp. 667–670, 2000.

[52] M. J. Keeling, P. Rohani, and B. T. Grenfell, "Seasonally forced disease dynamics explored as switching between attractors," *Physica D: Nonlinear Phenomena*, vol. 148, no. 3-4, pp. 317–335, 2001.

[53] W.-M. Liu, S. A. Levin, and Y. Iwasa, "Influence of nonlinear incidence rates upon the behavior of SIRS epidemiological models," *Journal of Mathematical Biology*, vol. 23, no. 2, pp. 187–204, 1986.

[54] P. Rohani, M. J. Keeling, and B. T. Grenfell, "The interplay between determinism and stochasticity in childhood diseases," *The American Naturalist*, vol. 159, no. 5, pp. 469–481, 2002.

WILEY | Hindawi

Retraction

Retracted: Cascading Failure Dynamics against Intentional Attack for Interdependent Industrial Internet of Things

Complexity

This article has been retracted by Hindawi following an investigation undertaken by the publisher [1]. This investigation has uncovered evidence of one or more of the following indicators of systematic manipulation of the publication process:

(1) Discrepancies in scope

(2) Discrepancies in the description of the research reported

(3) Discrepancies between the availability of data and the research described

(4) Inappropriate citations

(5) Incoherent, meaningless and/or irrelevant content included in the article

(6) Manipulated or compromised peer review

The presence of these indicators undermines our confidence in the integrity of the article's content and we cannot, therefore, vouch for its reliability. Please note that this notice is intended solely to alert readers that the content of this article is unreliable. We have not investigated whether authors were aware of or involved in the systematic manipulation of the publication process.

Wiley and Hindawi regrets that the usual quality checks did not identify these issues before publication and have since put additional measures in place to safeguard research integrity.

We wish to credit our own Research Integrity and Research Publishing teams and anonymous and named external researchers and research integrity experts for contributing to this investigation.

The corresponding author, as the representative of all authors, has been given the opportunity to register their agreement or disagreement to this retraction. We have kept a record of any response received.

References

[1] H. Peng, Z. Qian, Z. Kan, D. Zhao, J. Yu, and J. Han, "Cascading Failure Dynamics against Intentional Attack for Interdependent Industrial Internet of Things," *Complexity*, vol. 2021, Article ID 7181431, 15 pages, 2021.

WILEY | Hindawi

Research Article

Cascading Failure Dynamics against Intentional Attack for Interdependent Industrial Internet of Things

Hao Peng,[1] Zhen Qian,[1] Zhe Kan,[2] Dandan Zhao [ID],[1] Juan Yu,[1] and Jianmin Han[1]

[1]*Department of Computer Science and Engineering, Zhejiang Normal University, Jinhua 321004, China*
[2]*School of Cyber Science and Engineering, Shanghai Jiaotong University, Shanghai 200240, China*

Correspondence should be addressed to Dandan Zhao; ddzhao@zjnu.edu.cn

The emerging Industrial Internet of Things (IIoT) provides industries with an opportunity to collect, aggregate, and analyze data from sensors, including motion control, machine-to-machine communication, predictive maintenance, smart energy grid, big data analysis, and other smart connected medical systems. The physical systems and the cyber systems are organically integrated, forming an interdependent IIoT. This system provides us with enormous advantages, but at the same time, it also introduces the main safety challenges in the design and operation phase. To exploit the security threats of IIoT systems, in this paper, we propose a novel security-by-design approach for interdependent IIoT environments across two different levels, namely, theory modeling and runtime simulation. Our method theoretically analyzes the cascading failure dynamics of the intentional attack network. Simultaneously, we verified the theoretical results through simulations and gave the risk factors that affect the system's security to mitigate potential security attack threats. Besides, we prove its applicability through comparative simulation experiments to study application environments that rely on IIoT, which shows that our method helps identify risk factors and mitigate IIoT attacks' mechanism.

1. Introduction

In recent years, with human society's progress and the widespread use of the Internet, many emerging technologies and industries are booming. Emerging industries such as artificial intelligence, Internet of things, virtual reality, blockchain, big data, and cloud computing have accelerated the development and application of modern high-tech technologies.

With the rapid development of communication and sensor technology [1, 2], the Internet of things technology has attracted extensive attention in the emerging digital world. The goal of the Internet of things is to create a world of the Internet of things. The emergence of Internet of things technology has dramatically changed people's way of life, work, and entertainment. It has been everywhere in transportation, home furnishing, medical treatment, learning, and logistics. We found that the Internet of things technology has been embedded in people's daily life,

intelligently connecting things or objects around us. The industrial Internet of things is the deep integration of the Internet of things in industrialization and informatization. In 2011, Germany first proposed the concept of Industry 4.0 [3, 4] and took CPS (cyber-physical system) as the primary goal of Industry 4.0 development [5]. Industrial Internet of Things (IIoT) is a subset of the Internet of Things (IoT) [6], which requires a higher level of security, security, and reliable communication [7]. In the industrial field, future information application scenarios and CPS technology have high adaptability. CPS provides critical technology for the ubiquitous industrial Internet of things technology.

According to the US National Science Foundation (NSF), CPS seamlessly integrates computing and physical components. As the core architecture of IIoT, the goal of CPS is to realize the deep integration of information systems and physical systems [8]. CPS has been applied in many areas, such as intelligent transportation systems [9, 10], monitoring, and control [11, 12], national defense weapon

systems, intelligent aerospace, smart home, and other fields [13, 14]. CPS's impact is enormous, and its emergence will change the way people interact with the physical world [15]. In the modern industrial system [16], we pay special attention to the security of information technology [17]. CPS provides new opportunities in technology and brings more and more attention and challenges [18]. If these risks are not analyzed and handled appropriately, the consequences will be severe.

Part of the existing research focuses on the design and evaluation of CPS modeling. Because CPS is widely used in various industries, and the physical resource network and computing resource network of each industry are different, it is almost impossible to model CPS as a general model. Aiming at the information physical production system (CPPS), Ref. [19] proposes a system architecture that can adapt to the independent processing line. For the hierarchical control system, network physical modeling and network emergency assessment are carried out in Ref. [20]. In the context of targeted destructive impact, Pavlenko and Zegzhda [21] proposed a new network physical system security evaluation method. Ribeiro and Björkman [22] critically compare today's automation solutions with their potential network physical solutions. Wireless sensor actuator network is applied in industrial automation. Lu et al. [23] review the existing technology of industrial wireless control systems. Ref. [24] models and evaluates the energy management system of networked and automated electric vehicles and develops a network attack analysis method. The emergence of CPS attracts more people's attention to the physical network world, which is the opportunity.

However, we know that a general modeling method is not popular in the network physical world. The scale, topology, and connection heterogeneity of networks bring great challenges. We know that CPS is composed of two networks, and the two networks are interdependent. In network physical systems, physical devices such as batteries and sensors are regarded as physical components. Embedded computer and communication networks are considered network components. Generally, it is the interdependent computational-resource network and physical-resource network that the CPS model as Ref. [25]. In the interconnected system, the destruction of a node usually affects the whole system and brings essential influence. The interdependence between nodes leads to a node failure chain reaction called cascading failure [26]. Cascading failures will have a significant impact on CPS. Therefore, CPS needs to evaluate the risk of the coupled network.

This paper makes a significant contribution to the security of the IIoT system composed of CPS. Traditional fault analysis methods, such as fault tree analysis [27], are widely used in the CPS system [28]. However, this method does not consider the cascading failure of two networks in CPS due to the coupling relationship. Other scholars [29] have considered this cascading failure problem, but only under the deliberate attack strategy. In real life, the attack is often targeted and deliberate [30, 31]. In this paper, we model the IIoT system composed of computing resources and physical resources as two interdependent complex networks and elaborate the cascading failure dynamics of the cyber-physical system under the intentional attack strategy. We define the coupling relationship between physical resource networks and information resource networks through the model proposed in this paper. The specific contributions are as follows:

(i) We apply the percolation theory to the cascading failure of interdependent networks. Percolation theory is a process of removing network vertices and edges. We consider that both physical resource networks and computational resource networks are scale-free networks, and their degree distribution obeys power-law distribution. We analyze the robustness of our model in intentional attack strategy by calculating the proportion of functional nodes after cascading failure stops.

(ii) We use a mathematical method to analyze the cascading failure process of the coupling network in detail. The results show that, given the power-law exponent and initial attack parameters of the coupled network, there is always a threshold for the network to collapse and form a steady state. Beyond this threshold, the network will no longer have functional nodes. Within the threshold range, there are still functional nodes in the coupling network after cascading failure stops.

(iii) We further verify the accuracy of the theoretical and experimental results through simulation experiments. In addition, we analyze several essential parameters in the simulation phase, such as power-law index, attack parameters, etc. We find that the percolation threshold decreases with the increase of the power-law exponent of the network, which improves the robustness of the surface network. This work speeds up the understanding of the relationship between the online world and the physical world.

The essay proceeds as follows. The related work of this paper is addressed in Section 2. Section 3 presents the concept of the interdependent network model and the detailed cascading failure dynamics. In Section 4, the whole cascading failure dynamics is interpreted by the theoretical method. In Section 5, we solve the theoretical equation in Section 4 by numerical analysis and get the theoretical solution to give the simulation results. Section 6 summarizes the relevant conclusions and gives some possible works in the future.

2. Related Work

The Industrial Internet of Things system, composed of CPS, has always been the focus of scholars. We will mainly analyze and study the two critical theories of the security of the Industrial Internet of Things, namely the interdependent network and percolation theory.

2.1. Interdependent Networks. The scholarly study of the interdependent network mainly concentrates on the evolutionary dynamics and network structure's robustness [32–34]. The robustness of the network structure here refers to the integrity of network topology after some nodes fail. When a network in the cyber-physical system is attacked, it will split into a more extensive cluster and smaller groups. From the research of scholars [33, 35–37], it can be concluded that a node holds its function only if it meets two conditions as follows:

(i) Nodes in the current network must combine with those in another network.

(ii) The node should be part of the most extensive set of connected clusters.

Those who satisfy the conditions mentioned above are considered as functional nodes and features prominently in the entire network. When an attack comes, only these can remain. Once there exist no function nodes, the network would collapse completely.

In 2010, a "one-to-one correspondence" theoretical model was put forward by Buldyrev et al. [38] to abstract the robustness of coupled networks cascading failures into a model, and they found that the interdependent network under random attack is more fragile than the single network. This brings more scholars' attention to the coupled networks. Huang et al. [31] and others examined and put forward the interdependent networks' robustness model when being deliberately attacked. They transformed the targeted-attack model into a random attack model. They found that in an entirely random coupled scale-free network, even if the attack probability on a large vertex in one of the networks is reduced, the system is still fragile, which shows that it is complicated to protect the entirely random coupled scale-free network. Since then, Dong et al. [30] have also studied the degree-based attack of partial interdependent systems.

Parshani et al. [39] used the mathematical research method proposed by Buldyrev to study the partially interacted network. It was found when the degree of interdependence between the two subnetworks decreased, the network robustness would be enhanced; that is, the former first phase transition of network seepage is now transformed into the second phase transition. In 2014, Danziger studied a system of partially coupled spatial networks and presented cascade dynamics measurements. Chattopadhyay and Dai [40] researched some interdependent networks and established mathematical equations. Combining two attack models, random attack and target attack, we can learn more regarding the robustness of coupled interdependent networks.

In 2012, Gao et al. [34] jointly published a network paper on the interdependent network in the Journal of Nature Physics. They developed a more general mathematical method based on Buldyrev and others' mathematical framework, which further opened a new milestone for individuals to study the interdependence network.

In 2014, Shao et al. [41] researched the robustness of interdependent networks with clustering properties and noticed that the lower the clustering coefficient, the better the network robustness. In the same year, Zhou et al. [42] and others conducted an in-depth study on the cascading failure dynamics and found that a spontaneous second-order phase transition happened in the first-order phase transition point.

In recent years, experts and scholars have studied how to slow down coupled networks' cascading failure. Tootaghaj [43] had a comprehensive knowledge of failure location and focused on recovery strategies after failures. In this way, he developed two methods to solve the continuous cascading failure.

2.2. Percolation Theory. There are many theories in the research process of complex networks, such as game theory, communication theory, and percolation theory [42]. In network science, percolation theory becomes a significant part of the complex network structure's research evolution [39, 44]. Callaway et al. [45] first proposed the concept of percolation in 1957. Percolation theory is a method to estimate network reliability. There are two standard percolation modes: bond percolation and site percolation. In an $n * n * n$ mesh, the edges between nodes are preserved with probability p. Given a probability p, what is the probability of a path from the top to the bottom of the grid, called bond percolation [45]? If the mesh vertex is retained with probability p, then there is a question concerning the probability of a path from the top to the bottom of the mesh, called site percolation [46].

In [35, 38], the seepage theory is used to measure the coupled network's characteristics. In a single network, Cohen et al. [46] used percolation theory [47] to study network robustness and vulnerability.

In 2010, the percolation theory was used by Buldyrev et al. [38] to explore the robustness of interdependent networks. In 2013, Zhou et al. [48] researched the percolation phenomena of similar interdependent networks. In 2015, Dong et al. [49] and others delved into the percolation problem of the interdependent network with feedback dependent edges and found that in the case of strong coupling, the system with feedback dependent edges is more vulnerable.

The percolation research of interdependent networks mainly designs the network random evolution rules and the network seepage application [50, 51]. So far, there are a host of areas worth studying network seepage.

We will systematically analyze and study the security of IIoT by using the two methods of interdependent network theory and seepage theory. Compared with the above work, this paper's difference is that it analyzes the interdependent network's cascading failure dynamics based on the intentional attack mode, and the network type is closer to reality. We can better evaluate CPS's network security performance and industrial Internet of things through the combination of theory and simulation.

3. Proposed Model and Concepts

We propose a new modeling and analysis method of IIoT environment security from the two aspects of modeling and simulation. Figure 1 shows the primary process of our method. At the modeling level, we start with analyzing the network's cascading failure dynamics, studying the process of cascading failure mathematically, and proving when the network will come to an end. Furthermore, we get the critical value equation of network collapse. We find this threshold by image fitting. In the simulation, we build a cyber-physical network model of coupled networks. We will simulate the network's process being attacked deliberately, get the number of nodes remaining in the most connected group after the network crash, and find the network's critical value by drawing graphs. By analyzing these two levels, the emulation results can be fed back to the modeling results to analyze further the network security performance of the industrial Internet of things.

3.1. Modeling Level. In real life, the IIoT system is often based on CPS architecture, usually composed of a coupled computational-resource and physical-resource networks. As shown in Figure 2, these scenarios show the IIoT system based on CPS architecture. Many research and empirical data show that the number of nodes in a physical resource network is less than that in a computing resource network. Therefore, at the modeling level, we set the number of nodes of the two coupled networks to be 3 : 1. We use S and I to represent the two networks of computing and physical resources. The number of nodes is N_S and N_I, respectively. We call the connecting edge between S and I as internetwork connection and the connecting edge of the nodes in two networks as intranetwork connection. Both intranetwork and inter network connections are random. Nodes from different networks depend on each other by connecting edges. Failure of either party will result in the failure of the other party. It can be found that only a few nodes are linked to a large number of nodes, while most nodes are only connected with a small amount. We usually call the network with this distinct scale-free network. For the convenience of research, we consider the two coupled networks as scale-free networks. The degree distribution of scale-free networks follows the power-law distribution. In other words, $P(k) \propto k^{-\lambda}$ where $P(k)$ is the probability that a node has k edges and λ is a power-law exponent.

The computing and physical resources in IIoT are composed of many components, such as control devices, network devices, computers, and batteries. In the whole system, the damage of some devices has little effect on the network cascading failure. Therefore, in this paper, we only consider the impact of critical nodes on cascading failure of coupled networks. For example, in a smart grid, the power control node that provides power for communication network operation and the communication node that ensures the regular operation of the power network are the key nodes.

Some natural factors or emergencies may lead to some nodes' failure in the network in real life. However, more often than not, the network is deliberately attacked due to human factors. Therefore, in this paper, we assume that some computing resource network nodes suffer from intentional destruction. We use a deliberate attack strategy to delete the number of nodes in the network S, and the ratio is $1 - p$. The internetwork connection and intranetwork connection of these deleted nodes will be deleted. Due to interdependence, some nodes in the network I lose their connection, leading to dysfunction. As mentioned above, due to the coupling and interdependence between computing resource networks and physical resource networks, node failure in one network will affect another network. The node failure in another network will affect this network in turn, leading to the node failure in the network coupled with it. Therefore, it is a cycle process. We call this process a professional term: cascading failures, as shown in Figure 3.

The cascading failure dynamics have been described clearly, and we need to determine when it will stop. When the nodes in the two networks no longer fail or the coupled network collapses completely, we think the network has reached a stable state. At this point, cascading failures stop. We stipulate that only the nodes that meet the requirements of maintaining function in at least another network and belong to the largest connected cluster are called function nodes. Therefore, the functional nodes eventually survive. The following section will detailedly analyze the cascading failure dynamics by using mathematical methods.

3.2. Simulation Level. At the simulation level, the experimental data are used to verify the above theoretical results' accuracy. We will build two scale-free networks that are coupled and interdependent. The number of nodes in the two networks is set to 3000 and 9000, respectively. We know that three network nodes S establish a connection relationship with one network I. The nodes of network S and network I will also be connected randomly. Hence, we can compare the two networks. According to the targeted-attack model, intentional attacks between networks are skillfully transformed into equivalent random attacks. Referring to the above probability equations, which indicate targeted attacks, each node's failure probability is determined, and then nodes are deleted randomly. Due to the cascading failure, the nodes in one network are deleted, which will cause the nodes in another network to be affected and fail. In each step of the cascading failure dynamics, we will save the remaining nodes in the current network until there is no cascading failure in the network. The storage of these data will help us analyze the changes of network nodes. Algorithm 1 shows our simulation steps.

4. Mathematical Analysis of Cascading Failure Dynamics

In this section, we will use some mathematical methods to describe the process of cascading failures in coupled networks. Since the direct calculation of an intentional attack
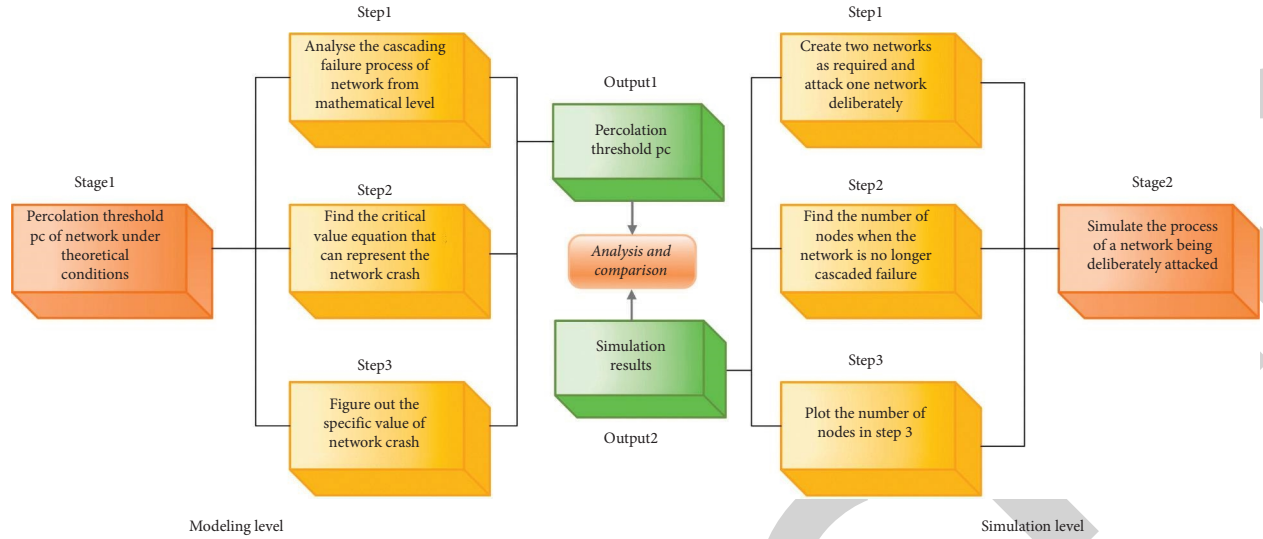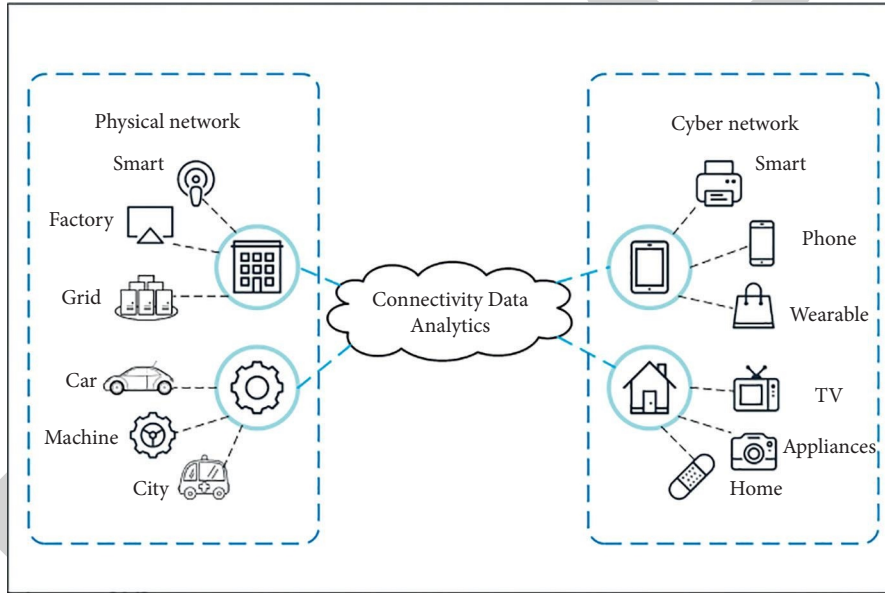
Figure 1: Process of the proposed method.

Figure 2: A conceptual view of industrial Internet of things system based on interdependent CPS architecture.

will increase the difficulty, we will use some scientific methods to convert an intentional attack into a random attack. After the transformation, we will analyze the process of network cascading failure step by step. Finally, we get the expression that the network finally reaches a steady state. The related symbols are defined in Table 1.

4.1. Stage 1: Intentional Attack in Network S. Various nodes in a network have different weights. Some nodes are crucial in the connectivity of the network. The criteria for evaluating node importance are not unique, and here we choose a more general one. Gallos et al. [36] proposed the influence of the degree of any vertices on network robustness. In Ref. [36], a family of functions is defined as follows:

$$Q_\alpha\left(k_i\right) = \frac{k_i^\alpha}{\sum_{i=0}^{N} k_i^\alpha}. \tag{1}$$

Assign $Q_\alpha(ki)$ to each node i with a corresponding degree of k_i, where $Q_\alpha(ki)$ implies the likelihood of nodes' failure caused by being attack.

By observing the function, we can know that when $\alpha < 0$ and the node degree is 0, the formula will become meaningless. From this, to keep the nodes with node degree 0 from being excluded and make them conform to the situation of the coupled system in real life, we improve the function equation and get the following functions:

$$Q_\alpha\left(k_i\right) = \frac{\left(k_i + 1\right)^\alpha}{\sum_{i=0}^{N} \left(k_i + 1\right)^\alpha}. \tag{2}$$
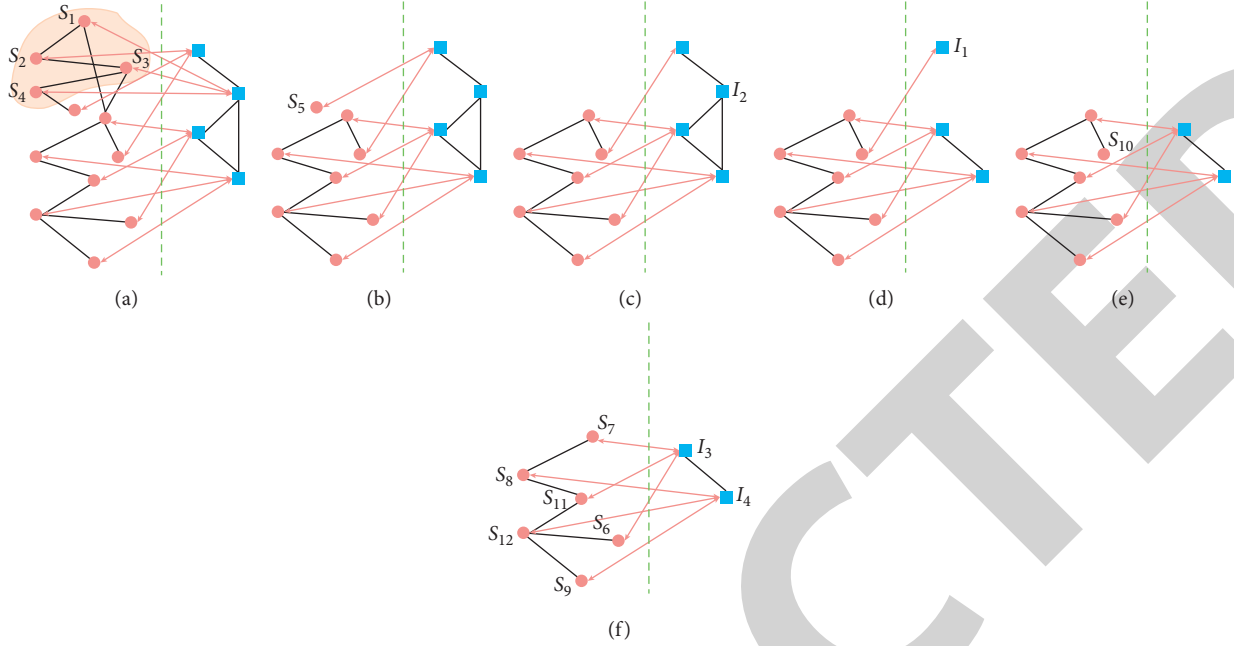
FIGURE 3: The process of cascading failure. (a) The left and right sides represent a computational-resource network and a physical-resource network, and the nodes are connected randomly. The shadow nodes $S_1 S_2 S_3 S_4$ indicate the deliberately damaged nodes of network S. (b) The damaged nodes are disconnected from network S and network I. Those belonging to the largest connected cluster in S will be preserved. Consequently, the node S_1 will be deleted. (c) Because of the node's failure in the network S, the node I_2 in the network I has no interlinks. I_2 also fails. (d) It demonstrates that the node I_1 does not belong to the giant network I and fails. (e) The nodes' failure occurs in the network I, and the interlink is disconnected from S_{10}. Thus, S_{10} fails. (f) The nodes of both networks do not fail anymore and reach a stable state.

```
(1)  for each i ∈ [0, 1] do
(2)    for i = 1 to 50 do
(3)      Target attack network S;
(4)      Remove the node of the attacked node network S;
(5)      int step;
(6)      while The number of network nodes is still changing do
(7)        step++;
(8)        if step% = 2 then
(9)          Delete the node in network S that has lost its normal function due to the failure of the node in network I;
(10)       else
(11)         Delete the node in network I that has lost its normal function due to the failure of the node in network S;
(12)       end if
(13)     end while
(14)   end for
(15)   Save the number of remaining nodes in the network;
(16) end for
```

ALGORITHM 1: Network cascading failure against intentional attack simulation.

When $\alpha < 0$, it is more vulnerable to fail low degree nodes, and those with high degrees are better protected. When $\alpha > 0$, the nodes with high degrees are more vulnerable to failure, and the nodes with a low degree are better protected. When $\alpha = 0$, $W_0 = 1/N$, all nodes have the same probability of failure, which is equivalent to being converted into a random attack. When $\alpha \longrightarrow +\infty$, the nodes with degrees from high to low are deleted in turn. On the contrary, when $\alpha \longrightarrow \infty$, the nodes with degrees from low to high are deleted in turn.

According to the previous description, our main method is to construct a network S', which is equivalent to the original network S. Therefore, the intentional attack on network S can be transformed into a random attack on network S'. According to Huang et al. [31] method, target attack is mapped to random attack. In the first step, according to equation (1), we first remove the $(1 - p)$ scale nodes from the network. The edges between the remaining nodes and the removed nodes are preserved. Then, the degree distribution of the remaining nodes $P_p(k)$ is as follows:

TABLE 1: Symbol definition.

Symbol	Explanation
N_S, N_I	The initial nodes of scale-free network S and I.
N'_{S_i}, N'_{I_i}	Number of nodes that have supporting interlink in the network S and I at stage i and j.
N_{S_i}, N_{I_i}	The giant components that remain functional in N'_{S_i} and N'_{I_i}.
μ_i, μ_j	The fraction corresponding to N_{S_i} and N_{I_i}.
μ'_i, μ'_j	The fraction corresponding to N'_{S_i} and N'_{I_i}.
λ_S, λ_I	Parameters of the degree distribution of network S and I.

$$P_p(k) = \frac{Q_p(k)}{pN_S}. \tag{3}$$

We assume $Q_p(k)$ describes the number of k-degree nodes among the resting part.

After deleting another node, $Q_p(k)$ will become as follows:

$$Q_{(p-1/N)}(k) = Q_p(k) - \frac{P_p(k)(k+1)^\alpha}{\sum_k P_p(k)(k+1)^\alpha}. \tag{4}$$

When $N \longrightarrow \infty$, equation (4) could be changed into a derivative of $Q_p(k)$ with respect to p:

$$\frac{dQ_p(k)}{dp} = N\frac{P_p(k)(k+1)^\alpha}{\sum_k P_p(k)(k+1)^\alpha}. \tag{5}$$

When $N \longrightarrow \infty$ combining equation (3) with equation (5), it can be seen that

$$-p\frac{dQ_p(k)}{dp} = P_p(k) - \frac{P_p(k)(k+1)^\alpha}{\sum_k P_p(k)(k+1)^\alpha}. \tag{6}$$

To better find a solution concerning the equation (6), a new function $G_\alpha(x) = \sum_k P(x)x^{(k+1)^\alpha}$ is defined and $d = G_\alpha^{-1}(p)$ [39], then we can solve equation (6) to get the following:

$$P_p(k) = \frac{1}{p}P(k)d^{(k+1)^\alpha}, \tag{7}$$

$$\sum P_p(k)(k+1)^\alpha = \frac{dG'_\alpha(d)}{G_\alpha(d)}. \tag{8}$$

Accordingly, the generating function of $P_p(k)$ is as follows:

$$G_{Sb}(x) \equiv \sum_k P_p(x)x^k = \frac{1}{p}\sum_k P(x)d^{(k+1)^\alpha}x^k. \tag{9}$$

Since network S is randomly connected, the probability that an edge ends at the remaining nodes is equal to the ratio of the number of edges sent from the remaining nodes to the total number of edges from all nodes of the original network:

$$\tilde{p} \equiv \frac{pN\langle k(p)\rangle}{N\langle k\rangle} = \frac{\sum_k P(k)kd^{(k+1)^\alpha}}{\sum_k P(k)k}. \tag{10}$$

Here, we define $\langle k\rangle$ as the original network's average degree, and set $\langle k(p)\rangle$ as the remaining nodes' average degree after the network being intentionally attacked. With

the method in Ref. [38], we obtain the remaining nodes' generating function as follows:

$$G_{Sc}(x) \equiv G_{Sb}(1 - \tilde{p} + \tilde{p}x). \tag{11}$$

Our goal is to transform the target attack on network S into random attack on network S'. Through some theoretical research, it can be found that the difference between a target attack and a theoretical attack is only in the first step of cascading failure. Therefore, as long as we seek out a network S', its generating function $G_{Sc}(x)$ and $\tilde{G}_{S0}(x)$ are equal after randomly deleting nodes with $(1-p)$ ratio. Then, the random attack analysis of network S' can replace the intentional attack analysis of network S. Based on the experience of Ref. [38], we use $\tilde{G}_{S0}(1 - p + px) = G_{Sc}(x)$ to get the following formula:

$$\tilde{G}_{S0}(x) = G_{Sb}\left(1 + \frac{\tilde{p}}{p}(x-1)\right). \tag{12}$$

Next, we use the random attack analysis process to continuously analyze the process of cascading failure under targeted attack, mainly searching the iterative process detailedly with the generation function and percolation theory. Then, we analyze the ratio of the current network's functional nodes amounts to the total quantity of nodes in the original network after each step of failure. The generating function of network S' has been obtained, as shown in equation (12). In light of the above generating function of network S', the generating function of the underlying branching process $\tilde{G}_{S1}(z)$ is as follows:

$$\tilde{G}_{S1}(z) = \frac{\tilde{G}'_{S0}(z)}{\tilde{G}'_{S0}(1)}. \tag{13}$$

When S' is randomly attacked to remove the nodes with the ratio of $(1-p)$, the remaining nodes' degree distribution will change while affecting the corresponding degree distribution in generating function. Therefore, the degree distribution of the remaining nodes in S' is $N'_{S1} = p * N_S$. The proportion of function nodes is as follows:

$$g_S(p) = 1 - \tilde{G}_{S0}[1 - p(1 - f_S)], \tag{14}$$

where we define f_S as the function of p, fs meets the following:

$$f_S = \tilde{G}_{S1}[1 - p(1 - f_S)]. \tag{15}$$

Next, we will analyze the cascading failure dynamics step by step.

4.2. Stage 2: Equivalent Failure Under Random Attack in Network S'.

In the previous paper, we have analyzed the process from intentional attack to random attack. Therefore, we think that the initial attack is a random attack on network S'. The $(1 - p)$ ratio of node failure. The quantity of remaining nodes is as follows:

$$N'_{S1} = p \cdot N_S = \mu'_1 \cdot N_S. \tag{16}$$

From equation (16), we could get $\mu'_1 = p$. Based upon the previous analysis, the quantity of nodes in the giant component in N'_{S1} is as follows:

$$N_{S1} = g_S(\mu'_1) \cdot N'_{S1} = \mu'_1 \cdot g_S(\mu'_1) \cdot N_S = \mu_1 \cdot N_S. \tag{17}$$

From equation (17), we obtain the following:

$$\mu_1 = \mu'_1 \cdot g_S(\mu'_1). \tag{18}$$

4.3. Stage 3: Cascading Failures in Network I Caused by S-Node Failures.

Through the analysis of the CPS system, we know that the nodes in the coupling network S' and I' are interdependent. Therefore, the failure of nodes in network S' may lead to the nodes crash in network I'. In our model, one node in network I' connects with three nodes of network S', and the internetwork connection and intranetwork connection are random. Consequently, the quantity of nodes remaining in network I' is as follows:

$$N'_{S3} = \mu_2 \cdot N_I \cdot \frac{\left[C_3^1 \cdot \mu_1 \cdot (1 - \mu_1)^2 \cdot 1 + C_3^2 \cdot \mu_1^2 \cdot (1 - \mu_1) \cdot 2 + \mu_1^3 \cdot 3 \right]}{\left[1 - (1 - \mu_1)^3 \right]}. \tag{23}$$

So

$$N'_{S3} = \mu_1 \cdot g_I(\mu'_2) \cdot N_S. \tag{24}$$

From N_{S1} to N'_{S3}, we know that

$$N_{S1} - N'_{S3} = (1 - g_I(\mu'_2)) \cdot N_{S1}. \tag{25}$$

Based upon the theory in Ref. [52], the nodes removed in the initial stage do not belong to N_{I2}, N_{S1} and N'_{S1}, so from the proportion of nodes removed in N_{S1} has the identical ratio with those nodes removed from N'_{S1}. So

$$N_{S1} - N'_{S3} = (1 - g_I(\mu'_2)) \cdot N_{S1} \\ = (1 - g_I(\mu'_2)) \cdot N'_{S1}. \tag{26}$$

The fraction of the total nodes removed to the original network S' is as follows:

$$1 - \mu'_1 + (1 - g_I(\mu'_2)) \cdot \mu'_1 = 1 - \mu'_1 \cdot g_I(\mu'_2). \tag{27}$$

From equation (27), we know the following:

$$\mu'_3 = \mu'_1 \cdot g_I(\mu'_2). \tag{28}$$

So, the quantity of nodes in the massive component in N'_{S3} is as follows:

$$N'_{I2} = \left[1 - (1 - \mu_1)^3 \right] \cdot N_I = \left(\mu_1^3 - 3 \cdot \mu_1^2 + 3 \cdot \mu_1 \right) \cdot N_I = \mu'_2 \cdot N_I, \tag{19}$$

$$\mu'_2 = \mu_1^3 - 3 \cdot \mu_1^2 + 3 \cdot \mu_1 = \mu'_1 \cdot g_S(\mu'_1) \cdot \left(\mu_1^2 - 3 \cdot \mu_1 + 3 \right). \tag{20}$$

Using the same analysis theory before, we can get the number of nodes in N'_{I2} that belongs to the huge connectivity component:

$$N_{I2} = g_I(\mu'_2) \cdot N'_{I2} = \mu'_2 \cdot g_I(\mu'_2) \cdot N_I = \mu_2 \cdot N_I. \tag{21}$$

From equation (21), we obtain the following:

$$\mu_2 = \mu'_2 \cdot g_I(\mu'_2). \tag{22}$$

4.4. Stage 4: Further Fragment in Network S'.

From the previous theoretical derivation of cascading failure, it is found that the number of nodes with dependency in those that remained and belonging to network S'. In the first step of random failure, it is derived that a node in network I may have a random connection to one to three nodes in network S'. In Table 2, we list the proportion of different connections.

According to our previous model, intralinks connection and interlinks connection are completely independent, which is a completely random event. Consequently, we get the quantity of nodes with dependency in S':

$$N_{S3} = \mu'_3 \cdot g_I(\mu'_3) \cdot N_S = \mu_3 \cdot N_S. \tag{29}$$

So,

$$\mu_3 = \mu'_3 \cdot g_S(\mu'_3). \tag{30}$$

4.5. Stage 5: Cascading Failures in I Once Again.

Because of the coupled CPS system, the network's nodes would occur breakdown caused by the previous failure of relevant nodes in the network S'. As in the second step, the quantity of dependent nodes in I is obtained.

$$N'_{I4} = \left[1 - (1 - \mu_3)^3 \right] \cdot N_I = \left(\mu_3^3 - 3 \cdot \mu_3^2 + 3 \cdot \mu_3 \right) \cdot N_I. \tag{31}$$

From N_{I2} to N'_{I4}, we can obtain the following:

$$N_{I2} - N'_{I4} = \left[\frac{1 - \left(\mu_3^3 - 3 \cdot \mu_3^2 + 3 \cdot \mu_3 \right)}{\mu_2} \right] \cdot N_{I2}. \tag{32}$$

Same as the previous analysis, we get the following:

$$N_{I2} - N'_{I4} = \left[\frac{1 - \left(\mu_3^3 - 3 \cdot \mu_3^2 + 3 \cdot \mu_3 \right)}{\mu_2} \right] \cdot N'_{I2}. \tag{33}$$

Table 2: The proportion of different nodes.

0	1	2	3
$(1 - \mu_1)^3$	$C_3^1 \cdot \mu_1 \cdot (1 - \mu_1)^2$	$C_3^2 \cdot \mu_1^2 \cdot (1 - \mu_1)$	μ_1^3

Thus, we know the fraction of the nodes that failed in network I is as follows:

$$1 - \mu_2' + \mu_2' \cdot \left[\frac{1 - \left(\mu_3^3 - 3 \cdot \mu_3^2 + 3 \cdot \mu_3 \right)}{\mu_2} \right] = 1 - \mu_1' \cdot \left(\mu_3^2 - 3 \cdot \mu_3 + 3 \right) \cdot g_S \left(\mu_3' \right). \tag{34}$$

So,

$$\mu_4' = \mu_1' \cdot \left(\mu_3^2 - 3 \cdot \mu_3 + 3 \right) \cdot g_S \left(\mu_3' \right). \tag{35}$$

It is found that the quantity of nodes in the largest component in N_{I4}' is as follows:

$$N_{I4} = \mu_4' \cdot g_I \left(\mu_4' \right) \cdot N_I. \tag{36}$$

So,

$$\mu_4 = \mu_4' \cdot g_I \left(\mu_4' \right). \tag{37}$$

Following the prior conclusions of the cascading failure dynamics method, we can identify the node size after each step of the process, which could be expressed by the following equations:

$$\begin{cases} \mu_{2i}' = \mu_1' \cdot \left(\mu_{2i-1}^2 - 3 \cdot \mu_{2i-1} + 3 \right) \cdot g_S \left(\mu_{2i-1}' \right), \\ \mu_{2i+1}' = \mu_1' \cdot g_I \left(\mu_{2i}' \right), \end{cases} \tag{38}$$

where $\mu_1' = p$.

In the next section, we will use numerical simulation and other methods to find Eq's solution (38). Thus, we can get the critical threshold of the coupled network.

5. Performance Analysis

5.1. Formula Calculation. Through the analysis in the previous section, it is clearly known that cascading failures will not occur again when the nodes in the coupled network are no longer in failure. Table 3 shows the specific state equations of the two networks at each stage. Therefore, in the coupled system, we can obtain the following equations when the cascading failure dynamics comes to an end:

$$\begin{cases} \mu_{2i}' = \mu_{2i-2}' = \mu_{2i+2}', \\ \mu_{2i+1}' = \mu_{2i-1}' = \mu_{2i+3}'. \end{cases} \tag{39}$$

In order to solve the above equations more efficiently, we define variables x, y:

$$\begin{cases} y = \mu_{2i}' = \mu_{2i-2}' = \mu_{2i+2}', \\ x = \mu_{2i+1}' = \mu_{2i-1}' = \mu_{2i+3}'. \end{cases} \quad (0 \le x, y \le 1). \tag{40}$$

Consequently, equation (38) can be shown as follows:

$$\begin{cases} y = p \cdot \left(\left(x \cdot g_S(x) \right)^2 - 3 \cdot x \cdot g_S(x) + 3 \right) \cdot g_S(x), \\ x = p \cdot g_I(y). \end{cases} \tag{41}$$

Simplify equation (41) to get the following:

$$x = p \cdot g_I \left[p \cdot \left(\left(x \cdot g_S(x) \right)^2 - 3 \cdot x \cdot g_S(x) + 3 \right) \cdot g_S(x) \right]. \tag{42}$$

In the process of solving the seepage threshold of a scale-free network, it is hard to directly replace the degree distribution of the network into the equation. Therefore, we need to rewrite equation (42) into two equations and make them infinitely approximate by drawing. Let's rewrite equation (42) into the following two equations:

$$\begin{cases} z = x, \\ z = p \cdot g_I \left[p \cdot \left(\left(x \cdot g_S(x) \right)^2 - 3 \cdot x \cdot g_S(x) + 3 \right) \cdot g_S(x) \right]. \end{cases} \tag{43}$$

According to the above equations, we draw the two equations in the figure. When the curve equation is tangent to the straight line, the intersection point is the seepage threshold as shown in Figure 4.

In Figure 4, we can see that when α is 1, the percolation threshold of the network is 0.5, while α is 2, it is 0.59. So far, we have solved the seepage threshold of the coupled network under different conditions. In order to verify the accuracy of the theoretical results, we will do some simulation experiments.

5.2. Case Results and Analysis. Simulation experiments in this section verify the correctness of the theoretical value. We analyze and verify the correctness of the theoretical data from several different dimensions. We write a C++ program to simulate the whole cascading failure process of interdependent networks in order to obtain the proportion of surviving nodes in the final steady state. Considering the actual situation, the power-law exponent of a scale-free network with power-law distribution is not a fixed value. We set this value between 2.0 and 3.0 to adapt and study different interdependent network systems. Whether the size of the network node affects the change of the experimental threshold is also the focus of our research. We set the network node size to different values. In addition to attack

TABLE 3: The stage of network S and network I.

	Network S	Network I
Stage 1	$\mu_1' = p \ \mu_1 = \mu_1' \cdot g_S(\mu_1')$	
Stage 2		$\mu_2' = \mu_1' \cdot g_S(\mu_1') \cdot (\mu_1^2 - 3 \cdot \mu_1 + 3) \ \mu_2 = \mu_2' \cdot g_I(\mu_2')$
Stage 3	$\mu_3' = \mu_1' \cdot g_I(\mu_2') \ \mu_3 = \mu_3' \cdot g_S(\mu_3')$	
Stage 4		$\mu_4' = \mu_1' \cdot g_S(\mu_3') \cdot (\mu_3^2 - 3 \cdot \mu_3 + 3) \ \mu_4 = \mu_4' \cdot g_I(\mu_4')$
...	...	...
Stage $2i$		$\mu_{2i}' = \mu_1' \cdot (\mu_{2i-1}^2 - 3 \cdot \mu_{2i-1} + 3) \cdot g_S(\mu_{2i-1}') \ \mu_{2i} = \mu_{2i}' \cdot g_I(\mu_{2i}')$
Stage $2i + 1$	$\mu_{2i+1}' = \mu_1' \cdot g_I(\mu_{2i}') \ \mu_{2i+1} = \mu_{2i+1}' \cdot g_S(\mu_{2i+1}')$	
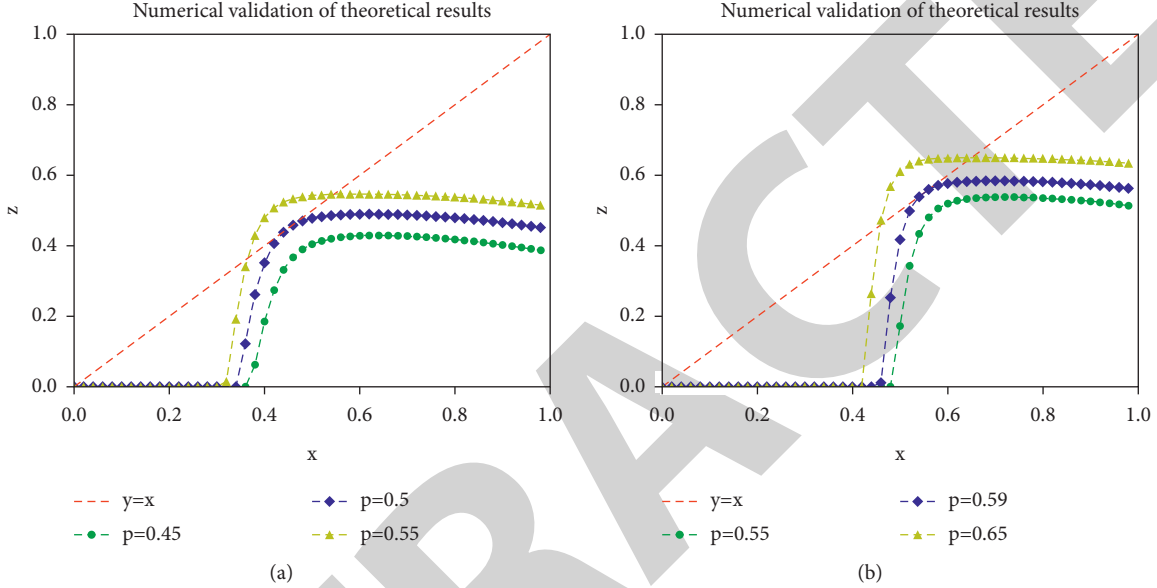
FIGURE 4: Solving iterative equations. We set the parameter λ of the network to 2.8 and change the value of α. (a) The intersection of a curve and a line stands for the critical threshold of the coupled system in the case of $\alpha = 1$. (b) The intersection of a curve and a line describes the critical threshold of the coupled system obtained with $\alpha = 2$.

parameters α, it is also essential to study cascading failure of coupled networks. We will set α between -1.0 and 2.0.

5.2.1. System Robustness. In Figure 5, we analyze the remaining nodes' proportion when the failure comes to an end in two networks with different p. From these three graphs, we can find that as p goes from pc + ε to pc − ε, the value of the ordinate suddenly drops from a nonzero finite value to 0, where ε is a value tending to 0. This shows that when the value of p is in this range, the remaining nodes' scale will reduce to an exceedingly small value by deleting one node in the network. Moreover, we can observe that the abscissa's value corresponding to the network's remaining nodes' phase transition corresponds to the theoretical value, verifying the formula's theoretical value.

From Figure 5, it is found that with the change of abscissa, the changing trend of network S and I is the same. Both networks are generic nodes or crash at the same time. When p approaches the critical threshold, the maximum connected component in the network will rise linearly, this indicates that when p exceeds the critical threshold, some nodes may exist, or the coupled system may collapse. This is consistent with our theoretical analysis.

In Figures 5(a) and 5(b), we set the attack parameter α to the same value and change the power-law index λ of a scale-free network to 2.6 and 2.8, respectively. Comparing the two graphs, we get that the greater the λ is, the smaller the percolation threshold is, and the more reliable the network is. The larger the λ of the scale-free network, the higher the likelihood that a few network nodes have the most connections. That is, the network connections are closed. So, the reliability of the network will be improved. In Figures 5(b) and 5(c), we change the attack parameter α of the network, one is set to 1, and the other is set to 2. The scale-free network is invariant. By comparison, we find that the larger the α, the bigger the pc. This shows that the reliability of the coupled network is getting worse. The larger the α, the more vulnerable the nodes are to attack, so the network reliability is reduced. These analyses correspond to our previous theoretical analysis.

From Figure 5, it can be seen that the blue line representing the percentage of the nodes that remained in network I is almost invariably above the red one, which represents that proportion in network S. Due to the initial attack in network S, every node in network I was linked with three nodes in network S, the network I receives a certain degree of protection. This has a particular significance for us
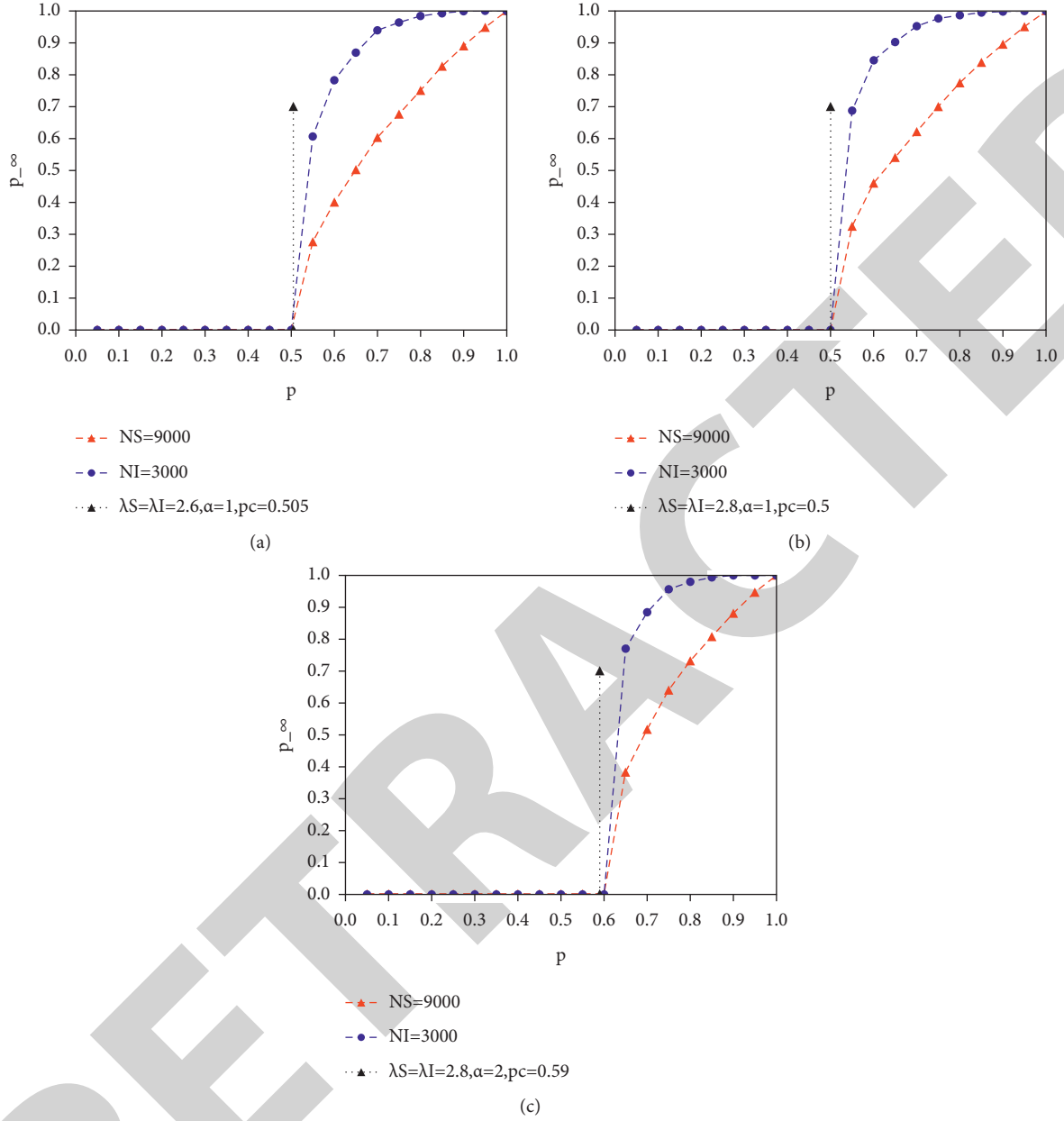
(a)

(b)

(c)

Figure 5: The fraction of survival nodes in network S and I. Abscissa p represents the proportion of nodes that are not attacked in the targeted-attack process and $1 - p$ represents the percentage of the attacked nodes. Ordinate p_∞ indicates the proportion of remaining nodes when cascading failure stops after the coupled network receives a targeted attack. The red line represents network S, the blue line represents network I, and the abscissa corresponding to the black line represents the theoretical value of the critical threshold when the networks fail.

in the construction of real-life infrastructure. We can connect more critical nodes in the coupled system to multiple dependent sides to improve its security.

5.2.2. Influence of Network Size. In Figure 6(a), various values of p are selected in the range [0.485, 0.545] near pc = 0.5, and we conduct 60 experiments at each point to calculate more accurately the times that the coupled system has not entirely failed. The same method is applied in Figure 6(b), except that the value of α is changed. By observing Figure 6, we can see that the curve is steadily

approaching critical importance as nodes' size increases. When network nodes' scale reaches a specific value, the first-order phase transition occurs near the critical threshold, distinct from the second-order phase transition of single networks.

5.2.3. Comparison between Different λ and α. Figure 7 compares the change of percolation threshold under different λ. We keep the other parameters unchanged. The abscissa represents the power-law index λ of the scale-free network, and the ordinate stands for the critical threshold pc
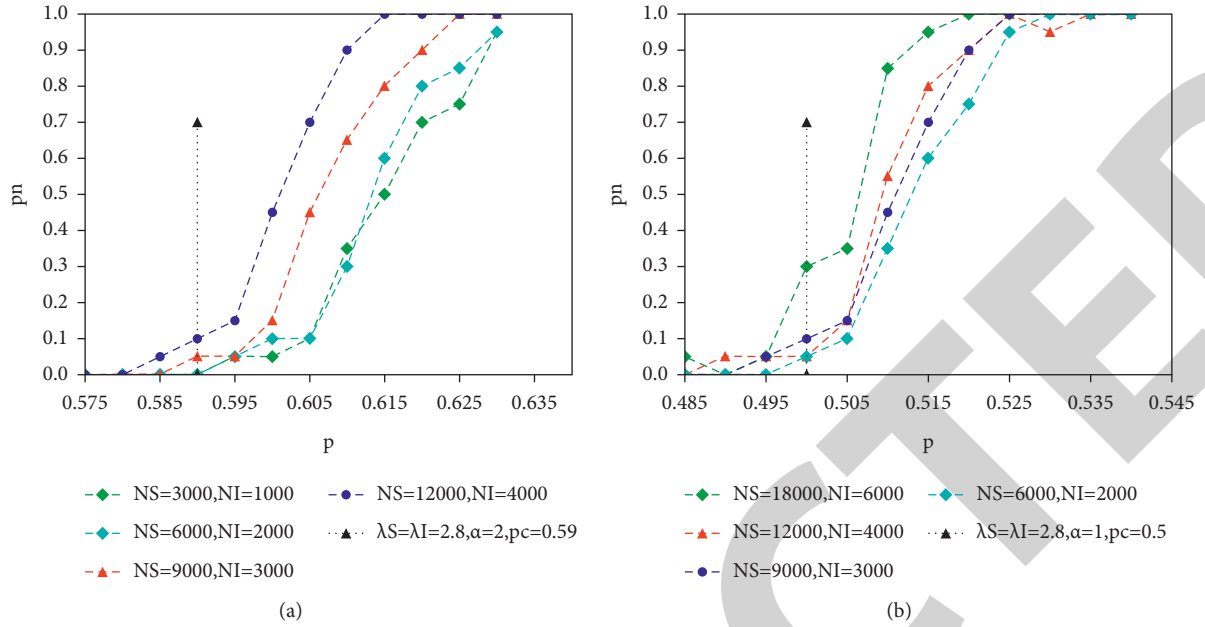
FIGURE 6: The existence probability of the huge component. We select several groups of points around the critical threshold for comparative analysis.
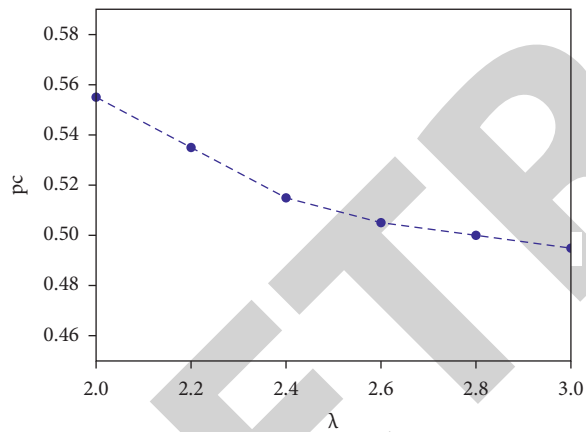

FIGURE 7: The relationship between pc and λ. We compare the transforming of pc in the case of different power-law indexes λ.

FIGURE 8: The relationship between pc and α. We compare different α with different critical threshold pc. The abscissa represents α, and the ordinate represents the essential threshold pc.

of the network. It can be found from the figure that the seepage threshold decreases with the increase of λ. This reduction is relatively small. This shows that the power-law index of scale-free networks is not a factor that significantly changes coupled networks' robustness. This has an efficient significance for us to analyze CPS.

In Figure 8, for comparison purposes, we set the rest of the network's parameters to the same, only changing the value of α. The λ of the network is 2.8, and the minimum degree of network is 3. We can see that the critical threshold pc increases with an increase of α. This implies that the robustness of the network is reduced. The greater α is, the more vulnerable the nodes with high degrees are. Hence, the network's robustness decreases. This also verifies the previous theoretical results. We can also find that the percolation threshold pc is not alike when the scale-free network
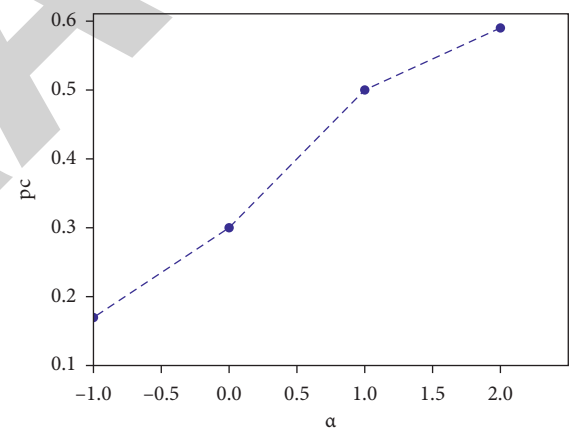
faces various targeted attacks. This is because of the characteristic that the least nodes of the scale-free network have the most connections, which leads to the difference between percolation thresholds in the face of different attacks. This is beneficial for us to protect the coupled network in real life. Correspondingly, we should analyze different situations according to the actual network structure.

5.3. Engineering Applications. As a typical CPS application, the smart grid provides us with many conveniences in real life [53]. Figure 9 shows a vast power grid system with isolated grids connected by long-distance transmission lines. A smart grid system is composed of a power grid network and communication network coupled and interdependent [35]. The power grid is controlled by the communication

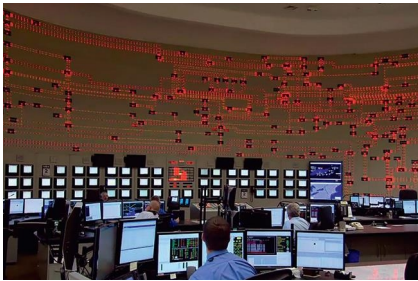FIGURE 9: A huge power grid system with isolated grids connected by long-distance transmission lines.

FIGURE 10: The grid nodes appear red in a large area.

network, which also needs power from the power grid [54]. This interdependence will increase the risk of the power grid, and the failure of a network node will cause the collapse of the whole power grid [55, 56].

The most classic blackout in the United States was in 2003 [45]. A circuit line is entangled with the roots of the trees growing under it. Due to the lack of timely measures, nearly 20 high-voltage lines were out of control. This led to more severe consequences. The interruption of one line made other high-voltage lines overburdened, and eventually, the entire New York State Grid collapsed. As shown in Figure 10, it can be seen that the power grid collapses in a large area, and the grid nodes appear red in large areas. Therefore, it is necessary to study the cascading failure dynamics of coupled networks.

We can use the network model to abstract the smart grid system into a system composed of two coupled networks. We can take the real power grid's data scale and the average degree of network nodes to study the cascading failure dynamics caused by partial node failure. According to the power grid failure process simulation, we can purposefully study the critical nodes in the network and study network nodes' influence and network size on the cascading failure dynamics. According to this data, we can improve the robustness of the smart grid more effectively.

6. Conclusion

The research work addressed the emerging IIoT concept and its cybersecurity concerns with probable outcomes. The security risk analysis is not yet developed, and various strategies, conceptual design, and technical implementations are expected in this paperwork. The cascading failure theory was

suggested for providing risk assessment services at the regional level by improving effectiveness, accessibility, and expandability. The risk analysis scheme proposed for security service corresponds to the interdependent IIoT application environment. The key risk factor is an essential part of ensuring IIoT system security; however, the research study addressed the mathematical mechanism analysis details of the emerging IIoT systems. We propose a novel risk analysis scheme for security modeling and analysis of such interdependent IIoT environments in the design. This method aims to support the development of secure IIoT environments at the modeling and simulation levels framework, and risk factors were hacked at the basic level itself. The methods utilized resistance and risk alleviation techniques. In the future, we plan to examine the environment of other complex application scenarios of our proposed risk analysis method, such as connected cars and houses, wearable devices, and smart medical care in intelligent interdependent IIoT applications. This will give us an in-depth understanding of the risks and challenges faced in these environments. They must be addressed to protect the security of interdependent distributed devices and all connected service-related participants, thereby limiting the risk elements that may affect the entire interdependent IIoT environment. Besides, we also aim to extend our work by including privacy requirements during the modeling and the analysis of such systems by including other risk requirements such as privacy protection and ciphertext retrieval in the modeling process. Through this extension, we will be able to protect user data security in interdependent IIoT systems and identify key risk factors that may affect user security requirements, such as anonymity, interconnectivity, unobservability, and undetectability, etc. Finally, we plan to introduce artificial intelligence and game theory methods for comparative analysis to determine the attacker's attack path mitigation technology.

Data Availability

All the data has been explained in detail in the manuscript.

Conflicts of Interest

The authors declare no conflicts of interest.

Acknowledgments

References

[1] K. Huang, Q. Zhang, C. Zhou, N. Xiong, and Y. Qin, "An efficient intrusion detection approach for visual sensor networks based on traffic pattern learnings," *IEEE Transactions on Systems, Man, and Cybernetics: Systems*, vol. 47, no. 10, pp. 2704–2713, 2017.

[2] W. Wu, N. Xiong, and C. Wu, "Improved clustering algorithm based on energy consumption in wireless sensor networks," *IET Networks*, vol. 6, no. 3, pp. 47–53, 2017.

[3] F. Shrouf, J. Ordieres, and G. Miragliotta, "Smart factories in industry 4.0: a review of the concept and of energy management approached in production based on the Internet of things paradigm," in *Proceedings of the IEEE International Conference on Industrial Engineering & Engineering Management*, Selangor, Malaysia, December 2015.

[4] Z. You and L. Feng, "Integration of industry 4.0 related technologies in construction industry: a framework of cyber-physical system," *IEEE Access*, vol. 8, pp. 122908–122922, 2020.

[5] A. Villalonga, G. Beruvides, F. Castaño, and R. E. Haber, "Cloud-based industrial cyber-physical system for data-driven reasoning: a review and use case on an industry 4.0 pilot line," *IEEE Transactions on Industrial Informatics*, vol. 16, no. 9, pp. 5975–5984, 2020.

[6] T. M. Fernández-Caramés and P. Fraga-Lamas, "A review on the application of blockchain to the next generation of cybersecure industry 4.0 smart factories," *IEEE Access*, vol. 7, pp. 45201–45218, 2019.

[7] M. Canizo, A. Conde, S. Charramendieta, R. Miñón, R. G. Cid-Fuentes, and E. Onieva, "Implementation of a large-scale platform for cyber-physical system real-time monitoring," *IEEE Access*, vol. 7, pp. 52455–52466, 2019.

[8] B. M. Lee and H. Yang, "Massive MIMO for industrial Internet of things in cyber-physical systems," *IEEE Transactions on Industrial Informatics*, vol. 14, pp. 2641–2652, 2017.

[9] G. Xiong, F. Zhu, X. Liu et al., "Cyber-physical-social system in intelligent transportation," *IEEE/CAA Journal of Automatica Sinica*, vol. 2, no. 3, pp. 320–333, 2015.

[10] D. B. Rawat, C. Bajracharya, and G. Yan, "Towards intelligent transportation cyber-physical systems: real-time computing and communications perspectives," in *Proceedings of the SoutheastCon 2015*, pp. 1–6, Fort Lauderdale, FL, USA, April 2015.

[11] E. Bartocci, J. Deshmukh, A. Donzé et al., "Specification-based monitoring of cyber-physical systems: a survey on theory, tools and applications," in *Lectures on Runtime Verification*, pp. 135–175, Springer, Berlin, Germany, 2018.

[12] X. Yuan, C. J. Anumba, and M. K. Parfitt, "Cyber-physical systems for temporary structure monitoring," *Automation in Construction*, vol. 66, pp. 1–14, 2016.

[13] Y. Lu, "Cyber physical system (CPS)-based industry 4.0: a survey," *Journal of Industrial Integration and Management*, vol. 2, no. 3, Article ID 1750014, 2017.

[14] R. M. Murray, K. J. Astrom, S. P. Boyd, R. W. Brockett, and G. Stein, "Future directions in control in an information-rich world," *IEEE Control Systems*, vol. 23, no. 2, pp. 20–33, 2003.

[15] M. Wollschlaeger, T. Sauter, and J. Jasperneite, "The future of industrial communication: automation networks in the era of the Internet of things and industry 4.0," *IEEE Industrial Electronics Magazine*, vol. 11, no. 1, pp. 17–27, 2017.

[16] Q. Zhang, C. Zhou, N. Xiong, Y. Qin, X. Li, and S. Huang, "Multimodel-based incident prediction and risk assessment in dynamic cybersecurity protection for industrial control systems," *IEEE Transactions on Systems Man & Cybernetics Systems*, vol. 46, pp. 1429–1444, 2017.

[17] S. Aamir, L. Malrey, Y. K. Lee et al., "Real time MODBUS transmissions and cryptography security designs and enhancements of protocol sensitive information," *Symmetry*, vol. 7, no. 3, pp. 1176–1210, 2015.

[18] H. I. AL-Salman and M. H. Salih, "A review cyber of industry 4.0 (cyber-physical systems (CPS), the internet of things (IoT) and the internet of services (IoS)): components, and security challenges," in *Proceedings of the 2nd International Conference on Advance & Scientific Innovation*, vol. 1424, Medan, Indonesia, July 2019.

[19] J. Herwan, S. Kano, R. Oleg, H. Sawada, and N. Kasashima, "Cyber-physical system architecture for machining production line," in *Proceedings of the 2018 IEEE Industrial Cyber-Physical Systems (ICPS)*, St. Petersburg, Russia, May 2018.

[20] S. Xin, Q. Guo, H. Sun, B. Zhang, J. Wang, and C. Chen, "Cyber-physical modeling and cyber-contingency assessment of hierarchical control systems," *IEEE Transactions on Smart Grid*, vol. 6, pp. 2375–2385, 2017.

[21] E. Pavlenko and D. Zegzhda, "Sustainability of cyber-physical systems in the context of targeted destructive influences," in *Proceedings of the 2018 IEEE Industrial Cyber-Physical Systems (ICPS)*, pp. 830–834, St. Petersburg, Russia, May 2018.

[22] L. Ribeiro and M. Björkman, "Transitioning from standard automation solutions to cyber-physical production systems: an assessment of critical conceptual and technical challenges," *IEEE Systems Journal*, vol. 12, no. 4, pp. 3816–3827, 2017.

[23] C. Lu, A. Saifullah, B. Li et al., "Real-time wireless sensor-actuator networks for industrial cyber-physical systems," *Proceedings of the IEEE*, vol. 104, no. 5, pp. 1013–1024, 2016.

[24] L. Guo, B. Yang, J. Ye et al., "Systematic assessment of cyber-physical security of energy management system for connected and automated electric vehicles," *IEEE Transactions on Industrial Informatics*, vol. 17, no. 5, pp. 3335–3347, 2021.

[25] G. Xu, J. Liu, Y. Lu, X. Zeng, Y. Zhang, and X. Li, "A novel efficient MAKA protocol with desynchronization for anonymous roaming service in global mobility networks," *Journal of Network and Computer Applications*, vol. 107, pp. 83–92, 2018.

[26] L. Ding and M. Tan, "Robustness of random scale-free networks against cascading failure under edge attacks," *Journal of Communications*, vol. 11, pp. 1088–1094, 2016.

[27] F. Imbault, M. Swiatek, R. D. Beaufort, and R. Plana, "The green blockchain: managing decentralized energy production and consumption," in *Proceedings of the IEEE International Conference on Environment & Electrical Engineering & IEEE Industrial & Commercial Power Systems Europe*, Milan, Italy, June 2017.

[28] S. Amin, G. A. Schwartz, and A. Hussain, "In quest of benchmarking security risks to cyber-physical systems," *IEEE Network*, vol. 27, no. 1, pp. 19–24, 2013.

[29] M. Rungger and P. Tabuada, "A notion of robustness for cyber-physical systems," *IEEE Transactions on Automatic Control*, vol. 61, no. 8, pp. 2108–2123, 2016.

[30] G. Dong, J. Gao, L. Tian, R. Du, and Y. He, "Percolation of partially interdependent networks under targeted attack," *Physical Review. E, Statistical, Nonlinear, and Soft Matter Physics*, vol. 85, no. 1 Pt 2, Article ID 016112, 2012.

[31] X. Huang, J. Gao, S. V. Buldyrev, S. Havlin, and H. E. Stanley, "Robustness of interdependent networks under targeted attack," *Physical Review. E, Statistical, Nonlinear, and Soft Matter Physics*, vol. 83, no. 6 Pt 2, Article ID 065101, 2011.

[32] D. T. Nguyen, Y. Shen, and M. T. Thai, "Detecting critical nodes in interdependent power networks for vulnerability assessment," *IEEE Transactions on Smart Grid*, vol. 4, no. 1, pp. 151–159, 2013.

[33] Z. Huang, C. Wang, S. Ruj, M. Stojmenovic, and A. Nayak, "Modeling cascading failures in smart power grid using interdependent complex networks and percolation theory," in

WILEY | Hindawi

Retraction

Retracted: Information Spreading on Memory Activity-Driven Temporal Networks

Complexity

This article has been retracted by Hindawi following an investigation undertaken by the publisher [1]. This investigation has uncovered evidence of one or more of the following indicators of systematic manipulation of the publication process:

(1) Discrepancies in scope

(2) Discrepancies in the description of the research reported

(3) Discrepancies between the availability of data and the research described

(4) Inappropriate citations

(5) Incoherent, meaningless and/or irrelevant content included in the article

(6) Manipulated or compromised peer review

The presence of these indicators undermines our confidence in the integrity of the article's content and we cannot, therefore, vouch for its reliability. Please note that this notice is intended solely to alert readers that the content of this article is unreliable. We have not investigated whether authors were aware of or involved in the systematic manipulation of the publication process.

Wiley and Hindawi regrets that the usual quality checks did not identify these issues before publication and have since put additional measures in place to safeguard research integrity.

We wish to credit our own Research Integrity and Research Publishing teams and anonymous and named external researchers and research integrity experts for contributing to this investigation.

The corresponding author, as the representative of all authors, has been given the opportunity to register their agreement or disagreement to this retraction. We have kept a record of any response received.

References

[1] L. Zhong, Y. Bai, C. Liu, J. Du, and W. Pan, "Information Spreading on Memory Activity-Driven Temporal Networks," *Complexity*, vol. 2021, Article ID 8015191, 8 pages, 2021.

WILEY | Hindawi

Research Article

Information Spreading on Memory Activity-Driven Temporal Networks

Linfeng Zhong [ID],[1] Yu Bai,[1] Changjiang Liu,[2] Juan Du,[3] and Weijun Pan [ID][1]

[1]*Civil Aviation Flight University of China, Guanghan 618307, China*
[2]*National Key Laboratory of Science and Technology on Blind Singnal Processing, Chengdu 610041, China*
[3]*Beijing Institute of Remote Sensing Information, Beijing 100192, China*

Correspondence should be addressed to Weijun Pan; wjpan@cafuc.edu.cn

Information spreading dynamics on temporal networks have attracted significant attention in the field of network science. Extensive real-data analyses revealed that network memory widely exists in the temporal network. This paper proposes a mathematical model to describe the information spreading dynamics with the network memory effect. We develop a Markovian approach to describe the model. Using the Monte Carlo simulation method, we find that network memory may suppress and promote the information spreading dynamics, which depends on the degree heterogeneity and fraction of bigots. The network memory effect suppresses the information spreading for small information transmission probability. The opposite situation happens for large value of information transmission probability. Moreover, network memory effect may benefit the information spreading, which depends on the degree heterogeneity of the activity-driven network. Our results presented in this paper help us understand the spreading dynamics on temporal networks.

1. Introduction

Extensive real-data analyses revealed that social network exhibits strong temporal properties [1–3], i.e., the edges and nodes do not always exist at any time, and may vary with time. For instance, in scientist collaborative networks, two researchers may collaborate to publish a paper but rarely collaborate at every time step [4–9]. Besides, two researchers may build their first collaboration. Another example is that in the transportation network, two cities may build expressways and high-speed trains. Thus, a new edge is added. The emergence and disappearance of edges and nodes widely exist for the online social network due to the login or log out of the online platforms. Therefore, the temporal network is a widely used method to describe the social network, in which nodes represent individuals and edges stand for their relationships.

For the information spreading on temporal networks, researchers from different disciplines made great contributions [10–19]. In what follows, we first review the progress of information spreading on social network. Different from the static networks, i.e., the network topology does not change with time, researchers found some important results [15, 20–23]. When the information is spreading on the static networks, scholars found that the existence of some hubs may eliminate the threshold point [24, 25]. Specifically, any values of information transmission probability can trigger the information spreading on social networks. Based on these results, we can understand why information can always spread on social platforms. Researchers further revealed that the network community, clustering, and degree-degree correlations could alter the spreading dynamics of information [26, 27]. In reality, sharing a piece of information is risky, and thus affirming its reality and reliability is fatal. Researchers used the threshold-based model to include this factor in the spreading dynamics, such as the Watts threshold model and other generalized models. For that threshold-based information spreading model, the phase transition of the dynamical system is always discontinuous, i.e., first-order phase transition [28]. Wang et al. [29, 30]

proposed nonredundant information spreading dynamics and revealed a transition between the continuous and discontinuous transition in the system.

When researchers studied the information spreading dynamics on temporal networks, scholars found that network temporality can suppress or promote the information spreading [1, 20, 21, 31–37]. Xue et al. proposed a mathematical model to describe a heterogeneous population, where a fraction of nodes adopts a complex contagion. They used a Markovian approach to describe the spreading dynamics. They found that the promotion or suppression of the network temporality is determined by the heterogeneities of population and degree distribution. Scholtes et al. [38] found that the non-Markovian temporal network may speed up or slow down the information spreading. Wang et al. [39] proposed a heuristic immunization strategy for information spreading and demonstrated the effectiveness of this strategy in real-world data.

For the temporal network, an essential factor is the network memory [38, 40–42], which means that edges that existed in the current time step may already occur in previous time steps. Sun et al. [43] revealed that network memory inhibits the spreading process for SIR models, in which the epidemic threshold is enlarged while the spreading size decreases. How memory affects the information spreading dynamics is an important question. To address this, we propose a mathematical model on temporal networks with memory. Then, we develop a Markovian theory for the dynamical model. Through extensive Monte Carlo simulations, we systematically investigate the dynamics. Finally, we conclude.

2. Information Spreading Model

In this section, we introduce the information spreading dynamics on temporal networks with network memory.

2.1. Activity-Driven Network with Memory. Mathematically, the temporal network $\mathcal{G}$ can be described as $\mathcal{G} = (\mathcal{G}_1, \ldots, \mathcal{G}_{t_{max}})$, where $\mathcal{G}_t$ represents the temporal network at time step t. For network $\mathcal{G}_t$, we use the temporal adjacency matrix A_t to represent the topology of $\mathcal{G}_t$. If $A_t(i, j) = 1$, there is an edge between nodes i and j at time t. Otherwise, $A_t(i, j) = 0$.

To build the activity-driven network with memory effect, we generalize the activity-driven model proposed in [44–46]. We build memory activity-driven network as follows.

(i) Assign value for network size N and potential activity x_i according to a given distribution $f(x)$. In this paper, we assume $f(x)$ follows a power-law distribution. That is to say, $f(x) = \varepsilon x^{-\gamma}$, where γ is the potential activity distribution exponent, $\varepsilon = 1/\sum_{x_{min}}^{x_{max}} x^{-\gamma}$, $x_{min} = 10^{-3}$, and $x_{max} = 0.99$. Mathematically, the larger the value of γ, the more homogeneous the degree distribution of the temporal network. Therefore, we can change γ to investigate the degree heterogeneity of the temporal network.

(ii) Generating temporal network $\mathcal{G}_t$: for each node i, there are two possible ways to build edges. If node i becomes active with probability $a_i = \eta x_i$, where η is a parameter, node i forwardly connects to m randomly selected nodes. If node i is inactive, it can only receive the connections from other active nodes.

(iii) At the end of the time step t, we delete every edge with probability $1 - \xi$. Therefore, the memory effect is induced. The higher the value of ξ, the more substantial the memory effect of the temporal network. For the case of $\xi = 0$, the temporal network is memoryless. When $\xi = 1$, the network is static.

According to the above steps, we know that the average degree of network $\mathcal{G}_t$ is $\langle k_t \rangle = 2m\eta\epsilon(\gamma - 1/\gamma - 2)$.

2.2. Information Spreading Model. We here adopt the information spreading model proposed in [47]. This model uses a generalized susceptible-infected-susceptible (SIS) model to describe the dynamics of information spreading. The susceptible nodes mean that they do not receive any information but may receive the information. The infected nodes represent that they have obtained the information and willing to share it with neighbors. In this model, we assume that there are two types of nodes, i.e., activists and bigots. The activists are willing to share the information with friends. Thus, we assume that they have a smaller adoption threshold $\theta_a = 1$. The bigots are less likely to accept the information. Therefore, we set those bigots with a higher adoption threshold $\theta_b > 1$. In this model, we randomly select a fraction of ω nodes as the bigots and the remaining $1 - \omega$ nodes as activists.

The information spreading dynamics evolve as follows:

(i) Randomly selecting ρ_0 fraction of nodes to receive the information and setting the rest as susceptible nodes.

(ii) At every time step, every infected node i tries to transmit the information to its very susceptible neighbor j with probability λ. If node j succeeds in receiving a piece of information, it would be represented by the mark +1 and the like. In this situation, we consider the state of node j. If node j is an activist, it becomes infected. If node j is a bigot, it becomes infected only when its received information is larger than θ_b.

(iii) Every infected node becomes a susceptible state with probability γ_r.

When the infected nodes no longer exist or the spreading dynamics has run 10000 times, the dynamics ends.

3. Theoretical Analyses

To obtain mathematical analysis results on the spreading dynamics, we use a generalized discrete Markovian approach, which is inspired by Refs. [39, 48–50]. In theory, we assume that there are no dynamical correlations among the

state of neighbors. That is to say, the infection probabilities of a susceptible node from informed neighbors are dependent. At any time step t, node i can only be susceptible or infected state. Define $x_i(t) = 1$ when node i is in the infected state and $x_i(t) = 0$ when in susceptible state. The probability of node i in the susceptible and infected states is $\Pr[x_i(t) = 0]$ and $\Pr[x_i(t) = 1]$, respectively. For the sake of simplicity, we denote $\Pr[x_i(t) = 0]$ and $\Pr[x_i(t) = 1]$ as $s_i(t)$ and $p_i(t)$, respectively.

For the evolution of $p_i(t)$, we should consider two situations: the evolutions of bigots and activists, which are denoted as $p_i^a(t)$ and $p_i^b(t)$, respectively. Therefore, we have

$$p_i(t) = p_i^a(t) + p_i^b(t). \tag{1}$$

In the following, we study the evolutions of $p_i^a(t)$ and $p_i^b(t)$. For an activist, such as node i, the evolution of $p_i^a(t)$ includes two situations. On the one hand, node i is in the infected state at time step t and does not recover to susceptible state with probability $(1 - \gamma)p_i(t)$. On the other hand, node i is susceptible at time step t and gets infected by neighbors at this time step with probability $(1 - p_i(t))(1 - q_i^0(t))$, where

$$q_i^0(t) = \prod_{j=1}^N \left(1 - \lambda \mathscr{A}_{ij}(t)p_j(t)\right), \tag{2}$$

represents the probability of node i remaining susceptible at time step t. The evolution of $p_i^a(t)$ is

$$p_i^a(t+1) = (1-\omega)\left[(1-\gamma)p_i(t) + (1 - p_i(t))\left(1 - q_i^0(t)\right)\right]. \tag{3}$$

For the bigots, the evolution of $p_i^b(t)$ is more complex. The bigots will only be infected if the information received is greater than the threshold θ_b. Therefore, we should first compute the number of information received by node i and denote $q_i^n(t)$ as n pieces of information received by node i at time step t. Using the results presented in Ref. [47], we have

$$q_i^n(t) = \sum_{\theta \subseteq \partial i, |\theta|=n} \prod_{j \in \theta} \lambda p_j(t) \prod_{j \in \partial i \backslash \theta} \left(1 - \lambda p_j(t)\right). \tag{4}$$

Until now, we have presented the expression of the evolution equations of the information spreading dynamics. In the steady state, i.e., $t \longrightarrow \infty$, we have $p_i(t+1) = p_i(t)$. We denote the fraction of nodes in the infected state in the steady state as ρ, which can be computed as

$$\rho = \frac{1}{N} \sum_{i=1}^N p_i. \tag{5}$$

We use ρ as the order parameter of the system in the following numerical studies.

4. Results

In this section, we use the Monte Carlo method to study the information spreading dynamics on temporal network with memory effect. When generating the temporal network, we set the average degree of every temporal network $\mathscr{G}_t$ with

average degree $\langle k_t \rangle = 10$. In the dynamical system, we set the order parameter ρ as

$$\rho = \frac{1}{1000} \sum_{t=t_{\max}}^{t_{\max}+1000} \rho(t), \tag{6}$$

where $t_{\max} = 5000$ and $\rho(t) = 1/N \sum_{i=1}^N \rho_i(t)$. We set $\theta_b = 2$. To numerically locate the steady state of the dynamical system, we compute the average values of $\rho(t)$. When the average value of variance $\rho(t)$ is smaller than 10^{-5}, the steady state of the system is reached.

In Figure 1, we first investigate the information spreading dynamics without bigots (i.e., $\xi = 0$). For different strengths of the memory effect, we find two distinct regions. When the information transmission probability λ is small, a strong memory effect suppresses the information spreading dynamics (see $\xi = 0$ and $\xi = 1$). That is to say, the temporal network is not beneficial in information transmission. However, for larger values of λ, the temporal network is beneficial for information spreading. For static networks, the network topology does change with time. The information can be accessed by more susceptible nodes for small values of λ since the giant connected cluster is larger. However, more different nodes will be connected to the temporal giant connected cluster for temporal networks and promote the information spreading for larger λ. Once the network memory effect is not strong enough, compared with the information spreading on static and temporal networks, the information is suppressed regardless of the information transmission probability. Thus, we know that the middle memory effect can suppress the information spreading.

We further investigate the information spreading on a given strength of memory effect for different values of bigots in Figure 2. We note that both the fraction of bigots and memory affect the information spreading. For a given network topology, we find that ρ increases with ω since bigots are not beneficial in transmitting the information. Besides, we note that the increase pattern of ρ versus λ is different for distinct values of ω. When $\omega = 0$, ρ increases continuously with λ. However, ρ discontinuously increases with λ when ω is large (e.g., $\omega = 1.0$ in Figures 2(b)–2(d) and 2(f)).

The network memory effect may benefit the information spreading, which depends on the degree heterogeneity of the activity-driven network. When the potential exponent is $\gamma = 2.1$ and 3.5, the network memory effect suppresses the information spreading (Figures 2(a), 2(c), 2(d), and 2(f)). However, when the potential exponent is $\gamma = 3.0$, the network memory effect promotes the information spreading, as shown in Figures 2(b) and 2(e).

Finally, we investigate the phase transition of the system with different initial seed sizes in Figure 3. Generally speaking, the phenomena are the same as those stated in Figure 2. We find that the system always has a hysteresis loop no matter what value ω and γ is assigned. In more detail, the final information spreading size ρ depends on ρ_0. The larger ρ_0, the higher ρ in the hysteresis loop region. We also note that the larger ω, the smaller ρ. That is to say, the bigots hinder the information spreading dynamics.
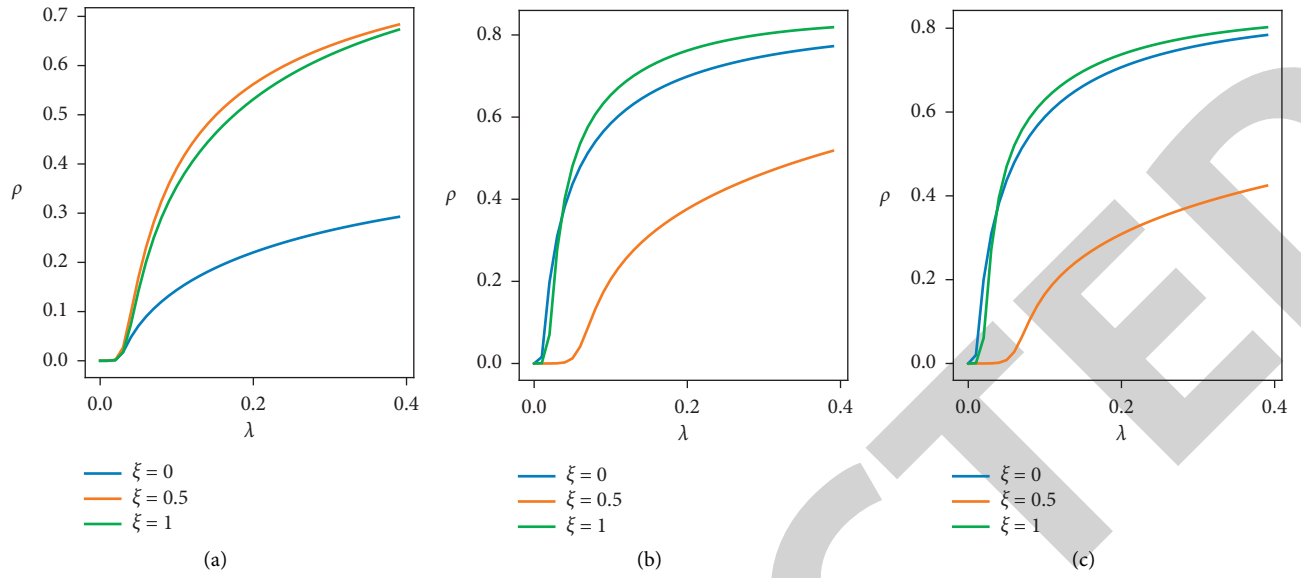
Figure 1: Information spreading on activity-driven networks. The final information spreading size ρ versus information transmission probability λ with $\gamma = 2.1$ (a), $\gamma = 3.0$ (b), and $\gamma = 3.5$ (c). We set the fraction of seeds as $\rho_0 = 0.1$ and the average degree as $\langle k_t \rangle = 10$, and there are no bigots (i.e., $\omega = 0.0$).
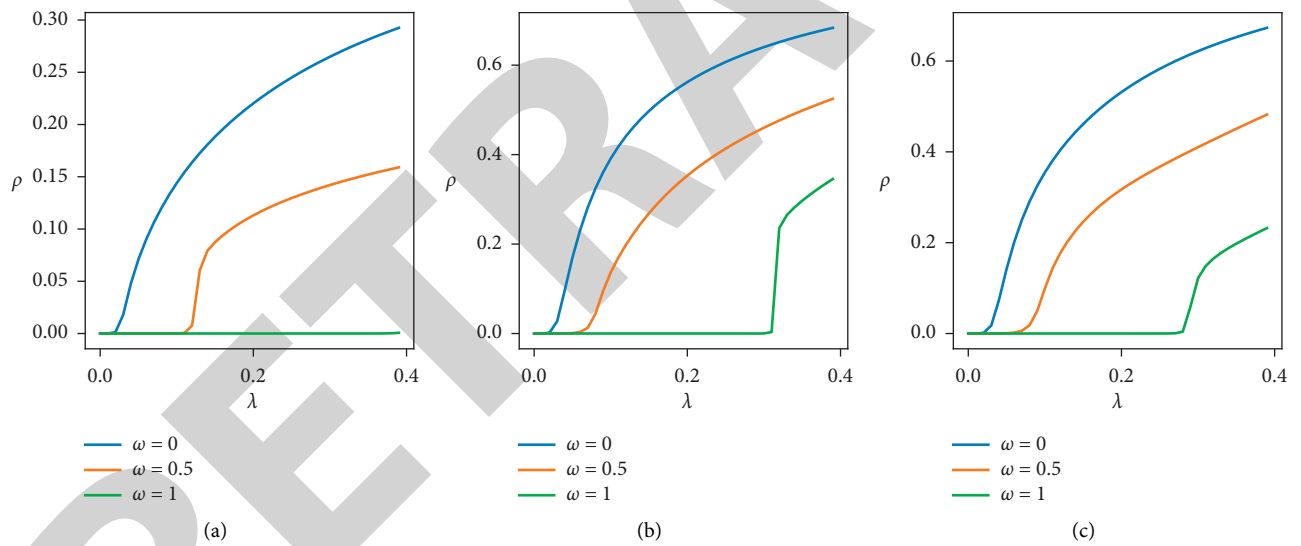

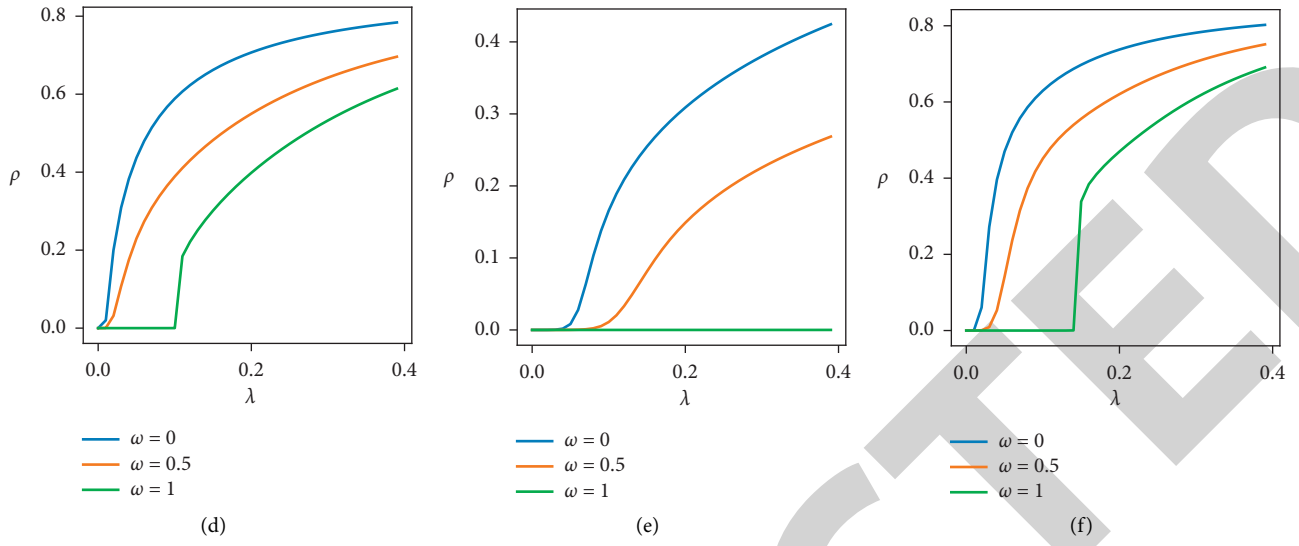Figure 2: Continued.

(d)   (e)   (f)

FIGURE 2: Information spreading on activity-driven networks. The final information spreading size ρ versus information transmission probability λ with $\gamma = 2.1$ (a), $\gamma = 3.0$ (b), and $\gamma = 3.5$ (c) for $\xi = 0.5$. ρ versus λ with $\gamma = 2.1$ (d), $\gamma = 3.0$ (e), and $\gamma = 3.5$ (f) for $\xi = 0$. We set $\rho_0 = 0.1$ and $\langle k_t \rangle = 10$.
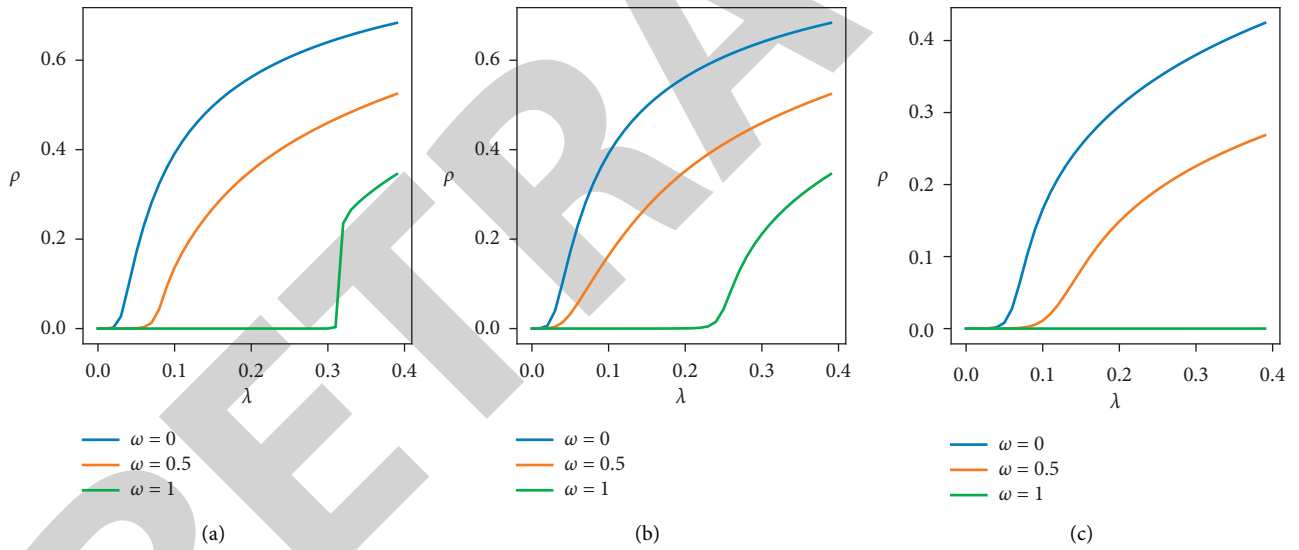

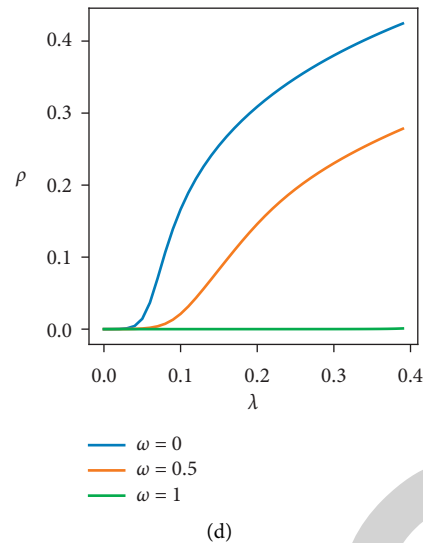(a)   (b)   (c)

FIGURE 3: Continued.

(d)

Figure 3: Information spreading on activity-driven networks. The final information spreading size ρ versus information transmission probability λ with $\rho_0 = 0.1$ (a) and $\rho_0 = 0.9$ (c) for $\gamma = 2.1$. ρ versus λ with $\rho_0 = 0.1$ (b) and $\rho_0 = 0.9$ (d) for $\gamma = 3.5$. We set $\xi = 0.5$ and $\langle k_t \rangle = 10$.

5. Conclusions

In this paper, we proposed a mathematical model to investigate the effects of network memory on the information spreading dynamics on temporal networks. We first proposed a dynamical model in which the temporal network has a memory effect. Specifically, the current temporal network can remember the previous interconnections. Furthermore, an information diffusion model is developed on this type of temporal network. Then, we used a Markovian approach to describe the information spreading dynamics. Finally, we used the Monte Carlo simulation method to study the information spreading model numerically and found that network memory may promote and suppress the dynamics. The effects depend on the heterogeneous degree distribution and the fraction of bigots in the populations.

The results presented in this paper may shed some light into investigating the dynamics of information on temporal networks. On the one hand, the Markovian theory may be used to study other dynamics on temporal networks. On the other hand, the memory effect of temporal network should be included when studying other dynamics. Finally, some further studies about memory of temporal network should be investigated, for instance, developing more accurate theory and designing more realistic models to describe the spreading dynamics.

Data Availability

The datasets used in the present study are available from the first author upon reasonable request (googlezlf@163.com).

Conflicts of Interest

The authors declare that they have no conflicts of interest.

References

[1] N. Masuda and P. Holme, *Temporal Network Epidemiology*, Springer, Berlin, Germany, 2017.
[2] P. Holme and J. Saramäki, *Temporal Network Theory*, Springer, Berlin, Germany, 2019.
[3] P. Holme, "Temporal network structures controlling disease spreading," *Physical Review E*, vol. 94, no. 2, Article ID 022305, 2016.
[4] L. M. Camarinha-Matos and H. Afsarmanesh, "Collaborative networks," in *Proceedings of the International Conference on Programming Languages for Manufacturing*, pp. 26–40, Springer, Berlin, Germany, May 2006.
[5] K.-H. Tsai, "Collaborative networks and product innovation performance: toward a contingency perspective," *Research Policy*, vol. 38, no. 5, pp. 765–778, 2009.
[6] M. Mandell, R. Keast, and D. Chamberlain, "Collaborative networks and the need for a new management language," *Public Management Review*, vol. 19, no. 3, pp. 326–341, 2017.
[7] J. Wang and J. Wang, "Cross-correlation complexity and synchronization of the financial time series on potts dynamics," *Physica A: Statistical Mechanics and its Applications*, vol. 541, Article ID 123286, 2020.
[8] J. Wang and J. Wang, "Measuring the correlation complexity between return series by multiscale complex analysis on Potts dynamics," *Nonlinear Dynamics*, vol. 89, no. 4, pp. 2703–2721, 2017.
[9] J. Wang, J. Wang, and H. E. Stanley, "Multiscale multifractal DCCA and complexity behaviors of return intervals for Potts price model," *Physica A: Statistical Mechanics and Its Applications*, vol. 492, pp. 889–902, 2018.

[10] H. P. Young, "The dynamics of social innovation," *Proceedings of the National Academy of Sciences*, vol. 108, no. 4, pp. 21285–21291, 2011.

[11] D. Centola, "The spread of behavior in an online social network experiment," *Science*, vol. 329, no. 5996, pp. 1194–1197, 2010.

[12] D. Centola, "Physician networks and the complex contagion of clinical treatment," *JAMA Network Open*, vol. 3, no. 1, Article ID e1918585, 2020.

[13] C. Castellano, S. Fortunato, and V. Loreto, "Statistical physics of social dynamics," *Reviews of Modern Physics*, vol. 81, no. 2, pp. 591–646, 2009.

[14] S. Boccaletti, G. Bianconi, R. Criado et al., "The structure and dynamics of multilayer networks," *Physics Reports*, vol. 544, no. 1, pp. 1–122, 2014.

[15] Z.-K. Zhang, C. Liu, X.-X. Zhan, X. Lu, C.-X. Zhang, and Y.-C. Zhang, "Dynamics of information diffusion and its applications on complex networks," *Physics Reports*, vol. 651, pp. 1–34, 2016.

[16] M. Kitsak, L. K. Gallos, S. Havlin et al., "Identification of influential spreaders in complex networks," *Nature Physics*, vol. 6, no. 11, pp. 888–893, 2010.

[17] W. Wang, Q.-H. Liu, J. Liang, Y. Hu, and T. Zhou, "Co-evolution spreading in complex networks," *Physics Reports*, vol. 820, pp. 1–51, 2019.

[18] Y. Yi, Z. Zhang, L. T. Yang, C. Gan, X. Deng, and L. Yi, "Reemergence modeling of intelligent information diffusion in heterogeneous social networks: the dynamics perspective," *IEEE Transactions on Network Science and Engineering*, vol. 8, pp. 828–840, 2020.

[19] L. Pan, W. Wang, L. Tian, and Y.-C. Lai, "Optimal networks for dynamical spreading," *Physical Review E*, vol. 103, no. 1, Article ID 012302, 2021.

[20] P. Holme and J. Saramäki, "Temporal networks," *Physics Reports*, vol. 519, no. 3, pp. 97–125, 2012.

[21] P. Holme, "Modern temporal network theory: a colloquium," *The European Physical Journal B*, vol. 88, no. 9, p. 234, 2015.

[22] W. Wang, M. Tang, H. Eugene Stanley, and L. A. Braunstein, "Unification of theoretical approaches for epidemic spreading on complex networks," *Reports on Progress in Physics*, vol. 80, no. 3, Article ID 036603, 2017.

[23] G. F. De Arruda, F. A. Rodrigues, and Y. Moreno, "Fundamentals of spreading processes in single and multilayer complex networks," *Physics Reports*, vol. 756, pp. 1–59, 2018.

[24] R. Pastor-Satorras and A. Vespignani, "Epidemic dynamics and endemic states in complex networks," *Physical Review E*, vol. 63, no. 6, Article ID 066117, 2001.

[25] R. Pastor-Satorras and A. Vespignani, "Epidemic dynamics in finite size scale-free networks," *Physical Review E*, vol. 65, no. 3, Article ID 035108, 2002.

[26] R. Pastor-Satorras, C. Castellano, P. Van Mieghem, and A. Vespignani, "Epidemic processes in complex networks," *Reviews of Modern Physics*, vol. 87, no. 3, pp. 925–979, 2015.

[27] W. Wang, M. Tang, H. Yang, Y. Younghae Do, Y.-C. Lai, and G. Lee, "Asymmetrically interacting spreading dynamics on complex layered networks," *Scientific Reports*, vol. 4, no. 1, p. 5097, 2014.

[28] D. J. Watts, "A simple model of global cascades on random networks," *Proceedings of the National Academy of Sciences*, vol. 99, no. 9, pp. 5766–5771, 2002.

[29] W. Wang, M. Tang, P. Shu, and Z. Wang, "Dynamics of social contagions with heterogeneous adoption thresholds: crossover phenomena in phase transition," *New Journal of Physics*, vol. 18, no. 1, Article ID 013029, 2016.

[30] H. Peng, W. Peng, D. Zhao, and W. Wang, "Impact of the heterogeneity of adoption thresholds on behavior spreading in complex networks," *Applied Mathematics and Computation*, vol. 386, Article ID 125504, 2020.

[31] S. Lee, L. E. C. Rocha, F. Liljeros, and P. Holme, "Exploiting temporal network structures of human interaction to effectively immunize populations," *PLoS One*, vol. 7, no. 5, Article ID e36439, 2012.

[32] J. Tang, M. Musolesi, C. Mascolo, and V. Latora, "Temporal distance metrics for social network analysis," in *Proceedings of the 2nd ACM Workshop on Online Social Networks*, pp. 31–36, New York, NY, USA, August 2009.

[33] N. Masuda and P. Holme, "Predicting and controlling infectious disease epidemics using temporal networks," *F1000 Prime Reports*, vol. 99, p. 5, 2013.

[34] K. M. Lee, C. D. Brummitt, and K. I. Goh, "Threshold cascades with response heterogeneity in multiplex networks," *Physical Review E*, vol. 90, no. 6, Article ID 062816, 2014.

[35] C. D. Brummitt, K. M. Lee, and K. I. Goh, "Multiplexity-facilitated cascades in networks," *Physical Review E*, vol. 85, no. 4, Article ID 045102, 2012.

[36] Z. Li, F. Yan, and Y. Jiang, "Cross-layers cascade in multiplex networks," *Autonomous Agents and Multi-Agent Systems*, vol. 29, no. 6, pp. 1186–1215, 2015.

[37] Q. Guo, X. Jiang, Y. Lei, M. Li, Y. Ma, and Z. Zheng, "Two-stage effects of awareness cascade on epidemic spreading in multiplex networks," *Physical Review E*, vol. 91, no. 1, Article ID 012822, 2015.

[38] I. Scholtes, N. Wider, R. Pfitzner, A. Garas, C. J. Tessone, and F. Schweitzer, "Causality-driven slow-down and speed-up of diffusion in non-Markovian temporal networks," *Nature Communications*, vol. 5, no. 1, pp. 5024–5029, 2014.

[39] W. Wang, Y. Ma, T. Wu, Y. Dai, X. Chen, and L. A. Braunstein, "Containing misinformation spreading in temporal social networks," *Chaos: An Interdisciplinary Journal of Nonlinear Science*, vol. 29, no. 12, Article ID 123131, 2019.

[40] N. Gour, J.-P. Ranjeva, M. Ceccaldi et al., "Basal functional connectivity within the anterior temporal network is associated with performance on declarative memory tasks," *Neuroimage*, vol. 58, no. 2, pp. 687–697, 2011.

[41] S. Unicomb, G. Iñiguez, J. P. Gleeson, and M. Karsai, "Dynamics of cascades on burstiness-controlled temporal networks," *Nature Communications*, vol. 12, no. 1, pp. 133–210, 2021.

[42] J. P. Gleeson and R. Durrett, "Temporal profiles of avalanches on networks," *Nature Communications*, vol. 8, no. 1, pp. 1227–1313, 2017.

[43] K. Sun, A. Baronchelli, and N. Perra, "Contrasting effects of strong ties on sir and sis processes in temporal networks," *The European Physical Journal B*, vol. 88, no. 12, pp. 1–8, 2015.

[44] N. Perra, B. Gonçalves, R. Pastor-Satorras, and A. Vespignani, "Activity driven modeling of time varying networks," *Scientific Reports*, vol. 2, no. 1, p. 469, 2012.

[45] M. Karsai, N. Perra, and A. Vespignani, "Time varying networks and the weakness of strong ties," *Scientific Reports*, vol. 4, no. 1, p. 4001, 2014.

[46] N. Perra, A. Baronchelli, D. Mocanu, B. Gonçalves, R. Pastor-Satorras, and A. Vespignani, "Random walks and search in time-varying networks," *Physical Review Letters*, vol. 109, no. 23, Article ID 238701, 2012.

[47] X. Xue, L. Pan, M. Zheng, and W. Wang, "Network temporality can promote and suppress information spreading,"